Chapter 11: Near-term Climate Change: Projections and Predictability

Coordinating Lead Authors: Ben Kirtman (USA), Scott Power (Australia)

Lead Authors: Akintayo John Adedoyin (Botswana), George Boer (Canada), Roxana Bojariu (Romania), Ines Camilloni (Argentina), Francisco Doblas-Reyes (Spain), Arlene Fiore (USA), Masahide Kimoto (Japan), Gerald Meehl (USA), Michael Prather (USA), Abdoulaye Sarr (Senegal), Christoph Schär (Switzerland), Rowan Sutton (UK), Geert Jan van Oldenborgh (Netherlands), Gabriel Vecchi (USA), Hui-Jun Wang (China)

Contributing Authors: Nathan Bindoff, Yoshimitsu Chikamoto, Thierry Fichefet, Javier García-Serrano, Paul Ginoux, Lesley Gray, Virginie Guémas, Ed Hawkins, Marika Holland, Christopher Holmes, Johnna Infanti, Masayoshi Ishii, Thomas Knutson, Gerhard Krinner, David Lawrence, Jian Lu, Vaishali Naik, Lorenzo Polvani, Alan Robock, Luis Rodrigues, Jan Sedlacek, Andrew Slater, Doug Smith, Bart van den Hurk, Steve Vavrus, Apostolos Voulgarakis, Oliver Wild, Tim Woollings

Review Editors: Pascale Delecluse (France), Tim Palmer (UK), Theodore Shepherd (Canada), Francis Zwiers (Canada)

Date of Draft: 5 October 2012

Notes: TSU Compiled Version

Table of Contents

Executive Summary

How will climate evolve over the next few decades? This chapter assesses the scientific literature describing estimates of future 'near-term' climate. 'Near-term' refers to future decades up to mid-century, the period for which the climate response to different future emissions scenarios is generally similar. Greatest emphasis is given to the period 2016–2035, though some information on projected changes before and after this period is also assessed. The near-term projections discussed in this chapter complement the mid-century and longer-term climate projections in Chapters 12 and 14. Projected changes in sea level are in Chapter 13. All projections of atmospheric composition, chemistry and air quality through 2100 are assessed in this chapter, except for CO_2, which is assessed in Chapter 12. Assessments are also provided here for the mechanisms responsible for near-term changes in climate, predictions of the evolution of natural variability of the climate system in the presence of changing emissions, the size of the externally-forced signal relative to internal natural variability, the degree of 'predictability' (as defined below) evident in the climate system, and the processes underpinning predictability. Much of the information in this chapter comes from climate model simulations that were performed as part of the Coupled Model Intercomparison Project Phase 5 (CMIP5) and Atmospheric Chemistry and Climate Model Intercomparison Project (ACCMIP), both following the RCP scenarios for emissions and GHG abundances. New results from CMIP5 projections generally corroborate key results in the IPCC Fourth Assessment Report (AR4) for the near term. Projections of continental-scale air quality to the end of the 21st century are also assessed using a hierarchy of modelling approaches, which includes coupled chemistry-climate modelling.

Predictability, Prediction and Projection

The evolution of near-term climate is the combined result of an externally forced component – due to greenhouse gasses, aerosols and other anthropogenic and natural radiative forcing agents – and an internally generated component, which is part of the natural variability of the climate system. A climate prediction attempts to simultaneously forecast the evolution of both of these components over the next several years, perhaps up to a decade, using models which are initialized with observation-based information. A climate projection, on the other hand, attempts to delineate the future evolution of the forced component only over several decades based on the past history of the external forcing and on future forcing scenarios. In climate science the 'predictability' of a given climatic feature is regarded as an intrinsic property of the climate system, which indicates the extent to which the future of the system could be predicted under ideal circumstances. For a particular case, the predictability represents an upper limit to the success with which a forecast system could predict the climate evolution in practice. Predictability, prediction and projection and the differences among them are discussed further in FAQ 11.1, Box 11.1 and Sections 11.1, 11.2.2, and 11.4.1.

Predictability

On decadal timescales, predictability studies are based mainly on the results from coupled climate models. There is a medium amount of evidence and agreement, based on model results, of the predictability of yearly to decadal averages of temperature both for the global average and for some geographical regions. For annual averages of temperature there is good agreement that, in general, the predictability associated with the specification of the initial state of the system decreases with time while that due to the externally forced component increases [Box 11.1, Section 11.2]. Results are model-dependent with medium agreement on common aspects and with multi-model approaches giving a 'consensus' view. It is *likely* that the predictability of the forced component is largest in tropical to middle latitudes and it is *likely* that of the internally generated component is largest for extra-tropical oceans and modest over extra-tropical land. [11.2.1]

Multi-model results for precipitation indicate a generally low level of predictability, although there are some exceptions at higher northern latitudes and longer timescales due mainly to the forced component. [Box 11.1, 11.2.2.1]

There is limited agreement and medium evidence that the Atlantic Multidecadal Variability (AMV) and Pacific Decadal Variability (PDV) patterns of climate variation exhibit predictability on timescales up to a decade. [11.2.2.1]

Decadal Prediction

Indices of global-mean temperature and Atlantic multi-decadal variability have statistically significant positive correlation with observations with *high confidence* for most forecast periods (i.e., four-year averages ranging from 1–4 to 6–10 years) considered [Section 11.2.2; Figure 11.7]. Retrospective prediction experiments have been used to assess forecast quality. The impact of the initialization is assessed by comparing the forecast quality of the initialized and the non-initialized (historical simulations and RCP4.5 projections after 2005) predictions [see Box 11.1 for distinction between prediction and projection; Section 11.2.2]. The initialization of the climate system improves the correlation and root mean square error compared with non-initialized predictions [Section 11.2, Figures 11.7 and 11.8]. The current retrospective prediction experiments suggest that the Interdecadal Pacific Oscillation (IPO) does not have statistically significantly positive skill computed over all initial states in the CMIP5 archive, although case studies suggest that there might be some initial states that can produce skill in predicting IPO-related decadal variability for some time periods. [11.2.3.4]

There is *high confidence* that the retrospective prediction experiments for forecast periods of 1 to 10 years have statistically significant regional temperature correlations with the observations (exceeding 0.6 over much of the globe) [Section 11.2.2]. **The initialization improves the temperature correlation over the North Atlantic, regions of the South Pacific and small continental areas of the Northern Hemisphere** [Section 11.2.2; Figure 11.8]. The differences between initialized predictions and the non-initialized predictions are not statistically significant with 90% confidence level. While there is high agreement that the initialization consistently improves several aspects of climate (like North Atlantic SSTs with more than 75% of the models agreeing on the improvement signal), there is also high agreement that it can consistently degrade others (like the equatorial Pacific temperatures). Probabilistic temperature predictions are reliable (see Section 11.2.3 for definition of reliability) with *medium confidence* [Section 11.2.3; Figure 11.9]. **On multi-annual and decadal time scales the retrospective predictions of continental precipitation have positive correlation with observations over several regions**, with maximum values of 0.6. These correlations are significant at the 95% confidence level, and are due mainly to the specified forcing because there is agreement that the initialization does not have an impact. [11.2.3]

Uncertainties in Future Anthropogenic and Natural Forcing

The range in anthropogenic aerosol emissions across all scenarios has a larger impact on near-term climate projections than the corresponding range in long-lived greenhouse gases, particularly on regional scales and for hydrological cycle variables [11.3.1.1, 11.3.6.1]. **The RCP scenarios do not span the range of future aerosol emissions found in the SRES and alternative scenarios**. The RCPs all assume future rapid reductions in aerosol emissions and there is robust evidence that collectively these represent the low end of future emissions scenarios for aerosols and other short-lived reactive gases, with the high end represented by the SRES A2 or A1FI scenarios. [1.3.x, 9.x.x, 11.5.3.1 and 11.3.6.1, Annex II Tables: AII.2.20–2.22 and AII.5.3–5.6]

If rapid reductions in sulphate aerosol are undertaken for improving air quality or as part of decreasing fossil-fuel CO_2 emissions, then there is *medium confidence* that this could lead to rapid near-term warming. There is robust evidence that accompanying controls on methane (CH_4) emissions would offset some of this sulphate-induced warming. While removal of black carbon aerosol could also counter warming associated with sulphate removal, uncertainties are too large to constrain the net sign of the global temperature response to black carbon emission reductions, which depends on co-emitted (reflective) aerosols and aerosol indirect effects. [11.3.6.1]

Including uncertainties in projecting the chemically reactive greenhouse gases methane (CH_4) and nitrous oxide (N_2O) from RCP emissions gives a range in abundance pathways that is *likely* 30% larger than the range in RCP concentrations used to force the CMIP5 climate models. Including uncertainties in emission estimates from agricultural, forest, and land use sources, in atmospheric lifetimes, and in chemical feedbacks, results in a much wider range of abundances for N_2O, CH_4, and HFCs and their radiative forcing. In the case of CH_4 it *likely* extends the range up to 500 ppb above RCP8.5 and 250 ppb below RCP2.6 through to 2100, with smaller ranges in the near term. [11.3.5]

1
2   **There is *low confidence* in projections of natural forcing.** Major volcanic eruptions cause a negative
3   radiative forcing up to several W m^{-2}, with a typical lifetime of one year, but the possible occurrence and
4   timing of future eruptions is unknown. Except for the 11-year solar cycle, changes in the total solar
5   irradiance are uncertain, see Chapter 8. Except where explicitly indicated, future volcanic eruptions and
6   changes in total solar irradiance additional to a repeating 11-year solar cycle are not included in the
7   projections of near term climate assessed in this chapter. [11.3.1.1]

8
9   *Projected Changes in Near-Term Climate*

10
11   While differences exist, projections of near-term climate change show modest sensitivity to contrasts in
12   greenhouse gas and aerosol emissions within the range of the RCP scenarios. These scenarios presume that
13   there are no major volcanic eruptions and that anthropogenic aerosol emissions are rapidly reduced during
14   the near term. [11.3.1, 11.3.2]

15
16   Projected changes given below are expressed as differences (i.e., anomalies) between the period 2016–2035
17   and the reference period of 1986–2005.

18
19   *Projected Changes in Temperature*

20
21   **The global mean surface air temperature anomaly for the period 2016–2035 relative to the reference**
22   **period of 1986–2005, will *likely* be in the range 0.4–1.0°C (*medium confidence*).** This conclusion
23   presumes that there are no major volcanic eruptions before or during 2016–2035 and no significant long term
24   changes in total solar irradiance, but takes into account the RCP and SRES emissions scenarios, and also
25   *medium evidence* that the CMIP5 models that warm most rapidly may be inconsistent with observations. It is
26   consistent with the AR4 Summary for Policymakers statement that 'For the next few decades a warming of
27   about 0.2°C per decade is projected for a range of SRES emission scenarios'. It is *more likely than not* that
28   that actual warming will be closer to the lower bound of 0.4°C than the upper bound of 1.0°C (*medium*
29   *confidence)*. [11.3.6.3; Figure 11.33]

30
31   **There is *high confidence* that higher concentrations of greenhouse gases and lower amounts of**
32   **sulphate aerosol lead to greater warming, but in the near term the differences between projections for**
33   **different RCP scenarios are typically smaller than the differences between projections from different**
34   **climate models.** In 2030, the CMIP5 multi-model ensemble mean values for global mean temperature differ
35   by less than 0.3 °C between the RCP scenarios, whereas the model spread (defined as the 5–95% range of the
36   decadal means of the models) is around 0.8 °C. The inter-scenario spread increases in time and by 2050 is
37   comparable to the model spread. In the near term, model uncertainty and natural variability therefore
38   dominate the uncertainty in projections of global mean temperature. Regionally, the largest differences in
39   surface air temperature between RCP scenarios are found in the Arctic. [11.3.2.1.1, 11.3.6.1, 11.3.6.3, Figure
40   11.32]

41
42   **The projected warming of global mean temperatures implies *high confidence* that new levels of**
43   **warming relative to pre-industrial climate will be crossed, particularly under higher greenhouse gas**
44   **emissions scenarios.** Assuming that the global mean warming prior to the reference period of 1986–2005
45   was 0.6°C, an assessment based on CMIP5 results suggests the following conclusions. By 2050: under
46   RCP2.6 it is *about as likely as not* that the 1.5°C level will be crossed and *very unlikely* that the 2°C level
47   will be crossed; under RCP4.5 and RCP6.0 it is *likely* that the 1.5°C level will be crossed, and *unlikely* that
48   the 2°C level will be crossed; and under RCP8.5 it is *very likely* that the 1.5 °C level will be crossed, and
49   *likely* that the 2°C level will be crossed. [11.3.1]

50
51   **A future volcanic eruption similar in size to the 1991 eruption of Mount Pinatubo would cause a rapid**
52   **drop in global mean surface air temperature of several tenths of 1°C in the following year, with**
53   **recovery over the next few years.** Larger eruptions, or several eruptions occurring close together in time,
54   would lead to larger and more persistent effects. [11.3.6.2.1]

55
56   **Possible future reductions in solar irradiance would act to cool global mean surface air temperature**
57   **but such cooling is *unlikely* to exceed –0.1°C by 2050 (medium confidence).** A return to conditions similar

1   to the Maunder Minimum is considered *very unlikely* in the near term but, were it to occur, would produce a
2   decrease in global temperatures much smaller than the warming expected from increases in anthropogenic
3   greenhouse gases. However, current understanding of the impacts of solar activity on regional climate
4   remains low. [11.3.6.2.2]
5
6   **The spatial patterns of near-term warming projected by the CMIP5 models following the RCP**
7   **scenarios are broadly consistent with the AR4.** It is *virtually certain* that anthropogenic warming of
8   surface air temperature over the next few decades will proceed more rapidly over land areas than over
9   oceans, and it is *very likely* that the anthropogenic warming over the Arctic in winter will be greater than the
10 global mean warming. Relative to background levels of natural internal variability there is *high confidence*
11 that the anthropogenic warming relative to the reference period will become apparent soonest in the summer
12 season in low latitude countries. Greatest atmospheric warming is projected to occur in the upper tropical
13 troposphere and in the lower troposphere in the northern high latitudes (*medium confidence*). While cooling
14 is projected in the middle-to-upper stratosphere (*high confidence*), there is less confidence in lower
15 stratospheric temperature changes due to opposing influences which include stratospheric O_3 recovery and
16 circulation changes driven by tropospheric warming. [11.4.2; Figures 11.12–14]
17
18 *Projected Changes in the Water Cycle*
19
20 **It is *more likely than not* that over the next few decades there will be increases in mean precipitation in**
21 **regions and seasons where the mean precipitation is relatively high, and decreases in regions and**
22 **seasons where mean precipitation is relatively low.** However, it is *likely* that these changes from 1986 to
23 2005 will only be significant, relative to natural internal variability, on the largest spatial scales (e.g., zonal
24 means), and changes in specific smaller regions may show departures from the large-scale pattern.
25 Anthropogenic aerosols and/or changes in atmospheric circulation could have important complicating or
26 dominant effects in some regions. [11.4.2, Figure 11.16]
27
28 **Over the next few decades increases in near-surface specific humidity are *very likely*. Models project**
29 **increases in evaporation in most regions.** There is little robustness in projected changes in soil moisture
30 and surface run off. Natural internal variability will continue to have a major influence on all aspects of the
31 water cycle. [11.4.2; Figure 11.18]
32
33 *Projected Changes in Atmospheric Circulation*
34
35 **Internal climate variability and multiple radiative forcing agents (e.g., volcanoes, greenhouse gases,**
36 **ozone and anthropogenic aerosols) will all contribute to near-term changes in the atmospheric**
37 **circulation**. For example, it is *likely* that the projected recovery of stratospheric ozone and increases in
38 greenhouse gas concentrations will have counteracting impacts on the width of the Hadley Circulation and
39 the meridional position of the Southern Hemisphere storm track. Therefore it is *unlikely* that they will
40 continue to expand poleward as rapidly as in recent decades. [11.3.2]
41
42 **There is low confidence in near-term projections for a poleward shift of the position and strength of**
43 **Northern Hemisphere storm tracks.** The estimated impact of internal climate variability on the position
44 and strength of Northern Hemisphere storm tracks is larger than the projected impact of greenhouse gases by
45 2016–2035 relative to 1986–2005. [11.3.2]
46
47 **There is low confidence in near-term projections for a weakening of the Walker circulation, relative to**
48 **1986–2005.** It is *more likely than not* that the Walker circulation will weaken by 2016–2035 relative to
49 1986–2005, but the projected weakening of the Walker circulation is small relative to simulated internally-
50 generated interdecadal variability. [11.3.2]
51
52 *Projected Changes in the Ocean*
53
54 **It is *virtually certain* that globally-averaged surface and upper ocean (top 700m) temperatures**
55 **averaged over 2016–2035 will be warmer than those averaged over 1986–2005** [11.4.4; Figure 11.28].
56 This conclusion presumes that there are no major volcanic eruptions during this period. It is *likely* that
57 internal climate variability will be a dominant contributor to changes in the depth and tilt of the equatorial

1   thermocline, and the strength of the east-west gradient of SST across the Pacific through the mid-21st
2   century, thus it is *likely* there will be multi-year periods with increases or decreases, but no clear longer term
3   trend. [11.3.3]

5   **There is *medium confidence* that there will be increases in salinity in the tropical and (especially)**
6   **subtropical Atlantic, and decreases in the western tropical Pacific over the next few decades** [11.4.4].
7   Overall, it is *likely* that there will be some decline in the Atlantic Meridional Overturning Circulation by
8   2050. However, the rate and magnitude of weakening is very uncertain and decades when this Circulation
9   increases are also to be expected [11.3.3].

11 *Projected Changes in the Cryosphere*

13 It is very likely that there will be continued near-term loss of sea ice extent in the Arctic, decreases of snow
14 cover, and reductions of permafrost at high latitudes of the Northern Hemisphere. Though there is the
15 possibility of sudden abrupt changes in the cryosphere, there is low confidence that these changes could be
16 predicted with any certainty over the next several decades. Based on an assessment of a subset of models that
17 more closely reproduce recent observed trends, a nearly ice-free Arctic in late summer before 2050 is a very
18 distinct possibility, even though later dates cannot be excluded. For the earlier near-term period of 2016–
19 2035 averaged over all the CMIP5 models compared to the 1986–2005 reference period, the projected
20 decreases of sea ice area for the RCP4.5 scenario are –28% for September, and –6% for February for the
21 Arctic. Projected changes for the Antarctic are decreases of –5% for September, and –13% for February.
22 Reductions in Northern Hemisphere sea ice volume for that same set of models, scenario and time period are
23 projected to be –23% for February, and –4% for September, while for the Southern Hemisphere those values
24 are –12% for February, and –7% for September. Multi-model averages from 21 models in the CMIP5
25 archive project decreases of Northern Hemisphere snow cover area of –4% ± 1.9% (one standard deviation)
26 for the 2016–2035 time period for a March to April average. The projected reduction in annual mean near-
27 surface permafrost (frozen ground) for the 2016–2035 time period compared to the 1986–2005 reference
28 period for the RCP4.5 scenario for 15 CMIP5 models is –2.9 x 10^6 km^2, or a decrease of about 18%. [11.3.4]

30 *Projected Changes in Temperature and Precipitation Extremes*

32 **It is *very likely* that in the next decades the frequency of warm days and warm nights will increase,**
33 **while the frequency of cold days and cold nights will decrease at the global scale. This trend will *likely***
34 **be visible in an increasing number of regions in the near term.** Models also project increases in the
35 duration, intensity and spatial extent of heat-waves and warm spells for the near term. These changes may
36 proceed at a different rate than the mean warming. For example, in regional climate modelling efforts for
37 Europe, high-percentile daytime summer temperatures are projected to warm at a faster rate than mean
38 temperatures, while daytime winter temperatures warm at a slower rate [11.3.2.5.1; Figure 11.22–23].

40 **In the near term, it is *likely* that the frequency and intensity of heavy precipitation events will increase**
41 **at the global scale. These changes are primarily driven by increases in atmospheric water vapor**
42 **content, but also affected by changes in atmospheric circulation**. While increases in heavy precipitation
43 are *likely* at the global scale and at high latitudes, the impact of anthropogenic forcing at regional scales is
44 less obvious regionally, as regional-scale changes are strongly affected by natural variability and also depend
45 upon the course of future aerosol emissions, volcanic forcing and land use changes. [11.3.2.5.2, Figure
46 11.22–23]

48 *Projected Changes in Tropical Cyclones*

50 **There is *low confidence* in basin-scale projections of trends in tropical cyclone (TC) frequency and**
51 **intensity to the mid-21st century**. Projections of basin-scale TC frequency change vary from basin to basin
52 and include increases and decreases. Increased TC intensity is projected by studies focusing on the North
53 Atlantic and South Pacific, consistent with projections to the end of the 21st century (Chapter 14), although
54 the limited number of studies available focusing on near-term intensity changes leads to only *medium*
55 *confidence* in these near-term intensity projections. It is *very likely* that tropical cyclone frequency, intensity
56 and spatial distribution globally and in individual basins will vary from year-to-year and decade-to-decade in
57 association with natural modes of variability including for example ENSO, AMO and the IPO. [11.3.2.5.3]

1
2 **We have *low confidence* that over the next few decades there will be global and regional increases in**
3 **the intensity of the strongest TCs, and the decrease in global TC frequency** as is projected for the end of
4 the 21st century in response to increasing greenhouse gases (Chapter 14). This low confidence reflects the
5 small number of studies exploring near-term TC activity, and the larger relative influence of internal
6 variability and non-greenhouse forcing of TC activity up to the mid-21st century than at the end of the 21st
7 century. [11.3.2.5.3]
8
9 *The Possibility of Abrupt Changes in Near-Term Climate*
10
11 There are various mechanisms that could lead to changes in global or – more likely – regional climate that
12 are abrupt by comparison with rates experienced in recent decades. The likelihood of such changes is
13 generally lower for the near term than for the long term, and for this reason the relevant mechanisms are
14 primarily assessed in Chapter 12. [11.3.6]
15
16 *Projected Changes in Air Quality*
17
18 **There is *high confidence* that baseline surface ozone (O_3) will change over the 21st century, although**
19 **projections across the RCP, SRES, and alternative scenarios for different regions range from –4 to +5**
20 **ppb by 2030 and –14 to +15 ppb by 2100**. Baseline values (i.e., those not influenced by local
21 anthropogenic emissions) are controlled by global emissions of ozone precursors, as well as climate change,
22 and these represent the abundances of surface ozone at remote sites and over large areas, upon which local
23 and regional pollution episodes build. A warming climate will change baseline levels: as water vapor rises
24 with temperature, there is *high confidence* that O_3 chemical destruction will increase in much of the
25 unpolluted lower troposphere; but there is *medium evidence* that other feedbacks may compensate in some
26 regions of the atmosphere, for example, where abundances of ozone precursors are high. [AII.7.1–3]
27
28 **There is *high confidence* that near-term air quality (surface O_3 and fine particulate matter (PM2.5))**
29 **will improve over North America and Europe under all RCPs except for O_3 in RCP8.5 but will be**
30 **degraded over Asia at least until mid-century under some scenarios**. Due to the assumption of
31 aggressive air quality controls globally across all RCP scenarios, there is *high confidence* that the range in
32 projected air quality changes is much narrower than under the SRES scenarios. By 2100, annual mean
33 surface O_3 over Europe, North America, and Asia declines by 3–14 ppb under all RCPs as projected with
34 CMIP5 and ACCMIP models, except for RCP8.5 which has increases of 1–5 ppb. Global, annual mean
35 surface O_3 rises steadily by 12 ppb in 2100 for SRES A2, but by only 3 ppb in RCP8.5. There is *medium*
36 *confidence* that the projected range in O_3 associated with chemical changes driven by short-lived pollutants
37 and CH_4 in the emission scenarios is much larger than that due to the physical climate changes driven by the
38 greenhouse gases. Aside from episodic dust and wildfire transport events, there is *high confidence* that
39 changes in PM2.5 are largely controlled by regional emissions except where large precipitation changes alter
40 the rainout of aerosols. Future changes at the local or urban level cannot be projected accurately with the
41 models and scenarios evaluated here. [Figures 11.31, 11.32ab, Annex II Tables AII.7.1–4]
42
43 **If the frequency of heat-waves and slow-moving high-pressure systems changes in the near-term, then**
44 **there is *medium confidence* that the frequency of extreme O_3 and PM2.5 pollution events would also**
45 **change**. Based on observations and models, there is *medium confidence* that these extreme weather events
46 can also trigger temperature-driven feedbacks on the sources and sinks of air pollutants, altogether
47 exacerbating O_3 and PM2.5 pollution events by enhancing smog-forming chemistry. The frequency and
48 severity of extreme future pollution events will depend also on changing baselines and local emissions of
49 pollutants not assessed here. [11.3.5.2]
50
51

11.1 Introduction

This chapter describes current scientific expectations for 'near-term' climate – including atmospheric composition and air quality – and it assesses the scientific basis for the expectations. In this chapter 'near term' refers to future decades up to mid-century, the period for which the climate response to different emissions scenarios for the future are generally similar. Greatest emphasis is given to the period 2016–2035, though some information on projected changes before and after this period (up to mid-century) is also assessed.

This emphasis on near-term climate arises from (i) a recognition of its importance to decision makers in government and industry; (ii) an increase in the international research effort aimed at improving our understanding of near-term climate; and (iii) a recognition that near-term projections are generally less sensitive to differences between future emissions scenarios than are long-term projections. Near-term decadal climate prediction (Keenlyside et al., 2008; Meehl et al., 2009c; Smith et al., 2007) provides information not available from existing seasonal to interannual (months to a year or two) predictions or from long-term (late 21st century and beyond) climate change projections (Chapters 12–14). Prediction efforts on seasonal to interannual timescales require accurate estimates of the initial climate state with less concern extended to changes in external forcing[1], while long-term climate projections rely more heavily on estimations of external forcing with little reliance on the initial state of internal variability. Estimates of near-term climate depend partly on the committed warming (caused by the inertia of the oceans as they respond to historical external forcing), the time evolution of internally-generated climate variability, and the future path of external forcing. Near-term climate is particularly sensitive to external forcings from rapid changes in short-lived climate forcing agents (Jacobson and Streets, 2009; Shindell et al., 2012c; UNEP and WMO, 2011; Wigley et al., 2009).

The need for near-term climate information has spawned a new field of climate science, decadal climate prediction (Meehl et al., 2009c; Meehl et al., 2012d). Reflecting this new activity, the Coupled Model Intercomparison Project phase 5 (CMIP5) experimental protocol includes, as one of its foci, near-term predictions (1–10 years), where there is an emphasis on the initialization of the climate system with observations. The goal with such predictions is to increase forecast skill by exploiting any predictability in internally-generated climate variability. This exploitation depends upon an accurate depiction of the initial state of internally generated climate variability (see Box 11.1). In practice there are several major technical challenges that need to be addressed in order to make decadal predictions using systems based on climate models. The challenges are now being addressed by the scientific community, and predictions are being provided. However, the solutions so far are imperfect, and major challenges remain. Estimates of the skill of such systems and the outstanding challenges are outlined in following sub-sections.

Some of these challenges connected with initialization are circumvented in he other focus of CMIP5: that is climate change experiments often referred to as 'uninitialized' or 'non-initialized' projections or simply as 'projections'. Such projections have been the main focus of assessments of future climate in previous IPCC assessments and are the focus of Chapters 12–14. The vast majority of attention in past asessments has been given to the properties of these projections in the late 21st century and beyond. However the projections also provide valuable information on externally-forced changes to near-term climate. Projections are therefore a very important source of information that complements information from the predictions.

The objectives of this chapter are to assess the state of the science for both near-term predictions and near-term projections. Thus both CMIP5 foci noted above are considered for the near term as well as other published near-term predictions and projections. The chapter consists of four major assessments:
(i)   the scientific basis for near-term prediction as reflected in estimates of predictability (see Box 11.1), and the dynamical and physical mechanisms underpinning predictability, and the processes that limit predictability (see Section 11.2);
(ii)   the current state of knowledge in near-term prediction (see Section 11.2). Here the emphasis is placed on the results from the decadal (10-year) multi-model prediction experiments in the CMIP5 database.

---

[1] Seasonal-to-interannual predictions typically include the impact of external forcing.

(iii)   the current state of knowledge in near-term projection (see Section 11.3). Here the emphasis is on
         what the climate in next few decades may look like relative to 1986–2005, based on near-term
         projections (i.e., the forced climatic response). The focus inis on the 'core' near-term period (2016–
         2035), but some information prior to this period and out to mid-century is also discussed. A key issue
         is when, where and how the signal of externally-forced climate change is expected to emerge from the
         background of natural climate variability;

(iv)   near-term projected changes in atmospheric composition and air quality, and their interactions with
         climate change, including new findings from the Atmospheric Chemistry and Climate Model
         IntercomParison (ACCMIP) initiative.

[START BOX 11.1 HERE]

Box 11.1: Climate Prediction, Projection and Predictability

This Box clarifies the meaning of various terms used extensively in this chapter, as they are defined in the
scientific literature on climate. FAQ 11.1 explains some of the terminology in a less technical manner, and it
clarifies the difference between climate prediction and weather predicton.

Internally generated and externally forced climate components
The black line in Figure 11.1a depicts the evolution of observation-based global annual average temperature,
$T(t)$, as the difference from the 1971–2000 average. A change in temperature or other climate system
variable is represented as $T(t) = T_f(t) + T_i(t)$, the sum of an *externally forced* and an *internally generated*
component. Changes in GHG concentrations, natural and anthropogenic aerosol loadings, land use and so on
provide the external forcings which determine $T_f(t)$, while $T_i(t)$ arises spontaneously due to the internal
workings of the climate system.

Climate projection
A *climate projection* attempts to determine the evolution of the forced component $T_f(t)$ and the envelope of
$T_i(t)$ over the next decade(s) but not the particular evolution of $T_i(t)$ that will occur. The yellow lines in the
Figure are from different realizations of the evolution of the global mean temperature from 1900 to 2000
produced by a climate model. This ensemble of realizations, which are not initialized from observations,
indicates a range of possible evolutions of the system for the given forcing and provides statistical
information on climate variability.

The separation of T, or other climate statistics, into externally forced and internally generated components
assumes that such a separation is meaningful and that the components are effectively independent and this
may not always be the case. Operationally, and in Figure 11.1a, T_f is obtained by averaging the different
realizations of T with $T_f(t)$ the component that survives ensemble averaging (the red curve) while $T_i(t)$
averages to near zero.

Climate prediction
A *climate prediction* or *climate forecast* is a statement about the future evolution of some aspect of the
climate system encompassing both forced and internally generated components. Climate predictions do not
attempt to forecast the actual day-to-day progression of the system but rather the evolution of some climate
statistic such as a seasonal, annual or decadal average which may be for a particular location, or a regional or
global average. The global and annually averaged temperature of Figure 11.1a is an example. Climate
predictions are usually made with numerical models which represent the system mathematically using the
equations of fluid mechanics, thermodynamics, cloud physics, radiative transfer and so on that account for
the energy flow and behaviour of the system. A climate prediction proceeds by integrating the governing
equations forward in time from observation-based initial conditions. The use of observational-based initial
conditions is a fundamental difference between a climate predition and a climate projection. Climate
predictions may also be made using statistical methods which relate current to future conditions using
statistical relationships derived from past system behaviour.

A climate model is deterministic in the sense that if the governing equations are integrated forward in time
from identical initial conditions the evolution of the system is reproducible. Nevertheless, because of the
chaotic and non-linear nature of the climate system, minor differences in initial conditions or in some aspect

1 of the model give different evolutions with time. Figure 11.1a gives an example of a forecast of global
2 annual mean temperature which is initiated in 2007. The thin blue lines are individual forecasts begun from
3 slightly different initial conditions and the dark blue line is the average of these forecasts.
4
5 A *deterministic forecast* takes the form of a numerical or categorical statement and attempts to trace out the
6 actual evolution of the climate variable of interest.The ensemble mean forecast (the dark blue line) attempts
7 to predict the actual evolution (the black line) in Figure 11.1a. If differences in initial conditions represent
8 observational and analysis errors, with trajectories that are affected by model deficiencies, the divergence of
9 the predicted from the actual evolution represents the growth of forecast error. Under suitable circumstances,
10 the spread among predictions (the light blue lines) gives an indication of the likelihood of a particular
11 forecast result which may be represented as a probability distribution.
12
13 A *probabilistic* climate prediction takes the form of a probability distribution. Typically, an ensemble of
14 climate prediction using slightly different initial condition and different models are used to contruct this
15 probability distribution. This probabilistic view is depicted in Figure 11.1b. The initial state has a sharply
16 peaked distribution representing the comparatively small uncertainty in the observation-based initial state.
17 The growth of error with forecast time broadens the probability distribution until, ultimately, it becomes
18 indistinguishable from that of an uninitialized climate projection.
19

Climate predictability

21 A physical system is deterministic if the current state determines all subsequent states. Predictability, as used
22 here, indicates the extent to which even minor imperfections in the knowledge of the current state or of the
23 representation of the system limits knowledge of subsequent states. As such it represents an upper limit to
24 forecast skill. The rate of separation or divergence of initially close states of the climate system with time
25 (the light blue lines in Figure 11.1a), or the rate of displacement and broadening of its probability
26 distribution (as in Figure 11.1b) are measures of the system's predictability. If initially close states separate
27 rapidly (or the probability distribution broadens quickly), the predictability of the system is low and vice
28 versa. Initial error grows rapidly if the predictability of the system is low but more slowly if predictability is
29 high. The inherent growth of small errors limits the duration of a useful prediction even for a highly accurate
30 forecast system. Formally, 'predictability' in climate science is a feature of the physical system itself, rather
31 than of our 'ability to make skilful predictions in practice'. The latter depends on the accuracy of models and
32 initial conditions and on the correctness with which the external forcing can be treated over the forecast
33 period. In other words, a highly predictable variable may be poorly predicted in practice because of
34 deficiencies in any (or all) of these aspects.
35
36 Estimating the degree of predictability on decadal timescales and understanding the physical mechanisms
37 involved is an important part of the scientific basis for climate prediction and of the assessment in the
38 Chapter. Climate predictability may be studied diagnostically, by analyzing past climate system behaviour
39 (observed or modelled), or prognostically by studying the behaviour of sequences of perturbed integrations
40 made with a model of the system. The rate of separation of initially close states or, in the probabilistic view,
41 the evolution of the probability distribution is studied and quantified. The predictability of different variables
42 in the atmosphere and ocean will be different and predictability will also vary with location and with the
43 spatial and temporal averaging applied. The predictability of a particular case will also differ from the
44 average predictability usually considered. Model-based estimates of the predictability of the climate system
45 provide broad insight into the possibility of, and the expected limitations to, skilful climate forecasts.
46

Forecast quality

48 Forecast (or prediction) quality measures the success of a prediction against observation-based information.
49 The average over a sequence of forecasts made for past cases, termed *retrospective forecasts* or *hindcasts*,
50 gives an indication of the quality that may be expected, on average, for future forecasts for a particular
51 variable at a particular location. Forecast quality measures the 'ability to predict' and, since forecast systems
52 are not without error, will generally be lower than the 'predictability' of the system. The terms forecast and
53 prediction are used synonymously throughout the remainder of the chapter as are the terms retrospective
54 prediction/forecast and hindcast.
55
56 Predictability and forecast quality, and their dependence on the time average and the range of the forecast,
57 are illustrated in Figure 11.2 which plots the global average of the local correlation skill score and the

1 corresponding predictability measure for temperatures averaged over periods from a month to a decade.
2 Initialized forecasts exhibit enhanced skill compared to uninitialized simulations at shorter time averages and
3 forecast ranges but this advantage declines for longer timescales. In this example at least (based on Boer et
4 al., 2012) the skill of the initialized predictions and of the uninitialized simulations become indistinguishable
5 beyond about a three-year average forecast. The corresponding predictability measures do not converge with
6 timescale, however, suggesting that gains in forecast skill may be possible.

7
8 **[INSERT FIGURE 11.1 HERE]**
9 **Figure 11.1a:** The evolution of observation-based global mean temperature $T(t) = T_f(t) + T_i(t)$ (the black line) as the
10 difference from the 1971–2000 average together with a model-based estimate of the externally forced component T_f (the
11 red line) and the internally generated component T_i (the difference between the black and red lines). An ensemble of
12 forecasts of global annual mean temperature, initialized in 2007, is plotted as thin blue lines and their average, the
13 ensemble mean forecast, as the dark blue line. The shading represent plus and minus one standard deviation for the
14 simulations (light grey shading) and the forecasts (light blue shading). The grey areas along the axis broadly indicate
15 the external forcing associated with volcanoes.

16
17 **Figure 11.1b:** Schematic evolution of predictability and error growth in terms of probability. The probability
18 distribution corresponding to the forced component $p(T_f,t)$ is in red with the deeper shades indicating higher probability.
19 The probabilistic representation of the forecast $p(T,t)$ is in blue. The initially sharply peaked distribution broadens with
20 time as information about the initial conditions is lost until the initialized climate prediction becomes indistinguishable
21 from an uninitialized climate projection (based on Branstator and Teng, 2010).

22
23 **[INSERT FIGURE 11.2 HERE]**
24 **Figure 11.2:** The global average of the local correlation skill score (solid lines) and the corresponding predictability
25 measure (dashed lines) for temperature averaged over periods from a month to a decade. Results plotted for the monthly
26 average correspond to the first month, those for the annual average to the first year and so on up to the decadal average.
27 The orange lines are the results for initialized forecasts which attempt to predict the evolution of both internally
28 generated and forced components of the climate. The green lines are the results for uninitialized forced climate
29 simulations.

30
31 **[END BOX 11.1 HERE]**

32
33 **11.2   Near-Term Predictions**

34
35 *11.2.1 Introduction*

36
37 Climate predictions on decadal timescales attempt to forecast the evolution of both externally-forced and
38 internally-generated near-term variations in climate. Although statistical methods can sometimes be used,
39 predictions are usually made with coupled climate models. The model is initialized by assimilating available
40 observations of the climate system and is integrated forward in time from this initial state with some
41 specification of the external forcing.

42
43 There are a range of difficulties and uncertainties that limit the effectiveness and skill of a decadal
44 prediction. Understanding the sources of uncertainty, quantifying uncertainties where possible and, of
45 course, reducing uncertainty with increased knowledge and improved models is necessary both to exploit
46 currently available predictive skill and to improve future predictions.

47
48 *Initial condition uncertainty*. Available observations of the climate system are 'assimilated' into the model to
49 produce initial conditions. To the extent that the initialization procedure is successful the model state will
50 incorporate the effect of past climate forcing. Initialization of decadal predictions is a complex process
51 which is limited by available observations, observational errors and, depending on the procedure used, may
52 be affected by uncertainty in the history of climate forcing. The initial conditions will contain errors that
53 grow as the forecast progresses thereby limiting the time for which the forecast will be useful.

54
55 *Model uncertainty*. Errors in the model's representation of the physical climate system will introduce errors
56 which also limit the skill of the forecast. Model error involves the representation of dynamical and physical
57 aspects of the climate as well as the model's response to external forcing.

58

Forcing uncertainty. Some representation of external forcing will be part of a decadal prediction. The initial forcing should be reasonably well known from observations but its projected evolution with time may introduce uncertainty. The forcing due to GHGs for instance will not change markedly over the decadal period of the forecast and its evolution may be specified in some simple manner. This is in contrast to the evolution of short timescale forcing that may occur, such as the effect of aerosols from a volcanic eruption for instance, which could be a source of appreciable forcing uncertainty.

Forecast uncertainty. Uncertainties in initial conditions, climate forcings and the model's representation of the climate system generate forecast uncertainty. Forecast uncertainty is typically probed by generating an ensemble of forecasts from initial conditions which are intended to reflect the uncertainty in the initial state. In some cases model uncertainty is probed in terms of the representation of physical processes in the model and/or by combining results from several models. The divergence of forecasts in an ensemble gives some indication of forecast uncertainty which may be represented as a probability distribution under suitable circumstances (see Box).

Forecast quality/skill. In the face of uncertainty, it is important that a decadal climate forecast (or any forecast for that matter) be accompanied by a measure of forecast quality which serves to indicate where and to what extent the forecast may be usefully employed. A long sequence of forecasts made for past cases typically provides the information on which forecast quality is assessed. This kind of information may also be used to adjust or calibrate forecasts, based on past experience, in order to improve skill.

11.2.2 Decadal Climate Prediction

The scientific impetus for decadal prediction arises from improved understanding of the physical basis of long timescale variations in climate and improvements in climate models (Chapter 9), the availability of information on the state of the atmosphere, ocean, cryosphere and land (Chapters 2–4) and from predictability studies, decadal forecasting attempts and from the development of multi-model and other approaches for combining, calibrating and verifying climate predictions. Decadal predictions are of interest for socio-economic reasons as discussed, for instance, in WMO (2009).

11.2.2.1 Predictability Studies

The innate behaviour of the climate system imposes limits on the ability to predict its evolution. Predictability studies indicate where and to what extent skillful climate predictions might be possible, although results are conditional on the verisimilitude with which the climate system is represented. Prognostic predictability studies analyze the time-dependent behaviour of actual or idealized predictions while diagnostic predictability studies are based on analyses (diagnoses) of observations of the climate system or on simulation results from climate models.

11.2.2.1.1 Prognostic predictability studies
The study of Griffies and Bryan (1997) is one of the earliest predictability studies of internally generated decadal variability in a coupled atmosphere/ocean climate model. It concentrates on the North Atlantic and the subsurface ocean temperature while the subsequent studies of Boer (2000) and Collins (2002) deal mainly with surface temperature. Long timescale temperature variability in the North Atlantic has received considerable attention (Figure 11.3) together with its possible connection to the variability of the Atlantic Meridional Overturning Circulation (AMOC) in predictability studies by Collins and Sinha (2003); Collins et al. (2006); Dunstone and Smith (2010); Dunstone et al. (2011); Grotzner et al. (1999); Hawkins and Sutton (2009); Latif et al. (2006); Latif et al. (2007); Msadek et al. (2010); Persechino et al. (2012); Pohlmann et al. (2004); Swingedouw et al. (2012); Teng et al. (2011). The predictability of the AMOC varies among models and, to some extent, with initial model states, ranging from several to 10 or more years. The predictability of the North Atlantic SST is typically weaker than that of the AMOC and the connection between the predictability of the AMOC and the SST is inconsistent among models.

Prognostic predictability studies of the Pacific are less plentiful even though Pacific Decadal Variability (PDV) itself has received considerable study. Sun and Wang (2006) suggest that some of the variability linked to the Pacific Decadal Oscillation (PDO) can be predicted approximately 7 years in advance. Teng et al. (2011) investigate the predictability of the first two EOFs of annual mean SST and upper ocean

temperature, identified with PDV, and find predictability of the order of 6–10 years. Meehl et al. (2010) focus on the low-frequency decadal component of SST in the Pacific (the Interdecadal Pacific Oscillation or IPO) both forced and internally generated components, in the broader Pacific region (to 40°S). Examination of past decadal shifts such as the 1970s climate shift that was shown to have both an internally generated component related to the IPO and an externally forced part (Meehl et al., 2009a), has led to more recent quantification of possible future decadal shifts that involve transitions of the IPO combined with external forcing to simulate decades with accelerated warming and decades with little warming (Meehl and Teng, 2012). Decadal timescale transitions of the IPO have also been shown to modulate interannual variability in the Indo-Pacific region associated with the Tropospheric Biennial Oscillation (TBO, see Chapter 14, Section 14.2.5.3) for both the mid-1970s shift, after which the TBO became weaker, and for the late 1990s shift, after which the TBO became stronger (Meehl and Arblaster, 2012), and to affect regional climate and sea level rise in the tropical eastern Indian and western Pacific Oceans (Han et al., 2012). Hermanson and Sutton (2010) report that predictable signals in different regions and for different variables may arise from differing initial conditions. Ocean variables, especially deep ocean quantities, are more predictable than atmospheric and surface variables. Branstator and Teng (2010) analyze upper ocean temperatures, and some SSTs, for the North Atlantic, North Pacific and the tropical Atlantic and Pacific in the NCAR model. Predictability associated with the initial state of the system decreases while that due to the forced component increases with time. The 'cross-over' time is longer in extratropical (7–11 years) compared to tropical (2 years) regions and in the North Atlantic compared to the North Pacific.

[INSERT FIGURE 11.3 HERE]
Figure 11.3: Predictability examples – Top panel shows results for perfect predictability of the Meridional Overturning Circulation (MOC) based on de-correlation time. Light blue curves correspond to multi-model results from Collins et al. (2006) for strong positive MOC cases, the dark blue curve is the multi-model mean and the dotted blue is de-correlation of persistence. Light red curves correspond to multi-model results from Collins et al. (2006) for strong negative MOC cases, the dark red curve is the multi-model mean and the dotted red is de-correlation of persistence. The think black curve the perfect predictability based on results from Msadek et al. (2010). Bottom panel shows CMIP5 multi-model extra-tropical upper (400 m) ocean heat content predictability as measured by potential de-correlation time. The blue curve corresponds to the Pacific and the red curves correspond to the Atlantic. Potential de-correlation (r) time is estimated from the mean squared distance (msd) as $r=1-msd/2$. The msd is from Branstator and Teng (2012) using an analogue method with a CMIP5 sub-set of models (see Branstator et al., 2012) for details).

11.2.2.1.2 Diagnostic predictability studies
Because long data records are needed, diagnostic decadal predictability studies based on observational data are few. Newman (2007) and Alexander et al. (2008) develop multivariate empirical Linear Inverse Models (LIMs) from observation-based SSTs and find predictability for ENSO and PDV type patterns that are generally limited to the order of a year although exceeding this in some areas. Hawkins and Sutton (2009) and Tziperman et al. (2008) apply similar methods to GFDL and Hadley Centre model output and find predictability of from one to several decades respectively for the AMOC and North Atlantic SST.

Branstator and Teng (2012) use analog and multivariate linear regression methods to quantify the predictability of the internally generated component of upper ocean temperature in six coupled models. Results differ across models but offer some common areas of predictability. Basin-average estimates indicate predictability for up to a decade in the North Atlantic and somewhat less in the North Pacific (Figure 11.3).

The percentage of the total variance that is accounted for by long timescales is termed the 'potential predictability'. It indicates where long timescales are important and where their lack limits predictability. The potential predictability of the internally generated component for temperature is studied in Boer (2000); Collins (2002); Pohlmann et al. (2004); Power and Colman (2006) and, in a multi-model context, in Boer (2004) and Boer and Lambert (2008). Power and Colman (2006) find that potential predictability in the ocean tends to increase with latitude and depth. Multi-model results for both externally forced and internally generated components are studied in Boer (2011) and Figure 11.4 displays the geographic distribution of potential predictability for both five year and decadal mean temperatures. The potential predictability of the forced and internally generated components depends on the time averages considered as seen also in Figure 11.2. Although not yet reanalyzed using CMIP5 results, the previous CMIP3-based multi-model result indicate that long-timescale potential predictability for precipitation is modest and associated with the forced component.

1 **[INSERT FIGURE 11.4 HERE]**
2 **Figure 11.4:** The potential predictability of five year and decadal means of temperature (lower panels), the contribution
3 from the forced component (middle panels) and from the internally generated component (upper panels). These are
4 multi-model results from CMIP5 RCP4.5 scenario simulations from 17 coupled climate models following the
5 methodology of Boer (2011). The results apply to the early 21st century.

6

7 *11.2.2.1.3 Summary*
8 At long timescales, predictability studies are based mainly on coupled models. Results are model dependent,
9 although there are commonalities, while multi-model approaches give a 'consensus' view. There is evidence
10 of predictability for both the internally generated and externally forced components of temperature with the
11 first dominating at shorter and the second at longer timescales. Long timescale predictability for precipitation
12 is modest and due mainly to the forced component. Predictability of temperature associated with the initial
13 state of the system decreases with time while that due to the forced component increases, with average cross-
14 over times of the order of 4–9 years.

15

16 *11.2.2.2 Climate Prediction on Seasonal to Decadal Timescales*

17

18 *11.2.2.2.1 Seasonal to decadal prediction*
19 Model-based seasonal predictions for the globe are routinely produced by some twelve WMO 'Global
20 Producing Centres (GPCs) for Long Range Forecasts' as well as by other global and regional centres. The
21 raw model results are often modified by statistical post-processing methods (e.g., Eyring et al., 2010;
22 Stephenson et al., 2005; Wang et al., 2009). Statistical methods are also used to produce seasonal forecasts
23 directly (e.g., Fan and Wang, 2009; van den Dool, 2007). Similar model-based and statistical methods are
24 used to make decadal predictions.

25

26 *11.2.2.2.2 Initial conditions*
27 A typical seasonal, interannual or decadal dynamical prediction consists of an ensemble of forecasts
28 produced by integrating a climate model forward in time from a set of observation-based initial conditions.
29 As forecast range increases, processes in the ocean become increasingly important and the sparseness, non-
30 uniformity and secular change in sub-surface ocean observations is a challenge to analysis and prediction
31 (Meehl et al., 2009b; Meehl et al., 2012d; Murphy et al., 2010) and can lead to differences among ocean
32 analyses (Stammer, 2006). Approaches to ocean initialization include (as listed in Table 11.1) 1) assimilation
33 only of SSTs and relying on ocean transports to initialize the sub-surface ocean indirectly (Keenlyside et al.,
34 2008), although studies suggest that the amplitude of the relaxation term is a key unknown (Dunstone and
35 Smith, 2010; Swingedouw et al., 2012), 2) the forcing of the ocean model with atmospheric observations
36 (e.g., Matei et al., 2012; Yeager et al., 2012) and/or the direct assimilation or insertion of ocean reanalyses
37 and atmospheric initial states (Du et al. 2012) and 3) more sophisticated alternatives based on fully coupled
38 data assimilation schemes (e.g., Sugiura et al., 2009; Zhang et al., 2007a).

39

40 Dunstone and Smith (2010) investigate the impact of SST and subsurface ocean data for initializing decadal
41 predictions in an idealized context and find expected improvement in skill when sub-surface information is
42 used. Assimilation of atmospheric data, however, gives little impact after the first year. The initialization of
43 sea ice, snow cover, frozen soil and soil moisture can potentially contribute to seasonal and subseasonal skill
44 (e.g., Chevallier and Salas-Melia, 2012; Koster et al., 2010; Paolino et al., 2012; Toyoda et al., 2011),
45 although an assessment of their benefit at longer time scales has not yet been attempted.

46

47 *11.2.2.2.3 Full-field and anomaly initialization*
48 Models may be initialized using *full-field* or *anomaly* approaches (Hazeleger et al., 2012b). Full-field
49 initialization constrains the model values to be near the observation-based values at the initial time.
50 However, the forecasts 'drift' from their initial observation-based state toward the model's climate (Doblas-
51 Reyes et al., 2011; Suckling and Smith, 2012) on timescales of a few years and this drift may be sufficient to
52 confound the evolution of the forecast. This may be at least partially offset by using anomaly initialization in
53 which observed anomalies are added to the model climate to produce initial conditions (see 11.2.3.1).

54

55 *11.2.2.2.4 Ensemble generation*
56 An ensemble of initial conditions is generated in order to sample the probability distribution of the
57 observation-based initial state of the system and the ensuing ensemble of forecasts to characterize its

1   evolution. Ensemble generation is important in seasonal prediction (e.g., Stan and Kirtman, 2008; Stockdale
2   et al., 1998) but not yet fully investigated for decadal prediction (Corti et al., 2012; Suckling and Smith,
3   2012). Methods being investigated include adding random perturbations to initial conditions, using
4   atmospheric states displaced in time, using parallel assimilation runs (Doblas-Reyes et al., 2011; Du et al.,
5   2012) and perturbing ocean initial conditions by ensemble assimilation (Mochizuki et al., 2010; Zhang et al.,
6   2007a). Perturbations leading to rapidly growing modes, common in weather forecasting have also been
7   investigated (Du et al., 2012; Hawkins and Sutton, 2009; Hawkins and Sutton, 2011; Kleeman et al., 2003;
8   Vikhliaev et al., 2007). The uncertainty associated with a model's representation of the climate system may
9   be partially represented by the perturbed physics (Murphy et al., 2007; Stainforth et al., 2005) or stochastic
10 physics (Berner et al., 2008) approaches applied to multi-annual and decadal predictions (Doblas-Reyes et
11 al., 2009; Smith et al., 2010), although the most common method is the multi-model approach.

13 The multi-model approach combines ensembles of predictions from a collection of models thereby
14 increasing the sampling of both initial conditions and model properties. Multi-model approaches are used
15 across timescales ranging from seasonal-interannual (eg. DEMETER; Palmer et al., 2004), to seasonal-
16 decadal (e.g., Weisheimer et al., 2011; van Oldenborgh et al., 2012), in climate change simulation (e.g.,
17 IPCC 2007, Chapter 10, Meehl et al., 2007b) and in the ENSEMBLES and CMIP5-based decadal predictions
18 assessed in Section 11.2.3.

20 **11.2.3   Prediction Quality**

22 *11.2.3.1   Decadal Prediction Experiments*

24 Decadal predictions for specific variables can be made by exploiting empirical relationships based on past
25 observations and expected physical relationships. Predictions of North Pacific Ocean temperatures have been
26 achieved using prior wind stress observations (Schneider and Miller, 2001). Regional predictions of surface
27 temperature have been made based on projected changes in external forcing and the state of the natural
28 variability at the start date (Ho et al., 2012; Krueger and von Storch, 2011; Lean and Rind, 2009; Newman,
29 2012). Some of these forecast systems are also used as benchmarks to compare with the dynamical systems
30 under development.

32 Modern comprehensive climate models produce prediction information for an array of variables although
33 most attention is paid to temperature and precipitation as the basic variables of practical interest. Evidence
34 for skilful interannual to decadal temperatures using dynamical models forced only by previous and
35 projected changes in anthropogenic greenhouse gases and aerosols and natural variations in volcanic aerosols
36 and solar irradiance is reported by Lee et al. (2006), Räisänen and Ruokolainen (2006) and Laepple et al.
37 (2008). To be clear, in the context of this report these studies are viewed as projections since no attempt is
38 made to use observational estimates for the initial conditions. Essentially, an uninitialized prediction is
39 synonymous with a projection. These projections or unitialized prediction are refered to synonymously in the
40 literature as 'NoInit,' or 'NoAssim' referring to the fact that no assimilated observations are used for the
41 specification of the initial conditions.

43 Additional skill can be realized by initializing the models with observations in order to also predict the
44 evolution of the internally generated component and to correct the model's response to previous and future
45 imposed forcings (Fyfe et al., 2011; Hawkins and Sutton, 2011; Kharin et al., 2007; Smith et al., 2010).
46 Again, to be clear this report makes the distinction that the studies attempting to initialize the models with
47 observations are a prediction, which should be contrasted with the projection sutides noted in the previous
48 paragraph where no attempt at initialization is made.

50 This recent recognition that decadal climate prediction is important has motivated the research community to
51 design coordinated experiments. The ENSEMBLES project (van Oldenborgh et al., 2012), for example, has
52 conducted a multi-model decadal retrospective prediction study, and the Coupled Model Intercomparison
53 Project phase 5 (CMIP5) proposed a coordinated experiment that focuses on decadal, or near-term, climate
54 prediction (Meehl et al., 2009b; Taylor et al., 2012). Prior to these initiatives, a few pioneering attempts at
55 initialized decadal prediction were made (Keenlyside et al., 2008; Mochizuki et al., 2010; Pierce et al., 2004;
56 Pohlmann et al., 2009; Smith et al., 2007; Troccoli and Palmer, 2007). Results from the CMIP5 coordinated
57 experiment (Taylor et al., 2012) are the basis for the assessment reported here.

Both ENSEMBLES and the CMIP5 near-term predictions involve a series of ten-year retrtospctive predictions initialized by observations every five years starting near 1960. A subsequent extension to the CMIP5 protocol calls for predictions initialized every year to increase the statistical robustness of the results. Initialized runs from three start dates, 1960, 1980, and 2005, were further extended to 30 years, a the range likely to be dominated by anthropogenic external forcing. Since the practice of decadal prediction is in its infancy, details of how to initialize the models was left to the discretion of the modeling groups and are described in Meehl et al. (2012d) and Table 11.1. In CMIP5 experiments, volcanic aerosol and solar cycle variability are prescribed along the integration using observation-based values up to 2005, and assuming a climatological 11-year solar cycle and a background volcanic aerosol load in the future. These forcings are shared with CMIP5 historical runs (i.e., unitialized projections) started from pre-industrial control simulations enabling an assessment of the impact of initialization. The specification of the volcanic aerosol load and the solar irradiance in the hindcasts gives an optimistic estimate of the forecast quality with respect to an operational prediction system. Table 11.1 summarizes forecast systems contributing to and the initialization methods used in the CMIP5 near-term experiment. The coordinated nature of ENSEMBLES and CMIP5 experiments offer a good opportunity to study *multi-model* ensembles (García-Serrano and Doblas-Reyes, 2012; van Oldenborgh et al., 2012) as a means of sampling model uncertainty while some modelling groups have also investigated this using perturbed parameter approaches (Smith et al., 2010).The relative impact of the different approaches for decadal predictions has yet to be assessed.

[INSERT TABLE 11.1]
Table 11.1: Initialization methods used in models that entered CMIP5 near-term experiments.

An important difficulty in climate prediction arises from model biases. When initialized with states close to the observations, models 'drift' towards their imperfect climatology, leading to systematic biases in the forecasts. The time scale of the drift is in most cases a few years (Hazeleger et al., 2012a; Suckling and Smith, 2012) and the magnitude can be comparable to the signals to be predicted. Biases can be largely removed by an a posteriori empirical correction computed from a collection of retrospective predictions (García-Serrano et al., 2012; Kharin et al., 2012). Figure 5 is an illustration of the time scale of the global SST drift, while at the same time showing the large systematic error of most of the forecast systems contributing to CMIP5. It should be noted, however, there are usually non-linear relationships between the mean state and the anomalies, which is one of the main limitations of this simple, linear approach.

[INSERT FIGURE 11.5 HERE]
Figure 11.5: Time series of global-mean sea surface temperature from the multi-model initialized hindcasts, where a different colour has been used for each start date, and the reference data (ERSST) is drawn in black. The hindcasts are displayed in two panels to prevent the curves from consecutive start dates to overlap. All time series have been smoothed out with a 24-month centred moving average that removes data for the first and last years of each time series.

Bias adjustment is a method of statistically post-processing forecasts that linearly corrects for model drift (e.g., Stockdale, 1997; García-Serrano and Doblas-Reyes, 2012). A temperature forecast, for instance, may be represented as $T(\tau) = \overline{T}(\tau) + T'(\tau)$, where the forecast range τ is the time beyond the initial time. The overbar represents the average over the hindcasts and $T'(\tau)$ the difference from the average. The observed temperatures corresponding to the forecasts are similarly expressed as $T_o(\tau) = \overline{T_o}(\tau) + T_o'(\tau)$. The average error or bias in this context is $b(\tau) = \overline{T}(\tau) - \overline{T}_o(\tau)$ which This estimates the rate at which the model drifts away from the observed climate and towards the model climate as the forecast evolves. The drift is subtracted from the forecast to give a bias-adjusted prediction $\hat{T}(\tau) = T(\tau) - b(\tau) = \overline{T}_o(\tau) + T'(\tau)$. This approach assumes that the model bias is stable over the prediction period (from 1960 onward in the CMIP5 experiment). This might not be the case if, for instance, the predicted temperature trend differs from the observed trend (Fyfe et al., 2011; Kharin et al., 2012). It has been recognized that including as many initial states as possible in computing the bias adjustments is more desirable than a greater number of ensemble members per initial state (Meehl et al., 2012a). A procedure for bias adjustment roughly following the technique outlined above has been recommended for the CMIP5 experiments (Office, 2011). A suitable adjustment depends also on there being a sufficient number of hindcasts for statistical robustness (García-Serrano et al., 2012; Kharin et al., 2012).

1   To reduce these problems, many of the early attempts at decadal prediction (Keenlyside et al., 2008;
2   Mochizuki et al., 2010; Pohlmann et al., 2009; Smith et al., 2007) use an approach called anomaly
3   initialization (Pierce et al., 2004; Schneider et al., 1999; Smith et al., 2007). The anomaly initialization
4   approach attempts to circumvent model drift and the need for a time-varying bias correction. The models are
5   initialized by adding observed anomalies to the model climate. The mean model climate is subsequently
6   subtracted from the predictions to obtain forecast anomalies. Sampling error in the calculation of the means
7   affects the success of this approach, which is also affected to a smaller degree by the drift (García-Serrano et
8   al., 2012). In both approaches, full or anomaly initialization, the forecast information essentially consists of
9   the evolution of the forecast *anomaly,* that is $T'(\tau)$. The relative merits of anomaly versus full initialization
10   have started to be quantified (Hazeleger et al., 2012a), although no initialization method was found to be
11   definitely better in terms of forecast quality. Ideally, model improvements are expected to reduce and
12   ultimately eliminate the need for bias correction or anomaly initialization although this will not be achieved
13   easily or quickly.
14
15   *11.2.3.2 Forecast Quality Assessment*
16
17   A distinction between model validation and forecast quality assessment is typically made NRC (2010a). The
18   quality of a forecast system is assessed by estimating the accuracy, skill and reliability of a set of hindcasts
19   (Jolliffe and Stephenson, 2011). No single metric can provide a complete picture of prediction quality, even
20   for a single variable. A suite of metrics needs to be considered, particularly when a forecast system is
21   compared with others or with previous versions. The accuracy of a forecast system refers to the precision
22   with which the forecast system tends to match the observed changes that the system is trying to predict. The
23   skill is the accuracy of the system relative to the accuracy of some reference prediction method (e.g.,
24   climatology or persistence). The reliability, which is a property of the specific forecast system, measures the
25   trustworthyness of the predictions, that is how well the predicted probability distribution matches the
26   observed relative frequency of the forecast event. In other words, a probabilistic prediction is considered
27   reliable if a user can rely on it to make a decision, even if the prediction is not skilful. Accuracy and
28   reliability are aspects of the forecast quality that can be improved by improving the individual forecast
29   systems or by combining several of them into a multi-model prediction. Furthermore, the reliability can be
30   increased by statistical post-processing of the predictions.
31
32   The assessment of forecast quality depends on what characteristics of the prediction are of greatest interest to
33   those who would use the information. WMO's Standard Verification System (SVS) for Long Range
34   Forecasts (LRF) (WMO, 2002) outlines specifications for long-range (sub-seasonal to seasonal) forecast
35   quality assessment. For deterministic forecasts, the recommended metrics: are the mean square skill score,
36   the relative operating characteristics (ROC) curve, area under the ROC curve (Mason and Weigel, 2009) for
37   the accuracy, and the correlation for skill. For probabilistic forecasts, the recommended metrics are the ROC
38   area, the Brier skill score and the reliability diagram. All these measures are described in Jolliffe and
39   Stephenson (2011) and Wilks (2006). Measures of reliability are related to the spread of the system. For
40   dynamical ensemble systems, a useful measure of the characteristics of an ensemble forecast system is its
41   spread. The relative spread can be described in terms of the ratio between the mean spread around the
42   ensemble mean and the ensemble-mean RMSE, or spread-to-RMSE ratio. A ratio of one is considered a
43   desirable feature for a Gaussian-distributed variable of a well-calibrated prediction system (Palmer et al.,
44   2006). It has been recently emphasized the importance of using statistical inference in forecast quality
45   assessments (García-Serrano and Doblas-Reyes, 2012; Goddard et al., 2012). This is even more important
46   when both the small samples available and the small number of degrees of freedom due to the
47   autocorrelation of multi-annual variability are taken into account, which creates problems such as the
48   negative bias in correlation induced by the commonly used leave-one-out cross-validation strategy (Gangstø
49   et al., 2012). Confidence intervals for the scores are typically computed using either parametric or bootstrap
50   methods (Guémas, 2012; Jolliffe, 2007; Lanzante, 2005).
51
52   Forecast skill and other measures of forecast quality are usually calculated as an average over the sequence
53   of hindcasts. Note that the brevity of the hindcast record and inhomogeneities in the initialisation data
54   generally leads to large uncertainty in the estimation of forecast quality measures. Additionally, the skill of
55   seasonal predictions can vary from generation to generation (Balmaseda et al., 1995; Power et al., 1999),
56   highlighting the possibility that the skill of decadal predictions might also vary from one period to another.
57   Certain initial conditions might precede more predictable near-term states than other intial conditions, and

1 this has the potential to be reflected in predictive skill assessments. A recommendation for a deterministic
2 metric for decadal climate predictions is the mean square skill score (MSSS), and for a probabilistic metric,
3 the continuous ranked probability skill skill score (CRPSS) as described more fully in Goddard et al. (2012)
4 and Meehl et al. (2012d).
5
6 *11.2.3.3 Pre-CMIP5 Decadal Prediction Experiments*
7
8 Early decadal prediction studies found little additional predictability from initialization, over that due to
9 changes in radiative forcing, on global (Pierce et al., 2004) and regional scales (Troccoli and Palmer, 2007),
10 but neither of these studies considered more than two start dates. More comprehensive tests, which
11 considered at least nine different start dates indicated temperature skill (Doblas-Reyes et al., 2011; García-
12 Serrano and Doblas-Reyes, 2012; García-Serrano et al., 2012; Keenlyside et al., 2008; Mochizuki et al.,
13 2010; Pohlmann et al., 2009; Smith et al., 2007; Smith et al., 2010; Sugiura et al., 2009; van Oldenborgh et
14 al., 2012). Moreover, this skill was enhanced by the initialization mostly over the ocean, in particular over
15 the North Atlantic and subtropical Pacific oceans (Doblas-Reyes et al., 2012). Some skill improvements have
16 also been found for precipitation (Volpi et al., 2012).
17
18 The largest of those tests in a multi-model context was offered by the ENSEMBLES experiment.
19 ENSEMBLES multi-model consists of four forecast systems: CERFACS, ECMWF, IFM-GEOMAR and
20 Met Office with the HadGEM2 model (van Oldenborgh et al., 2012). Three-member ensemble hindcasts
21 were run for ten years starting on November 1 from 1960 to 2005 every five years. Volcanic aerosol
22 concentrations from eruptions before the analysis date were relaxed to zero with a time scale of one year in
23 the IFM-GEOMAR system (Keenlyside et al., 2008), while the other three models did not include any
24 volcanic aerosol effect. In all cases, the effects of eruptions during the hindcasts were not included to
25 reproduce a realistic forecasting context. The treatment of volcanoes is major difference the CMIP5
26 experiment and the ENSEMBLES experiment. Three of the four models (the ECMWF, Met Office and
27 CERFACS systems) used a full initialisation strategy. In contrast, IFM-GEOMAR used observed SST
28 anomaly information to generate the initial conditions. A second ENSEMBLES contribution (DePreSys;
29 Smith et al., 2010) was run by the Met Office using a nine-member ensemble of HadCM3 model variants
30 sampling modelling uncertainties through perturbations to poorly constrained atmospheric and surface
31 parameters. Ten-year long hindcasts were started on the first of November in each year from 1960 to 2005.
32 In order to assess the impact of initialization an additional parallel set of hindcasts (referred to as NoAssim)
33 with the same nine model versions was also made. The NoAssim hindcasts are identical to those of
34 DePreSys except that they are not explicitly initialized with the contemporaneous state of the climate system,
35 the initial conditions obtained from the restarts of the corresponding long-term climate change integrations.
36 NoAssim is used to assess the impact of the initial conditions in near-term climate prediction.
37
38 *11.2.3.4 CMIP5 Decadal Prediction Experiments*
39
40 Global-mean temperature, and the Atlantic multi-decadal variability (AMV) and the interdecadal Pacific
41 oscillation (IPO) as well as global mean temperature indices are used as benchmarks to assess the ability of
42 decadal forecast systems to predict multi-annual averages (Goddard et al., 2012; van Oldenborgh et al.,
43 2012; see also Figure 11.6), the AMV (Trenberth and Shea, 2006) and IPO (Power et al., 1999).
44
45 Non-initialized predictions (or projections) of the global-mean temperature are statistically significantly
46 skilful for most of the forecast ranges considered, due to the almost monotonic increase in temperature,
47 pointing at the large role played by the time-varying radiative forcing (Kim et al., 2012; Murphy et al.,
48 2010). In other words, non-initialized predictions (or projections) could have provided skilful temperature
49 information over the past 50 years. This holds whether the changes in the external forcing (i.e., changes in
50 natural and/or anthropogenic atmospheric compostion) are specified (i.e., CMIP5) or are projected
51 (ENSEMBLES and DePreSys). CMIP5 and DePreSys have similar skill behaviour along the forecast time,
52 with subtle differences between the skill of the two forecast systems (Doblas-Reyes et al., 2012). The skill of
53 the global-mean temperature improves with the initialization, although only in the RMSE sense.
54
55 The AMV index, computed as the SST anomalies averaged over the region Equator –60ºN and 80º–0ºW
56 minus the SST anomalies averaged over 60ºS–60ºN (Trenberth and Shea, 2006), shows decadal variability
57 and has multi-year predictability (García-Serrano and Doblas-Reyes, 2012; Murphy et al., 2010) and has

1   important impacts on temperature and precipitation over land (van Oldenborgh et al., 2012). The AMV has
2   been connected to multi-decadal variability of Atlantic tropical cyclones (Dunstone et al., 2011; Goldenberg
3   et al., 2001; Zhang and Delworth, 2006). As for the global-mean temperature, the robust high correlation of
4   the non-initialized AMV predictions is consistent with the view that recent variability is due to the external
5   forcings (Booth et al., 2012). Figure 11.6 shows that the CMIP5 multi-model ensemble mean has a similar
6   skill as a function of the forecast time, which is statistically significant at the 95% level, and generally larger
7   than for the single-model forecast systems (García-Serrano and Doblas-Reyes, 2012; Kim et al., 2012). The
8   skill of the AMV index improves with the initialization for the early forecast ranges while the mean square
9   error is significantly reduced with the initialization for the global-mean temperature for all forecast ranges.
10
11 The Pacific decadal variability is associated with potentially important climate impacts, including rainfall
12 over America, Asia, Africa and Australia (Deser et al., 2004; Li et al., 2012; Power et al., 1999; Zhu et al.,
13 2011). The combination of Pacific and Atlantic variability and climate change appears to explain much of
14 the multidecadal US drought frequency (Burgman et al., 2010; McCabe et al., 2004) including key events
15 like the American dustbowl of the 1930s (Schubert et al., 2004). Figure 11.6 shows that the IPO predictions
16 seldom show statistically significant positive correlation along the forecast range, even when initialized. van
17 Oldenborgh et al. (2012) reported weak skill of the IPO in the ENSEMBLES multi-model, although Doblas-
18 Reyes et al. (2012) show that the ensemble-mean skill of the ENSEMBLES multi-model IPO is barely
19 significant for all forecast systems and shows no consistent impact of the initialization. Although the current
20 retrospective prediction experiments suggest that the IPO does not have statistically significant positive skill
21 computed over all initial states, although case studies suggest that there might be some initial states that can
22 produce skill in predicting IPO-related decadal variability for some time periods (e.g., Chikamoto et al.,
23 2012b; Meehl and Teng, 2012).
24
25 The higher AMV and global-mean temperature skill of the CMIP5 predictions with respect to the DePreSys
26 and ENSEMBLES hindcasts (Doblas-Reyes et al., 2012) might be partly due to the former multi-model
27 using specified instead of projected aerosol load (especially the volcanic aerosol) and solar irradiance
28 variations during the simulations. As these forcings can not be specified in a real forecast setting, DePreSys
29 and ENSEMBLES offer a better estimate of the skill of a real-time forecast system.
30
31 **[INSERT FIGURE 11.6 HERE]**
32 **Figure 11.6:** Decadal prediction forecast quality of several climate indices. Top row: Time series of the 2–5 year
33 average ensemble-mean initialized hindcast anomalies and the corresponding non-initialized experiments for three
34 climate indices: global-mean temperature (left), the Atlantic multidecadal variability (AMV, middle) and interdecadal
35 Pacific oscillation (IPO, right). The observational time series, GISS global-mean temperature and ERSST for the AMV
36 and IPO, are represented with dark grey (positive anomalies) and light grey (negative anomalies) vertical bars, where a
37 four-year running mean has been applied for consistency with the time averaging of the predictions. Predicted time
38 series are shown for three different sets of the CMIP5 Init (solid) and NoInit (dotted) simulations: hindcasts with start
39 dates every five years (eleven systems, green), with start dates every year (five systems, yellow) and the five systems
40 with yearly start dates sampled using only one start date every five years (red), all over the period 1960–2005. The
41 AMV index was computed as the SST anomalies averaged over the region Equator –60ºN and 80º–0ºW minus the SST
42 anomalies averaged over 60ºS–60ºN. The IPO index is the principal component of the leading EOF of each model using
43 SSTs in the region 50ºS–50ºN / 100ºE–290ºE where the mean SST over 60ºS–60ºN for each forecast system and
44 forecast period has been previously removed. Middle row: Ensemble-mean correlation with the observational reference
45 along the forecast time for four-year averages of the three sets of CMIP5 hindcasts for Init (solid) and NoInit (dashed).
46 The one-sided 95% confidence level with a t distribution is represented in grey (dark grey) for the hindcasts with five
47 (one) year start date sampling. The number of degrees of freedom has been computed taking into account the
48 autocorrelation of the observational time series. A two-sided t test (where the number of degrees of freedom has been
49 computed taking into account the autocorrelation of the observational time series) has been used to test the differences
50 between the correlation of the initialized and non-initialized experiments, but no differences where found significant
51 with a confidence equal or higher than 90%. Bottom row: Ensemble-mean root mean square error along the forecast
52 time for four-year averages of the three sets of CMIP5 hindcasts for Init (solid) and NoInit (dashed). A two-sided F test
53 (where the number of degrees of freedom has been computed taking into account the autocorrelation of the
54 observational time series) has been used to test the ratio between the RMSE of the Init and NoInit, and those forecast
55 time with differences significant with a confidence equal or higher than 90% are indicated with an open square. The
56 number of degrees of freedom has been computed taking into account the autocorrelation of the observational time
57 series.
58

1 Near-term prediction systems have significant skill for temperature over large regions (Figure 11.7),
2 especially over the oceans, but also over land (Doblas-Reyes et al., 2011; Kim et al., 2012; Smith et al.,
3 2010; van Oldenborgh et al., 2012). A robust skill increase due to the initialization (Figure 11.7) is limited to
4 areas of the North Atlantic, in agreement with previous results (Mochizuki et al., 2012; Pohlmann et al.,
5 2009; Smith et al., 2010), the southeast Pacific and areas of the Southern Ocean. Some improvements are
6 also found over land in the Mediterranean and northern Eurasia. Similar results are found in individual
7 forecast systems (e.g., Bellucci et al., 2012; Müller et al., 2012).

8
9 The skill in the North Atlantic basin in Figure 11.7 is consistent with previous studies (e.g., Knight et al.,
10 2005) linking Atlantic multi-decadal variability (AMV) with variations of the AMOC. The improvement in
11 retrospective AMV predictions from initialization (Dunstone et al., 2011; García-Serrano et al., 2012;
12 Hazeleger et al., 2012b; Smith et al., 2010; Wouters et al., 2012) suggest that internal variability was
13 important to AMV in the past. However, the interpretation is complicated because the impact on the skill
14 varies slightly with the forecast quality measure used. The improvements in certain areas, like over the
15 northern Indian (an effect, as for the global-mean temperature, of the bias correction of the modelled climate
16 response induced by the initialization) or the western Pacific Oceans (in agreement with Chikamoto et al.,
17 2012b), depend on the skill measure and the variable considered. This has been attributed to the different
18 impact of the local trends on the scores used (Goddard et al., 2012). The impact of the initialization on the
19 skill, though robust (as shown by the agreement between the different CMIP5 systems), is small. This fact
20 linked to the limited sample available (nine or ten start dates, depending on the forecast time), make the
21 correlation differences between Init and NoInit not statistically significant with 90% confidence. Although
22 some single forecast systems show larger skill improvements, the lack of agreement in the spatial
23 distribution of the skill differences reduces the positive impact of the initialization.

24
25 Initialization of the sub-polar Atlantic, which was shown to be skilful in Figures 11.6 and 11.7, provides skill
26 (García-Serrano et al., 2012; Robson et al., 2012b). In an idealized predictability study of the Atlantic
27 tropical storm frequency (Dunstone et al., 2011) it was found that the AMV, and in particular its subpolar
28 branch, was behind the skill of multi-year North Atlantic tropical storm frequency predictions (Smith et al.,
29 2010). However, another study argued that the nominal improvement in multi-year forecasts of North
30 Atlantic hurricane frequency was due to persistence of a climate signal (Vecchi et al., 2012b).

31
32 Sugiura et al. (2009) report using a single forecast system skill in hindcasts of the Pacific Decadal
33 Oscillation (PDO), which is ascribed to the interplay between Rossby waves and a clockwise propagation of
34 ocean heat content anomalies along the Kuroshio-Oyashio extension and subtropical subduction pathway.
35 However, as Figure 11.7 shows, the Pacific Ocean is the basin with the lowest temperature skill overall, with
36 no consistent impact of the initialization. The central North Pacific has zero or negative skill, which is partly
37 linked to the large relative importance of the interannual variability, the generalized failure in predicting the
38 largest warming events (Guémas et al., 2012) beyond a few months into the forecast, the low skill of the
39 SST-based PDO (Lienert and Doblas-Reyes, 2012) and the different behaviour of surface temperature and
40 upper ocean heat content predictions for the PDO (Chikamoto et al., 2012a; Mochizuki et al., 2012;
41 Mochizuki et al., 2010). There is a robust negative skill difference between Init and NoInit in the equatorial
42 Pacific. The complex basin-wide forecast quality explains that the IPO ensemble-mean skill is very low for
43 every forecast system considered (Figure 11.6).

44
45 **[INSERT FIGURE 11.7 HERE]**
46 **Figure 11.7:** Near surface air temperature forecast quality for the forecast time 2–5 (left column) and 6–9 (right
47 column) years. Top row: Ensemble-mean correlation of the CMIP5 Init multi-model with five-year interval between
48 start dates over the period 1960–2005. A combination of temperatures from GHCN/CAMS air temperature over land,
49 ERSST and GISTEMP 1200 over the polar areas is used as a reference. Black dots correspond to the points where the
50 correlation is statistically significant with 95% confidence using a one-sided t-test taking into account the
51 autocorrelation of the observational time series. Second row: Ensemble-mean correlation difference between the
52 CMIP5 Init and NoInit multi-model experiments. A Fisher Z-transform of the correlations has been computed, the
53 colours showing the Z difference in correlation space. Contours are used for areas where the ensemble-mean correlation
54 of at least 75% of the single forecast systems has the same sign as the multi-model ensemble mean correlation. Dots are
55 used for the points where the Z differences are statistically significant with 90% confidence taking into account the
56 autocorrelation of the observational time series. Third row: Root mean square skill score for the multi-model ensemble
57 mean of CMIP5 Init experiment. Black dots correspond to the points where the skill score is statistically significant
58 with 95% confidence using a one-sided F-test taking into account the autocorrelation of the observation minus

prediction time series. Bottom row: Ratio between the ensemble-mean root mean square error of Init and NoInit. Dots are used for the points where the ratio is significantly above or below one with 90% confidence using a two-sided F-test taking into account the autocorrelation of the observation minus prediction time series. Contours are used for areas where the ratio of at least 75% of the single forecast systems has a value above or below one according to the multi-model ensemble mean correlation. Poorly observationally sampled areas are masked in grey. The model original data have been bilinearly interpolated to the observational grid. The ensemble mean of each forecast system has been estimated before computing the multi-model ensemble mean.

The initialization has been suggested to be responsible for skill improvements over land mainly through atmospheric teleconnections from improved surface temperature predictions in the North Atlantic and subtropical Pacific (Dunstone et al., 2011; Smith et al., 2010). Skill in predicting the AMV is thought to be related to skill in predicting the AMOC (Knight et al., 2005). An assessment of the impact of observing systems on AMOC predictability indicates that the recent dense observations of oceanic temperature and salinity are crucial to constraining the AMOC in one model Zhang et al. (2007a), while the observing system representative of the pre-2000s was not as effective, indicating that inadequate observations in the past might also have limited the impact of initialization on the predictions. This has been confirmed by Wouters et al. (2012) using decadal predictions.

In spite of the positive role of the initialization, recent studies (Booth et al., 2012; Chang et al., 2011; Evan et al., 2009; Villarini and Vecchi, 2012b) suggest that the observed AMV over the 20th century was strongly influenced by changes in atmospheric (natural and anthropogenic) aerosol loading. It is likely that changes in aerosol forcing were influential in observed variations in the North Atlantic, yet the influence on the AMV of aerosols relative to other processes remains uncertain. Assessments of the skill of prediction systems to hindcast past variability in the AMOC have been attempted by Matei et al. (2012) for example, although their claimed skill may not yet go beyond reproducing average seasonal cycles (Vecchi et al., 2012a). At any rate, direct measures of the AMOC are far too short to underpin a reliable estimate of skill, and longer histories are poorly known. The fact remains that there is very low confidence in current estimates of the skill of the AMOC hindcasts. It is essential to estabilish sustained ocean observations, such as Argo and RAPID-MOCHA, in order to build our capability to understand and predict AMOC.

Decadal predictions have been mainly considered from a deterministic point of view, in most cases using a single prediction or the mean of an ensemble. However, climate prediction is, by nature, probabilistic. Probabilistic predictions are expected to be not just skilful, but also reliable. The word 'reliable' has a specific technical meaning in probability forecasting, a meaning that can allow potential users to assess whether decadal predictions are trustworthy. Suppose a decadal forecast probability of some event E, say that temperature lies above the long-term climatological tercile value, is equal to 0.6. For a reliable forecast system, one could assert that E would actually occur on 60% of the time where E was predicted with a probability of 0.6. However, probabilistic forecast systems are often not fully reliable. Decadal predictions should ultimately be evaluated on the basis of whether they give an accurate estimation of the relative frequency of the predicted outcome. This question can be addressed using, among other tools, attributes diagrams (Mason, 2004). They measure how closely the forecast probabilities of an event correspond to the actual chance of observing the event. They are based on a discrete binning of many forecast probabilities taken over a given geographical region.

Figure 11.8 illustrates the CMIP5 multi-model Init and NoInit attributes diagrams for predictions of the North Atlantic SSTs to be below the lower tercile. For perfect reliability the forecast probability and the frequency of occurrence should be equal, and the plotted points should lie on the diagonal (solid black line in the figure). When the line joining the bullets (the reliability curve) has positive slope indicates that as the forecast probability of the event occurring increases, as does the verified chance of observing the event. The predictions therefore can be considered as moderately reliable. However, if the slope of the curve is less than the diagonal, then the forecast system is overconfident. If the reliability curve is mainly horizontal, then the frequency of occurrence of the event does not depend on the forecast probabilities. In this situation a user might make some very poor decision based on such uncalibrated probabilities. An ideal forecast should have high resolution whilst retaining reliability, it should be both sharp and reliable.

In agreement with Corti et al. (2012), CMIP5 multi-model predictions are to some degree reliable, in particular for the North Atlantic, although with a tendency to be overconfident. For the North Atlantic, the initialization also improves the reliability of the predictions, which translates in an increase of the Brier skill

1   score. However, the uncertainty associated with these estimates is not negligible. This is mainly due to the
2   small sample, which makes that the number of predictions in a given probability bin is too small to give a
3   meaningful estimate of the observed relative frequency (Brocker and Smith, 2007).
4
5   **[INSERT FIGURE 11.8 HERE]**
6   **Figure 11.8:** Attributes diagram for the CMIP5 multi-model decadal initialized (panels a and c) and non-initialized
7   (panels b and d) hindcasts for the event 'SST anomalies below the lower tercile' over a) and b) the global oceans
8   (60ºN–60ºS) and c) and d) the North Atlantic (87.5ºN–30ºN, 80ºW–10ºW) for the forecast time 2–5 years. The number
9   of red bullets in the figure corresponds to the number of probability bins (10 in this case) used to estimate forecast
10 probabilities. The size of the bullets represents the number of forecasts in a specific probability category and is a
11 measure of the sharpness of the predictions. The blue horizontal and vertical lines indicate the climatological frequency
12 of the event in the observations and the mean forecast probability, respectively. Grey vertical bars indicate the
13 uncertainty in the observed frequency for each probability category estimated at 95% level of confidence with a
14 bootstrap resampling procedure based on 1000 samples. The longer the bars, the more the vertical position of the bullets
15 may change as new hindcasts become available. The black dashed line separates skilful from unskilled regions in the
16 diagram in the Brier skill score sense. The Brier skill score with respect to the climatological forecast is drawn in the
17 top left corner of each panel.
18
19 The skill for land precipitation (Figure 9) is much lower than the skill for temperature, with several regions,
20 especially in the Northern Hemisphere, displaying statistically significantly positive values. The positive
21 precipitation skill can be attributed mostly to the specification or projection of the atmospheric concentration
22 as the initialization improves the skill very little (Doblas-Reyes et al., 2012; Goddard et al., 2012). The skill
23 in areas like Europe and West Africa might be associated with the positive AMV skill (even in non-
24 initialized predictions), the AMV being a descriptor of the interannual precipitation over those regions (van
25 Oldenborgh et al., 2012).
26
27 **[INSERT FIGURE 11.9 HERE]**
28 **Figure 11.9:** Precipitation forecast quality for the forecast time 2–5 (left column) and 6–9 (right column) years. Top
29 row: Ensemble-mean correlation of the CMIP5 Init multi-model with five-year interval between start dates over the
30 period 1960–2005. GPCC precipitation is used as a reference. Black dots correspond to the points where the correlation
31 is statistically significant with 95% confidence using a one-sided t-test taking into account the autocorrelation of the
32 observational time series. Second row: Ensemble-mean correlation difference between the CMIP5 Init and NoInit
33 multi-model experiments. A Fisher Z-transform of the correlations has been computed, the colours showing the Z
34 difference in correlation space. Contours are used for areas where the ensemble-mean correlation of at least 75% of the
35 single forecast systems has the same sign as the multi-model ensemble mean correlation. Dots are used for the points
36 where the Z differences are statistically significant with 90% confidence taking into account the autocorrelation of the
37 observational time series. Third row: Root mean square skill score for the multi-model ensemble mean of CMIP5 Init
38 experiment. Black dots correspond to the points where the skill score is statistically significant with 95% confidence
39 using a one-sided F-test taking into account the autocorrelation of the observation minus prediction time series. Bottom
40 row: Ratio between the ensemble-mean root mean square error of Init and NoInit. Dots are used for the points where the
41 ratio is significantly above or below one with 90% confidence using a two-sided F-test taking into account the
42 autocorrelation of the observation minus prediction time series. Contours are used for areas where the ratio of at least
43 75% of the single forecast systems has a value above or below one according to the multi-model ensemble mean
44 correlation. The model original data have been bilinearly interpolated to the observational grid. The ensemble mean of
45 each forecast system has been estimated before computing the multi-model ensemble mean.
46
47 The small amount of statistically significant differences found between the initialized and non-initialized
48 experiments does not necessarily mean that the impact of the initialization does not have a physical basis. A
49 comparison of the global-mean temperature and AMV forecast quality using one- and five-year intervals
50 between start dates (Figure 11.6) suggests that, although a five-year interval sampling allows an estimate of
51 the level of skill, local maxima as a function of forecast lead-time might well be due to poor sampling of the
52 start dates (Doblas-Reyes et al., 2012; García-Serrano and Doblas-Reyes, 2012; Goddard et al., 2012).
53 Several signals, such as the skill improvement for temperature over the North Atlantic, are robust as it is
54 found in a large fraction of forecast systems (more than 75%). However, it is difficult to obtain statistical
55 significance with these limited samples. The low start date sampling frequency is one of the limitations of
56 the core CMIP5 near-term prediction experiment. Results estimated with yearly start dates are clearly more
57 robust than with a five-year start date frequency, and offer an increased number of statistically significant
58 results. However, even with one-year start date frequency, the impact of the initialization is similar (Figure
59 11.10a; note that the CMIP5 multi-model ensemble in this case includes five individual systems instead of
60 eleven). The spatial distribution of the skill does not change substantially with the different start date

1 frequency. The skill and the initialization impact are both slightly reduced in the results with yearly start
2 dates, but at the same time the spatial variability is substantially reduced. Apart from the low sampling of the
3 start dates, the length of the forecasting period is limited to the period over which reasonably accurate
4 estimates of the ocean initial state can be made, which starts around 1960. This fact also limits the sample
5 size to estimate the forecast quality.

6

7 **[INSERT FIGURE 11.10a HERE]**
8 **Figure 11.10a:** Impact of the number of start dates on the air temperature forecast quality of the 2–5 year forecast time
9 with five-year (left) and one-year (right) interval between start dates over the period 1960–2005. Top row: Ensemble-
10 mean correlation of the CMIP5 Init multi-model, where the same multi-model ensemble with five individual forecast
11 systems has been used in both panels. A combination of temperatures from GHCN/CAMS air temperature over land,
12 ERSST and GISTEMP 1200 over the polar areas is used as a reference. Black dots correspond to the points where the
13 correlation is statistically significant with 95% confidence using a one-sided t-test taking into account the
14 autocorrelation of the observational time series. Second row: Ensemble-mean correlation difference between the
15 CMIP5 Init and NoInit multi-model experiments. A Fisher Z-transform of the correlations has been computed, the
16 colours showing the Z difference in correlation space. Contours are used for areas where the ensemble-mean correlation
17 of at least 75% of the single forecast systems has the same sign as the multi-model ensemble mean correlation. Dots are
18 used for the points where the Z differences are statistically significant with 90% confidence taking into account the
19 autocorrelation of the observational time series. Third row: Ratio between the ensemble-mean root mean square error of
20 Init and NoInit. Dots are used for the points where the ratio is significantly above or below one with 90% confidence
21 using a two-sided F-test taking into account the autocorrelation of the observation minus prediction time series.
22 Contours are used for areas where the ratio of at least 75% of the single forecast systems has a value above or below
23 one according to the multi-model ensemble mean correlation.

24

25 These results confirm that there is substantial skill in multi-annual predictions of temperature and non-trivial
26 skill for land precipitation. Most of the skill is due to the slowly varying changes in atmospheric
27 composition, both natural and anthropogenic. The initialization of the forecast systems robustly improves
28 several aspects of the forecast quality of temperature over the North Atlantic and other regions, although it
29 can also degrade the skill in other areas like the tropical Pacific. Responding to the gains in decadal skill in
30 certain regions due to the initialization, a coordinated quasi-operational initiative has been organized (Smith
31 et al., 2012). Different institutions regularly exchange initialized decadal predictions. The forecast systems
32 used are based on those of CMIP5 and some statistical predictions, and individually have been evaluated for
33 forecast quality. The forecast is experimental, since the skill of the particular multi-model system is as yet
34 unknown, provides a consensus view to prevent overconfidence in predictions from any single model. An
35 example is illustrated in Figures 11.10b and 11.10c, where the initialized predictions started near the end of
36 2012 are shown for the forecast period 1–5 years as well as the differences between the initialized and non-
37 initialized predictions. Uncertainties are large for individual years and the initialization has little impact
38 beyond the first four years in most regions. Relative to the non-initialized predictions, initializing causes
39 substantial warming of the north Atlantic sub-polar gyre, cooling of the north Pacific throughout the decade
40 and cooling over most land and ocean regions and in the global average out to several years ahead. However,
41 in the absence of volcanic eruptions, global temperature is predicted to continue to rise.

42

43 **[INSERT FIGURE 11.10b HERE]**
44 **Figure 11.10b:** Forecast and observed temperature anomalies for 2013–2017 initialized near the end of 2012. a)-j)
45 Ensemble mean forecast from each forecast system. All anomalies are degrees centigrade relative to the average of the
46 period 1971 to 2000.

47

48 **[INSERT FIGURE 11.10c HERE]**
49 **Figure 11.10c:** Impact of initialization (initialized minus non-initialized ensemble means) on forecasts of the period
50 2013 to 2017 initialized near the end of 2012. Unstippled regions in (i) indicate a 90% or higher probability that
51 differences between the initialized and non-initialized ensemble means did not occur by chance (based on a 2 tailed t-
52 test of differences between the two ensemble means assuming the ensembles are normally distributed).

53

54 The coordinated experiments, such as ENSEMBLES and CMIP5, not only enable overall assessments of the
55 present level of decadal prediction skill, but also provide valuable opportunity for case studies when
56 successful or less successful retrospective predictions are made. For example, a good understanding is being
57 obtained through detailed process studies on the cause and predictability of a stepwise increase in SSTs over
58 the North Atlantic during mid-1990s (Robson et al., 2012a) or large deviations from the mean in the North
59 Pacific in the 1960s (Guémas et al., 2012). It has been shown that enhancement of oceanic northward heat

transport as a response to prolonged atmospheric forcing associated with positive NAO played the key role (Lohmann et al., 2009; Robson et al., 2012a) and some CMIP5 models showed successful hindcasts of such a process (Robson et al., 2012b; Yeager et al., 2012). Possible impact of this Atlantic event on tropical Pacific climate is also being discussed (Chikamoto et al., 2012a; Chikamoto et al., 2012b). Meehl and Teng (2012) has shown that there is added skill by initialization in NCAR CCSM hindcasts of mid-1970s shift (Trenberth and Hurrell, 1994) and early 2000s hiatus (Easterling and Wehner, 2009) in the Pacific. Such case studies should provide physical bases for the development of decadal prediction systems (Meehl et al., 2012d).

11.2.3.5 Realizing Potential

Although idealized model experiments show considerable promise for predicting internal variability, realizing this potential is a challenging task. There are 3 main hurdles: (1) the limited availability of data to initialize and verify predictions, (2) limited progress in initialization techniques for decadal predictions and (3) dynamical model shortcomings.

It is expected that the availability of temperature and salinity data in the top two km of the ocean through the global deployment of Argo floats will give a step change in our ability to initialize and predict ocean heat and density anomalies (Zhang et al., 2007a). Another important recent advancement is the availability of altimetry data. Argo and altimeter data only became available in 2000 and 1992 respectively, so an accurate estimate of their impact on real forecasts has to wait (Dunstone and Smith, 2010).

Improved initialization of other aspects such as sea ice, snow cover, frozen soil and soil moisture, may also have potential to contribute to predictive skill beyond the seasonal timescale. This could be investigated, for example by using measurements of soil moisture from the planned Soil Moisture and Ocean Salinity (SMOS) satellite, or by initializing sea ice thickness with observations from the planned CryoSat-2 satellite.

Many of the current decadal prediction systems use relatively simple initialization schemes and do not adopt fully coupled initialization/ensemble generation schemes. Sophisticated assimilation schemes, such as 4DVAR (Sugiura et al., 2008) and ensemble Kalman filter (Zhang et al., 2007a), offer opportunities for fully coupled initialization including assimilation of variables such as sea ice, snow cover and soil moisture.

Bias correction is used to reduce the effects of model drift, but the non-linearity in the climate system (e.g., Power, 1995) might limit the effectiveness of bias correction and thereby reduce the forecast quality. Understanding and reducing both drift and systematic errors is important, as it is also for seasonal-to-interannual climate prediction and for climate change projections. While improving models is the highest priority, efforts to quantify the degree of interference between model bias and predictive signals should not be overlooked.

11.3 Near-Term Projections

11.3.1 Introduction

In this section the outlook for global and regional climate up to mid-century is assessed, based on climate model projections. In contrast to the predictions discussed in 11.2, these projections are not initialized using observations; instead, they are initialized from historical simulations of the evolution of climate from pre-industrial conditions up to the present. The historical simulations are forced by estimates of past anthropogenic and natural climate forcing agents, and the projections are obtained by forcing the models with scenarios for future climate forcing agents. Major use is made of the CMIP5 model experiments forced by the RCP scenarios discussed in Chapters 1 and 8.

Projections of climate change in this and subsequent chapters are expressed relative to the reference period: 1986–2005. Most emphasis is given to the period 2016–2035, but some information on changes projected before and after this period (up to mid-century) is also provided. Longer-term projections are assessed in Chapters 12 and 13.

1   Key assessment questions addressed in this section are: *what is the externally forced signal of near-term*
2   *climate change, how large is it compared to natural variability, and does the signal emerge from the natural*
3   *variability during the near term?* From the point of view of climate impacts, the absolute magnitude of
4   climate change may be less important than the magnitude relative to the local level of natural variability.
5   Because many systems are naturally adapted to the background level of variability, it is changes that move
6   outside of this range that are most likely to trigger impacts that are unprecedented in the recent past (e.g.,
7   Lobell and Burke, 2008; for crops). It follows that the future date at which the climate change signal reaches
8   sufficient magnitude to 'emerge' clearly from the noise of natural variability is an important issue for climate
9   risk assessments and adaptation planning.
10
11   An important conclusion of the AR4 (Chapter 10, Section 10.3.1) was that near-term climate projections are
12   not very sensitive to plausible alternative non-mitigation scenarios for greenhouse gas concentrations
13   (specifically the SRES scenarios – see discussion of comparison with RCP scenarios in Chapter 1), that is in
14   the near term different scenarios give rise to similar magnitudes and patterns of climate change. For this
15   reason, most of the projections presented in this chapter are based on one specific RCP scenario, RCP4.5.
16   RCP4.5 was chosen because of its intermediate greenhouse gas forcing. However, there is greater sensitivity
17   to other forcing agents, in particular anthropogenic aerosols. Consequently, a further question addressed in
18   this section is: *to what extent are near-term climate projections sensitive to alternative scenarios for*
19   *anthropogenic forcing?*
20
21   Note that a great deal of information on near-term projections of surface air temperatrue and precipitation is
22   also provided in Annex I. This annex presents a series of figures showing global and regional patterns of
23   climate change computed from CMIP5 models (Taylor et al., 2012). Time series for temperature and relative
24   precipitation changes are shown for global land and sea averages, the 26 sub-continental SREX regions
25   (IPCC, 2012) augmented with polar regions and the Caribbean, two Indian Ocean and three Pacific Ocean
26   regions. Maps are only shown for the RCP4.5 scenario, however the time series presented show how the
27   area-average response varies among the RCP2.6, RCP4.5, RCP6.0 and RCP8.5 scenarios. Spatial maps for
28   the other RCP scenarios are presented in the supplementary material.
29
30   *11.3.1.1 Uncertainty in Near-Term Climate Projections*
31
32   Climate projections are subject to three sources of uncertainty. The first arises from natural *internal*
33   *variability,* which is intrinsic to the climate system, and includes phenomena such as variability in the mid-
34   latitude storm tracks and the Interdecadal Pacific Oscillation (IPO). The existence of internal variability
35   places fundamental limits on the precision with which future climate variables can be projected. The second
36   is uncertainty concerning the past, present and future *forcing* of climate system by natural and anthropogenic
37   forcing agents such as greenhouse gases, aerosols and land use change. Forcing agents may be specified in
38   various ways, for example as *emissions* or as *concentrations* (see 12.2). The third is uncertainty related to the
39   *response* of the climate system to the specified forcing agents.
40
41   Quantifying the uncertainty that arises from each of the three sources is an important challenge. For
42   projections, no attempt is made to predict the evolution of the internal variability. Instead, the statistics of
43   this variability are sometimes included as a component of the uncertainty associated with a projection. The
44   magnitude of internal variability can be estimated from observations (Chapter 2) or from climate models
45   (Chapter 9). Challenges arise in estimating the variability on decadal and longer time scales, and for rare
46   events such as extremes, as observational records are often too short to provide robust estimates.
47
48   Uncertainty concerning the past forcing of the climate system arises from a lack of direct or proxy
49   observations, and from observational errors. This uncertainty can influence future projections of some
50   variables (particularly large-scale ocean variables) for years or even decades ahead (e.g., Gregory, 2010;
51   Meehl and Hu, 2006; Stenchikov et al., 2009). Uncertainty about future forcing arises from the inability to
52   predict future anthropogenic emissions and land use change, and natural forcings (e.g., volcanoes), and from
53   uncertainties concerning carbon cycle and other biogeochemical feedbacks (Chapters 6, 12 and Annex
54   II.4.1). The uncertainties in future anthropogenic forcing are typically investigated through the development
55   of specific socio-economic scenarios, such as the RCP scenarios (Chapters 1 and 8). Different scenarios give
56   rise to different climate projections, and the spread of such projections is commonly described as *scenario*

uncertainty. The sensitivity of climate projections to alternative scenarios for future anthropogenic emissions is discussed especially in 11.3.6.1

To project the climate response to specified forcing agents, climate models are required. The term *model uncertainty* describes uncertainty about the extent to which any particular climate model provides an accurate representation of the real climate system. This uncertainty arises from approximations required in the development of models. Such approximations affect the representation of all aspects of the climate including natural internal variability and the response to external forcings. The term *model uncertainty* is sometimes used in a narrower sense to describe the spread between projections generated using different models or model versions; however, such a measure is crude as it takes no account of factors such as model quality (Chapter 9) or model independence (e.g., Pennell and Reichler, 2011; Masson and Knutti, 2011; Power et al., 2012; Power and Delage, 2012). The term *model response uncertainty* is used here to describe the dimension of model uncertainty that is directly related to the response to external forcings. To obtain projections of extreme events such as tropical cyclones, or regional phenomena such as orographic rainfall, it is sometimes necessary to employ a dynamical or statistical downscaling procedure. Such downscaling introduces an additional dimension of model uncertainty (e.g., Alexandru et al., 2007).

The relative importance of internal variability, uncertainty in the specification of future forcing agents and uncertainty in the response to the imposed forcings depends on the variable of interest, the space and time scales involved (Meehl et al., 2007b; Section 10.5.4.3), and the lead-time of the projection. Figure 11.11 provides an illustration of these dependencies based on an analysis of CMIP5 projections (following Hawkins and Sutton, 2009; Hawkins and Sutton, 2010;Yip et al., 2011). In this example, the forcing-related uncertainty is estimated using the spread of projections for different RCP scenarios (i.e., scenario uncertainty), whilst the spread amongst different models for individual RCP scenarios is used as a measure of the model response uncertainty. Key points are: 1) the uncertainty in *near-term* projections is dominated by internal variability and model response uncertainty. This finding provides some of the rationale for considering near-term projections separately from long-term projections. Note, however, that the RCP scenarios do not sample the full range of uncertainty in future anthropogenic forcing, and that uncertainty in aerosol forcings in particular may be more important than is suggested by Figure 11.11 (see Section 11.3.6.1); 2) internal variability becomes increasingly important on smaller space and time scales; 3) for projections of precipitation, forcing uncertainty is less important and (on regional scales) internal variability is generally more important than for projections of surface air temperature.

A key quantity for any climate projection is the 'signal-to-noise' ratio (Christensen et al., 2007), where the 'signal' is a measure of the amplitude of the projected climate change, and the noise is a measure of the uncertainty in the projection. Higher signal-to-noise ratios indicate more robust projections of change and/or changes that are large relative to background levels of variability. Depending on the purpose, it may be useful to identify the noise with the total uncertainty, or with a specific component such as the internal variability). The evolution of the signal-to-noise ratio with lead-time depends on whether the signal grows more rapidly than the noise, or vice versa. Figure 11.11 (top right) shows that, when the noise is identified with the total uncertainty, the signal-to-noise ratio for surface air temperature is typically higher at lower latitudes and has a maximum at a lead time of a few decades (Cox and Stephenson, 2007; Hawkins and Sutton, 2009). The former feature is primarily a consequence of the greater amplitude of internal variability in mid-latitudes. The latter feature arises because over the first few decades, when scenario uncertainty is small, the signal grows most rapidly, but subsequently the contribution from scenario uncertainty grows more rapidly than does the signal, so the signal-to-noise ratio falls.

[INSERT FIGURE 11.11 HERE]
Figure 11.11: Sources of uncertainty in climate projections as a function of lead time based on an analysis of CMIP5 results. a) Projections of global mean decadal mean surface air temperature to 2100 together with a quantification of the uncertainty arising from internal variability (orange), model response uncertainty (blue), and forcing uncertainty (green). b) shows the signal-to-uncertainty ratio for various global and regional averages. The signal is defined as the simulated multi-model mean change in surface air temperature relative to the simulated mean surface air temperature in the period 1986–2005, and the uncertainty is defined as the total uncertainty. c), d), e), f) show the fraction of variance explained by each source of uncertainty for: global mean decadal and annual mean temperature (c), European (30˚–75˚N, 10˚W–40˚E) decadal mean boreal winter (December to February) temperature (d) and precipitation (f), and East Asian (5˚–45˚N, 67.5˚–130˚E) decadal mean boreal summer (June to August) precipitation (e). See text and Hawkins and Sutton (2009); Hawkins and Sutton (2011) for further details.

1
2   ***11.3.2   Near-Term Projected Changes in the Atmosphere and Land Surface***
3
4   *11.3.2.1   Surface Temperature*
5
6   *11.3.2.1.1 Global mean surface air temperature*
7   For a given greenhouse gas concentration scenario, different climate models project different rates of global
8   mean surface air temperature change due to different representations of a wide range of processes, including
9   radiative transfer, clouds, and physical climate feedbacks (see Chapters 9, 10 and 12). In addition, the
10   climate forcing by aerosols and ozone cannot be specified as a global mean abundance, and hence climate
11   models use different physical-chemical models to calculate the anthropogenic radiative forcing from
12   emissions of short-lived species. Figure 11.12 (a) shows projections for the CMIP5 models under RCP4.5.
13   The 5–95% range for the projected anomaly in global mean surface air temperature for the period 2016–35,
14   relative to the reference period 1986–2005, is 0.47–1.02 K. However, this range provides only a very crude
15   measure of the uncertainty in future global mean temperature change under this scenario. In particular, it
16   takes no account of model quality (Chapter 9), and there is no guarantee that the real world must lie within
17   the range spanned by the CMIP5 models.
18
19   Obtaining trustworthy estimates of the uncertainty in future global mean temperature change is an important
20   challenge. There are two main approaches. One involves applying weights to individual models according to
21   some measure of their quality (see Chapter 9). A second approach, known as ASK (Allen et al., 2000; Stott
22   and Kettleborough, 2002) is based on the use of results from detection and attribution studies (Chapter 10),
23   in which the fit between observations and model simulations of the past is used to scale projections of the
24   future. ASK may be viewed as a variant of the first approach, but it requires specific simulations to be
25   carried out with individual forcings (e.g., anthropogenic greenhouse gas forcing alone). Only some of the
26   centres participating in CMIP5 have carried out the necessary integrations. Biases in ASK derived
27   projections may arise from errors in the specified forcings and from errors in the model-simulated patterns of
28   response.
29
30   Figure 11.12 (b) shows the projected range of global mean surface air temperature change derived using the
31   ASK approach for RCP4.5 (Stott, 2012; Stott and G. Jones, 2012), and compares this with the range derived
32   from the CMIP5 models. In this case decadal means are shown. The 5–95% confidence interval for the
33   projected temperature anomaly for the period 2016 to 2035, based on the ASK method, is 0.39–0.87 K. Both
34   the lower and upper values are below the corresponding values obtained from the raw CMIP5 results,
35   although there is substantial overlap between the two ranges. The ASK results suggest that those CMIP5
36   models that warm most rapidly may be inconsistent with the observations. This possibility is also suggested
37   by comparing the models with the observed rate of warming since 1986, but see Chapter 10 for a full
38   discussion of this comparison. There are also indications that the 30-year CMIP5 decadal predictions
39   initialised in 2006 warm less rapidly than free running projections, but these are preliminary results for one
40   model (Meehl and Teng, 2012). Lastly, Figure 11.12 also shows a statistical prediction for global mean
41   surface air temperature, using the method of Lean and Rind (2009). This prediction is very similar to the
42   CMIP5 multi-model mean.
43
44   As already emphasised, the projections shown in Figure 11.12 are based on the RCP4.5 scenario. There are
45   additional uncertainties in projections of global mean surface air temperature associated with uncertainties in
46   future anthropogenic, particularly for near-term climate forcing agents such as methane and aerosols, and
47   natural forcing agents, and the climate response to these forcing agents. These additional uncertainties are
48   discussed in Section 11.3.6, and an overall assessment of the likely range for future global mean surface air
49   temperature is provided there.
50
51   The ASK method is only useful for quantifying the uncertainty in large-scale and well-observed variables
52   such as global mean surface air temperature. Consequently, for the remaining projections in this chapter the
53   spread amongst the CMIP5 models is used as a simple, but crude, measure of uncertainty. The extent of
54   agreement between the CMIP5 projections provides some rough guidance about the likelihood of a particular
55   outcome. But it must be kept firmly in mind that the real world could fall outside of the range spanned by
56   these particular models. See Section 11.3.6 for further discussion.
57

1   **[INSERT FIGURE 11.12 HERE]**
2   **Figure 11.12:** a) Projections of global mean, annual mean surface air temperature 1986–2050 (anomalies relative to
3   1986–2005) under RCP4.5 from CMIP5 models (grey and blue lines, one ensemble member per model), with four
4   observational estimates (HadCRUT3: Brohan et al., 2006; ERA-Interim: Simmons et al., 2010; GISTEMP: Hansen et
5   al., 2010; NOAA: Smith et al., 2008) for the period 1986–2011 (black lines); b) as a) but showing the 5–95% range
6   (grey shades, with the multi-model median in white) of decadal mean CMIP5 projections using one ensemble member
7   per model from RCP4.5 scenario, and decadal mean observational estimates (black lines). The maximum and minimum
8   values from CMIP5 are shown by the grey lines. An estimate of the projected 5–95% range for decadal mean global
9   mean surface air temperature for the period 2016–2040 derived using the ASK methodology applied to several CMIP5
10   GCMs (dashed black lines; from Stott, 2012). The red line shows a statistical prediction based on the method of Lean
11   and Rind (2009), updated for RCP 4.5.

12

13   *11.3.2.1.2 Regional and seasonal patterns of surface warming*
14   The geographical pattern of near-term surface warming simulated by the CMIP5 models (Figure 11.13) is
15   consistent with previous IPCC reports and observational trends in a number of key aspects. First,
16   temperatures over land increase more rapidly than over sea (e.g., Manabe et al., 1991; Sutton et al., 2007).
17   Processes that contribute to this land-sea warming contrast are the ocean heat uptake (Lambert and Chiang,
18   2007), the partitioning of the surface energy budget over arid regions (e.g., Vidale et al., 2007), the
19   nonlinearity of the moist-adiabatic lapse rate in a warming environment and its disproportionate influence
20   over the ocean (Joshi et al., 2011), as well as radiative and cloud feedbacks associated with a reduction of
21   relative humidity over land (Fasullo, 2010; Shimpo and Kanamitsu, 2009).

22

23   Second, the projected warming in wintertime shows a polar amplification that is particularly large over the
24   Arctic. This feature is found in virtually all coupled model projections, but the CMIP3 simulations generally
25   appeared to underestimate this effect in comparison to observations (Callaghan and Power, 2011; Screen and
26   Simmonds, 2010; Stroeve et al., 2007). Several studies have isolated mechanisms behind this amplification,
27   which include: reductions in snow cover and retreat of sea ice (e.g., Serreze et al., 2007; Comiso et al.,
28   2008); changes in atmospheric and oceanic circulations (Chylek et al., 2010; Chylek et al., 2009; Simmonds
29   and Keay, 2009); presence of anthropogenic soot in Arctic environment (Flanner et al., 2007b; Jacobson,
30   2010; Quinn et al., 2008; Ramana et al., 2010); and increases in cloud cover and water vapour. Most studies
31   argue that changes in sea ice are central to the polar amplification – see Section 11.3.4.1 for further
32   discussion. Further information about the regional changes in surface air temperature projected by the
33   CMIP5 models is presented in the Atlas (Annex I).

34

35   **[INSERT FIGURE 11.13 HERE]**
36   **Figure 11.13:** CMIP5 multi-model ensemble mean of projected changes in surface air temperature for the period 2016–
37   2035 relative to 1986–2005 under RCP4.5 scenario (left panels). The right panels show an estimate of the natural
38   internal variability in the quantity plotted in the left panels (see Annex I Atlas for details of method). Hatching in left-
39   hand panels indicates areas where projected changes are small compared to the natural variability (i.e., smaller than one
40   standard deviation of estimated natural variability of twenty-year means), and stippling indicates regions where the
41   multi-model mean projections deviate significantly from the control (by at least two standard deviations of internal
42   variability in twenty-year means) and where at least 90% of the models agree on the sign of change). See Box 12.1 in
43   Chapter 12 for further details and discussion.

44

45   As discussed in Sections 11.1 and 11.3.1, the signal of climate change is emerging against the background of
46   natural internal variability. The natural internal variability of surface air temperature is greater in some
47   regions than others (see Chapters 9 and 10, and Figure 11.13). For example, it is greater at mid latitudes than
48   in the tropics. The regional variation in the (spatially varying) magnitude of the signal relative to the
49   (spatially varying) magnitude of the internal variability has implications for the emergence of the climate
50   change signal. Information on the time at which a significant mean warming signal is expected to emerge in
51   different regions was presented in tabular form in the AR4 (Chapter 11, Table 11.1). Consistent with the
52   AR4, Mahlstein et al. (2011) recently showed using CMIP3 simulations that the earliest emergence of
53   significant mean warming occurs in the summer season in low latitude countries (~25°S–25°N), and that in
54   many low latitude regions significant local mean warming, relative to pre-industrial climate, has already
55   occurred.

56

57   Figure 11.14 quantifies the 'Time of Emergence' (ToE) of the mean warming signal relative to the recent
58   past (1986–2005), based on the CMIP5 RCP4.5 projections, using a spatial resolution of 5° latitude x 5°
59   longitude and using the standard deviation of interannual variations as the measure of internal variability.

1 (Note that choosing the standard deviation of decadal variations would result in earlier ToE, whilst
2 considering smaller spatial scales would result in later ToE. The choice of signal-to-noise threshold also
3 affects the ToE, with a higher threshold leading to later ToE.) Using a signal-to-noise threshold of 1, these
4 projections suggest that the median time at which a significant half-year-mean warming emerges is before
5 2020 throughout most of the tropics, whereas over mid latitudes the median time is typically a decade or so
6 later. Over North Africa and Asia emergence occurs sooner for the warm half-year (April to September) than
7 for the cool half-year, consistent with Mahlstein et al. (2011). ToE generally occurs sooner for larger space
8 and time scales, because the variance of natural internal variability decreases with averaging (Section
9 11.3.1.1 and AR4, Chapter 10, Section 10.5.4.3). This tendency can be seen in Figure 11.14 by comparing
10 the median value of the histograms for area averages with the area average of the median ToE inferred from
11 the maps (e.g., for Region 3). The histograms also illustrate the large range of values for ToE that is implied
12 by different CMIP5 models. This large range, which can be as much as 30 years, is a consequence of
13 differences in both the magnitude of the warming signal simulated by the models (i.e., uncertainty in the
14 climate response, see Section 11.3.1.1) and in the amplitude of simulated natural internal variability. Note
15 finally, that Figure 11.14 describes only the emergence of changes in the half-year *mean* temperature. In
16 many cases, changes in extreme events may be of greater importance for impacts, and significant changes in
17 some extremes may become apparent sooner than changes in mean climate. See 11.3.2.5 for further
18 discussion.
19
20 In summary, it is *very likely* that anthropogenic warming of surface air temperature over the next few
21 decades will proceed more rapidly over land areas than over oceans, and that the warming over the Arctic in
22 winter will be greater than the global mean warming. Relative to background levels of natural internal
23 variability it is *likely* that the anthropogenic warming of mean climate relative to the recent past will become
24 increasingly apparent soonest in the summer season in low latitude countries, because natural internal
25 variability has lower amplitude in these regions.
26
27 **[INSERT FIGURE 11.14 HERE]**
28 **Figure 11.14:** Time of emergence of significant local warming derived from CMIP5 models under the RCP 4.5
29 scenario. Warming is quantified as the half-year mean temperature anomaly relative to 1986–2005, and the noise as the
30 standard deviation of half-year mean temperature derived from a control simulation of the relevant model. Central
31 panels show the median time at which the signal-to-noise ratio exceeds a threshold value of 1 for (left) the October to
32 March half year and (right) the April to September half year, using a spatial resolution of 2.5° x 2.5°. Histograms show
33 the distribution of emergence times for area averages over the regions indicated obtained from the different CMIP5
34 models. Blue histograms are when using each model's estimate of noise, and green when a median estimate of noise is
35 used. Full details of the methodology may be found in Hawkins and Sutton (2011).
36
37 *11.3.2.2 Free Atmospheric Temperature*
38
39 Changes in zonal mean temperature for the near-term period (2016–2035 compared to the base period 1986–
40 2005) for the multi-model CMIP5 ensemble in Figure 11.15 shows a pattern similar to that in the IPCC AR4,
41 with warming in the troposphere and cooling in the stratosphere of a couple of degrees that is significant
42 even in the near-term period. There is relatively greater warming in the tropical upper troposphere and
43 northern high latitudes in both DJF and JJA as well as in the annual mean. Stratospheric cooling extends
44 nearly into the tropopause in the high southern latitudes in JJA, but that is not evident in DJF or the annual
45 mean.
46
47 **[INSERT FIGURE 11.15 HERE]**
48 **Figure 11.15:** Zonal mean temperature differences, 2016–2035 minus 1986–2005, for the CMIP5 multi-model
49 ensemble (°C), for a) DJF, b) JJA, and C) annual mean. Stippling as in Figure 11.13.
50
51 *11.3.2.3 The Water Cycle*
52
53 As discussed in the AR4 (Meehl et al., 2007b) and the IPCC Technical Paper on Climate Change and Water
54 (Bates et al., 2008) a general intensification of the global hydrological cycle, and of precipitation extremes,
55 are expected for a future warmer climate (e.g., Chou et al., 2009; Dery et al., 2009; Huntington, 2006; Kao
56 and Ganguly, 2011; Lu and Fu, 2010; Muller et al., 2011; O'gorman and Schneider, 2009; Seager et al.,
57 2010; Wild et al., 2008; Williams et al., 2007; Wu et al., 2010). In this section projected changes in the time-
58 mean hydrological cycle are discussed; changes in extremes, are discussed in Section 11.4.2.5.

There are very close links between the global water and energy cycles. A rapid increase in atmospheric water vapour content ($\sim 7\%$ K^{-1}) is an expected and observed response to warming, as a consequence of the Clausius–Clapeyron equation (Allen and Ingram, 2002; Trenberth et al., 2003). However, global mean precipitation and evaporation are projected to increase more slowly (1–3% K^{-1}), constrained by the atmospheric and surface energy budgets (Allan, 2009; Held and Soden, 2006; Lambert and Webb, 2008; O'gorman and Schneider, 2008; Pall et al., 2007; Stephens and Ellis, 2008; Vecchi and Soden, 2007; Wild and Leipert, 2010). There is evidence that shortwave forcings with little atmospheric radiative absorption including scattering anthropogenic aerosols, and natural solar variability, can be more effective than thermal greenhouse gas forcings in modifying the intensity of the global hydrological cycle (Andrews et al., 2010; Bala et al., 2010; Frieler et al., 2011; Lambert et al., 2008; O'gorman et al., 2012; Previdi, 2010; Wild and Leipert, 2010), although Stephens and Hu (2010) strongly emphasise the role of longwave radiation. Further discussion of the global mean hydrological cycle is provided in Chapter 12, Section 12.4.5.2.

AR4 projections of the spatial patterns of precipitation change in response to greenhouse gas forcing showed consistency between models on the largest scales, but large uncertainty on smaller scales. The consistent pattern was characterized by increases in wet regions (including the maxima in mean precipitation found in the tropics and at high latitudes), and decreases in dry regions (including large parts of the subtropics). Large uncertainties in the sign of projected change were seen especially in regions located on the borders between regions of increases and regions of decreases. More recent research has highlighted the fact that if models agree that the projected change is small relative to internal variability in some sense, then agreement on the sign of the change is not expected (Power et al., 2012; Tebaldi et al., 2011). This recognition led to the identification of subregions within the border regions, where models agree that projected changes are either zero or small (Power and Delage, 2012; Power et al., 2012). This, and other considerations, also led to the realisation that the consensus amongst models on precipation projections is more widespread than might have been inferred on the basis of the projections described in the AR4 (Power et al., 2012).

Since the AR4 there has also been considerable progress in understanding the factors that govern the spatial pattern of change in precipitation (P) and precipitation-evaporation (P-E), and inter-model differences in these patterns. The general pattern of wet-get-wetter (also referred to as 'rich-get-richer', e.g., Allan et al., 2010; Chou et al., 2009; Held and Soden, 2006) and dry-get-drier has been confirmed, and it has been demonstrated that this pattern implies an enhanced seasonal precipitation range between wet and dry seasons in the tropics, and enhanced inter-hemispheric precipitation gradients (Chou et al., 2007). The basic structure of this pattern is a direct consequence of the increases in atmospheric water vapour, and enhancement of horizontal moisture transports (Chou et al., 2009; Held and Soden, 2006; Seager et al., 2010). However, this basic thermodynamic response is modified by dynamical changes in atmospheric circulation, some of which are less well understood and less consistent between different models (Allan, 2012; Chou et al., 2009; Seager et al., 2010; Williams and Ringer, 2010). The dynamical changes can increase or decrease P and P-E anomalies (Chou et al., 2009; Seager et al., 2010; Vecchi and Soden, 2007).

Some aspects of tropical circulation changes in response to GHGs, in particular a projected weakening of the tropical divergent circulation (Held and Soden, 2006; Vecchi and Soden, 2007) and an expansion of the Hadley Circulation (see Section 11.4.2.4.3; Lu et al., 2007) have important consequences for regional changes in the water cycle. For example, Lu et al. (2007) argue that poleward expansion of the Hadley Circulation leads to poleward expansion of the subtropical dry zone (defined in terms of zonal mean P-E; see also Seager et al., 2010). However, these circulations can be strongly impacted by radiative forcing agents other than GHGs (see Section 11.4.2.4), and even the GHG-driven changes in tropical circulation can be masked on multi-decadal time-scales by substantial internal climate variability (see Section 11.4.2.4).

It has recently been proposed that analysis of the energy budget, previously applied only to the global mean, may provide further insights into the controls on regional changes in precipitation (Levermann et al., 2009; Muller and O'gorman, 2011; O'gorman et al., 2012). Muller and O'gorman (2011) argue in particular that changes in radiative and surface sensible heat fluxes provide a guide to the local P response over land. Projected and observed patterns of oceanic precipitation change in the tropics tend to follow patterns of SST change because of local changes in atmospheric stability, such that regions warming more than the tropics as a whole tend to exhibit an increase in local precipitation, while regions warming less tend to exhibit reduced precipitation (Johnson and Xie, 2010; Xie et al., 2010).

A further result of the AR4 was that, especially in the near term, and on regional or smaller scales, the magnitude of projected changes in mean precipitation was small compared to the magnitude of natural internal variability – the signal-to-noise ratio is much lower than for projected changes in surface air temperature. Recent work has confirmed this result, and provided more quantification (e.g., Deser et al., 2012; Hawkins and Sutton, 2011; Hoerling et al., 2011; Power et al., 2012; Rowell, 2011). Hawkins and Sutton (2011) presented further analysis of CMIP3 results and found that, on spatial scales O (1000 km), internal variability contributes 50–90% of the total uncertainty in all regions for projections of decadal and seasonal mean precipitation change for the next decade, and is the most important source of uncertainty for many regions for lead times up to three decades ahead. Thereafter, response uncertainty is generally dominant. Forcing uncertainty (except for that relating to aerosols, see Section 11.4.7) is generally negligible for near-term projections. The signal-to-noise ratio for seasonal mean precipitation is highest in the subtropics and at high-latitudes.

Tebaldi et al. (2011) and Power et al. (2012) demonstrated that some of the apparent differences between the CMIP3 models in their simulation of the sign of the precipitation response to greenhouse gas forcing occur in regions where the models tend to agree that the signal-to-noise ratio is low. These studies highlight that agreement on precipitation changes amongst models is more widespread than might have previously been interpreted from the AR4. Rowell (2011) investigated relationships between model formulation and response uncertainty. He found that the contribution of response uncertainty to the total uncertainty (response plus internal variability) in local precipitation change is highest in the deep tropics, particularly over South America, Africa, the east and central Pacific, and the Atlantic. He also showed that over tropical land and summer mid-latitude continents the representation of SST changes, atmospheric processes, land surface processes, and the terrestrial carbon cycle all contribute to the uncertainty in projected changes in rainfall.

In addition to the response to greenhouse gas forcing, the forcing that arises from natural and anthropogenic aerosols has the potential to exert significant impacts on regional patterns of precipitation change (as well as on global mean precipitation, see above). Precipitation responses may arise as a consequence of temperature changes caused by aerosol effects on radiation and atmospheric heating, and/or as a direct consequence of aerosol effects on clouds (Chapter 7). Future emissions of aerosols and aerosol precursors are subject to large uncertainty, and further large uncertainties arise in assessing the responses to these emissions. These issues are discussed in Sections 11.4.4 and 11.4.7 (see also Chapter 14).

Figures 11.16 and 11.17 present projections of near-term changes in precipitation from CMIP5. The basic pattern of wet regions tending to get wetter and dry regions tending to get dryer is apparent. However, the large response uncertainty is evident in the substantial spread in the magnitude of projected change simulated by different climate models (Figure 11.17). In addition, it is important to recognize – as discussed in previous sections – that models may agree and still be in error (e.g., Power et al., 2012). In particular, there is some evidence from comparing observations with simulations of the recent past that climate models might be underestimating the magnitude of changes in precipitation. This evidence is discussed in detail in Chapter 10 (Section 10.3.2), and could imply that projected future changes in precipitation are underestimated by current models; however, the magnitude of any underestimation has yet to be quantified, and is subject to considerable uncertainty.

Figures 11.16 and 11.17 also highlight the large amplitude of the natural internal variability of mean precipitation. Desertic areas from Sahara to Arabia exhibit high values of standard deviation associated to the small absolute changes in these regions. For zonal means (Figure 11.17), the projected changes are substantially larger than the estimated standard deviation of internal variability only at high latitudes. On regional scales, the median projected changes are almost everywhere less than the estimated standard deviation of natural internal variability. The only exceptions are at northern high latitudes.

Overall, it is *more likely than not* that over the next few decades there will be increases in mean precipitation in regions and seasons where the mean precipitation is relatively high, and decreases in regions and seasons where mean precipitation is relatively low. However, it is likely that these changes will only be significant, relative to natural internal variability, on the largest spatial scales (e.g., zonal means), and changes in specific smaller regions may show departures from the large-scale pattern. Anthropogenic aerosols and/or changes in atmospheric circulation could have important complicating or dominant effects in some regions.

1

2   **[INSERT FIGURE 11.16 HERE]**
3   **Figure 11.16:** CMIP5 multi-model ensemble mean of projected changes in precipitation for the period 2016–2035
4   relative to 1986–2005 under RCP4.5 in % for October to March (top left-hand panel) and April to September (bottom
5   left-hand panel). The right-hand panels show the corresponding estimates of the natural internal variability in the
6   quantity plotted in the left-hand panels (see Annex I Atlas for details of method). Hatching and stippling in left-hand
7   panels as in Figure11.13.

8

9   **[INSERT FIGURE 11.17 HERE]**
10   **Figure 11.17:** CMIP5 multi-model projections of changes in annual mean zonal mean precipitation (mm/day) for the
11   period 2016–2035 relative to 1986–2005 under RCP4.5. The box plots indicate projected changes (median, interquartile
12   range, and 5–95% range of model changes). Shading indicates 1 standard deviation of the estimated natural internal
13   variability (see Annex I Atlas for details of method).

14

15   *11.3.2.3.1 Changes in evaporation, run-off, soil moisture, and specific humidity*
16   As discussed in the AR4 (Meehl et al., 2007b; Trenberth et al., 2007) and the IPCC Technical Paper on
17   Climate Change and Water (Bates et al., 2008), global mean increases in evaporation are required to balance
18   increases in precipitation in response to greenhouse gas forcing. Based upon bulk formula used in models,
19   global evaporation is constrained by the Clausius Clapeyron equation to increase at around 7%/K. However,
20   a more 'muted' response, consistent with increases in global P, is achieved in CMIP3 models through small
21   yet systematic decreases in wind stress and near-surface temperature lapse rate and increases in relative
22   humidity (Richter and Xie, 2008). Changes in evapotranspiration over land are influenced not only by the
23   response to radiative forcing due to greenhouse gases, but also by vegetation responses to elevated CO_2
24   concentrations. Physiological effects of CO2 may involve both the stomatal response, which acts to restrict
25   evapotranspiration (e.g., Cao et al., 2009, 2010; Field et al., 1995; Hungate et al., 2002; Lammertsma et al.,
26   2011), and an increase in plant growth and leaf area, which acts to increase evapotranspiration (e.g., El Nadi,
27   1974). Simulation of the latter process requires the inclusion of a vegetation modelmodels that allow spatial
28   and temporal variability in the amount of active biomass, either by changes in the phenological cycle or
29   changes in the biome structure.

30

31   Soil moisture plays an important role in climate and the hydrological cycle, and directly influences
32   evapotranspiration. In response to greenhouse gas forcing, dry land areas tend to show a reduction of
33   evaporation and often precipitation, accompanied by drying of the soil and an increase of surface
34   temperature, as a result of the decrease in latent heat flux from the surface (e.g., Fischer et al., 2007;
35   Seneviratne et al., 2010). Jung et al. (2010) use a mixture of observations and models to illustrate a recent
36   global mean decline in land-surface evaporation due to soil moisture limiations. Accompanying effects with
37   precipitation are more subtle, as there are significant uncertainties and geographical variations regarding the
38   sign of the soil-moisture precipitation feedback (Hohenegger et al., 2009; Taylor et al., 2011). AR4
39   projections Meehl et al. (2007b) of annual mean soil moisture changes for the 21st century showed a
40   tendency for decreases in the subtropics, southern South America and the Mediterranean region, and
41   increases in limited areas of east Africa and central Asia. Changes seen in other regions were mostly not
42   consistent or statistically significant. Future GCM projections with prescribed soil moisture climatologies
43   corresponding with present day conditions show that projected changes in soil moisture affect daily mean
44   temperature (generally higher values due to reduced evaporative cooling), while high temperature values
45   (above 95 percentile) exhibit a stronger response than daily mean (Seneviratne et al., 2012).

46

47   Changes in runoff from are coupled to changes in precipitation, evapotranspiration and soil moisture. AR4
48   projections of 21st century runoff changes (Meehl et al., 2007c) showed consistency in sign among models
49   indicating reductionannual mean reductions in southern Europe and increases in Southeast Asia and at high
50   northern latitudes. Projected changes in global mean runoff associated with the physiological effecteffects of
51   doubled carbon dioxide concentrations show increases of 6–8% relative to pre-industrial levels, an increase
52   that is comparable to that simulated in response to radiative forcing changes (11 ± 6%) (Betts et al., 2007;
53   Cao et al., 2010). Gosling et al. (2011) assess the projected impacts of climate change on river runoff from
54   global and basin-scale hydrological models obtaining increased runoff with global warming in the Liard
55   (Canada), Rio Grande (Brazil) and Xiangxi (China) basins and decrease for the Okavango (southwest
56   Africa).

57

1   The global distribution of the 2016–2035 changes in annual mean evaporation, surface run-off, soil moisture
2   and surface-level specific humidity from the CMIP5 multi-model ensemble under RCP4.5 are shown in
3   Figure 11.18, together with estimates of the natural internal variability in these quantitiesChanges in
4   evaporation over land are mostly positive, except in north-western Africa, with largest values at northern
5   high latitudes in agreement with projected temperature increases (Figure 11.18). Over the oceans,
6   evaporation is also projected to increase in most regions. Projected changes are larger than the estimated
7   standard deviation of internal variability only at high latitudes and over the tropical oceans. Annual mean
8   soil moisture shows decreases in most subtropical regions and in central Europe, and increases in the
9   Maritime continent and other regions of northern mid-to-high latitudes, but in all regions the projected
10   changes are smaller than the estimated natural internal variability.

12   Changes in near-surface specific humidity are mostly positive with largest values at northern high latitudes
13   in agreement with the projected increases in temperature and the Clausius-Clapeyron relationship. These
14   changes are larger than the estimated standard deviation of internal variability almost everywhere: the only
15   exceptions are north-western Africa and the northern North Atlantic. In comparison, changes in near-surface
16   relative humidity (not shown) are much smaller, on the order of a few percent, with general decreases over
17   most land areas, and increases over the oceans. Most of these changes are not significant for the near term,
18   though this general pattern grows in amplitude with time and is projected to become more significant later in
19   the 21st century (Chapter 12). Spatial patterns of changes in JJA relative humidity (not shown) broadly
20   coincide with the spatial structure of annual mean soil moisture changes (Figure 11.18).

22   Over the next few decades increases in near-surface specific humidity are *very likely*, and models project
23   increases in evaporation in most regions. There is low confidence in projected changes in soil moisture and
24   surface run off. Natural internal variability will continue to have a major influence on all aspects of the water
25   cycle.

27   **[INSERT FIGURE 11.18 HERE]**
28   **Figure 11.18:** CMIP5 multi-model mean projected changes in annual mean evaporation (%), surface runoff (%), soil
29   moisture (%) and near-surface specific humidity (%) for the period 2016–2035 relative to 1986–2005 under RCP4.5
30   (left panels). All changes are listed as relative changes with respect to control conditions. Right-hand panels and
31   stippling/hatching are defined as in Figure11.13.

33   *11.3.2.4 Atmospheric Circulation*

35   *11.3.2.4.1 Northern Hemisphere extra-tropical circulation*
36   In the Northern Hemisphere extra-tropics, some AOGCMs indicate changes to atmospheric circulation from
37   anthropogenic forcing by the mid-21st century resembling the projected response at the end of the 21st
38   century. This includes a poleward shift of the jet streams and associated zonal mean storm tracks (Miller et
39   al., 2006a; Paeth and Pollinger, 2010; Pinto et al., 2007) and a strengthening of the Atlantic storm track
40   (Pinto et al., 2007), Figure 11.19. Changes in the tropical Pacific influence in response to anthropogenic
41   forcing can influence extratropical circulation in AOGCMs (Haarsma and Selten, 2012). However, there is
42   considerable response uncertainty across AOGCMs for northern hemisphere storm track position (Ulbrich et
43   al., 2008), stationary waves (Brandefelt and Kornich, 2008) and the jet streams (Ihara and Kushnir, 2009;
44   Miller et al., 2006a; Woollings and Blackburn, 2012). The response of the Northern Hemisphere jet streams
45   and stationary waves can be sensitive even to small changes in model formulation (Sigmond et al., 2007),
46   and to features that are known to be poorly simulated in many climate models, such as oceanic and
47   stratospheric dynamics and high- and low-latitude physics (Rind, 2008; Woollings, 2010), and many
48   AOGCMs fail to capture observed multi-decadal changes in the NAO (Scaife et al., 2009). Several
49   stratosphere-resolving models exhibit an equatorward shift of the storm track and jet stream in response to
50   greenhouse forcing (Huebener et al., 2007; Morgenstern et al., 2010; Scaife et al., 2012).

52   Further, the response of NH extra-tropical circulation to even strong greenhouse forcing can be weak
53   compared to recent multi-decadal changes (Miller et al., 2006b; Woollings and Blackburn, 2012), with some
54   AOGCMs simulating multi-decadal NAO variability as large as recently observed changes with no external
55   forcing (Selten et al., 2004; Semenov et al., 2008). This suggests that natural variability could dominate the
56   anthropogenically forced response in the near term. Some studies have predicted a shift to the negative phase
57   of the Atlantic Multidecadal Oscillation (AMO) over the coming few decades, with potential impacts on

1   atmospheric circulation around the Atlantic sector (Folland et al., 2009; Knight et al., 2005; Sutton and
2   Hodson, 2005). It has also been suggested that there may be significant changes in solar forcing over the
3   next few decades, which could have an important influence on NAO-related atmospheric circulation
4   (Lockwood et al., 2011), although these predictions are highly uncertain (see Section 11.2.2.2).
5
6   Regionally changes of the mean atmospheric circulation may be imposed by systematic patterns of surface
7   warming. Haarsma et al. (2009) illustrate a systematic increase in NW European easterlies during summer in
8   response to strong surface drying and warming in the Mediterranean. A systematic survey of this kind of
9   responses is lacking.
10
11 The large response uncertainty and the potentially large influence of internal variability mean there is limited
12 confidence in near-term projections of Northern Hemisphere circulation change.
13
14 *11.3.2.4.2 Southern Hemisphere extra-tropical circulation*
15 A key issue in projections of near-term Southern Hemisphere (SH) extra-tropical circulation change is the
16 extent to which changes driven by stratospheric ozone recovery will counteract changes driven by increasing
17 greenhouse gases. Over the late 20th century and early 21st century, the impacts of stratospheric ozone
18 depletion and increasing greenhouse gases have reinforced each other to contribute to a poleward expansion
19 of SH tropospheric circulation (a positive *Southern Annular Mode, or SAM*) (Arblaster and Meehl, 2006;
20 Fogt et al., 2009; Gillett and Thompson, 2003; Roscoe and Haigh, 2007; Shindell and Schmidt, 2004).
21 Recovery of the Antarctic ozone hole will impact the SH circulation in the austral summer, but there is
22 expected to be competition between the ozone recovery producing an equatorward shift of the circumpolar
23 trough around Antarctica, and ongoing increases of GHGs maintaining the southward-shifted circumpolar
24 trough (Arblaster et al., 2011; McLandress et al., 2011). Even though a full recovery of the ozone hole is not
25 expected until the 2060s–2070s (Table 5.4, WMO, Rep. No. 52, 2010; see Chapter 12), it is likely that over
26 the near term there will be a reduced rate in the summertime poleward shift of the circumpolar trough
27 compared to its movement over the past 30 years as indicated by AOGCMs and stratosphere-resolving
28 models that suggest some near-term poleward shifts in SH extra-tropical storm tracks and winds (Figure
29 11.19).
30
31 *11.3.2.4.3 Tropical circulation*
32 As with near-term changes in SH extra-tropical circulation, a key for near-term projections of the structure of
33 the Hadley Circulation (Figure 11.20) is the extent to which future stratospheric ozone recovery will
34 counteract the impact of greenhouse gases. The poleward expansion of the Hadley Circulation, particularly
35 of the SH branch during austral summer, during the later decades of the 20th century has been largely
36 attributed to the combined impact of stratospheric ozone depletion (Son et al., 2009a; Son et al., 2009b; Son
37 et al., 2008; Thompson and Solomon, 2002) and the concurrent increase in GHGs (Arblaster and Meehl,
38 2006; Arblaster et al., 2011) as discussed in the previous section. The poleward expansion of the Hadley
39 Circulation driven by the response of the atmosphere to increasing GHGs (Butler et al., 2012; Chen and
40 Held, 2007; Kang and Polvani, 2011; Korty and Schneider, 2008; Lorenz and DeWeaver, 2007; Lu et al.,
41 2007) would be counteracted in both hemispheres by reduced stratospheric ozone depletion but depends on
42 the rate of ozone recovery (UNEP and WMO, 2011). Increases in the incoming solar radiation can lead to a
43 widening of the Hadley Cell (Haigh, 1996; Haigh et al., 2005), so future solar variations could also lead to
44 variations in the width of the Hadley Cell. The poleward extent of the Hadley Circulation and associated dry
45 zones can exhibit substantial internal variability (e.g.*,* Lu et al., 2007), which can be as large as its near-term
46 projected changes (Figure 11.20). There is also considerable uncertainty in the amplitude of the poleward
47 shift of the Hadley Circulation in response to GHGs across multiple AOGCMs (Lu et al., 2007; Figure
48 11.20). Because of the counteracting impacts of future changes in stratospheric ozone and greenhouse gas
49 concentrations, it is unlikely that it will continue to expand poleward in either the northern and southern
50 hemisphere as rapidly as it did in recent decades. Because of the strong influences of internal variability, it is
51 very likely that there will be variations in the position and strength of the Hadley circulation over the coming
52 decades.
53
54 Global climate models and theoretical considerations suggest that a warming of the tropics should lead to a
55 reduction of the strength of atmospheric circulation in general, primarily by weakening the tropical divergent
56 circulation – largely in the zonally-asymmetric or Walker circulation (Gastineau et al., 2009; Held and
57 Soden, 2006; Knutson and Manabe, 1995; Vecchi and Soden, 2007). Aerosol forcing can modify both

1   Hadley and Walker circulations, which – depending on the details of the aerosol forcing – may lead to
2   temporary reversals or enhancements in any GHG-driven weakening of the Walker circulation (Bollasina et
3   al., 2011; DiNezio et al., 2012; Merrifield, 2011; Sohn and Park, 2010). Meanwhile, the strength and
4   structure of the Walker circulation are impacted by internal climate variations, such as the El Niño/Southern
5   Oscillation (e.g., Battisti and Sarachik, 1995), the PDO (e.g., Zhang et al., 1997) and the IPO (Meehl and Hu,
6   2006; Meehl and Arblaster, 2011; Meehl and Arblaster, 2012; Meehl et al., 2012a; Power et al., 1999; Power
7   and Kociuba, 2011b; Power et al., 2006). Even on timescales of thirty to one hundred years, substantial
8   variations in the strength of the Pacific Walker circulation in the absence of changes in radiative forcing are
9   possible (Power et al., 2006; Vecchi et al., 2006). Estimated near-term weakening of the Walker circulation
10 from CMIP3 models under the A1B scenario (Power and Kociuba, 2011a; Vecchi and Soden, 2007) are very
11 likely to be smaller than the impact of internal climate variations over fifty-year timescales (Vecchi et al.,
12 2006). There is also considerable response uncertainty in the amplitude of the weakening of Walker
13 Circulation in response to GHG increase across multiple AOGCMs (DiNezio et al., 2009a; Power and
14 Kociuba, 2011a, 2011b; Vecchi and Soden, 2007). It is *very likely* that there will be decades in which the
15 Walker circulation strengthens and weakens due to internal variability through the mid-century as the
16 externally forced change is small compared to internally-generated decadal variability (Figure 11.21).
17
18 In response to projected increases in GHGs the (see Section 14.3.10) there is an expectation for a reduction
19 in the strength of the monsoonal circulations, yet an increase in monsoon rainfall. There are indications that
20 changes in aerosol loading can influence monsoonal circulation and precipitation (Bollasina et al., 2011;
21 Gautam et al., 2009; Lau and Kim, 2006; Lau et al., 2006; Ramanathan et al., 2005). However, some studies
22 suggest that increasing aerosols should act to increase monsoon rainfall and circulation (e.g., Lau et al.,
23 2006; Lau and Kim, 2006), others indicate that the monsoon should be weakened in response to increasing
24 aerosols (e.g., Ramanathan et al., 2005; Meehl et al., 2008; Bollasina et al., 2011), with some studies
25 suggesting an intraseasonal redistribution of monsoon rainfall and circulation in response to aerosols
26 (Gautam et al., 2009). Further, internal climate variations associated such as ENSO, TBO, IOD and AMO
27 (see Section 14.2.5) can influence monsoon rainfall and circulation (Ashok et al., 2004; Gadgil et al., 2004;
28 Li et al., 2008; Meehl and Arblaster, 2011; Meehl and Arblaster, 2012; Nolte et al., 2008; Yuan et al., 2008;
29 Zhang and Delworth, 2006). Therefore, over the next few decades it is likely that the expected weakeing of
30 monsoon circulation in response to GHGs will be modulated by internal climate variations. Lack of
31 agreement regarding the expected response of the monsoon to aerosol forcing presents a key source of
32 uncertainty in monsoon projections over the first half of the 21st century.
33
34 **[INSERT FIGURE 11.19 HERE]**
35 **Figure 11.19:** [PLACEHOLDER FOR FINAL DRAFT: to make final] Projected changes in annual-averaged zonal
36 (west-to-east) wind at 850hPa based on the average of 23 AOGCMs from the CMIP3 (Meehl et al., 2007b) multi-model
37 ensemble, under 21st century Emissions Scenario SRESA1B. Gray shading indicates where the multi-model average
38 AOGCM anomalies are smaller than two standard deviations of the multi-AOGCM estimate of internal variability from
39 the control climate integrations. Values referenced to the 1986–2005 climatology.
40
41 **[INSERT FIGURE 11.20 HERE]**
42 **Figure 11.20:** Projected changes in the annual-averaged poleward edge of the Hadley Circulation (horizontal axis) and
43 sub-tropical dry zones (vertical axis) based on 15 AOGCMs from the CMIP5 (Taylor et al., 2012) multi-model
44 ensemble, under 21st century Representative Concentratio Pathway 4.5. Orange symbols show the change in the
45 northern edge of the Hadley Circulation/dry zones, while blue symbols show the change in the southern edge of the
46 Hadley Circulation/dry zones. Open circles indicate the multi-model average, while horizontal and vertical colored lines
47 indicate the ±1-standard deviation range for internal climate variability estimated from each model. Values referenced
48 to the 1986–2005 climatology. Figure based on the methodology of Lu et al. (2007).
49
50 **[INSERT FIGURE 11.21 HERE]**
51 **Figure 11.21:** Projected changes in the strength of the Pacific Walker Circulation, as estimated using the east-west sea
52 level pressure gradient across the equatorial Pacific (Vecchi and Soden, 2007; Vecchi and Soden, 2007), based on 24
53 AOGCMs from the CMIP3 (Meehl et al., 2007b) multi-model ensemble, under 21st century Emissions Scenario
54 SRESA1B. Thin gray lines indicate the five-year running average for each model, red line indicates the multi-model
55 five-year running average. Blue horizontal lines indicate the 2016–2035 values for each model, with the orange line
56 indicating the multi-model averaged projection for 2016–2035. Values referenced to the 1986–2005 climatology.
57
58 *11.3.2.5 Atmospheric Extremes*
59

Extreme events in a changing climate and their impacts upon the natural physical environment are the subject of Chapter 3 (Seneviratne et al., 2012) of the IPCC Special Report on Managing the Risks of Extreme Events and Disasters to Advance Climate Change Adaptation (SREX). This previous comprehensive IPCC chapter provides an assessment of more than 1000 studies and forms the basis of much of the AR5 assessment on extremes.

The overwhelming majority of past studies on extremes in a changing climate have addressed long-term projections (i.e., 50 to 100 years into the future), while the focus of the current section is on near-term projections. When addressing near-term changes in extremes, natural variability plays an important role in determining the uncertainties (see Section 11.2). In addition, the uncertainty strongly depends upon the type of extremes considered, and is larger for small-scale extremes (such as heavy precipitation events) than for large-scale extremes (such as temperature extremes).

11.3.2.5.1 Temperature extremes
In the AR4 (Meehl et al., 2007b), cold episodes were projected to decrease significantly in a future warmer climate and it was considered *very likely* that heat waves would be more intense, more frequent and last longer towards the end of the 21st century. These conclusions have generally been confirmed in subsequent studies addressing both global scales (e.g., Orlowsky and Seneviratne, 2011; Sillmann et al., 2011) and regional scales (e.g., Alexander and Arblaster, 2009; Fischer and Schar, 2009, 2010; Gutowski et al., 2008; Marengo et al., 2009; Meehl et al., 2009a). In the SREX assessment it is concluded that increases in the number of warm days and nights and decreases in the number of cold days and nights are *virtually certain* on the global scale.

None of the aforementioned studies specifically addressed the near term, but detection and attribution studies (see also Chapter 10) show that temperature extremes already increase in many regions consistent with climate change projections, and analyses of CMIP5 global projections show that this trend will continue and become more notable. The CMIP5 model ensemble exhibits a general significant decrease in the frequency of cold nights, an increase in the frequency of warm days and nights, and an increase in the duration of warm spells (Sillmann J. et al., 2012) These changes are particularly evident in global mean projections (see Figure 11.22). The figure shows that for the next few decades – as discussed in the introduction to the current chapter – these changes are remarkably insensitive to the emission scenario considered.

[INSERT FIGURE 11.22 HERE]
Figure 11.22: Global mean projections for the occurrence of (a) warm days, (b) cold days, and (c) wet days from CMIP5 for the RCP2.6, RCP4.5 and RCP8.5 scenarios relative to 1986–2005. Panel (a) shows percentage of warm days (tx90p: Tmax exceeds the 90th percentile), panel (b) shows percentage of cold days (tx10p: Tmax below the 10th percentile), and panel (c) shows relative change of simple precipitation intensity (sdii: average daily precipitation amount for wet days). Results for CMIP3 are also indicated. From Sillmann J. et al. (2012).

Near-term results from the ENSEMBLES projections (van der Linden and Mitchell, 2009) for Europe are shown in Figure 11.23, displaying near-term changes in mean and extreme temperature (left-hand panels) and precipitation (right-hand panels) relative to the control period 1986–2005. In terms of JJA temperatures (Figure 11.1b23a-b), projections show a warming of 0.6–1.5°C, with highest changes over the land portion of the Mediterranean. The north-south gradient in the projections is consistent with the AR4. Figure 11.23 shows that daytime extreme summer temperatures in southern and central Europe (Figure 11.23b) are projected to warm substantially faster than mean temperatures (compare Figure 11.23a and 11.23b). This difference between changes in mean and extremes can be explained by increases in interannual and/or synoptic variability, or increases in diurnal temperature range (Fischer and Schar, 2010; Gregory and Mitchell, 1995; Quesada et al., 2012; Schar et al., 2004; Seneviratne et al., 2012). There is some evidence, however, that this effect is overestimated in some models (Fischer et al., 2012; Stegehuis et al., 2012), leading to a potential overestimation of the projected Mediterranean summer mean warming (Boberg et al., 2010). With regards to near-term projections of record heat compared to record cold, Meehl et al. (2009c) show, for one model, that over the U.S. the ratio of daily record high temperatures to daily record low temperatures could increase from an early 2000s value of roughly 2 to 1, to a mid-century value of about 20 to 1.

In terms of DJF temperatures (Figure 11.23c-d), projections show a warming of 0.3°C–1.8°C, with high intensity in the N-NE part of Europe. This pattern tends to persist to the end of century (van der Linden and

1   Mitchell, 2009). In contrast to JJA temperatures, daytime high-percentile winter temperatures are projected
2   to warm slower than mean temperatures (compare panels (c) and (d)), which is indicative of reductions in
3   variability. Such variability reductions might be linked to changes in storm track activity, reductions in
4   diurnal temperature range and changes in snow cover (e.g., Colle et al.; 2012; Dutra et al., 2011).
5
6   **[INSERT FIGURE 11.23 HERE]**
7   **Figure 11.23:** European-scale projections from the ENSEMBLES regional climate modelling project for 2016–2035
8   relative to 1986–2005, with top and bottom panels applicable to JJA and DJF, respectively. For temperature, projected
9   changes (°C) are displayed in terms of ensemble mean changes of (a, c) mean seasonal surface temperature, and (b, d)
10 the 90th percentile of daily maximum temperatures. For precipitation, projected changes (%) are displayed in terms of
11 ensemble mean changes of (e, g) mean seasonal precipitation and (f, h) the 95th percentile of daily precipitation. The
12 stippling in (e-h) highlights regions where 80% of the models agree in the sign of the change (for temperature all
13 models agree on the sign of the change). The analysis includes the following 10 RCM-GCM simulation chains for the
14 SRES A1B scenario (naming includes RCM group and GCM simulation): HadRM3Q0-HadCM3Q0, ETHZ-
15 HadCM3Q0, HadRM3Q3-HadCM3Q3, SMHI-HadCM3Q3, HadRM3Q16-HadCM3Q16, SMHI-BCM, DMI-
16 ARPEGE, KNMI-ECHAM5, MPI-ECHAM5, DMI-ECHAM5 (Rajczak et al., 2012; courtesy of Jan Rajczak).
17
18 *11.3.2.5.2   Heavy precipitation events*
19 The AR4 concluded that heavy precipitation events were *likely* to increase over most areas of the globe in
20 the 21st century (IPCC, 2007). The SREX concluded that increases in heavy precipitation events were likely
21 strongest in high latitudes and stronger in winter than summer, but were subject to considerable uncertainties
22 related to climate model uncertainties, statistical downscaling and natural variability. Increases were also
23 found in some regions where the total precipitation was projected to decrease (assessed with medium
24 confidence by SREX). For precipitation extremes, results depend more strongly upon the region under
25 consideration than with temperature extremes.
26
27 Since AR4, a larger number of additional studies have been published using global and regional climate
28 models (Fowler et al., 2007; Gutowski et al., 2007; Hanel and Buishand, 2011; Heinrich and Gobiet, 2011;
29 Im et al., 2008; Meehl et al., 2012c; O'gorman and Schneider, 2009). For the near term, CMIP5 global
30 projections confirm a clear tendency for increases in heavy precipitation events in the global mean (Figure
31 11.22c), but there are significant variations across regions (Sillmann et al., 2011; Sillmann J. et al., 2012).
32 Past observations have also shown that interannual and decadal variations in mean and heavy precipitation
33 are large, and are in addition strongly affected by natural variations (e.g., El Niño), volcanic forcing, and
34 anthropogenic aerosol loads (see Section 2.3.1.2). In general models have difficulties to represent these
35 variations, particularly in the tropics (see Section 9.4.4.2).
36
37 Simulations with regional climate models demonstrate that the response in terms of heavy precipitation
38 events to anthropogenic climate change may become evident in some but not all regions in the near term. For
39 instance, ENSEMBLES projections for Europe (see Figure 11.23e-h) confirm the previous IPCC results that
40 changes in mean precipitation as well as heavy precipitation events are characterized by a pronounced north-
41 south gradient in the extratropics, especially in the winter season, with precipitation increases (decreases) in
42 the higher latitudes (subtropics). While this pattern starts to emerge in the near term, these projected changes
43 are statistically significant only in a fraction of the domain. The results appear to be affected by changes in
44 water vapour content as induced by large-scale warming, and the large-scale circulation changes. Figure
45 11.23e-h also shows that projections for changes in extremes and means are qualitatively very similar in the
46 near term.
47
48 The increase in precipitation with increasing atmospheric water vapour content is not uniform over the entire
49 precipitation intensity range, but is more pronounced for short-term events associated with thunderstorms
50 (Lenderink and Van Meijgaard, 2008). Lenderink et al. (2011) show that extreme precipitation exhibits a
51 stronger increase per degree surface dewpoint temperature than expected based on the Clausius-Clapeyron
52 equation. In a wide range of surface dewpoint temperature this scaling is uniform over climate regimes, but
53 this uniformity breaks down at high temperature, possibly due to limitations in moisture supply or
54 convective activity.
55
56 Other aspects of the precipitation climate may also be important when considering the associated impacts.
57 For instance, changes in snow line have a significant impact on runoff. Increases in snow line imply

increases in rain at the expense of snow, with potentially significant implication on runoff formation (e.g., Bosshard et al., 2012; Lambert and Hansen, 2011).

11.3.2.5.3 Tropical cyclones

Two recent reports, the SREX (IPCC, 2012; particularly Seneviratne et al., 2012) assessment and a WMO Expert Team report on tropical cyclones and climate change (Knutson et al., 2010) indicate the response of global tropical cyclone frequency to projected radiative forcing changes is likely to be either no change or a decrease of up to a third by the end of the 21st century. The projected response of tropical cyclones at the end of the 21st century is summarized in Chapter 14, Box 14.3.

There are only a limited number of studies that have explored near-term projections of tropical cyclone activity. An analysis of five CMIP3 models found that the observed increase of TC activity over subtropical East Asia, and reduced TC activity over the South China Sea, was projected to continue through the 2040s (Wang et al., 2011). An analysis with a family of CMIP5 models projects a 10–15% decrease in tropical cyclone frequency in the Western North Pacific averaged over 2016–2035 relative to 1979–2007, with the greatest reduction occurring in the South China Sea (Mori et al., 2012). A dynamical downscaling study of CMIP3 models focused on the South Pacific (Leslie et al., 2007) projects negligible changes in the overall frequency of tropical storms, but significant (~15%) increase in the number of Category 4–5 tropical cyclones, by 2050. A statistical downscale of North Atlantic tropical storm frequency with the CMIP3 models over the first half of the 21st century found a non-significant decrease (~5% over fifty years) averaged across a 17-model ensemble, with the model ensemble range spanning −50 to +30% over fifity years (Villarini et al., 2011). Meanwhile, the application of the same statistical framework to the CMIP5 models projects an increase in North Atlantic tropical storm frequency over the first half of the 21st century in the multi-model average driven by changes in aerosol forcing (ranging from 4 to 10% over fifty years across three RCP scenarios), with the 10 to 90% range of model projections ranging between −5 to +40% over fifty years (Villarini and Vecchi, 2012a). A related statistical downscaling technique projects an increase in Atlantic tropical cyclone intensity over the first half of the 21st century, duebothto greenhouse gas increases and aerosol changes (Villarini and Vecchi, 2012b). Dynamical downscaling of CMIP5 conditions 2026–2035 relative 1980–2005 using the Zhao et al. (2009) global atmospheric model found a tendency for frequency increases (range between +20 and +60%) in North Atlantic hurricane frequency and a decrease (range of −5 to −40%) in East Pacific hurricane frequency (Maloney et al., 2012); these projected changes in Atlantic and East Pacific hurricane frequency followed the surface temperautre changes projected for each basin relative to tropical-mean SST changes, as has been found in dynamical downscaling of projections for the end of the 21st century (Knutson et al., 2012b; Villarini et al., 2011; Zhou et al., 2008). Studies using the CMIP3 and CMIP5 models found that projected changes in Atlantic tropical storm frequency over the first half of the 21st century were smaller than the overall uncertainty estimated from the CGCMs, with internal climate variability being a leading source of uncertainty through the mid-21st century (Villarini and Vecchi, 2012a; Villarini et al., 2011). Therefore, based on the limited literature available, the conflicting mid-term projections in basins with more than one study, the large influence of internal variability, the lack of detected/attributed changes in TC activity (Chapter 10), and the conflicting projections for basin-wide TC activity at the end of the 21st century (Chapter 14), there is currently limited confidence in basin-scale projections of trends in tropical cyclone frequency to the mid-21st century. There is medium agreement and limited evidence for projections of increased TC intensity in the coming decades.

The CMIP3 and CMIP5 AOGCMs indicate continued year-to-year and decade-to-decade variations in North Atlantic tropical storm frequency through the mid-21st century. Modes of climate variability that in the past have led to variations in the intensity, frequency and structure of tropical cyclones across the globe – such as the El Niño Southern Oscillation are very likely continue to exist through the mid-21st century (Callaghan and Power, 2011; Collins et al., 2010; Vecchi and Wittenberg, 2010). Therefore, it is very likely that over the next few decades tropical cyclone frequency, intensity and spatial distribution globally, and in individual basins, will vary from year-to-year and decade-to-decade, as they have in the past (Chapters 2, 10, and 14).

11.3.3   Near-Term Projected Changes in the Ocean

11.3.3.1   Temperature

1   Globally-averaged surface and near-surface ocean temperatures are projected by AOGCMs to warm over the
2   early 21st century, in response to both present day atmospheric concentrations of greenhouse gases
3   ('committed warming'; e.g., Meehl et al., 2006), and projected changes (Figure 11.24). Globally-averaged
4   SST shows substantial year-to-year and decade-to-decade variability (e.g., Knutson et al., 2006; Meehl et al.,
5   2011), whereas the variability of depth-averaged ocean temperatures is much less (e.g., Meehl et al., 2011;
6   Palmer et al., 2011). The rate at which globally-averaged temperatures rise in response to a given scenario
7   for radiative forcing shows a considerable spread between models (an example of response uncertainty, see
8   Section 11.2), due to differences in climate sensitivity and ocean heat uptake (e.g., Gregory and Forster,
9   2008). In the CMIP3 models under SRESA1B globally averaged SSTs increase by 0.3°C–0.6°C over the
10   near term relative to 1986–2005 (Figure 11.24).

12   A key uncertainty in the future evolution of globally averaged oceanic temperature are possible future large
13   volcanic eruptions, which could impact the radiative balance of the planet for 2–3 years after their eruption
14   and act to reduce oceanic temperature for decades into the future (Delworth et al., 2005; Gregory, 2010;
15   Stenchikov et al., 2009). An estimate using the GFDL-CM2.1 coupled AOGCM (Stenchikov et al., 2009)
16   suggests that a single Tambora (1851)-like volcano could erase the projected global ocean depth-averaged
17   temperature increase for many years to a decade. A Pinatubo (1991)-like volcano could erase the projected
18   increase for 2–10 years. See Section 11.3.6 for further discussion.

20   In the absence of multiple major volcanic eruptions or other 'surprises' (see 11.3.6.2), it is *extremely likely*
21   that globally-averaged surface and upper ocean (top 700m) temperatures averaged 2016–2035 will be
22   warmer than those averaged over 1986–2005.

24   Projected ocean temperature changes tend to be largest near the surface, and decrease with depth (Figures
25   11.24, 11.25 and 11.26). This results in an increase in the near-surface stratification of temperature,
26   particularly in the tropical Pacific and Indian Oceans. In the Atlantic and Southern Oceans models suggest
27   that warming penetrates more rapidly to greater depths (Figure 11.27). Projections for the Arctic Ocean
28   suggest a subsurface maximum in warming, at a depth of a few hundred meters.

30   There are regional variations in the projected amplitude of ocean temperature change (Figure 11.26), which
31   are influenced by ocean circulation as well as surface warming (DiNezio et al., 2009b; Timmermann et al.,
32   2007; Vecchi and Soden, 2007; Xie et al., 2010; Yin et al., 2009; Yin et al., 2010). Inter-decadal variability
33   of upper ocean temperatures is larger in mid-latitudes, particularly in the Northern Hemisphere, than in the
34   tropics (Figure 11.27). A consequence of this contrast is that it will take longer in the mid-latitudes than in
35   the tropics for the anthropogenic warming signal to emerge from the noise of internal variability (Figure
36   11.26, Wang et al., 2010).

38   The Southern Ocean shows significant local spread in its temperature projections, particularly in the Weddell
39   Gyre and north of the Ross-Sea gyre. These differences between models tend to be displaced from regions of
40   high internal variability and are likely to be caused by the same model biases of the surface mixed layer
41   depths and water mass formation found in century scale simulations (Sloyan and Kamenkovich, 2007; Figure
42   11.26 lower panels). The relative roles of stratospheric ozone and anthropogenic forcing on the Southern
43   Ocean temperature and salinity remains for the recent past and near term are important issues (Sections 9.3.2
44   and 10.3), but the role of these forcings on the near-term projections on ocean circulation have not been
45   assessed in the literature.

47   Projected changes to thermal structure of the tropical Indo-Pacific are strongly dependent on future
48   behaviour of the Walker circulation (DiNezio et al., 2009a; Timmermann et al., 2010; Vecchi and Soden,
49   2007), in addition to changes in heat transport and changes in surface heat fluxes. Since the projected
50   weakening of the Walker circulation through the mid-21st century is smaller than the expected variability on
51   timescales of decades to years (Section 11.3.2.4.3), it is *likely* that internal climate variability will be a
52   dominant contributor to changes in the depth and tilt of the equatorial thermocline, and the strength of the
53   east-west gradient of SST across the Pacific through the mid-21st century, thus it is *likely* there will be multi-
54   year periods with increases or decreases, but no clear longer term trend.

56   **[INSERT FIGURE 11.24 HERE]**

1   **Figure 11.24:** Projected changes in annual-averaged, globally-averaged, depth-averaged ocean temperature based on
2   twelve AOGCMs from the CMIP3 (Meehl et al., 2007b) multi-model ensemble, under 21st century Emissions Scenario
3   SRESA1B. Top panel shows changes of sea surface temperature, middle panel ocean temperature changes averaged
4   over the upper 700 meters of the ocean, bottom panel shows changes averaged over the full ocean depth. Thin black
5   lines show the evolution for each of the twelve AOGCMs, red line shows the average of all twelve projections, the blue
6   line indicates an estimate of the average magnitude of internal variability of all twelve AOGCMs (2sigma).Gray
7   horizontal lines indicate the 2016–2035 average anomaly for each of the twelve AOGCMs, while the orange horizontal
8   line indicates the multi-model average 2016–2035 anomaly. The fifty-year running average from each model's control
9   climate integration was removed from each line. Values referenced to the 1986–2005 climatology of each AOGCM.
10
11 **[INSERT FIGURE 11.25 HERE]**
12 **Figure 11.25:** Projected changes, as a function of depth, in annual-averaged, globally-averaged ocean temperature
13 based on the average of twelve AOGCMs from the CMIP3 (Meehl et al., 2007b) multi-model ensemble, under 21st
14 century Emissions Scenario SRESA1B. Gray shading indicates where the multi-model average AOGCM anomalies are
15 smaller than two standard deviations of the multi-AOGCM estimate of internal variability from the control climate
16 integrations. The fifty-year running average from each model's control climate integration was removed from each line.
17 Values referenced to the 1986–2005 climatology of each AOGCM.
18
19 **[INSERT FIGURE 11.26 HERE]**
20 **Figure 11.26:** Upper panels show the projected changes averaged 2016–2035 relative to 1986–2005 in sea surface
21 temperature (left panels) and temperature averaged over the upper 700 meters of the ocean (right panels), as a function
22 of latitude and longitude. Lower panels show the standard deviation of twenty-year averages of sea surface temperature
23 (left panels) and temperature averaged over the upper 700 meters of the ocean (right panels) arising from internal
24 climate variability in these models. Figures based on the average of twelve AOGCMs from the CMIP3 (Meehl et al.,
25 2007b) multi-model ensemble, under 21st century Emissions Scenario SRESA1B. Gray shading indicates where the
26 multi-model average AOGCM anomalies are smaller than two standard deviations of the multi-AOGCM estimate of
27 internal variability from the control climate integrations, black stippling indicates where at least four (1/3) of the models
28 disagree on the sign of the change. The fifty-year running average from each model's control climate integration was
29 removed from each line.
30
31 **[INSERT FIGURE 11.27 HERE]**
32 **Figure 11.27:** [PLACEHOLDER FOR FINAL DRAFT: Currently shaded at 1 sigma. Same as Figure 11.25, but for
33 regional averages.]
34
35 *11.3.3.2 Salinity*
36
37 Changes in sea surface salinity are expected in response to changes in precipitation, evaporation and run-off
38 (see Section 11.3.2.3); in general (but not in every region), salty regions are expected to become saltier and
39 fresh regions fresher (e.g., Durack and Wijffels, 2010). As discussed in Chapter 10, observation-based and
40 attribution studies have found some evidence of an emerging anthropogenic signal in salinity change, in
41 particular increases in surface salinity in the subtropical North Atlantic, and decreases in the west Pacific
42 warm pool region (Durack and Wijffels, 2010; Stott et al., 2008; Terray et al., 2012). However, the extent to
43 which the observed changes are clearly outside the range of natural internal variability, and the extent to
44 which current models are providing an adequate simulation of salinity change, has yet to be firmly
45 established (Durack and Wijffels, 2010; Terray et al., 2012). This said, models generally predict increases in
46 salinity in the tropical and (especially) subtropical Atlantic, and decreases in the western tropical Pacific
47 over the next few decades (Figure 7b of Terray et al., 2012).
48
49 Projected near-term increases in fresh water flux into the Arctic Ocean produce a fresher surface layer and
50 increased transport of fresh water into the North Atlantic (Holland et al., 2006; Holland et al., 2007; Vavrus
51 et al., 2012). Such contributions to decreased density of the ocean surface layer in the North Atlantic could
52 help stabilize deep ocean convection there and contribute to a near-term reduction of strength of Atlantic
53 Meridional Ocean Circulation. However, the strength of the AMOC can also be modulated by changes in
54 temperature, such as those from changing radiative forcing (Delworth and Dixon, 2006). There is also a
55 projected increase in the temperature of intermediate depth water penetrating the Arctic from the North
56 Atlantic with greater warming than the surface layer (Vavrus et al., 2012).
57
58 *11.3.3.3 Circulation*
59

1   As discussed in previous assessment reports, the AMOC is generally projected to weaken over the next
2   century in response the increase in anthropogenic greenhouse gases. However, the rate and magnitude of
3   weakening is very uncertain. Response uncertainty is likely to be a dominant contribution in the near term,
4   but the influence of anthropogenic aerosols and natural radiative forcings (solar, volcanic) cannot be
5   neglected, and could be as important as the influence of greenhouse gases (e.g., Delworth and Dixon, 2006;
6   Stenchikov et al., 2009). For example, the rate of weakening of the AMOC in two models with different
7   climate sensitivities is quite different, with the less sensitive model (CCSM4) showing less weakening and a
8   more rapid recovery, with the more sensitive model (CESM1/CAM5) indicating stronger weakening and a
9   slower recovery (Meehl et al., 2012b). In addition, the natural variability of the AMOC on decadal
10 timescales is poorly known and poorly understood, and could dominate any anthropogenic response in the
11 near term (Drijfhout and Hazeleger, 2007). The AMOC is known to play an important role in the decadal
12 variability of the North Atlantic Ocean (Figure 11.26), but climate models show large differences in their
13 simulation of both the amplitude and spectrum of AMOC variability (e.g., Bryan et al., 2006; Msadek et al.,
14 2010). In some AOGCMs changes in southern hemisphere surface winds influence the evolution of the
15 AMOC on timescales of many decades (Delworth and Zeng, 2008), so the delayed response to southern
16 hemisphere wind changes, driven by the historical reduction in stratospheric ozone along with its projected
17 recovery, could be an additional confounding issue (Section 11.4.2.3). Overall, it is *likely* that there will be
18 some decline in the AMOC by 2050, but decades during which the AMOC increases are also to be expected.
19 There is *low confidence* in projections of when an anthropogenic influence on the AMOC might be detected.
20
21 The high uncertainty in projections for the AMOC should not be interpreted as ruling out the possibility of a
22 sudden major reduction or 'shutdown' – see Section 11.3.6 and Chapter 12.
23
24 Projected changes to oceanic circulation in the Indo-Pacific are strongly dependent on future response of the
25 Walker circulation (DiNezio et al., 2009a; Vecchi and Soden, 2007). The projected radiatively-forced
26 weakening of the Walker circulation through the mid-21st century is smaller than the expected variability on
27 timescales of decades to years (Section 11.3.2.4.3), therefore it is more likely than not that internal climate
28 variability will be a dominant contributor to changes in the strength of equatorial circulation, the shallow
29 subtropical overturning in the Pacific, and the Indonesian Throughflow over the coming decades. The
30 dominant contribution of internal climate variability precludes a confident assessment of their likely changes
31 through the mid-21st century; however, it is very likely that there will be substantial variations in their
32 strength on timescales of years to decades.
33
34 ### 11.3.4   Near-Term Projected Changes in the Cryosphere
35
36 This section assesses projected near-term changes of elements of the cryosphere. These consist of sea ice,
37 snow cover and near-surface permafrost (frozen ground), changes to the Arctic Ocean, and possible abrupt
38 changes involving the cryosphere. Glaciers and ice sheets are addressed in Chapter 13. The IPCC AR4
39 showed time series of Arctic and Antarctic sea ice extent following the SRES scenarios in the 21st century,
40 and geographical plots of sea ice extent for those regions only for the end of the 21st century. A comparable
41 time series plot of projected sea ice extent for the duration of the 21st century is shown for the CMIP5 multi-
42 model ensemble in Chapter 12, Section 12.4.6 where there are more detailed discussions of some of the
43 relevant processes involved with future changes in the cryosphere. There was no assessment of near-term
44 changes of snow cover or permafrost in the AR4. Here we assess near-term changes in the geographical
45 coverage of sea ice, snow cover and near-surface permafrost. Trends in many observed quantities seem to
46 show evidence of anthropogenic forcing, however, for many of these, the trend exists alongside considerable
47 interannual and decadal variability that complicates our ability to make specific/precise short-term
48 projections, and confounds the emergence of a forced signal above the noise.
49
50 *11.3.4.1   Sea Ice*
51
52 Though more than 90% of CMIP5 models project a nearly ice-free Arctic at the end of summer by 2100 in
53 the RCP8.5 scenario (see 12.4.6.1 and Figure 12.30), some show large changes in the near term as well.
54 Some previous models project an ice-free summer period in the Arctic Ocean by 2040 (Holland et al., 2006),
55 and even as early as the late 2030s using a criterion of 80% sea ice area loss (e.g., Zhang, 2010). By scaling
56 six CMIP3 models to recent observed September sea ice changes, a nearly ice free Arctic in September is
57 projected to occur by 2037, reaching the first quartile of the distribution for timing of September sea ice loss

1   by 2028 (Wang and Overland, 2009). However, a number of models that have fairly thick Arctic sea ice
2   produce a slower near-term decrease in sea ice extent compared to observations (Stroeve et al., 2007). An
3   example of an estimate of when there could be a nearly ice-free late-summer (September) in the Arctic, from
4   a subselection of CMIP5 models that meet criteria related to simulation quality of sea ice, show a range of
5   2040 to at least 2100 for RCP4.5, and 2041–2060 for RCP8.5 (Massonnet et al., 2012).

7   The credibility of near-term predictions for an ice-free Arctic before mid-century depend on at least a
8   reasonable simulation of extent and spatial distribution of present-day ice thickness, accurate representation
9   of the surface energy budget and its influence on the sea ice mass budget, atmospheric energy transports,
10 local feedbacks associated with the stable boundary layer and polar clouds, and the relationship of reduction
11 in ice area per ice thickness change (Bitz, 2008; Holland et al., 2008). Additionally an increase in ocean heat
12 flux convergence to the Arctic could contribute to more rapid ice melt (Bitz et al., 2006; Holland et al., 2008;
13 Winton, 2006). An analysis of CMIP3 model simulations indicates that for near-term predictions the
14 dominant factor for decreasing sea ice is increased ice melt, and reductions in ice growth play a secondary
15 role (Holland et al., 2008). Arctic sea ice has larger volume loss when there is thicker ice initially across the
16 CMIP3 models, with a projected accumulated mass loss of about 0.5 m by 2020, and roughly 1.0 m by 2050
17 with considerable model spread (Holland et al., 2008). The CMIP3 models tended to under-estimate the
18 observed rapid decline of summer Arctic sea ice during the satellite era, but these recent trends are more
19 accurately simulated in the CMIP5 models (see 12.4.6.1). Results from the CMIP5 models indicate
20 September Arctic sea ice extent per degree annual mean global surface warming of $-2.0 \pm 2.5 \times 10^6$ km^2 °C^{-1}
21 which is more sensitive compared to recent observed trends (see 12.4.6.1 and Figure 12.32). Acceleration of
22 sea ice drift observed over the last 3 decades, underestimated in CMIP3 projections (Rampal et al., 2011)
23 and presence of fossil-fuel and biofuel soot in Arctic environment (Jacobson, 2010) could also contribute to
24 ice-free late summer conditions over the Arctic in the near term. Details on the transition to ice-free summer
25 over Arctic regardless the particular aspects of near term projections are presented in Chapter 12 (12.4.6.1
26 and 12.5.5.3).

28 As discussed in Chapter 12 (12.4.6.1), by combining all available studies and focusing particularly on
29 models that do the best job in simulating recent observed trends, the following time intervals are obtained for
30 when there could be a late-summer (September) ice-free Arctic: 2020–2100 and beyond, for the SRESA1B
31 scenario and RCP4.5, with a best estimate in the range of 2035–2065 (Boe et al., 2009; Massonnet et al.,
32 2012; Stroeve et al., 2012; Wang and Overland, 2012; Wang and Overland, 2009; Zhang, 2010), and 2020–
33 2060 for RCP8.5, with a best estimate in the range of 2035–2050 (Massonnet et al., 2012; Wang and
34 Overland, 2012). Thus, there is a distinct possibility that there could be a late-summer (September) ice-free
35 Arctic before mid-century.

37 In early 21st century simulations, Antarctic sea ice cover is projected to decrease more slowly than in the
38 Arctic in the CMIP5 models, though CMIP3 and CMIP5 models simulate recent decreases in Antarctic sea
39 ice extent compared to slight increases in the observations (Chapter 12, Section 12.4.6.1 and Figure 12.31).
40 However, it has been noted that there is the possibility that melting of the Antarctic ice sheet could actually
41 be changing the vertical ocen temperature stratification around Antarctica and encourage sea ice growth
42 (Bintanja et al., 2012). The decreases of sea ice area for the time period 2016–2035 averaged across all
43 models in the CMIP5 multi-model ensemble average for the RCP4.5 scenario are –28% for September
44 (Figure 11.28), and –6% for February for the Arctic (Figure 11.28). Changes for the Antarctic are –5% for
45 September (Figure 11.28), and –13% for February (Figure 11.28). Reductions in Northern Hemisphere sea
46 ice volume for that same set of models, scenario and time period are –23% for February, and –43% for
47 September, while for the Southern Hemisphere those values are –12% for February, and –7% for September.

49 *11.3.4.2 Snow Cover*

51 Decreases of snow cover area (SCA) are strongly connected to a shortening of seasonal snow cover duration
52 (Brown and Mote, 2009) and are related to both precipitation and temperature changes (see 12.4.6.2). This
53 has implications for snow on sea ice where loss of sea ice area in autumn delays snowfall accumulation, with
54 CMIP5 multi-model mean values of snow depth in April north of 70°N reduced from about 28 cm to roughly
55 18 cm for the 2031–2050 period compared to the 1981–2000 average (Hezel et al., 2012). The snow
56 accumulation season by mid-century in one model is projected to begin later in autumn with the melt season
57 initiated earlier in the spring (Lawrence and Slater, 2010). Some climate models have simulated reductions

1   in annual snow cover of –4 to –7% by 2011–2030, and –5 to –13% by 2041–2060 with largest decreases in
2   northern spring (March-April-May) (Committee, 2010). As discussed in greater detail in 12.4.6.2, projected
3   increases in snowfall across much of the northern high latitudes act to increase snow amounts, but warming
4   reduces the fraction of precipitation that falls as snow. Additionally, the reduction of Arctic sea ice also
5   provides an increased moisture source for snowfall (Liu et al., 2012). Whether the average SCA decreases or
6   increases by mid-century depends on the balance between these competing factors. The dividing line where
7   models transition from simulating increasing or decreasing maximum snow water equivalent roughly
8   coincides with the –20°C isotherm in the mid-20th century November to March mean surface air temperature
9   (Raisanen, 2008).
10
11 Time series of projected changes in relative SCA are shown in Figure 12.34. Multi-model averages from 21
12 models in the CMIP5 archive show decreases of Northern Hemisphere snow cover area of –4.2 ± 1.9% (one
13 standard deviation) for the 2016–2035 time period for a March to April average using a 15% extent threshold
14 for RCP4.5 (Brutel-Vuilmet et al., 2012).
15
16 *11.3.4.3 Near Surface Permafrost (Frozen Ground)*
17
18 Virtually all near-term projections indicate a substantial amount of near-surface permafrost degradation, and
19 thaw depth deepening over much of the permafrost area (Committee, 2010; Lawrence et al., 2008; Sushama
20 et al., 2006; Guo and Wang, 2012). As discussed in more detail in 12.4.6.2, these projections have increased
21 credibility compared to the previous generation of models assessed in the AR4 because current climate
22 models represent permafrost more accurately (Alexeev et al., 2007; Lawrence et al., 2008; Nicolsky et al.,
23 2007). The reduction in annual mean permafrost area for the 2016–2035 time period compared to the 1986–
24 2005 reference period for the RCP4.5 scenario for 15 CMIP5 models for the Northern Hemisphere is 2.91 x
25 10^6 km^2, or a decrease of –18%.
26
27 *11.3.4.4 Possible Near-Term Abrupt Climate Change Involving the Cryosphere*
28
29 Periods of rapid summer-time retreat of the Arctic sea ice margin, such as that which occurred in the late
30 2000s (see Chapter 4) has been noted to occur in a climate model, raising the possibility of abrupt sea ice
31 retreat events sometime in the next 50 years (Holland et al., 2006). In summer, the oceanic heat anomaly is
32 enhanced by ice–albedo feedback, but in winter the excess oceanic heat is lost to the atmosphere due to a
33 lack of insulating sea ice cover, and this raises the possibility of sudden irreversible loss of Arctic summer
34 sea ice during warming conditions (Winton, 2006), even though there is evidence that the loss of Arctic
35 summer could be reversible. Increases in mostly low clouds in autumn, or decreases in summer, can promote
36 rapid sea ice loss events (Vavrus et al., 2011). A more detailed discussion of these processes is given in
37 12.5.5.3. The interactions of clouds and sea ice introduce another element of uncertainty to short term
38 predictions of abrupt changes in sea ice coverage (DeWeaver et al., 2008; Gorodetskaya et al., 2008; Vavrus
39 et al., 2009).
40
41 Though permafrost thaw and active layer deepening could initiate abrupt changes in Arctic hydrological,
42 biogeochemical, and ecosystem processes (McGuire et al., 2006), the impact of these potential climate
43 feedbacks is not well quantified for short term climate change (Euskirchen et al., 2006; O'connor et al.,
44 2010).
45
46 It is very likely that there will be continued near-term loss of sea ice extent in the Arctic, decreases of snow
47 cover, and reductions of permafrost at high latitudes of the Northern Hemisphere and Tibetan Plateau.
48 Though there is the possibility of sudden abrupt changes in the cryosphere, there is low confidence that these
49 changes could be predicted with any certainty over the next several decades.
50
51 **[INSERT FIGURE 11.28 HERE]**
52 **Figure 11.28:** February and September CMIP5 multi-model mean sea ice concentrations (%) in the Northern and
53 Southern Hemispheres for the periods (a) 1986–2005, (b) 2016–2035 under RCP4.5. Only one member per model is
54 taken into account in the analysis. The number of models is given in parentheses. The pink lines show the observed
55 15% sea ice concentration limits averaged over 1986–2005 (Comiso et al., 2008).
56

1 ### 11.3.5   Changes in Atmospheric Composition and Air Quality
2
3 Future atmospheric composition depends on anthropogenic emissions, natural emissions and uptake (Chapter
4 6), and chemical-physical processes in the atmosphere (Chapters 2, 6, 7, 8). IPCC emission scenarios
5 prescribe only emissions that can be directly ascribed to human activities (anthropogenic) and do not include
6 projections for shifting natural emissions or other forcings. The latter may occur in response to changes in
7 climate or land use, changes in the solar flux or volcanic aerosols, all of which alter climate and composition
8 (Chapter 8). This chapter assesses changes in the atmospheric abundances of CH_4, N_2O, other well-mixed
9 greenhouse gases, plus O_3 and aerosol optical depth, projected over the 21st century from the RCP scenarios
10 (Meinshausen et al., 2011; Moss et al., 2010; van Vuuren et al., 2011; Section 11.3.5.1). Projected CO_2
11 abundances, controlled by anthropogenic emissions and interaction with the terrestrial and oceanic carbon
12 cycle, are discussed in Chapters 6 and 12. The 21st-century scenarios, from emissions to radiative forcing are
13 collected in the tables of Annex II.
14
15 Also included here (Section 11.3.5.2) is an assessment of projected changes in ambient air quality at the
16 continental scale, specifically surface O_3 and PM (particulate matter, a measure of aerosol concentration) as
17 they are influenced by climate change and global-scale anthropogenic pollution. The connections between
18 air pollution, global atmospheric chemistry and climate change were recognized in the TAR (Jacob et al.,
19 1993; Johnson et al., 1999; Penner et al., 1993; Prather et al., 2001). The SRES scenarios were assessed for
20 changes in surface O_3 from emissions (Prather et al., 2003), changes in radiative forcing from emissions of
21 air pollutants (Gauss et al., 2003; Shindell et al., 2007), and changes in global tropospheric O_3 driven by
22 climate (Johnson et al., 2001). In the AR4, these SRES scenarios were contrasted with newer near-term
23 scenarios to 2030, the Current Legislation (CLE) and Maximum Feasible Reductions (MFR) scenarios, to
24 illustrate the impacts of explicit air pollution control strategies on air pollution, global atmospheric
25 chemistry, and near-term climate (Dentener et al., 2005; Dentener et al., 2006; Stevenson et al., 2006). In
26 terms of air quality, the RCPs all assume stringent air pollution policies as opposed to the unconstrained but
27 broader range within SRES. The RCPs do not cover the range of future pollution emissions found in the
28 literature (van Vuuren et al., 2011), all tending toward the MFR scenarios. In addition, changes in diet,
29 production of food or biofuels (Chapter 6), technology shifts in the agricultural or energy sectors (e.g.,
30 Galloway et al., 2008; Jacobson, 2008a; Schultz et al., 2003; Unger et al., 2009; van Ruijven et al., 2011), or
31 changes in land use/cover affecting biospheric emissions and dry deposition (Chen et al., 2009a; Ganzeveld
32 et al., 2010; Wu et al., 2012) could alter future air quality but are not assessed here. Section 11.3.6.1
33 discusses the climate impacts of efforts directed at improved air quality.
34
35 #### 11.3.5.1   Reactive Greenhouse Gases and Aerosols
36
37 The IPCC has assessed previous emission-based scenarios for future greenhouse gases and aerosols in the
38 SAR (IS92) and TAR/AR4 (SRES). The new RCP scenarios, developed independently of the IPCC
39 assessment and review process, each have an integrated but simplified single model, which goes from human
40 activities to emissions to greenhouse gases to climate change (Lamarque et al., 2011a; Meinshausen et al.,
41 2011; Meinshausen et al., 2011; van Vuuren et al., 2011). The RCP-prescribed emissions, abundances and
42 radiative forcing used in the CMIP5 model ensembles do not reflect current best understanding of natural
43 and anthropogenic emissions, atmospheric chemistry and biogeochemistry, and radiative forcing of climate
44 (see e.g., Dlugokencky et al., 2011; Prather et al., 2012). Emissions of highly reactive, non-greenhouse
45 species (e.g., SO_2, NH_3, NOx, CO, NMVOC) control much of global atmospheric chemistry, viz.,
46 tropospheric O_3, aerosols, global air quality, and indirectly the abundances of CH_4 and HFCs. These
47 emissions are difficult to quantify or project, and alternative near-term scenarios have been proposed (Cofala
48 et al., 2012; Cofala et al., 2007; Dentener et al., 2005; Kloster et al., 2008). The uncertainty in projecting
49 RCP emissions into radiative forcing and climate change is not negligible, see below, but is still generally
50 less than the range of RF between the RCP2.6 and RCP8.5 scenarios. Where appropriate, results from the
51 SAR (IS92a) and TAR (SRES B1&A2) are included.
52
53 ##### 11.3.5.1.1 CH_4, N_2O, and the fluorinated F-gases
54 Kyoto greenhouse gases abundances projected to 2100 (AII.4.1–15) show both RCP published values
55 (Meinshausen et al., 2011) and those estimated in this assessment (denoted RCP&) where uncertainty is
56 estimated as ±1 standard deviation. The Kyoto GHG RFs, based on Chapter 8 methodology, are summarized
57 in AII.6.1–4. While anthropogenic emissions of fossil-fuel CO_2 (AII.2.1a) are generally accurate to 10% or

1   less based on bottom-up inventory methods, emissions of CH_4 and N_2O, primarily from the agriculture,
2   forestry and other land use sectors (AFOLU, AII.2.1b, AII.2.3–4), have uncertainties typically 25% or more
3   (NRC, 2010b; Prather et al., 2009). Following the method of Prather et al. (2012), a best estimate and
4   uncertainty range for present day (year 2010) anthropogenic and natural emissions of CH_4 and N_2O are
5   derived using updated AR5 values (see Chapters 2, 5, 6). The RCP emissions are normalized here at 2010
6   and then used as indices to scale the future anthropogenic CH_4 and N_2O emissions for 2010–2100. Such
7   harmonization was done for the SRES emissions in the TAR (Prather et al., 2001) and the RCPs
8   (Meinshausen et al., 2011) but with different values for lifetimes and natural sources.
9
10 Combining CH_4 observations (pre-industrial, present, and present trends, Chapter 2), lifetime estimates for
11 present day (Montzka et al., 2011; Prather et al., 2012) and the ACCMIP studies (Voulgarakis et al., 2012),
12 plus estimates of changing natural sources (Chapter 6), the current budget is derived as: anthropogenic
13 emissions in the year 2010 of 318 ± 48 Tg–CH_4 yr^{-1} with total emissions of 504 ± 43 Tg–CH_4 yr^{-1}. The RCP
14 (anthropogenic) emissions for 2010 lie within 10% of this value, and thus the scaling factor for RCPs over
15 the 21st century is small (see AII.2.2). A projection of the tropospheric OH lifetime of CH4 (AII.5.9) is
16 based on the ACCMIP simulations of the RCPs for 2100 time slice simulations (Voulgarakis et al., 2012),
17 other modeling studies (John et al., 2012; Stevenson et al., 2006) and the multi-model sensitivity analyses of
18 factors controlling OH (Holmes et al., 2012). The latter outlines the method for projecting the lifetime of
19 CH4 and the HFCs with uncertainties attached. Future changes in natural sources of CH_4 may be important
20 (Chapter 6) and are estimated in a few CMIP5 models, but there is not sufficient confidence to include these
21 in projections here. The resulting projections of CH4 anthropogenic emissions and abundances are compared
22 with the RCP values in Figure 11.29. For RCP2.6, CH_4 abundances are projected to decline continuously
23 over the century by about 30%; whereas RCP 4.5 and 6.0 peak in mid-century and then decline below 2010
24 abundances. By 2020 the spread in CH_4 abundances across RCPs is large, 1720 to 1920 ppb, with model
25 uncertainty estimated at only ± 20 ppb. This spread continues to diverge by 2050, 1400 to 2700 ppb, with
26 model uncertainty increasing to ± 160 ppb. Only RCP8.5 with its large increasing anthropogenic emissions
27 has consistently increasing abundances, doubling by 2080. Uncertainty in projecting future abundances is
28 much smaller than the difference between scenarios.
29
30 **[INSERT FIGURE 11.29 HERE]**
31 **Figure 11.29:** Projected CH_4 (a) anthropogenic emissions (Tg–CH_4 yr^{-1}) and (b) atmospheric abundances (ppb) for the
32 four RCP scenarios (2010–2100). The thick solid lines show the published RCP values: red plus, RCP8.5; orange
33 square, RCP6.0; light blue circle, RCP4.5; dark blue asterisk, RCP2.6. Thin lines with markers show values from this
34 assessment based on Holmes et al. (2012). The shaded region shows the ± 1 standard deviation from the Monte Carlo
35 calculations that consider uncertainties, including the current magnitude of the anthropogenic emissions.
36
37 Even with the emergence of N_2O as the number three long-lived GHG, less effort has gone into studying and
38 projecting its budget and lifetime. Observations of N_2O (pre-industrial, present, and present trends, Chapter
39 2) are combined with two modern studies of the N_2O lifetime (Fleming et al., 2011; Hsu and Prather, 2010)
40 and a Monte Carlo method (Prather et al., 2012) to derive a best present-day budget: anthropogenic
41 emissions of 6.5 ± 1.0 Tg–$N(N_2O)$ yr^{-1} with total emissions of 15.6 ± 1.0 Tg–$N(N_2O)$ yr^{-1}. Adjustments to
42 the RCP anthropogenic N_2O emissions (-20%) are larger than for CH_4 because of the different lifetime
43 (AII.2.3). Projections of N_2O here (AII.4.3) include a shifting lifetime due to changing circulation and
44 chemistry in the stratosphere (Fleming et al., 2011) and the feedback of increasing N_2O reducing its own
45 lifetime. Recent multi-model, chemistry-climate studies (CCMVal) project a more vigorous stratospheric
46 overturning and shorter N_2O lifetime by 2100 (Oman et al., 2010a; Strahan et al., 2011), but did not diagnose
47 the N_2O lifetime. By 2020 the spread in mean N_2O abundances across RCPs is small, 329–332 ppb, and it
48 grows slowly by 2050 to 345–365 ppb, with model uncertainty remaining relatively small at only ± 4 ppb.
49 The RCP published range shows N_2O increasing from 323 pbb in 2010 to 344–435 ppb in 2100. Accounting
50 for chemical feedbacks on the lifetime reduces this range for 2100 by 20%, from 354–424 ppb.
51
52 The industrially produced, synthetic fluorinated (F-)gases would seemingly have reliable bottom-up
53 inventories (AII.2.4–15). Recent measurements show that for Europe HFC-23 emissions are greatly under
54 reported (Keller et al., 2011) while HFC-125 and 152a are roughly consistent with emissions inventories
55 (Brunner et al., 2012). Globally, HFC-365mfc and HFC-245fa emissions are overestimated (Vollmer et al.,
56 2011) while SF_6 appears to be under reported (Levin et al., 2010). Without clear guidance on how to correct
57 or place uncertainty on these F-gas emissions, this assessment uses the RCP emissions as reported. For the
58 very long-lived SF_6 and per-fluorocarbons (CF_4, C_2F_6, etc.) uncertainty in lifetimes does not significantly

1   affect the projected abundances over the 21st century (AII.4.4–7), and the RCP values are adopted without
2   uncertainty. For the HFCs, whose lifetimes are determined primarily by tropospheric OH, their future
3   abundances are projected with uncertainties using the RCP emissions with the probability distribution of OH
4   described for the CH_4 projections above (AII.4.8–15).
5
6   Scenarios for the ozone-depleting GHG under control of the Montreal Protocol (CFCs, HCFCs, halons in
7   AII.4.16) are taken from scenario A1 of the 2010 WMO Ozone Assessment (WMO, 2011, Table 5–A3). All
8   of the CFC abundances decline throughout the century, but some of the HCFC's increase to 2030 before
9   their phase-out and decline. Their combined RF (Table AII.6.5) is calculated using the methodology in
10 Chapter 8 plus a simple estimate of uncertainty in their decay from 2005 to 2100 as described in the table
11 notes. Radiative forcing from the sum of these Montreal gases decreases from a peak value of 0.33 ± 0.01 W
12 m^{-2} in 2010, to 0.29 W m^{-2} in 2030, to 0.20 W m^{-2} in 2050, and to 0.10 ± 0.02 W m^{-2} in 2100.
13
14 *11.3.5.1.2 Tropospheric and stratospheric O_3*
15 Projected O_3 changes are broken into tropospheric and stratospheric columns (DU, AII.5.1–2) because each
16 has different driving factors and opposite-signed impacts on RF (Chapter 8). Tropospheric O_3 changes are
17 driven by anthropogenic emissions of CH_4, NOx, CO, NMVOC (AII.2.2.16–18) and are projected to follow
18 these emission trends over the next few decades (e.g., decreasing in all RCPs by 2100 as global NO_x
19 declines, but increasing in RCP8.5 due to CH_4 increases despite falling NOx emissions). Overall,
20 tropospheric climate change drives a decline in tropospheric O_3, but enhanced stratospheric circulation can
21 counter that (Kawase et al., 2011; Lamarque et al., 2011b; Shindell et al., 2006; Zeng et al., 2008a). Natural
22 emissions of NOx, particularly lightning NOx, and biogenic NMVOC are also important (Wild, 2007; Wu et
23 al., 2007), but reliable estimates of their change with climate cannot be made. Best estimates for tropospheric
24 O_3 change (Table AII.5.2) are based on ACCMIP time slice simulations for 2030 and 2050 with chemistry-
25 climate models (Young et al., 2012) and the CMIP5 runs (Eyring et al., 2012). Similar results are obtained
26 with multi-model studies of tropospheric O_3 response to key factors like individual emissions, climate-driven
27 increases in water vapour and temperature, and increased stratospheric influx (Oman et al., 2010a; Prather et
28 al., 2001; Stevenson et al., 2006; Wild et al., 2011; Wild et al., 2012). The ACCMIP models show a wide
29 range in tropospheric O_3 burden changes from 2000 to 2100: –5 DU (–15%) in RCP2.6 to +6 DU (18%) in
30 RCP8.5. The CMIP5 results are similar but not identical: –3 DU (RCP26) to +10 DU (RCP85). In both
31 cases, one standard deviation of the model ensemble (about 10%) is comparable to the change in the multi-
32 model average/median. For RCP60 the ACCMIP and CMIP5 models project opposite but small changes by
33 2100, –5 and +3%, respectively. Tropospheric O_3 changes in the near term (2030–2040) are smaller but
34 mostly positive across all scenarios and models. The RF from these tropospheric O_3 changes (AII.6.7)
35 parallels the O_3 burden change (Stevenson et al., 2012). The RF in year 2000 is estimated to be 0.36 ± 0.06
36 W m^{-2}, and to diverge according to scenario: by 2030 the range over RCPs is 0.32–0.44 W m^{-2}, and by 2100
37 it is 0.16–0.60 W m^{-2}. RCP2.6 always has the (Oman et al., 2010b) lowest tropospheric O_3 RF; and RCP8.5,
38 the highest. Model uncertainty is less than the spread across scenarios.
39
40 Stratospheric O_3 is being driven by declining chlorine levels, changing N_2O and CH_4, cooler temperatures
41 from increased CO_2, and a more vigorous overturning circulation driven by more wave propagation under
42 climate change (Butchart et al., 2006; Eyring et al., 2010; Oman et al., 2010b). Overall stratospheric O_3 is
43 expected to increase in the coming decades, reversing the majority of the loss that occurred between 1980
44 and 2000. The O_3 recovery and increased stratospheric circulation is proposed to increase tropospheric O_3
45 (Bauer et al., 2007b; Shindell et al., 2006; Unger et al., 2006c; Zeng et al., 2008b; Zeng et al., 2010b). This
46 effect is difficult to quantify separately from other changes, but it is included in some of the
47 ACCMIP/CMIP5 models used to project tropospheric O_3. The CCMVal modeling studies of ozone recovery
48 over the 21st century have highlighted uncertainties, but assessment of the differences among RCP scenarios
49 is less extensive (Eyring et al., 2010; Oman et al., 2010b). Best estimates for global mean stratospheric O_3
50 change (Table A.5.1) are taken from the CMIP5 results (Eyring et al., 2012) and by 2100 show a 5–7%
51 increase above 2000-levels for all RCPs, recovering to within 1% of the pre-ozone-hole 1980-levels by 2050.
52
53 *11.3.5.1.3 Aerosols*
54 Aerosol species can be emitted directly (mineral dust, sea salt, black carbon and some organic carbon) or
55 indirectly through precursor gases (sulfate, ammonium, nitrate, some organics). Anthropogenic aerosol
56 sources are projected to change under the RCPs and alternative scenarios. CMIP5 models (Lamarque et al.,
57 2011c) have projected changes in aerosol burden (Tg) and optical depth (AOD) to 2100 (AII.5.3–8). Total

AOD is dominated by dust and sea salt, but absorbing aerosol optical depth (AAOD) is primarily of anthropogenic origin. Key anthropogenic aerosol changes are documented in the species-specific burdens. Uniformly, anthropogenic aerosols decrease under RCPs. By 2030 both sulfate and black carbon aerosol burdens decrease by 13–26%, and by 2050 they drop by 20% (RCP6.0) up to 40% (RCP2.6). By 2100, the decline across all scenarios is 45–60% relative to 2010. See also Section 11.3.6.1. For the aerosol direct and indirect forcing under the RCPs see Chapter 8.

11.3.5.1.4 Natural emissions and uncertainties
Natural emissions of CO_2, CH_4 and N_2O, plus highly reactive species like NOx, CO, and NMVOC control in part the abundance of most greenhouse gases and some aerosols. Models predict that these emissions will change in a warming climate and with land use change, but we are unable to quantify such changes for the RCPs, see Chapter 6.

Uncertainty estimates in projecting atmospheric composition under a changing climate are based in large part on expert judgment. Our understanding of the atmospheric processes that control the abundance of greenhouse gases and aerosols has been tested and calibrated with intensive in situ observations over the past couple decades, and has been incorporated into modern three-dimensional chemistry-transport or chemistry-climate models (CTMs or CCMs) (Chapter 9). With climate change, the atmospheric processes calibrated under historical conditions (e.g., harmonization of N_2O observations, budgets, and lifetimes) are expected to shift, and thus uncertainty in projecting changes under a given emissions scenario will be greater than the errors in current models.

11.3.5.2 Projections of Air Quality

Air quality changes in the 21st century are tied first to local anthropogenic emissions, then to global and neighboring anthropogenic emissions, and finally to changes in physical climate and related biogenic emissions (e.g., Carlton et al., 2010; Doherty et al., 2009; Hoyle et al., 2011; Meleux et al., 2007; Steiner et al., 2006; Steiner et al., 2010; Tai et al., 2010; Tao et al., 2007; Wu et al., 2008b). For example, extreme air quality episodes are associated with changing weather patterns, such as heat waves and stagnation episodes (Cox and Chu, 1996; Logan, 1989; Mickley et al., 2004; Stott et al., 2004; Vukovich, 1995). Neither the global climate-chemistry models used here, nor the RCP scenarios, are adequate to assess pollution driven by local emissions, for example within an air quality management district. See WGII Chapters 9 and 14 for evaluation of climate projections at the regional-urban scale. The WGI global models, with horizontal resolutions of 100 km at best, are able to assess the latter two elements. Thus, air quality changes are assessed here based on (i) the impact of climate change as expressed in temperature, water vapor, local meteorology, and natural emissions (Section 11.3.5.2.1), and (ii) the impact of global and regional anthropogenic emissions of short-lived pollutants and methane (Section 11.3.5.2.2). The emphasis on ozone and aerosols reflects the large focus in the literature to date on the response of these chemical species to climate and emission changes (e.g., Dentener et al., 2006; HTAP, 2010c; TFHTAP, 2007; Wild et al., 2012). For nitrogen and acid deposition see Chapter 6 and AII.7.3–4. Air toxics such as mercury and persistent organic pollutants (HTAP, 2010a, 2010b; Jacob and Winner, 2009; NRC, 2009) and biological aerosols such as pollen (Jacobson and Streets, 2009) are not considered here.

The air quality projections assessed here include estimates from: off-line chemical transport models (CTMs) or AOGCMs run with stable climate but changing emissions; a parameterization developed from sensitivities diagnosed from a coordinated multi-model set of regional emission perturbation simulations with CTMs; CTMs using meteorological fields projected from separate AOGCMs; a suite of linked climate and atmospheric chemistry models from global to regional scales; and global and regional climate models with interactive chemistry. Empirical relationships between local meteorological variables and air quality provide constraints for model evaluation under current conditions and could potentially be used to extrapolate these links to future climate (e.g., Bloomer et al., 2009; Lin et al., 2001; Rasmussen et al., 2011; Tai et al., 2010). Their application for such statistical downscaling of local air quality (e.g., Holloway et al., 2008; Mahmud et al., 2008) may be limited by non-linear sensitivities and changing spatial emissions and temperature sensitivities in a changing climate (e.g., Butler et al., 2012; Dawson et al., 2009; Forkel and Knoche, 2006; Murazaki and Hess, 2006; Nolte et al., 2008; Steiner et al., 2010; Weaver et al., 2009). Downscaling based on air quality relationships with current synoptic conditions may offer a more robust approach (e.g., Appelhans et al., 2012; Dharshana et al., 2010; Tai et al., 2012a; Tai et al., 2012b) but are subject to the same

1   problems with predictability in a changing climate as is the downscaling of regional climate from the CMIP5
2   results (Chapters 9 and 14, WGII).
3
4   *11.3.5.2.1 Climate-driven changes from meteorology and natural emissions*
5   Recent reviews summarize the role of specific temperature-driven processes on O_3 and PM air quality (Fiore
6   et al., 2012; Isaksen et al., 2009; Jacob and Winner, 2009). Reliable air quality projections require
7   confidence in the projected regional climate change, including synoptic meteorology, precipitation,
8   convection, mixing depths, wind speed, and cloud cover (e.g., Jacob and Winner, 2009; Liang et al., 2006;
9   Weaver et al., 2009) and are only as good as the regional climate modeling (Chapter 9 and 14). Ecosystem
10   interactions are particularly uncertain since vegetation acts as both a source and a sink for many air
11   pollutants (e.g., Andersson and Engardt, 2010) and incomplete understanding of chemical oxidation
12   pathways limits confidence in the sign of O_3 and PM responses to changing biogenic emissions (e.g., Carlton
13   et al., 2009; Hallquist et al., 2009; Ito et al., 2009; Pacifico et al., 2009; Paulot et al., 2009).
14
15   *Ozone*
16
17   Climate change exerts opposing influences on surface O_3: decreasing baseline O_3 in the unpolluted
18   atmosphere, but increasing O_3 in some polluted regions and seasons. These competing effects are assessed
19   here. As an example, published estimates for the surface ozone response to climate change alone between
20   2000 and 2030 are summarized in Figure 11.30 (CLIMATE, blue lines). A major caveat is that many
21   published simulations for present-day and future climate conditions span only a few years each, and the short
22   simulation length precludes separating climate change from climate variability (e.g., Langner et al., 2012a;
23   Nolte et al., 2008). The inter-annual variability is evident from the multi-model mean O_3 changes from the
24   transient simulations shown in Figure 11.31a; year-to-year variability in a single model realization is much
25   larger. The ranges in Figure 11.30 reflect spatial variability, model differences, near-term climate scenarios,
26   and differences in reported O_3 statistics. In unpolluted regions, surface O_3 levels are very likely to decrease
27   in a warmer climate because higher water vapor abundances enhance O_3 destruction in low-NO_x regions of
28   the atmosphere where the increase in temperature itself has little impact on O_3 chemistry (Jacobson, 2008b).
29   Hence the global O_3 changes are smaller than in the northern hemisphere regions that contain most of the
30   global pollutant emissions. In polluted regions, a warmer, wetter atmosphere can enhance local O_3,
31   particularly during the peak pollution season. For example, climate-driven increases of 2–6 ppb are projected
32   within Central Europe by 2030 during the peak-O_3 season (Figure 11.30 blue dashed line). Studies
33   examining spatial variations with regional models for summer daytime statistics tend to simulate a wider
34   range of climate-driven changes (e.g., Zhang et al., 2008) with most results available for 2050 (see Fiore et
35   al., 2012).
36
37   Climate-driven increases in biogenic emissions from vegetation and soils, lightning NO_x, influx of
38   stratospheric O_3, as well as shifts in intercontinental transport pathways for pollutants, have not been well
39   assessed in these studies shown in Figure 11.30. With the exception of intercontinental transport, they are
40   generally expected to increase surface O_3 in some regions (Doherty et al., 2012; Isaksen et al., 2009; Johnson
41   et al., 1999). The integrated effect of these processes on regional O_3 remains poorly understood relative to
42   the temperature and water vapor impacts on O_3 photochemistry.
43
44   The observed correlation of high-O_3 events with temperature in polluted regions is well documented and
45   largely reflects the correlation of temperature with stagnation episodes and cloud-free enhanced
46   photochemistry, which are unlikely to scale linearly with temperature in a warming world. Other
47   temperature-related factors (e.g., more rapid thermal decomposition of organo-nitrates to NO_x, higher
48   biogenic emissions, more frequent wildfires) may continue to increase with overall warming (e.g., AR4
49   Chapter 7 Box; Doherty et al., 2012; Fiore et al., 2012; Jacobson, 2008b; Katragkou et al., 2011; Kawase et
50   al., 2011; Nolte et al., 2008; Racherla and Adams, 2008; Wu et al., 2008a; Wu et al., 2008b; Zeng et al.,
51   2008a; Zeng et al., 2010a), though some of these feedback processes are known to have optimal temperature
52   ranges (e.g., Guenther et al., 2006; Sillman and Samson, 1995; Steiner et al., 2010). Some modeling studies
53   find a longer season for O_3 pollution (e.g., Avise et al., 2009; Carvalho et al., 2011; Jacob and Winner, 2009;
54   Jacobson and Streets, 2009; Jaffe et al., 2008; Leibensperger et al., 2008; Menon and et al., 2008; Mickley et
55   al., 2004; Murazaki and Hess, 2006; Nolte et al., 2008; Ordóñez et al., 2005; Weaver et al., 2009; Wu et al.,
56   2008b). Altogether, multiple lines of evidence indicate that climate change alone is *likely* to increase O_3
57   exposure in the more polluted regions while lowering it in others.

1

2   On a regional scale, models are sometimes consistent in the sign of the O_3 response to a warming climate
3   (e.g., increases in Northeastern United States and Southern Europe; decreases in Northern Europe), but they
4   often disagree (e.g., the Midwest, Southeast, and Western United States – Jacob and Winner, 2009; Langner
5   et al., 2012a; Langner et al., 2012c; Weaver et al., 2009). Consistency across these regional studies is
6   difficult to achieve due to variations in the regional climate responses used in each model as well as in
7   emissions and chemical feedbacks. Given the large climate variability at regional to local scales, detection of
8   a climate-change impact on air quality will require many ensembles. Over the Northeastern United States,
9   the consistency across models may reflect the dominance and regularity of synoptic meteorology over
10   feedbacks with the biosphere (Jacob and Winner, 2009; Tai et al., 2012a; Tai et al., 2012b; Weaver et al.,
11   2009). One study finds decreasing cyclone passages over the 21st century (Turner et al., 2012), which are
12   identified as a major driver of variability in O_3 pollution events (Leibensperger et al., 2008). Trends in the
13   number of summertime cyclones may be model-dependent in many regions (Lang and Waugh, 2011), and
14   more evidence is needed to confirm the robustness of this relationship with air quality under a changing
15   climate.

16

17   Overall, there is *high confidence* that a warming climate will change baseline O_3 levels by reducing
18   tropospheric O_3 as water vapor rises with temperature, increasing the O_3 chemical loss rate in much of the
19   unpolluted lower troposphere. Both evidence and agreement are more limited regarding the impact of
20   climate change on pathways for long-range transport of air pollution or the feedbacks from emissions from
21   the biosphere, leading to *low confidence* in their potential importance for future air quality.

22

23   *Aerosols*

24

25   Evaluations as to whether climate change will worsen or improve aerosol (PM) pollution are model-
26   dependent, confounded by opposing influences on individual PM components, and the large inter-annual
27   variability (e.g., Mahmud et al., 2010). Warmer temperatures generally decrease nitrate aerosol (volatility)
28   but increase sulphate aerosol, reflecting faster production although synoptic transport may play a role (e.g.,
29   Aw and Kleeman, 2003; Hedegaard et al., 2008; Kleeman, 2008; Liao et al., 2006; Pye et al., 2009; Racherla
30   and Adams, 2006; Tai et al., 2012b; Unger et al., 2006b). PM in surface air will also increase in locations
31   where surface stability increases, or under higher humidity that enhances aerosol growth (Jacobson, 2008b).
32   Natural aerosols may increase with temperature, particularly carbonaceous aerosol from wildfires, mineral
33   dust, and biogenic secondary organic aerosol (SOA) (Carvalho et al., 2011; Fiore et al., 2012; Jiang et al.,
34   2010; Jickells et al., 2005; Mahowald, 2007; Mahowald and Luo, 2003; Mahowald et al., 2006; Spracklen et
35   al., 2009; Tegen et al., 2004; Woodward et al., 2005; Yue et al., 2010). In some regions, biogenic SOA is
36   expected to grow as temperatures rise due to enhanced emissions and gas-to-particle conversion (Heald et
37   al., 2008; Liao et al., 2007; Tagaris et al., 2007).

38

39   Most components of PM are expected to correlate negatively with precipitation (Tai et al., 2010), such that
40   aerosol burdens will likely decrease in regions with increased precipitation (Avise et al., 2009; Liao et al.,
41   2007; Pye et al., 2009; Racherla and Adams, 2006; Tagaris et al., 2007; Zhang et al., 2008). Projecting
42   precipitation at the regional or urban scale is much more uncertain than temperature, and additional
43   uncertainties apply to polluted regions where aerosols are likely to interfere with the hydrologic cycle
44   (Chapters 7, 14). Seasonal differences in aerosol burdens versus precipitation preclude simple scaling of
45   aerosol response to precipitation changes (Fang et al., 2011; Kloster et al., 2010a). Other meteorological
46   changes, such as mixing depths and ventilation of the continental boundary layer, also influence the sign of
47   the aerosol changes (e.g., Dawson et al., 2009; Jacob and Winner, 2009; Kleeman, 2008; Mahmud et al.,
48   2010) and may in turn be sensitive to aerosol feedbacks on the vertical temperature structure (e.g., Roelofs,
49   2012; Zhang et al., 2010).

50

51   The coupling between physical climate and precursor emissions, both biogenic and anthropogenic, of O_3 and
52   aerosols is recognized but not well understood. For example, biogenic aerosol formation depends on
53   anthropogenic emissions and atmospheric oxidizing capacity (Carlton et al., 2010; Jiang et al., 2010). In
54   addition to climate-driven feedbacks from the biosphere, future land use changes may also influence regional
55   air quality (Chen et al., 2009a; Cook et al., 2009; Heald et al., 2008; Wu et al., 2012).

56

1 While PM is *likely* to decrease in regions where precipitation increases, consensus is lacking regarding the
2 relative importance of other potential impacts from changes in the physical climate, including feedbacks
3 from the biosphere, leading to *low confidence* in the overall impact of climate change alone on PM
4 distributions.
5
6 *11.3.5.2.2 Changes driven by regional and global anthropogenic pollutant emissions*
7 Projections for annual-mean surface O_3 and PM with diameter <2.5 μm ($PM_{2.5}$) for 2000 through 2100 are
8 shown in Figures 11.31a and 11.31b, respectively. Changes are spatially averaged over selected world (land-
9 only) regions and include the combined effects of emission and climate change under the RCPs. Results
10 include both multi-model ensembles of CMIP5 transient chemistry-climate simulations and the ACCMIP
11 time slice simulations. Values for the 1986–2005 reference period from the CMIP5 ensemble and for the
12 average of the 1980 and 2000 time slices for the ACCMIP ensemble are given in the top of each regional
13 box and show that the two different groups of models have markedly different reference O_3 pollution levels
14 in the northern hemisphere. Large inter-annual and regional variations are evident, as even the average of the
15 CMIP5 ensemble has noticeable year-to-year variations. In the near term (2030) surface O_3 under
16 RCP26/45/60 decreases or changes negligibly (<+1 ppb) over all major regions except South and East Asia;
17 while under RCP85, it degrades everywhere by as much as +4 ppb. In the long term (2100) under
18 RCP26/45/60, all major regions show improvements with decreases of –3 to –12 ppb, while under RCP85,
19 all regions show degradation with increases of up to +5 ppb (see Figures 11.30, 11.31a; and Annex II Tables
20 AII.7). Considering only RCP scenarios and the regions in Figure 11.31a, multi-model average surface O_3
21 changes of –4 to +5 ppb are projected by 2030 and –14 to +5 ppb by 2100.
22
23 The largest surface O_3 changes under the RCP scenarios are much smaller than those projected under the
24 older SRES scenarios (Figures 11.30, 11.31a; Annex II Tables AII.7; Lamarque et al., 2011a; Wild et al.,
25 2012). By 2100, global annual multi-model mean surface O_3 rises steadily by 12 ppb in SRES A2, but by 3
26 ppb in RCP8.5. The differences between 2030 projections with the CLE and MFR scenarios (–2.3 to +0.7
27 ppb; Dentener et al., 2005) are larger than the ACCMIP range of RCP26/45/60 (–1.5 to +0.3 ppb), but less
28 the RCP85 value (+1.7 ppb; see Figure 11.30, Tables AII.7). In particular, much larger O_3 decreases are
29 projected to occur by 2030 under MFR (Figure 11.31) which assumes that existing control technologies are
30 applied uniformly across the globe (Dentener et al., 2005). Under RCP8.5 the prominent rise in methane
31 abundances raises background O_3 levels, including in regions with aggressive controls on other O_3
32 precursors (Kawase et al., 2011; Lamarque et al., 2011c; Wild et al., 2012). Numerous earlier studies have
33 demonstrated the potential for rising global anthropogenic emissions of O_3 precursors, such as CH_4 and NO_x,
34 to enhance baseline O_3, offsetting local emission reductions, and lengthening the O_3 pollution season (Avise
35 et al., 2009; Chen et al., 2009b; Fiore et al., 2002; Fiore et al., 2009; Granier et al., 2006; Hogrefe et al.,
36 2004; HTAP, 2010c; Huang et al., 2008; Jacob et al., 1999; Lin et al., 2008; Prather et al., 2001; Prather et
37 al., 2003; Szopa et al., 2006; Tao et al., 2007; Wild et al., 2012; Wu et al., 2008a). Intercontinental transport
38 of O_3 has also been shown to contribute to individual high-O_3 events (Holloway et al., 2003; HTAP, 2010c;
39 Li et al., 2002; Lin et al., 2012; NRC, 2009; Yienger et al., 2000; Zhang et al., 2008).
40
41 The O_3 changes driven by RCP emissions scenarios with fixed, present-day climate (Figure 11.30; Wild et
42 al., 2012) are roughly equivalent to the changes estimated with the full chemistry-climate models (Figure
43 11.31a). While the regions considered are not identical, the evidence supports a major role for global
44 emissions in determining near-term O_3 air quality. Overall, the magnitude associated with the influence of
45 near-term climate change on global and regional O_3 air quality, as measured by the ranges across models
46 reported in the literature, is smaller than that of emission-driven changes (Figure 11.30; HTAP, 2010c; Wild
47 et al., 2011). In many regions and seasons, the influence of climate change on air quality may nevertheless
48 be important (Section 11.3.5.2.1).
49
50 Aerosol changes driven by anthropogenic emissions depend somewhat on oxidant levels (e.g., Kleeman,
51 2008; Unger et al., 2006a), but generally sulphate follows SO_2 emissions and carbonaceous aerosols follow
52 the primary elemental and organic carbon emissions. Changes in NO_x emissions influence nitrate aerosols to
53 a lesser extent than for SO_2 and sulphate due to competition between sulphate and nitrate for ammonium.
54 This competition leads to an inverse dependence between sulphate and nitrate such that increasing ammonia
55 (NH_3; precursor gas to ammonium in aerosol) while reducing sulphate offsets some of the benefit from SO_2
56 controls (Pye et al., 2009; see Chapters 7 and 8). Continued reductions in SO_2 emissions alongside rising
57 NH_3 emissions, as occurs in the RCP scenarios (Annex II) could lead to nitrate aerosol levels equivalent to or

1　surpassing sulphate aerosol levels in some regions over the next few decades (Bauer et al., 2007a; Bellouin
2　et al., 2011).
3
4　Projected changes in regional PM2.5 from the CMIP5 and ACCMIP chemistry-climate models following the
5　RCP scenarios suggest an overall decline over the 21st century for much of the globe, with little difference
6　across the individual scenarios except for the South and East Asia regions (Figure 11.31b). The noisy
7　projections over Africa, the Middle East, and to some extent Australia, reflect dust sources and their strong
8　dependence on meteorological variability from year to year. Over the two Asian regions, different PM2.5
9　levels between the RCPs are due to (i) OC emission trajectories over South Asia and (ii) combined changes
10　in carbonaceous aerosol and SO_2 over East Asia (Fiore et al., 2012).
11
12　Global emissions of aerosols and precursors also contribute to high-PM events under some situations. For
13　example, seasonal dust events are observed to increase aerosols in regions downwind of major source
14　regions, including trans-oceanic transport (Chin et al., 2007; Grousset et al., 2003; HTAP, 2010c; Huang et
15　al., 2008; Prospero, 1999). Other modelling studies document intercontinental transport of dust and other
16　aerosols, which can degrade downwind air quality (e.g., HTAP, 2010c; Liu et al., 2009; Ramanathan and
17　Feng, 2009). One study (Leibensperger et al., 2011a) suggests that intercontinental influences of NO_x and
18　CO emissions on PM can exceed those from SO_2 emissions particularly in regions with high PM pollution.
19　The balance between the relative importance of regional and global anthropogenic emissions versus climate-
20　driven changes for aerosol is likely to vary regionally with projected changes in precipitation, wildfires, dust,
21　and biogenic emissions (Section 11.3.5.2.1). Furthermore, the attribution to natural versus anthropogenic is
22　indirect and highly uncertain for dust and SOA (e.g., Ginoux et al., 2012; Hoyle et al., 2011).
23
24　In summary, there is *high confidence* that the range in air quality projections under the RCP scenarios is
25　much smaller than earlier estimates using the SRES scenarios, which projected a wider range of air pollutant
26　emissions. Comparison of air quality projections based solely on changes in climate versus that in
27　anthropogenic emissions of short-lived pollutants including CH_4 indicates that the range in projected surface
28　O_3 is wider for emission-driven changes than for physical climate changes driven by the greenhouse gases.
29　Aside from episodic dust and wildfire transport events particulate matter (PM) pollution is largely controlled
30　by regional emissions except in regions where precipitation changes dominate.
31
32　*11.3.5.2.3　Extreme weather and air pollution*
33　Air pollution events are typically associated with stagnation events, usually concurrent with heat waves,
34　whose frequency of occurrence can vary greatly from decade to decade (AR4 Chapter 7 Box; Leibensperger
35　et al., 2008; Tai et al., 2010). The 2003 European heat wave was associated with high air pollution and
36　related mortalities (Filleul et al., 2006; Stedman, 2004). In general all heat waves are associated with poor air
37　quality (Hodnebrog et al., 2012; Struzewska and Kaminski, 2008; Ordóñez et al., 2005; Tressol et al., 2008;
38　Vautard et al., 2005; Vieno et al., 2010). Anthropogenic climate change, even over the next few decades, has
39　increased the risk of such heat waves (Clark et al., 2010; Diffenbaugh and Ashfaq, 2010; Stott et al., 2004;
40　see Section 11.3.2.5.1). Globally, an index of warm spell duration increases under all of the RCP scenarios
41　for the CMIP5 model ensemble (Sillman et al., 2012), implying that in the absence of emission reductions,
42　the incidence of extreme air pollution events may also increase although a direct scaling is not appropriate
43　due to the dependence of air pollution on the local emissions (Section 11.3.5.2.1).
44
45　Meteorological conditions tied to O_3 and PM pollution events are likely to increase in frequency and duration
46　with climate change, although the severity of pollution events depend on the local emissions scenario (Chen
47　et al., 2009b; Forkel and Knoche, 2006; Hogrefe et al., 2004; Jiang et al., 2008; Liao et al., 2009; Mahmud et
48　al., 2008; Mickley et al., 2004; Murazaki and Hess, 2006; Nolte et al., 2008; Racherla and Adams, 2008;
49　Struzewska and Kaminski, 2008; Szopa et al., 2006; Tagaris et al., 2007; Tai et al., 2010; Vautard et al.,
50　2005; Wu et al., 2008b). Positive feedbacks from vegetation (higher emissions of O_3 and aerosol precursors
51　and lower stomatal O_3 deposition), wildfires, urbanization, and shifts in prevailing wind directions, may
52　further worsen air pollution during heat waves waves (Andersson and Engardt, 2010; Flannigan et al., 2009;
53　Hodnebrog et al., 2012; Jaffe and Wigder, 2012; Jiang et al., 2008; Royal Society, 2008; Vieno et al., 2010).
54　Over the United States and Europe, some studies suggest near-term increases in extreme O_3 events, but they
55　do not agree at the regional level (Huszar et al., 2011; Jacob and Winner, 2009; Jacobson, 2008b; Kleeman,
56　2008; Langner et al., 2012b; Weaver et al., 2009). Our understanding based on observations and models

1 indicates it is *likely* that, statistically, a warming climate will exacerbate extreme O_3 and PM pollution events
2 for some populated regions in the near term, even if the effect is not uniform.

3

4 **[INSERT FIGURE 11.30 HERE]**
5 **Figure 11.30:** Changes in surface O_3 (ppb) between year 2000 and 2030 averaged globally and over four northern mid-
6 latitude source regions as used in the Hemispheric Transport of Air Pollution (HTAP) studies (HTAP, 2010c). Results
7 are taken from the literature and include changes driven by climate alone (CLIMATE) as well as those driven by
8 emissions alone, following emission scenarios (SRES A1, A2, B1, B2; RCP 2.6, 4.5, 6.0, 8.5; MFR, CLE). Results
9 from individual studies are labeled by letters underneath the corresponding plot symbols. Solid vertical bars represent a
10 combination of ranges as reported in the literature: (A) multi-model mean and standard deviations in annual mean,
11 spatial averages from the ACCENT/Photocomp study (Dentener et al., 2006); (C) a parameterized model developed
12 from the multi-model HTAP ensemble (Wild et al., 2012). Dotted vertical bars represent spatial ranges as estimated
13 with one model: (S) globally (Stevenson et al., 2005), (V) within each of the HTAP regions (Dentener et al., 2005); (F,
14 D) over Europe (Forkel and Knoche, 2006; Szopa et al., 2006). Filled squares represent: (Q, T, U) regional averages
15 over the globe (Fiore et al., 2008; Unger et al., 2006b; West et al., 2006); and (W) over the United States (Fiore et al.,
16 2002). Regional definitions, methods, and reported metrics (e.g., 24-hour versus daily maximum values over a 1-hour
17 or 8-hour averaging period, annual or seasonal averages) vary across studies, and are the major contributor to the
18 apparent discrepancies between the blue (climate change only) solid and dashed lines (Section 11.3.5.2). Climate
19 change scenarios vary across studies, but are combined into ranges denoted by blue bars because there is little
20 detectable cross-scenario difference in the climate response by 2030 and it would not be detectable with the simulations
21 here (Sections 11.3.5.2.1 and 11.3.6). Adapted from Figure 3 of Fiore et al. (2012).

22

23 **[INSERT FIGURE 11.31a HERE]**
24 **Figure 11.31a:** Projected changes in annual mean surface O_3 (ppb mole fraction) from 2000 to 2100 following the RCP
25 scenarios (8.5 red, 6.0 orange, 4.5 light blue, 2.6 dark blue). Results in each box are averaged over the shaded land
26 regions with continuous colored lines denoting the average of 4 CMIP5 chemistry-climate models (GFDL-CM3, GISS-
27 E2-R, LMDz-ORINCA, NCAR-CAM3.5) and colored dots denoting the average of 3, 9, 2, and 11 (or fewer) ACCMIP
28 models contributing results for the decadal time slices centered on 2010, 2030, 2050 and 2100, respectively. The
29 shading about the lines and the vertical bars on the dots represent the full range across models. Changes are relative to
30 the 1986–2005 reference period for the CMIP5 transient simulations, and relative to the average of the 1980 and 2000
31 decadal time slices for the ACCMIP ensemble. The average value and model standard deviation for the reference period
32 is shown in each panel with CMIP5 models on the upper left and ACCMIP models on the upper right. In cases where
33 multiple ensemble members are available from a single model, they are averaged prior to inclusion in the multi-model
34 mean. Adapted from Fiore et al. (2012).

35

36 **[INSERT FIGURE 11.31b HERE]**
37 **Figure 11.31b:** Projected changes in annual-mean surface PM2.5 (ng per g air) from 2000 to 2100 following the RCP
38 scenarios (8.5 red, 6.0 orange, 4.5 light blue, 2.6 dark blue). PM2.5 values are calculated as the sum of individual
39 aerosol components (black carbon + organic carbon + sulfate + secondary organic aerosol + 0.1*dust + 0.25*sea salt).
40 Nitrate was not reported for most models and is not included here. See Figure 11.31a, but note that fewer models
41 contribute: GFDL-E2-R and GFDL-CM3 from CMIP5; CICERO-OsloCTM2, GFDL-AM3, MIROC-CHEM, and
42 NCAR-CAM3.5 from ACCMIP. Adapted from Fiore et al. (2012).

43

44 *11.3.6 Additional Uncertainties in Projections of Near-Term Climate*

45

46 As discussed in 11.3.1, most of the projections presented in 11.3.2–11.3.4 are based on the RCP4.5 scenario
47 and rely on the spread amongst the CMIP5 ensemble of opportunity as an ad-hoc measure of uncertainty. It
48 is possible that the real world might follow a path outside (above or below) the range projected by the
49 CMIP5 models. Such an eventuality could arise if there are processes operating in the real world that are
50 missing from, or inadequately represented in, the models. Two main possibilities must be considered: 1)
51 Future radiative and other forcings may diverge from the RCP4.5 scenario and, more generally, could fall
52 outside the range of *all* the RCP scenarios; 2) The response of the real climate system to radiative and other
53 forcing may differ from that projected by the CMIP5 models. A third possibility is that internal fluctuations
54 in the real climate system are inadequately simulated in the models. The fidelity of the CMIP5 models in
55 simulating internal climate variability is discussed in Chapter 9.

56

57 Future changes in radiative forcing will be caused by anthropogenic and natural processes. The
58 consequences for near-term climate of uncertainties in anthropogenic emissions and land use are discussed in
59 11.3.6.1. The uncertainties in natural radiative forcing that are most important for near term climate are those
60 associated with future volcanic eruptions and variations in the radiation received from the sun (solar output),

1   and are discussed in 11.3.6.2. In addition, carbon cycle and other biogeochemical feedbacks in a warming
2   climate could potentially lead to abundances of CO_2 and CH_4 (and hence radiative forcing) outside the range
3   of the RCP scenarios, but these feedbacks are not expected to play a major role in near term climate – see
4   Chapters 6 and 12 for further discussion.
5
6   The response of the climate system to radiative and other forcing is influenced by a very wide range of
7   processes, not all of which are adequately simulated in the CMIP5 models (Chapter 9). Of particular concern
8   for projections are mechanisms that could lead to major 'surprises' such as an abrupt or rapid change that
9   affects global-to-continental scale climate. Several such mechanisms are discussed in this assessment report;
10 these include: rapid changes in the Arctic (11.3.4.4 and Chapter 12); rapid changes in the ocean's
11 overturning circulation (Chapter 12); rapid change of ice sheets (Chapter 13); and rapid changes in regional
12 monsoon systems and hydrological climate (Chapter 14). Additional mechanisms may also exist as
13 synthesized in Chapter 12. These mechanisms have the potential to influence climate in the near term as well
14 as in the long term, albeit the likelihood of substantial impacts increases with global warming and is
15 generally lower for the near term. Section 11.3.6.3 provides an overall assessment of projections for global
16 mean surface air temperature, taking into account all known quantifiable uncertainties.
17
18 *11.3.6.1   Uncertainties in Future Anthropogenic Forcing and the Consequences for Near-Term Climate*
19
20 As discussed in Section 11.3.2.1.1, climate projections for the near term are not very sensitive to plausible
21 alternative scenarios for anthropogenic CO_2 emissions (Hawkins and Sutton, 2009; Meehl et al., 2007a; Stott
22 and Kettleborough, 2002; AR4 Chapter 10, Section 10.5.4.5; see also Section 11.2.2.1). However, near-term
23 projections may nevertheless be sensitive to alternative scenarios involving rapid reduction in emissions of
24 climate forcing agents with lifetimes shorter than CO_2, particularly the greenhouse gases CH_4 (lifetime of
25 about a decade; Annex II Table AII.5.8) and tropospheric O_3 (lifetime of weeks), as well as tropospheric
26 aerosols (lifetime of days). We assess here the potential for changes in near-term anthropogenic forcing to
27 induce climate responses that differ from the range of responses described in previous sections.
28
29 The range of near-term climate responses across the RCPs (Figure 11.32) provides one estimate for the
30 possible range in climate responses to different emission trajectories. For global mean temperatures in 2030,
31 the CMIP5 multi-model ensemble projects differences of less than 0.3 C between the RCP scenarios. This
32 inter-scenario spread reflects the sum of cross-scenario differences in CO_2 abundances, other greenhouse
33 gases, and aerosol forcings (see AII.6.12). For comparison, the inter-model spread for an individual scenario
34 (defined as the 5–95% range of the decadal means of the models) is around 0.8° C. The inter-scenario spread
35 increases with time, but remains smaller than the inter-model spread for a single scenario throughout the
36 near-term, becoming comparable by 2050.
37
38 The emission trajectories for aerosols and their precursors along the RCPs, however, span a narrow range.
39 The small range reflects the assumption underlying all four RCP scenarios of a uniformly aggressive
40 reduction of anthropogenic carbonaceous aerosol, sulphur dioxide (SO_2; the precursor gas to sulphate
41 aerosol) and other air pollutant emissions due to the implementation of abatement control technologies
42 globally (Lamarque et al., 2011a; van Vuuren et al., 2011; Annex II Table AII.2.20–22). The RCP emission
43 trajectories for SO_2, the precursor to sulphate aerosol, fall at the low end of the possible pathways in the
44 published literature and may not represent the most likely possible future (Hawkins and Sutton, 2009;
45 Hawkins and Sutton, 2010).
46
47 Anthropogenic aerosol impacts on global radiative forcing and temperatures are dominated by sulphate (see
48 Chapters 7 and 8). The rapid decline in sulphate that occurs with aggressive mitigation of air pollution or
49 fossil-fuel CO_2 emissions, such as projected under the RCPs and other scenarios, is projected to produce a
50 rapid rise in surface temperatures (e.g., Jacobson and Streets, 2009; Wigley et al., 2009; Makkonen et al.,
51 2012; Raes and Seinfeld, 2009). For example, the aerosol emission reductions following RCP4.5 induce a
52 few tenths of a degree warming by 2040–2050 (Levy et al., 2012). Kloster et al. (2010b) show that following
53 a maximum feasible aerosol-abatement scenario for 2030 results in a near doubling of the warming from
54 greenhouse gases alone (from +1 to +2 K). If the aggressive abatement strategies projected in the RCPs are
55 not achieved, then near-term warming will be less than is projected in the CMIP5 results. For this reason we
56 consider here additional scenarios, including the SRES used in the TAR and AR4. Although the RCPs and
57 SRES span a similar range of total radiative forcing, they include different ranges of aerosol, methane, and

1 tropospheric O_3 radiative forcing (Annex II Tables AII.6.2, AII.6.7, AII.6.9). Unfortunately, the SRES
2 aerosol emissions and RF were poorly defined and not uniformly applied in CMIP3 (see TAR Appendix II).
3 Most CMIP5 models include some representation of aerosol indirect effects (AIE) that were largely
4 neglected in CMIP3, however, processes related to AIE are model dependent and remain highly uncertain
5 (Chapters 7–10).
6
7 In the SRES and RCP scenarios, near-term CH_4 abundances and RF increase except for RCP2.6, which
8 projects decreases over the whole century (AII.4.2, 6.3; Lamarque et al., 2011c; Meinshausen et al., 2011).
9 From 2000 to 2030 the direct CH_4 RF changes range from –0.07 (RCP2.6) to +0.16 (RCP8.5 & SRES A2)
10 W m^{-2},(see AII.4.2, AII.6.2). By 2030 the RF change due to tropospheric O_3 changes since 2000 diverges
11 according to scenario from –0.04 (RCP2.6) to +0.08 (RCP8.5) W m^{-2}, and continues to diverge by 2100
12 from –0.20 (RCP2.6) to +0.24 (RCP8.5) W m^{-2}, reaching a total RF of up to 0.60 W m^{-2} (see Stevenson et
13 al., 2012; AII.6.7) From 2000 to 2030, multi-model global mean aerosol RF (AIE not included) increases by
14 0.01 (RCP8.5) to 0.09 (RCP2.6) W m^{-2} in CMIP5 and ACCMIP models, but the sign varies regionally and
15 the spread across the individual models is much larger, with one model projecting larger negative forcing
16 due to the inclusion of nitrate aerosol which is neglected in many CMIP5 models (Shindell et al., 2012a).
17
18 Projections under the most rapidly warming scenario (RCP8.5) emerge from the likely range of the other
19 RCP scenarios by 2040–2050. The enhanced warming by 2040 and 2050 in RCP8.5 and the UNEP Ref
20 scenario in Figure 11.32a (as well as the SRES A1-A2-B2; see AII4.2, TAR Appendix II) partially reflects
21 the rapid growth of methane as compared with the RCP2.6-4.5-6.0 scenarios (and SRES B1). One study
22 examined the range in global mean surface temperatures following extreme reductions in greenhouse gas
23 emissions: if all Annex I Kyoto greenhouse gas emissions (about 50% of all anthropogenic) were cut in 1990
24 then global cooling would reach –0.11 ± 0.03°C twelve years later (e.g., Jacobson and Streets, 2009; Wigley
25 et al., 2009). In contrast, reductions of reflective (cooling) aerosols in the RCP scenarios may enhance near-
26 term warming. For example, the larger warming in some CMIP5 models at 2020–2030 in RCP2.6 compared
27 to some of the other RCP scenarios (Figure 11.32a; compare upper likely and very likely ranges), may reflect
28 the much more rapid decline of SO_2 emissions under RCP2.6 than the other RCPs (e.g., Chalmers et al.,
29 2012).
30
31 By 2040, differences of 0.5°C–1.0°C between RCP2.6 and RCP8.5 emerge over substantial portions of the
32 globe in both summer and winter hemispheres, with projected warming over the Arctic differing by >1.5°C
33 during boreal winter. These patterns are further amplified by 2050, with temperature differences of more
34 than 1 K over large continental regions and >2.5°C during Arctic winter (Figure 11.32b). Applying pattern
35 scaling across future scenarios that have large decreases in aerosols such as the RCPs may not be valid. From
36 current literature it is unclear whether the spatial pattern of surface temperature response to aerosol forcing
37 mirrors that from greenhouse-gas forcing or, rather, follows local aerosol forcing patterns (Allen and
38 Sherwood, 2010, and references therein; Bollasina et al., 2011; Leibensperger et al., 2011b; Ming and
39 Ramaswamy, 2011; Ming et al., 2011; Ming et al., 2010; Ott et al., 2010; Randles and Ramaswamy, 2010).
40 A multi-model analysis suggests strong sensitivity of the surface temperature response to the latitudinal
41 forcing distribution but limited sensitivity to longitude, which may partially reconcile these discrepancies
42 (Shindell et al., 2010). At the regional scale, however, internal variability and model response uncertainty
43 may still dominate in the near-term (Ceppi et al., 2010; van Oldenborgh et al., 2010; van Oldenborgh et al.,
44 2009b).
45
46 Several studies have identified approaches to slowing near-term climate warming while also improving air
47 quality by decreasing CH_4, tropospheric O_3, and absorbing aerosols, particularly black carbon aerosols (Moss
48 et al., 2010; van Vuuren et al., 2011). To illustrate the potential impact of mitigation strategies targeting
49 near-term climate forcing species (methane and black carbon), the three UNEP/WMO scenarios (UNEP and
50 WMO, 2011) are also included in Figure 11.32a. These estimates are made with only two climate models
51 and thus do not have the same level of assessment and uncertainty ranges derived from the CMIP3 and
52 CMIP5 ensembles. Under one scenario, current control technology for CH_4 emissions, implemented
53 worldwide by 2030 (a 24% decrease in anthropogenic CH_4 emissions relative to 2010-levels) lessens
54 warming by 0.2–0.4 K (estimated central range) between 2030 and 2050. This temperature change is
55 comparable to the near-term spread across the RCP scenarios. Under a second scenario, current control
56 technologies are implemented for both methane and black carbon. The controls on black carbon (a 78%
57 decrease from 2010-levels) and co-emitted species worldwide by 2030 lessen warming by an additional 0.0–

1   0.2 K but with larger uncertainties. Some models also suggest relatively greater responses over the Arctic to
2   black carbon aerosol controls (Flanner et al., 2007a; Jacobson, 2010; Quinn et al., 2008; Ramana et al.,
3   2010). While removal of black carbon (BC) aerosol could counter some of the sulphate impact on surface
4   temperature, there is considerable uncertainty as to the net impact of BC due to poor understanding of
5   aerosol indirect effects as well as of the ratio of BC to co-emitted reflective organic carbon (OC) aerosols,
6   their size distributions and mixing states (Dentener et al., 2005; Fiore et al., 2008; Fiore et al., 2002; Hansen
7   et al., 2000; Jacobson, 2010; United Nations and World Meteorological Organization, 2011; Royal Society,
8   2008; West et al., 2006).
9
10   In addition to their influence on surface temperature, changes in anthropogenic aerosol sources may induce
11   changes in regional atmospheric circulation and precipitation. Precipitation responses to changes in aerosol
12   optical depth, anthropogenic aerosols, and specific fuel emissions sectors for 2030 and 2050 have been found
13   in several modeling studies (e.g., Jacobson and Streets, 2009; Menon and et al., 2008; Roeckner et al., 2006).
14   Changes in aerosols have been shown to contribute to circulation changes, influencing aspects such as the
15   width of the tropics, Arctic-Oscillation phasing, monsoons, jet locations, and associated precipitation (Allen
16   and Sherwood, 2010, and references therein; Bollasina et al., 2011; Leibensperger et al., 2011b; Ming and
17   Ramaswamy, 2011; Ming et al., 2010; Ming et al., 2011; Ott et al., 2010; Randles and Ramaswamy, 2010).
18   Regionally observed precipitation trends over Africa, South Asia and northern China over the past decades
19   have been attributed at least partially to anthropogenic aerosol forcing (Bollasina et al., 2011; Ramanathan
20   and Carmichael, 2008; Shindell et al., 2012c), suggesting that aerosol decreases in these regions over the
21   next century could reverse these trends (cf. also Chapters 10 and 14). Positive feedbacks with soil moisture
22   and low cloud cover imply a larger sensitivity of extremes (heat waves and associated air pollution events)
23   over the United States to the aerosol emission scenario (Leibensperger et al., 2011b; Mickley et al., 2011).
24   Similar amplifying feedbacks have been implicated for European warming, including through fog reduction
25   (Ceppi et al., 2010; van Oldenborgh et al., 2010; van Oldenborgh et al., 2009b). The lack of uniformity
26   across studies, which addressed different regions and relative balances of reflecting versus absorbing
27   aerosols, complicates generalization of these findings.
28
29   Land use and changes in land use (LULUC) including deforestation and forest degradation can alter climate
30   forcing through changing surface albedo, hydrological cycle, greenhouse gases, or atmospheric aerosols.
31   These LULUC changes in albedo have been assessed since the TAR as part of the radiative forcing (Chapter
32   8). The other major LULUC impact has been on CO_2 emissions, and future LULUC is expected to alter CO_2
33   abundances (see Chapters 6 and 12). Changes in CH_4 emissions due to agriculture and other land use are
34   anticipated in the RCP scenarios. In the RCPs, land use change projections vary widely depending on the
35   underlying socio-economic storylines, but on the global scale, the relative area of land projected to be
36   subject to change for the coming decades is relatively modest (Hurtt et al., 2011) Land use change can give
37   rise to systematic changes in the regional climate, as shown by both case studies and coordinated global
38   modelling experiments (e.g., Pitman et al., 2009). Apart from first order regional climate effects related to
39   changes in the surface albedo upon transferring natural vegetation into cropland or pasture, alterations in the
40   seasonal cycle of the energy balance may cause changes to a number of variables that at the regional scale
41   are of similar magnitude (but opposite sign) to the signal induced by greenhouse warming (de Noblet-
42   Ducoudre et al., 2012). The expected impacts of LULUC are, for the most part, long term and not expected
43   to drive substantial climate change on regional or larger scales in the near term. On local scales, larger
44   impacts are possible through changes in hydrometeorology, but such local impacts are beyond the scope of
45   this report.
46
47   In summary, whilst climate projections for the near term are not very sensitive to plausible alternative
48   scenarios for anthropogenic emissions of CO_2 and other long-lived greenhouse gases, emissions of
49   anthropogenic aerosols and their effects on climate are a major source of uncertainty in near term
50   projections, especially on regional scales. Removal of sulphate aerosol as in the RCPs, whether undertaken
51   as measures to decrease CO_2 emissions or to improve air quality, could lead to rapid near-term warming.
52   There is strong evidence that accompanying controls on CH_4 emissions would offset some of this sulphate-
53   induced warming. While removal of black carbon aerosol could also counter warming associated with
54   sulphate removal, uncertainties are too large to constrain the net sign of the global temperature response to
55   BC emission reductions, which depends on co-emitted (reflective) aerosols and AIE. Finally, an
56   overestimate of sulphate reductions under the RCP scenarios implies that the CMIP5 models would project
57   excessive near-term warming.

[INSERT FIGURE 11.32a HERE]

Figure 11.32a: Near-term increase in global mean surface air temperatures across scenarios. Increases in 10-year mean (2016–2025, 2026–2035, 2036–2045 and 2046–2055) relative to the reference period (1986–2005) of the globally averaged surface air temperatures (K). Results are shown for the CMIP5 model ensembles (see Annex I for listing of models included) for RCP2.6 (dark blue), RCP4.5 (light blue), RCP6.0 (orange), and RCP8.5 (red), respectively) and the CMIP3 model ensemble (22 models for SRES A1b (black). The multi-model median (square), 17–83% (likely) range (wide boxes), 5–95% (very likely) range (whiskers) across all models are shown for each decade and scenario. Also shown are estimates for scenarios that implement technological controls on methane emissions (UNEP CH_4) and on emissions of methane and black carbon as well as co-emitted species such as carbon monoxide, organic carbon and nitrogen oxides (UNEP CH_4 + BC). These changes are calculated relative to a reference scenario (UNEP Ref) but adjusted to reflect the 1986–2005 reference period shown here. UNEP results are based on two chemistry-climate models and shown only as a range (whiskers) derived from uncertainties in radiative forcing components and climate sensitivity (Shindell et al., 2012b; UNEP and WMO, 2011). The thick horizontal lines indicate increases in global mean surface air temperature relative to a reference period of 1850–1900 (rather than 1986–2005).

[INSERT FIGURE 11.32b HERE]

Figure 11.32b: Global maps of near-term differences in surface air temperature across the RCP scenarios. Differences between the high (RCP8.5) and low (RCP2.6) scenarios for the CMIP5 model ensemble (12 models) are shown for averages over 2026–2035 (left), 2036–2045 (middle) and 2046–2055 (right) in boreal winter (DJF; top row) and summer (JJA; bottom row).

11.3.6.2   Uncertainties in Future Natural Radiative Forcing and the Consequences for Near-Term Climate

11.3.6.2.1   The effects of future volcanic eruptions
Natural climate forcing with the largest shock value in the near-term is likely to be explosive volcanic eruptions like that of Mount Pinatubo in 1991, regarded as one of the largest in recent times with a return period of about 3 times per century, but dwarfed by Tamobora in 1815 (Gao et al., 2008). Pinatubo caused a rapid drop in a global mean surface air temperature of about –0.5°C over the following year, but this signal disappeared over the next five years (Bender et al., 2010; Hansen et al., 1992; Soden et al., 2002). As discussed in Chapter 8, explosive volcanic eruptions are the major cause of natural variations in radiative forcing on interannual to decadal time scales. Most important are large tropical and subtropical eruptions that inject substantial amounts of sulfur dioxide gas (SO_2) directly into the stratosphere. The subsequent formation of sulphate aerosols leads to a negative radiative forcing of several W m^{-2}, with a typical lifetime of a year (Robock, 2000). In addition to global mean cooling, there are effects on the hydrological cycle (e.g., Trenberth and Dai, 2007), atmosphere and ocean circulation (e.g., Stenchikov et al., 2006). The surface climate response typically persists for a few years, but the subsurface ocean response can persist for decades or centuries, with consequences for sea level rise (Delworth et al., 2005; Gregory, 2010; Stenchikov et al., 2009).

Whilst it is possible to detect when various existing volcanoes become more active, or are more likely to erupt, the precise timing of an eruption, the amount of sulfur dioxide emitted and its distribution in the stratosphere are not predictable until after the eruption. Eruptions comparable to Mount Pinatubo can be expected to cause a short term cooling of the climate with related effects on surface climate that persist for a few years before a return to warming trajectories discussed in Section 11.3.2. Larger eruptions, or several eruptions occurring close together in time, would lead to larger and/or more persistent effects.

11.3.6.2.2   The effects of future changes in solar forcing
The future CMIP5 climate simulations using the RCP scenarios include an 11-year variation in total solar irradiance (TSI) but no underlying trend beyond 2005. Chapter 10 noted that there has been little observed trend in TSI during a time period of rapid global warming since the late 1970s, but that the 11-year solar cycle does introduce a significant and measurable pattern of response in the troposphere (10.3.1.1.3). As discussed in Chapter 8 (8.3.1), the Sun is in a 'grand solar maximum' of magnetic activity on the multi-decadal timescale. However, the most recent solar minimum was the lowest and longest since 1920. Some studies (e.g., Lockwood, 2010) suggest there may be a continued decline towards a much quieter period in the coming decades, but there is no consensus on this point (see 8.3.1.3). Using historical analogues of the current solar state to project TSI (Jones et al., 2012) gives a mean TSI value for the period 2030–2050 that is approximately 0.03% lower than the average for the historical reference period 1986–2005. At the lower end of these projections, the range includes the possibility that TSI may fall by 2060 to levels last seen during the

1   Maunder Minimum (MM; late 17th century). However, a smaller decline is more likely: Lockwood et al.
2   (2010) suggests an 8% chance that the Sun will have returned to MM conditions by 2060 (and a 50% chance
3   by 2120). The mean of the projected TSI changes corresponds to a mean change in solar Radiative Forcing
4   (RF) of approximately –0.1 W m^{-2} by 2050 (using TOA instantaneous RF – see Section 8.3.1). Assuming a
5   climate sensitivity parameter of 0.8 K (W m^{-2})$^{-1}$ this translates to a global mean temperature change of –0.08
6   K, and this anomaly is unlikely to exceed –0.1 K. Using a simplified coupled climate model, Feulner and
7   Rahmstorf (2010) showed that a grand solar minimum, similar to that of the Maunder Minimum in the 17th
8   century, would produce a decrease in global temperatures much smaller than the warming expected from
9   increases in anthropogenic greenhouse gases; however, regional impacts could be more significant (Gray et
10 al., 2010; Ineson et al., 2011; Mann et al., 2009; Xoplaki et al., 2001).
11
12 As discussed in Section 8.2.1.4.1, a recent satellite measurement (Harder et al., 2009) found much greater
13 than expected reduction at UV wavelengths in the recent declining solar cycle phase. Changes in solar uv
14 drive stratospheric O$_3$ chemistry and can change RF. Haigh et al. (2010) show that if these observations are
15 correct, they imply the opposite relationship between solar RF and solar activity over that period than has
16 hitherto been assumed. These new measurements therefore increase uncertainty in estimates of the sign of
17 solar RF, but they are unlikely to alter estimates of the maximum absolute magnitude of the solar
18 contribution to RF, which remains small (Chapter 8). However, they do suggest the possibility of a much
19 larger impact of solar variations on the stratosphere than previously thought, and some studies have
20 suggested that this may lead to significant regional impacts on climate (as discussed in 10.3.1.1.3), that are
21 not necessarily reflected by the RF metric (see 8.2.16).
22
23 In summary, possible future reductions in solar irradiance would act to cool global mean surface air
24 temperature but such cooling is *unlikely* to exceed –0.1°C by 2050 (medium confidence). A return to
25 conditions similar to the Maunder Minimum is considered *very unlikely* in the near term but, were it to
26 occur, would produce a decrease in global temperatures much smaller than the warming expected from
27 increases in anthropogenic greenhouse gases. However, current understanding of the impacts of solar activity
28 on regional climate remains low.
29
30 *11.3.6.3   Synthesis of Projections for Global Mean Surface Air Temperature*
31
32 Figure 11.33 provides a synthesis of near term projections of global mean surface air temperature from
33 CMIP5, CMIP3, and studies that have attempted to use observations to quantify the projection uncertainty
34 (Rowlands et al., 2012; Stott et al., 2012; see 11.3.2.1). On the basis of this evidence, an attempt is made
35 here to assess a likely range for global mean temperature in the period 2016–2035. Such an overall
36 assessment is not straightforward. The following points are particularly important to recognise:
37 1) No likelihoods are associated with the different RCP or other scenarios. For this reason, previous IPCC
38   Assessment Reports have only presented projections that are conditional on specific scenarios. The
39   arguments for taking a different approach here are that: a) near term projections are not highly sensitive
40   to alternative scenarios, and b) there is some evidence, discussed in 11.3.6.1, that anthropogenic aerosols
41   may not decline as rapidly as assumed in the RCP scenarios, and therefore that the CMIP5 projections
42   may tend to overestimate the rate of near term warming. Figure 11.33c shows that the CMIP3 projections
43   based on the SRES B1, A1B and A2 scenarios are generally cooler than the CMIP5 projections based on
44   the RCP scenarios.
45 2) As discussed in 11.3.6.2, the RCP scenarios assume no underlying trend in total solar irradiance and no
46   future volcanic eruptions. However, future volcanic eruptions cannot be predicted and there is low
47   confidence in projected changes in solar irradiance (Chapter 8). Consequently the possible effects of
48   future changes in natural forcings are excluded from the assessment in this section.
49 3) There is no consensus in the literature regarding the best way to use observations to constrain the
50   uncertainty in projections. As discussed in 11.3.2.1.1, results using the ASK method (Stott, 2012)
51   suggest a lower range than is obtained from the raw CMIP5 results (i.e., that the models that warm most
52   rapidly are *unlikely* to be consistent with observations). Biases in ASK derived projections could arise
53   from errors in the specified forcings and/or from errors in the model-simulated patterns of response. It is
54   not clear that such errors should introduce a systematic bias (of either sign), but they are more likely to
55   make the projections over-confident, so the ASK ranges might be too narrow. The Rowlands et al.
56   (2012) results for the SRES A1B scenario, which are based on a very large perturbed physics ensemble
57   of simulations, show a larger range of uncertainty than the corresponding CMIP3 results, and the ASK

results for RCP4.5 and RCP8.5, but the observational constraint only used observations of the past 50 years (much shorter than for ASK). Rowlands et al. (2012) also report that using a longer observational record (though still shorter than used for the ASK results) reduces the upper bound on their likely range by about 0.2 K at 2050.

4) Over the last two decades the rate of global warming that has been observed is at the lower end of rates simulated by CMIP5 models. Evidence assessed in Chapter 10 (10.3.1.1.3) indicates that part of the explanation is likely to be internal variability, suggesting that some acceleration in the rate of warming may be expected in the next decade or so. On the other hand, there may be a contribution from errors in the anthropogenic or natural forcings specified in the models, and/or errors in model sensitivity. If forcing or model errors are dominant, there is no obvious reason to expect an imminent acceleration in the rate of observed warming.

5) All the projections rely on climate models to some extent. As emphasised in the Introduction to 11.3.6, there may be processes operating in the real world that are missing from, or inadequately represented in, the models.

Overall, in the absence of major volcanic eruptions – which would cause significant but temporary cooling – and, assuming no significant long term changes in solar irradiance, it is *likely* (>66% probability) that the global mean surface air temperature anomaly for the period 2016–2035, relative to the reference period of 1986–2005 will be in the range 0.4–1.0°C *(medium confidence)*. This range spans the likely ranges obtained from all the raw CMIP3 and CMIP5 results, except for the upper bound obtained for RCP8.5. An upper bound above 1.0°C is considered inappropraite in view of the ASK results, the evidence that anthropogenic aerosols may not decline as rapidly as assumed in the RCP scenarios, and the sensitivity of the Rowlands et al. (2012) results to using a longer observational record. The 0.4–1.0°C range is consistent with the AR4 SPM statement that 'For the next few decades a warming of about 0.2°C per decade is projected for a range of SRES emission scenarios'. Note also that the projections in Figure 11.33c suggest that the uncertainty in future global mean temperature is skewed; on the basis of this evidence it is *more likely than not* that that actual warming will be closer to the lower bound of 0.4˚C than the upper bound of 1.0˚C *(medium confidence)*.

[INSERT FIGURE 11.33 HERE]

Figure 11.33: Synthesis of near-term projections of global mean surface air temperature. a) Projections of global mean, annual mean surface air temperature (SAT) 1986–2050 (anomalies relative to 1986–2005) under all RCPs from CMIP5 models (grey and coloured lines, one ensemble member per model), with four observational estimates (HadCRUT3: Brohan et al., 2006; ERA-Interim: Simmons et al., 2010; GISTEMP: Hansen et al., 2010; NOAA: Smith et al., 2008) for the period 1986–2011 (black lines); b) as a) but showing the 5–95% range for RCP4.5 (light grey shades, with the multi-model median in white) and all RCPs (dark grey shades) of decadal mean CMIP5 projections using one ensemble member per model, and decadal mean observational estimates (black lines). The maximum and minimum values from CMIP5 are shown by the grey lines. An assessed *likely* range for the mean of the period 2016–2035 is indicated by the black solid bar. The '2°C above pre-industrial' level is indicated with a thin black line, assuming a warming of global mean SAT prior to 1986–2005 of 0.6°C. c) A synthesis of ranges for the mean SAT for 2016–2035 using SRES CMIP3, RCPs CMIP5, observationally constrained projections (Stott et al., 2012; Rowlands et al., 2012; updated to remove simulations with large future volcanic eruptions), and an overall assessment. The box and whiskers represent the *likely* (66%) and *very likely* (90%) ranges. The dots for the CMIP3 and CMIP5 estimates show the maximum and minimum values in the ensemble. The median (or maximum likelihood estimate for Rowlands et al., 2012) are indicated by a grey band.

The results shown in Figures 11.32 and 11.33 may be used to assess the likelihood that global mean surface temperatures will cross policy-relevant levels, such 1.5°C or 2°C above pre-industrial conditions, by specific dates (Joshi et al., 2011). Table 11.2 shows likelihoods of crossing specific temperature levels by 2050, based on the raw CMIP5 results and also moderated assessments that take into account the evidence discussed in 11.3.2.1.1 and 11.3.6.3 that those CMIP5 models that warm most rapidly may be inconsistent with observations. These results assume that the warming of global mean temperature prior to the reference period of 1986–2005 was 0.6°C, based on a comparison with the mean for 1850–1900 using the HadCRUT4 dataset (Morice et al., 2012). Note that it is expected that specific temperature levels will be temporarily crossed in individual years before a permanent crossing is established (Joshi et al., 2011).

Key results from Table 11.2 are as follows. By 2050: under RCP2.6 it is *about as likely as not* that the 1.5°C level will be crossed and *very unlikely* that the 2°C level will be crossed; under RCP4.5 and RCP6.0 it is

1   *likely* that 1.5°C level will be crossed, and *unlikely* that the 2°C threshold will be crossed; under RCP8.5 it is
2   *very likely* that the 1.5°C level will be crossed and *likely* that the 2°C level will be crossed.
3
4
5   **Table 11.2:** Likelihood of global mean surface air temperature (SAT) crossing specified temperature levels relative to
6   an estimate of pre-industrial climate. The tabulated numbers show the percentage of CMIP5 models that show a
7   warming of decadal mean SAT greater than or equal to the specified level by 2050, based on all available models.
8   (Very similar results are obtained if only the models for which data for all four RCP scenarios are available is used.)
9   The assessed likelihoods are moderated based on the evidence discussed in 11.3.2.1.1 and 11.3.6.3 that those CMIP5
10   models that warm most rapidly may be inconsistent with observations. These results assume that the warming of global
11   mean temperature prior to the reference period of 1986–2005 was 0.6°C, based on a comparison with the mean for
12   1850–1900 using the HadCRUT4 dataset (Morice et al., 2012), and assume no future volcanic eruptions.

Temperature Threshold	RCP Scenario:	RCP2.6	RCP4.5	RCP6.0	RCP8.5
1.5°C by 2050	% of CMIP5 Models	52	95	80	100
	Assessed Likelihood	*about as likely as not*	*likely*	*likely*	*very likely*
2.0°C by 2050	% of CMIP5 Models	19	38	25	86
	Assessed Likelihood	*very unlikely*	*unlikely*	*unlikely*	*likely*

13
14
15   **[START BOX 11.2 HERE]**
16
17   **Box 11.2: Ability of Climate Models to Simulate Observed Regional Trends**
18
19   [PLACEHOLDER FOR FINAL DRAFT: Within which chapter this Box will be placed is to be decided.]
20
21   Past performace of climate models on regional scales can be used to investigate the relationship between the
22   multi-model ensemble spread and the uncertainty arising from local forcing uncertainty and model
23   deficiencies. Agreement between observed and simulated regional trends, taking natural variability and
24   model spread into account, builds confidence in near-term projections. On sub-continental and smaller scales
25   the trends are, in general, not represented well by climate models (Benestad, 2012; Stott et al., 2010).
26   Downscaling with RCMs does not affect seasonal mean trends except near mountains or coastlines. Given
27   the statistical nature of the comparisons, it is currently not possible to say in which regions observed
28   discrepancies are due to coincidental natural variability and in which regions they are due to forcing or
29   model deficiencies. They show that the CMIP5 ensemble cannot be taken as a probability forecast, but that
30   the true uncertainty can be larger than the model spread indicated in the maps in this chapter and Annex I.
31
32   *Temperature*
33   Räisänen (2007) and Yokohata et al. (2012) compared regional linear temperature trends during 1955–2005
34   with corresponding trends in the CMIP3 ensemble. They found that the range of simulated trends captured
35   the observed trend in nearly all locations, even though the range in global mean temperature is larger than
36   observed (Chapter 2). Using another metric, Knutson et al. (2012a) found that CMIP5 models did slightly
37   better than CMIP3 in reproducing linear trends (Figure 11.34, see also Figure 10.2 FOD). However, some of
38   the apparent agreement appears to be for the wrong reason. Many of the models that appear to correctly
39   simulate observed high regional trends do so because they have a high climate response (i.e., the global
40   temperature rises quickly) and do not simulate the observed spatial pattern of trends (Kumar et al., 2012). To
41   address his, Bhend and Whetton (2012) and Drijfhout and van Oldenborgh (2012) used another definition of
42   the local trend: the regression of the local temperature on the (low-pass filtered) global mean temperature.
43   This definition separates the local temperature response pattern from the global-mean climate response. They
44   found highly significant discrepancies in the CMIP3 and CMIP5 trend patterns from the variety of estimates
45   of observed trend estimates. In December–February the observed Arctic amplification in Asia and North
46   America extends further south than modelled, in June–August southern Europe and North Africa have
47   warmed significantly faster than both CMIP3 and CMIP5 models (van Oldenborgh et al., 2009a), The
48   observed Indo-Pacific warm pool trend were significantly higher than the models year-round (Funk et al.,
49   2012; Shin and Sardeshmukh, 2011; Williams and Funk, 2011), and the North Pacific and the southeastern
50   US and adjoining ocean trends were lower. Direct causes for many of these discrepancies are known (e.g.,
51   circulation trends that differ between the observation and the models [Bhend and Whetton, 2012; Gillett et

1   al., 2005; Gillett and Stott, 2009; van Oldenborgh et al., 2009a] or teleconnections from other areas with
2   trend biases [Deser and Phillips, 2009; Meehl et al., 2012b]), but the causes of the underlying discrepancies
3   are often unknown. Possibilities include an underestimation of the low-frequency variability (Knutson et al.,
4   (2012a) show evidence that this is not likely), unrealistic local forcing (e.g., aerosols; Ruckstuhl and Norris,
5   2009), or missing or misrepresented processes in models (e.g., fog; Ceppi et al., 2010; Vautard et al., 2009).

7   *Precipitation*
8   Regional linear precipitation trends have been found to differ significantly between observations and CMIP3
9   models, both in the zonal mean (Allan and Soden, 2007; Zhang et al., 2007b) and regionally (Räisänen,
10 2007). In Europe there are large-scale differences in GCMs and RCMs (Bhend and von Storch, 2008), which
11 are ascribed to circulation change discreoancies in winter and in summer SST trend biases (Haren et al.,
12 2011, 2012; Lenderink et al., 2009) and the misrepresentation of Summer NAO teleconnections (Bladé et al.,
13 2012). Precipitation trends discrepancies in East Africa have been traced to the Indo-Pacific warm pool
14 warming (Williams and Funk, 2011). Larger northwest Australian rainfall increases than in CMIP3 are
15 driven by ozone forcings in one climate model (Kang et al., 2011) and aerosols in another (Rotstayn et al.,
16 2012). The CMIP5 patterns seem to reproduce the observed ones somewhat better than the CMIP3 patterns
17 (Bhend and Whetton, 2012; Figure 11.xx)

19 **[INSERT FIGURE 11.34 HERE]**
20 **Figure 11.34:** a) Observed linear December to February temperature trend 1950–2010 (CRUTEM3/HadSST2)
21 [°C/century], b) the equivelant CMIP5 ensemble mean trend and c) quantile of the observed trend in the ensemble.
22 d,e,f) Same for June to August. g,h,i) Same for October to March precipitation (CRU TS 3.10.01) [% per century]. j,k,l)
23 Precipitation in April to September. Based on Räisänen (2007).

25 **[END BOX 11.2 HERE]**

27 **[START FAQ 11.1 HERE]**

29 **FAQ 11.1: If You cannot Predict the Weather Next Month, How can You Predict Climate for the**
30 **Coming Decade?**

32 *Climate can sometimes be predicted with a degree of skill much further into the future than weather can be*
33 *predicted accurately. In order to understand why, we first need to recognise that, while weather and climate*
34 *are intertwined, they are in fact very different things. Weather is defined as the state of the atmosphere at a*
35 *given time and place, and can change from hour to hour and even minute to minute. Climate, on the other*
36 *hand, generally refers to the statistics of weather conditions over a decade or more.*

38 *Weather forecasts typically provide detailed information on future air temperature, precipitation and many*
39 *other factors at specific times in the future. To make accurate predictions, weather forecasters need detailed*
40 *information about the current state of the atmosphere. Even the tiniest error in that depiction inevitably*
41 *typically leads to very poor forecasts beyond a week or two. This is the so-called 'butterfly effect'.*

43 *Climate predictions, on the other hand, can have some accuracy for periods far beyond one week into the*
44 *future. Warming of the planet in response to anthropogenic greenhouse gas emissions, for example, can*
45 *change the statistics of future weather conditions, as can other factors, such as sulphate aerosols. Some of*
46 *these changes can be predicted to an extent by climate scientists, even though they cannot predict the hour-*
47 *to-hour or day-to-day evolution of weather conditions beyond a week or so.*

49 *In a similar manner it can be confidently predicted at the end of spring, that the average surface air*
50 *temperature over the coming summer in Capetown (for example) will very likely be higher than the average*
51 *temperature during the most recent spring—even though the day-to-day weather during the coming summer*
52 *cannot be predicted with accuracy beyond a week. While the reasons for this stark contrast in accuracy are*
53 *different, the underlying principle is the same: a degree of accuracy in predicting changes in the statistics of*
54 *weather over a coming season or decade does not depend on accuracy in predicting the weather over the*
55 *same period.*

The statistics of weather conditions used to define climate include long-term averages of air temperature and rainfall, as well as statistics of their variability, such as the standard deviation of year-to-year rainfall variability from the long-term average, or the frequency of days below 5°C. Averages of climate variables over long periods of time are called climatological averages. They can apply to individual months, seasons or the year as a whole. A climate prediction will address questions like: 'How likely will it be that the average temperature during the coming summer will be higher than the long-term average of past summers?' or: 'How likely will it be that the next decade will be warmer than past decades?' More specifically, a climate prediction might provide an answer to the question: 'What is the probability that temperature (in Australia, for instance) averaged over the next ten years will exceed the temperature in Australia averaged over the past 30 years?' Climate predictions do not provide forecasts of the detailed day-to-day evolution of future weather. Instead, they provide probabilities of long-term changes to the statistics of future climatic variables.

Weather forecasts, on the other hand, provide predictions on future day-to-day weather changes. They help to address questions like: 'Will it rain tomorrow?' or 'How much rain will fall?' Sometimes, weather forecasts are given in terms of probabilities. For example, the weather forecast might state that: 'the likelihood of rainfall in Apia tomorrow is 75%'.

Climate scientists do not attempt or claim to predict the detailed future evolution of the weather – its chaotic nature generally makes accurate predictions beyond a week impossible. There is, on the other hand, a sound scientific basis for supposing that aspects of climate can be predicted, albeit imprecisely.

We know, for example, that increases in long-lived atmospheric greenhouse gas concentrations tend to increase surface temperature in future decades. Thus, information from the past can and does help predict future climate.

Naturally occurring so-called 'internal' variability can—in theory at least—extend our capacity to predict future climate. Internal climatic variability mostly arises from natural instabilities in the climate system. The El Niño-Southern Oscillation phenomenon is probably the most famous example of this. If such variability includes or causes extensive, long-lived, upper ocean temperature anomalies, this will drive changes in the overlying atmosphere, both locally and remotely.

Some internal variability—including the El Niño-Southern Oscillation—unfolds in a partially predictable fashion. Meteorological services and other agencies exploit this. They have developed seasonal-to-interannual prediction systems that enable them to routinely predict seasonal climate anomalies. These systems have demonstrable predictive skill, though that skill varies markedly from place to place, season to season, and variable to variable. Skill tends to diminish the further the prediction delves into the future and in some locations or seasons, there is no skill at all. In case you are wondering, 'skill' is used here in its technical sense. It is a measure of how much greater the accuracy of a prediction is, compared with the accuracy of some typically simple prediction method like assuming that recent anomalies will persist during the period being predicted, or that the weather is just typical for that time of year.

Unlike seasonal-to-interannual prediction systems, decadal prediction systems are very much in their infancy. These systems are designed to exploit both externally-forced and internally-generated sources of predictability. Climate scientists distinguish between decadal predictions and decadal projections, which only exploit the predictive capacity arising from external forcing. While previous IPCC Assessment Reports focussed exclusively on projections, this report also assesses decadal prediction research and its scientific basis.

Despite their infancy, decadal prediction systems exhibit statistically significant (though imperfect) skill in predicting near-surface temperature over much of the globe out to at least nine years. The bulk of this skill is thought to arise from external forcing. Theory indicates that skill in predicting decadal surface temperature should exceed skill in predicting decadal precipitation, and this has proven to be the case.

Current research is aimed at improving decadal prediction systems, and understanding the reasons for any apparent skill. Ascertaining the degree to which the extra information from internal variability actually translates to skill beyond that arising from external forcing alone is a key issue.

1
2   While prediction systems are expected to improve over coming decades, the chaotic nature of the climate
3   system will always impose unavoidable limits on predictive skill.
4
5   **[END FAQ 11.1 HERE]**
6
7   **[BEGIN FAQ 11.2 HERE]**
8
9   **FAQ 11.2: How Do Volcanic Eruptions Affect Climate and Our Ability to Predict Climate?**
10
11   *Large volcanic eruptions affect the climate by injecting sulphur dioxide gas into the upper atmosphere,*
12   *which reacts with water to form clouds of sulphuric acid droplets. These clouds reflect sunlight back to*
13   *space, preventing its energy from reaching the Earth's surface, thus cooling it, along with the lower*
14   *atmosphere. These upper atmospheric sulphuric acid clouds also locally absorb energy from the sun, the*
15   *Earth and the lower atmosphere, which heats the upper atmosphere (see FAQ 11.2, Figure 1). In terms of*
16   *surface cooling, the 1991 Mt. Pinatubo eruption in the Philippines, for example, injected about 20 million*
17   *tons of sulphur dioxide into the stratosphere, cooling the Earth by about 0.5°C for a year. Globally,*
18   *eruptions also reduce precipitation, because the cooler the Earth's surface, the less water that is available in*
19   *the atmosphere.*
20
21   *For the purposes of predicting climate, we can expect an eruption to cause significant global surface cooling*
22   *and upper atmospheric heating for the next year or so. The problem is that, while we can detect when a*
23   *volcano has become more active, we cannot predict the precise timing of an eruption, or the amount of*
24   *sulphur dioxide injected into the upper atmosphere and how it might disperse. This is a source of uncertainty*
25   *in climate predictions.*
26
27   Large volcanic eruptions produce lots of particles, called ash or tephra. However, these particles fall out of
28   the atmosphere quickly, within days or weeks, so they do not affect the global climate. For example, the
29   1980 Mount St. Helens eruption affected surface temperatures in the northwest United States for several
30   days but, because it emitted little sulphur dioxide into the stratosphere, it had no detectable global climate
31   impacts. If large, high-latitude eruptions inject sulphur into the stratosphere, they will only have an effect in
32   the hemisphere where they erupted, and the effects will only last a year at most, as the stratospheric cloud
33   they produce only has a lifetime of a few months.
34
35   Tropical or subtropical volcanoes produce more global surface or tropospheric cooling. This is because the
36   resulting sulphuric acid cloud in the upper atmosphere lasts between one and two years, and can cover much
37   of the globe. However, their regional climatic impacts are difficult to predict, because dispersion of
38   stratospheric sulfate aerosols depends heavily on atmospheric wind conditions at the time of eruption.
39   Furthermore, the surface cooling effect is typically not uniform: because continents cool more than the
40   ocean, the summer monsoon can weaken, reducing rain over Asia and Africa.
41
42   The climatic response is further complicated by the fact that upper atmospheric clouds from tropical
43   eruptions also absorb sunlight and heat from the Earth, which produces more upper atmosphere warming in
44   the tropics than at high latitudes. This can change planetary wind patterns, with a stronger jet stream. During
45   the Northern Hemisphere winter, this can blow more warm air onto the continents from the oceans,
46   counteracting surface cooling associated with the reduction in sunlight.
47
48   **[INSERT FAQ 11.2, FIGURE 1 HERE]**
49   **FAQ 11.2, Figure 1:** Schematic of how large tropical or sub-tropical volcanoes impact upper atmospheric
50   (stratospheric) and lower atmospheric (tropospheric) temperatures.
51
52   The largest volcanic eruptions of the past 250 years stimulated scientific study. After the 1783 Laki eruption
53   in Iceland, there were record warm summer temperatures in Europe, followed by a very cold winter. Several
54   studies failed to prove a connection, but subsequent famines in Egypt, India, China, and Japan have been
55   linked to weakened summer monsoon precipitation over Africa and Asia.
56

1 Two large eruptions, an unidentified one in 1809, and the 1815 Tambora eruption caused the 'Year Without a
2 Summer' in 1816 (which inspired Frankenstein, written by Mary Shelley on the shores of Lake Geneva).
3 Agricultural failures in Europe and the United States that year led to food shortages, famine and riots.
4
5 The largest eruption in more than 50 years, that of Agung in 1963, led to many modern studies, including
6 observations and climate model calculations. Two subsequent large eruptions, El Chichón in 1982 and
7 Pinatubo in 1991, inspired the work that led to our current understanding of the effects of volcanic eruptions
8 on climate.
9
10 Volcanic clouds only remain in the stratosphere for a couple of years, so their impact on climate is
11 correspondingly short. But the impacts of consecutive large eruptions can last longer: for example, at the end
12 of the 13th century there were four large eruptions—one every ten years. The first, in 1258 CE, was the
13 largest in 1000 years. That sequence of eruptions cooled the North Atlantic Ocean, and Arctic sea ice
14 expanded so much that the period was dubbed the Little Ice Age. The 1452 CE Kuwae eruption perpetuated
15 this cooling, and the climate did not warm again until greenhouse gases from human activities became the
16 dominant cause of climate change in the past century.
17
18 Volcanologists can detect when a volcano becomes more active, but they cannot predict whether it will
19 erupt, or if it does, how much sulphur it might inject into the stratosphere. Nevertheless, volcanoes affect our
20 ability to predict climate in three distinct ways. First, if a violent eruption injects significant volumes of
21 sulphur dioxide into the stratosphere, we can include this effect in our climate predictions for the next couple
22 of years.
23
24 There are substantial challenges involved, such as collecting good observations of the volcanic cloud, and
25 calculating how it will move and change during its lifetime. But, based on our observations, and successful
26 modelling of recent eruptions, we are confident that the next large tropical eruption will produce global
27 cooling for about two years, and winter warming of the Northern Hemisphere continents for one or two
28 years. There will also be reduced summer monsoon precipitation over Asia and Africa. A large Northern
29 Hemisphere high-latitude eruption, if it occurs in spring or summer, will also produce a weak summer
30 monsoon.
31
32 The second effect is that volcanic eruptions are a potential source of uncertainty in our predictions. We
33 cannot predict eruptions in advance, but they will occur, causing short-term climatic impacts on both local
34 and global scales. In principle, we can also account for this potential uncertainty by including random
35 eruptions, or eruptions based on some scenario in our near-term ensemble climate predictions. This area of
36 research needs further exploration. The projections in this report do not include volcanic eruptions.
37
38 Thirdly, we can use the historical climate record, along with estimates of observed sulphate aerosols, to test
39 the fidelity of our climate simulations. While the climatic response to explosive volcanic eruptions is a useful
40 analogue for some other climatic forcings, there are limitations. For example, successfully simulating the
41 impact of one eruption can help validate models used for seasonal and interannual predictions. But they
42 cannot test all the mechanisms involved in global warming over the next century, because they involve long-
43 term oceanic feedbacks, which have a longer time scale than the response to individual volcanic eruptions.
44
45 **[END FAQ 11.2 HERE]**
46

References

Alexander, L. V., and J. M. Arblaster, 2009: Assessing trends in observed and modelled climate extremes over Australia in relation to future projections. *Int J Climatol*, **29**, 417-435.

Alexander, M. A., L. Matrosova, C. Penland, J. D. Scott, and P. Chang, 2008: Forecasting Pacific SSTs: Linear inverse model predictions of the PDO. *J Climate*, **21**, 385-402.

Alexandru, A., R. de Elia, and R. Laprise, 2007: Internal variability in regional climate downscaling at the seasonal scale. *Monthly Weather Review*, **135**, 3221-3238.

Alexeev, V. A., D. J. Nicolsky, V. E. Romanovsky, and D. M. Lawrence, 2007: An evaluation of deep soil configurations in the CLM3 for improved representation of permafrost. *Geophys Res Lett*, **34**.

Allan, R. P., 2009: Examination of Relationships between Clear-Sky Longwave Radiation and Aspects of the Atmospheric Hydrological Cycle in Climate Models, Reanalyses, and Observations. *J Climate*, **22**, 3127-3145.

——, 2012: Regime dependent changes in global precipitation. *Clim. Dyn.*, **in press**.

Allan, R. P., and B. J. Soden, 2007: Large discrepancy between observed and simulated precipitation trends in the ascending and descending branches of the tropical circulation. *Geophys Res Lett*, **34**.

Allan, R. P., B. J. Soden, V. O. John, W. Ingram, and P. Good, 2010: Current changes in tropical precipitation. *Environ Res Lett*, **5**.

Allen, M. R., and W. J. Ingram, 2002: Constraints on future changes in climate and the hydrologic cycle. *Nature*, **419**, 224-+.

Allen, M. R., P. A. Stott, J. F. B. Mitchell, R. Schnur, and T. L. Delworth, 2000: Quantifying the uncertainty in forecasts of anthropogenic climate change. *Nature*, **407**, 617-620.

Allen, R., and S. Sherwood, 2010: The impact of natural versus anthropogenic aerosols on atmospheric circulation in the Community Atmosphere Model. *Clim Dynam*. doi:10.1007/s00382-010-0898-8, 1-20.

Andersson, C., and M. Engardt, 2010: European ozone in a future climate: Importance of changes in dry deposition and isoprene emissions. *J. Geophys. Res.*, **115**, D02303.

Andrews, T., P. M. Forster, O. Boucher, N. Bellouin, and A. Jones, 2010: Precipitation, radiative forcing and global temperature change. *Geophys Res Lett*, **37**.

Appelhans, T., A. Sturman, and P. Zawar-Reza, 2012: Synoptic and climatological controls of particulate matter pollution in a Southern Hemisphere coastal city. *Int J Climatol*.

Arblaster, J. M., and G. A. Meehl, 2006: Contributions of external forcings to southern annular mode trends. *J Climate*, **19**, 2896-2905.

Arblaster, J. M., G. A. Meehl, and D. J. Karoly, 2011: Future climate change in the Southern Hemisphere: Competing effects of ozone and greenhouse gases. *Geophys Res Lett*, **38**.

Ashok, K., Z. Y. Guan, N. H. Saji, and T. Yamagata, 2004: Individual and combined influences of ENSO and the Indian Ocean Dipole on the Indian summer monsoon. *J Climate*, **17**, 3141-3155.

Avise, J., J. Chen, B. Lamb, C. Wiedinmyer, A. Guenther, E. Salathé, and C. Mass, 2009: Attribution of projected changes in summertime US ozone and PM2.5 concentrations to global changes. *Atmos. Chem. Phys.*, **9**, 1111-1124.

Aw, J., and M. J. Kleeman, 2003: Evaluating the first-order effect of intraannual temperature variability on urban air pollution. *J. Geophys. Res.*, **108**, 4365.

Bala, G., K. Caldeira, and R. Nemani, 2010: Fast versus slow response in climate change: implications for the global hydrological cycle. *Clim Dynam*, **35**, 423-434.

Balmaseda, M. A., M. K. Davey, and D. L. T. Anderson, 1995: Decadal and Seasonal Dependence of Enso Prediction Skill. *J Climate*, **8**, 2705-2715.

Bates, B. C., Z. W. Kundzewicz, S. Wu, and J. P. Palutikof, 2008: Climate Change and Water. Technical Paper of the Intergovernmental Panel on Climate Change. IPCC, 210.

BATTISTI, D., and E. SARACHIK, 1995: UNDERSTANDING AND PREDICTING ENSO. *Reviews of Geophysics*. 1367-1376.

Bauer, S. E., D. Koch, N. Unger, S. M. Metzger, D. T. Shindell, and D. G. Streets, 2007a: Nitrate aerosols today and in 2030: a global simulation including aerosols and tropospheric ozone. *Atmos. Chem. Phys.*, **7**, 5043-5059.

——, 2007b: Nitrate aerosols today and in 2030: a global simulation including aerosols and tropospheric ozone. *Atmospheric Chemistry and Physics*, **7**, 5043-5059.

Bellouin, N., J. G. L. Rae, A. Jones, C. E. Johnson, J. M. Haywood, and O. Boucher, 2011: Aerosol forcing in the CMIP5 simulations by Hadgem2-ES and the role of ammonium nitrate. *J. Geophys. Res.-Atmospheres*. doi:10.1029/2011JD016074.

Bellucci, A., et al., 2012: Decadal climate predictions with a coupled OAGCM initialized with oceanic reanalyses. *Clim. Dyn.*, **submitted**.

Bender, F. A. M., A. M. L. Ekman, and H. Rodhe, 2010: Response to the eruption of Mount Pinatubo in relation to climate sensitivity in the CMIP3 models. *Clim Dynam*, **35**, 875-886.

Benestad, R., 2012: Global evaluation of surface temperature trends simulated by multi-model ensembles. *J.Climatolog.*, **submitted**.

1   Berner, J., F. J. Doblas-Reyes, T. N. Palmer, G. Shutts, and A. Weisheimer, 2008: Impact of a quasi-stochastic cellular
2   automaton backscatter scheme on the systematic error and seasonal prediction skill of a global climate model.
3   *Philos T R Soc A*, **366**, 2561-2579.
4   Betts, R. A., et al., 2007: Projected increase in continental runoff due to plant responses to increasing carbon dioxide.
5   *Nature*, **448**, 1037-U1035.
6   Bhend, J., and H. von Storch, 2008: Consistency of observed winter precipitation trends in northern Europe with
7   regional climate change projections. *Clim Dynam*, **31**, 17-28.
8   Bhend, J., and P. Whetton, 2012: Consistency of simulated and observed regional changes in temperature, sea level
9   pressure and precipitation. *Clim. Dyn.*, **submitted**.
10 Bintanja, R., G. J. van Oldenborgh, S. S. Drijfhout, B. Wouters, and C. A. Katsman, 2012: Expanding Antarctic sea ice
11   caused by climate warming? *Geophys Res Lett*. submitted.
12 Bitz, C., 2008: Some aspects of uncertainty in predicting sea ice thinning. Arctic Sea Ice Decline: Observations,
13   Projections, Mechanisms, and Implications. *Geophysical Monographs, 180,* American Geophysical Union, 63-
14   76.
15 Bitz, C. M., P. R. Gent, R. A. Woodgate, M. M. Holland, and R. Lindsay, 2006: The influence of sea ice on ocean heat
16   uptake in response to increasing CO2. *J Climate*, **19**, 2437-2450.
17 Bladé, I., D. Fortuny, G. J. van Oldenborgh, and B. Liebmann, 2012: The summer North Atlantic Oscillation in CMIP3
18   models and related uncertainties in projected summer drying in Europe. *J. Geophys. Res.*, **117**.
19 Bloomer, B. J., J. W. Stehr, C. A. Piety, R. J. Salawitch, and R. R. Dickerson, 2009: Observed relationships of ozone air
20   pollution with temperature and emissions. *Geophys. Res. Lett.*, **36**, L09803.
21 Boberg, F., P. Berg, P. Thejll, W. J. Gutowski, and J. H. Christensen, 2010: Improved confidence in climate change
22   projections of precipitation further evaluated using daily statistics from ENSEMBLES models. *Clim Dynam*, **35**,
23   1509-1520.
24 Boe, J. L., A. Hall, and X. Qu, 2009: September sea-ice cover in the Arctic Ocean projected to vanish by 2100. *Nat
25   Geosci*, **2**, 341-343.
26 Boer, G. J., 2000: A study of atmosphere-ocean predictability on long time scales. *Clim Dynam*, **16**, 469-477.
27 ——, 2004: Long time-scale potential predictability in an ensemble of coupled climate models. *Clim Dynam*, **23**, 29-44.
28 ——, 2011: Decadal potential predictability of twenty-first century climate. *Clim Dynam*, **36**, 1119-1133.
29 Boer, G. J., and S. J. Lambert, 2008: Multi-model decadal potential predictability of precipitation and temperature.
30   *Geophys Res Lett*, **35**.
31 Boer, G. J., V. Kharin, and W. J. Merryfield, 2012: Decadal predictability and forecast skill. *Clim. Dyn.*, **submitted**.
32 Bollasina, M. A., Y. Ming, and V. Ramaswamy, 2011: Anthropogenic Aerosols and the Weakening of the South Asian
33   Summer Monsoon. *Science*. doi:10.1126/science.1204994.
34 Booth, B. B. B., N. J. Dunstone, P. R. Halloran, T. Andrews, and N. Bellouin, 2012: Aerosols implicated as a prime
35   driver of twentieth-century North Atlantic climate variability (vol 484, pg 228, 2012). *Nature*, **485**, 534-534.
36 Bosshard, T., S. Kotlarski, M. Zappa, and S. Schär, 2012: Hydrological climate-impact projections for the Rhine river:
37   GCM-RCM uncertainty and separate temperature and precipitation effects. *Journal Hydrometeorology*,
38   **submitted**.
39 Brandefelt, J., and H. Kornich, 2008: Northern Hemisphere Stationary Waves in Future Climate Projections. *J Climate*.
40   doi:DOI 10.1175/2008JCLI2373.1, 6341-6353.
41 Branstator, G., and H. Y. Teng, 2010: Two Limits of Initial-Value Decadal Predictability in a CGCM. *J Climate*, **23**,
42   6292-6311.
43 ——, 2012: Potential impact of initialization on decadal predictions as assessed for CMIP5 models. *Geophys Res Lett*,
44   **39**.
45 Branstator, G., H. Teng, G. A. Meehl, M. Kimoto, J. R. Knight, M. Latif, and A. Rosati, 2012: Systematic Estimates of
46   Initial-Value Decadal Predictability for Six AOGCMs. *J Climate*, **25**, 1827-1846.
47 Brocker, J., and L. A. Smith, 2007: Increasing the reliability of reliability diagrams. *Weather and Forecasting*, **22**, 651-
48   661.
49 Brohan, P., J. J. Kennedy, I. Harris, S. F. B. Tett, and P. D. Jones, 2006: Uncertainty estimates in regional and global
50   observed temperature changes: A new data set from 1850. *Journal of Geophysical Research-Atmospheres*, **111**.
51 Brown, R. D., and P. W. Mote, 2009: The Response of Northern Hemisphere Snow Cover to a Changing Climate. *J
52   Climate*, **22**, 2124-2145.
53 Brunner, D., S. Henne, C. A. Keller, S. Reimann, M. K. Vollmer, S. O'Doherty, and M. Maione, 2012: An extended
54   Kalman-filter for regional scale inverse emission estimation. *Atmos. Chem. Phys.*, **12**, 3455-3478.
55 Brutel-Vuilmet, C., M. Menegoz, and G. Krinner, 2012: An analysis of present and future seasonal Northern
56   Hemisphere land snow cover simulated by CMIP5 coupled climate models. *Cryosphere*, **submitted**.
57 Bryan, F. O., G. Danabasoglu, N. Nakashiki, Y. Yoshida, D. H. Kim, J. Tsutsui, and S. C. Doney, 2006: Response of
58   the North Atlantic thermohaline circulation and ventilation to increasing carbon dioxide in CCSM3. *J Climate*,
59   **19**, 2382-2397.
60 Burgman, R., R. Seager, A. Clement, and C. Herweijer, 2010: Role of tropical Pacific SSTs in global medieval
61   hydroclimate: A modeling study. *Geophys Res Lett*, **37**.
62 Butchart, N., et al., 2006: Simulations of anthropogenic change in the strength of the Brewer-Dobson circulation. *Clim
63   Dynam*, **27**, 727-741.

Butler, T. M., Z. S. Stock, M. R. Russo, H. A. C. Denier van der Gon, and M. G. Lawrence, 2012: Megacity ozone air quality under four alternative future scenarios. *Atmos. Chem. Phys.*, **12**, 4413-4428.

Callaghan, J., and S. B. Power, 2011: Variability and decline in the number of severe tropical cyclones making land-fall over eastern Australia since the late nineteenth century. *Clim Dynam*, **37**, 647-662.

Cao, L., G. Bala, K. Caldeira, R. Nemani, and G. Ban-Weiss, 2009: Climate response to physiological forcing of carbon dioxide simulated by the coupled Community Atmosphere Model (CAM3.1) and Community Land Model (CLM3.0). *Geophys Res Lett*, **36**.

——, 2010: Importance of carbon dioxide physiological forcing to future climate change. *Proc. Natl. Acad. Sci. U. S. A.*, **107**, 9513-9518.

Carlton, A. G., C. Wiedinmyer, and J. H. Kroll, 2009: A review of Secondary Organic Aerosol (SOA) formation from isoprene. *Atmos. Chem. Phys.*, **9**, 4987-5005.

Carlton, A. G., R. W. Pinder, P. V. Bhave, and G. A. Pouliot, 2010: To What Extent Can Biogenic SOA be Controlled? *Environmental Science & Technology*, **44**, 3376-3380.

Carvalho, A., A. Monteiro, M. Flannigan, S. Solman, A. I. Miranda, and C. Borrego, 2011: Forest fires in a changing climate and their impacts on air quality. *Atmos Environ*, **45**, 5545-5553.

Ceppi, P., S. C. Scherrer, A. M. Fischer, and C. Appenzeller, 2010: Revisiting Swiss temperature trends 1959–2008. *Int J Climatol*. doi:10.1002/joc.2260, n/a-n/a.

Chalmers, and et_al, 2012: Aerosol contribution to the rapid warming of near-term climate under RCP 2.6. *Geophys. Res. Lett.*, **39**.

Chang, C. Y., J. C. H. Chiang, M. F. Wehner, A. R. Friedman, and R. Ruedy, 2011: Sulfate Aerosol Control of Tropical Atlantic Climate over the Twentieth Century. *J Climate*, **24**, 2540-2555.

Chen, G., and I. M. Held, 2007: Phase speed spectra and the recent poleward shift of Southern Hemisphere surface westerlies. *Geophys Res Lett*, **34**.

Chen, J., J. Avise, A. Guenther, C. Wiedinmyer, E. Salathe, R. B. Jackson, and B. Lamb, 2009a: Future land use and land cover influences on regional biogenic emissions and air quality in the United States. *Atmos Environ*, **43**, 5771-5780.

Chen, J., et al., 2009b: The effects of global changes upon regional ozone pollution in the United States. *Atmos. Chem. Phys.*, **9**, 1125-1141.

Chevallier, M., and D. Salas-Melia, 2012: The Role of Sea Ice Thickness Distribution in the Arctic Sea Ice Potential Predictability: A Diagnostic Approach with a Coupled GCM. *J Climate*, **25**, 3025-3038.

Chikamoto, Y., M. Kimoto, M. Watanabe, M. Ishii, and Mochizuki, 2012a: Relationship between the Pacifc and Atlantic stepwise climate change during the 1990s. *Geoph. Res. Lett.*, **submitted**.

Chikamoto, Y., et al., 2012b: Predictability of a Stepwise Shift in Pacific Climate during the Late 1990s in Hindcast Experiments Using MIROC. *J Meteorol Soc Jpn*, **90A**, 1-21.

Chin, M., T. Diehl, P. Ginoux, and W. Malm, 2007: Intercontinental transport of pollution and dust aerosols: implications for regional air quality. *Atmospheric Chemistry and Physics*, **7**, 5501-5517.

Chou, C., J. Y. Tu, and P. H. Tan, 2007: Asymmetry of tropical precipitation change under global warming. *Geophys Res Lett*, **34**.

Chou, C., J. D. Neelin, C. A. Chen, and J. Y. Tu, 2009: Evaluating the "Rich-Get-Richer" Mechanism in Tropical Precipitation Change under Global Warming. *J Climate*, **22**, 1982-2005.

Christensen, J. H., et al., 2007: Regional Climate Projections. *Climate Change 2007: The Physical Science Basis. Contribution of Working Group I to the Fourth Assessment Report of the Intergovernmental Panel on Climate Change*, S. Solomon, et al., Eds., Cambridge University Press.

Chylek, P., C. K. Folland, G. Lesins, and M. K. Dubey, 2010: Twentieth century bipolar seesaw of the Arctic and Antarctic surface air temperatures. *Geophys Res Lett*, **37**.

Chylek, P., C. K. Folland, G. Lesins, M. K. Dubey, and M. Y. Wang, 2009: Arctic air temperature change amplification and the Atlantic Multidecadal Oscillation. *Geophys Res Lett*, **36**.

Clark, R. T., J. M. Murphy, and S. J. Brown, 2010: Do global warming targets limit heatwave risk? *Geophys. Res. Lett.*, **37**, L17703.

Cofala, J., et al., 2012: Global long-term air pollution emission scenarios. *Journal of X*.

Cofala, J., M. Amann, Z. Klimont, K. Kupiainen, and L. Hoglund-Isaksson, 2007: Scenarios of global anthropogenic emissions of air pollutants and methane until 2030. *Atmos Environ*, **41**, 8486-8499.

Colle, B. A., Z. Zhang, K.A. Lombardo, E. Chang, P. Liu, M. Zhang, and S. Hameed, 2012: Historical and Future Predictions of Eastern North America and Western Atlantic Extratropical Cyclones in CMIP5 During the Cool Season. *J. Climate*, **submitted**.

Collins, M., 2002: Climate predictability on interannual to decadal time scales: the initial value problem. *Clim Dynam*, **19**, 671-692.

Collins, M., and B. Sinha, 2003: Predictability of decadal variations in the thermohaline circulation and climate. *Geophys Res Lett*, **30**.

Collins, M., et al., 2006: Interannual to decadal climate predictability in the North Atlantic: A multimodel-ensemble study. *J Climate*, **19**, 1195-1203.

Collins, M., et al., 2010: The impact of global warming on the tropical Pacific ocean and El Nino. *Nat Geosci*, **3**, 391-397.

Comiso, J. C., C. L. Parkinson, R. Gersten, and L. Stock, 2008: Accelerated decline in the Arctic Sea ice cover. *Geophys Res Lett*, **35**.

Committee), I. I. A. S., 2010: Arctic Climate Impact Assessment (full report). *Encyclopedia of Earth*, P. Saundry, Ed., Environmental Information Coalition, National Council for Science and the Environment.

Cook, B. I., R. L. Miller, and R. Seager, 2009: Amplification of the North American "Dust Bowl" drought through human-induced land degradation. *Proceedings of the National Academy of Sciences*, **106**, 4997-5001.

Corti, S., A. Weisheimer, T.N. Palmer, F. J. Doblas-Reyes, and L. Magnusson, 2012: Reliability of decadal predictions. *Geoph. Res. Lett.*, **submitted**.

Cox, P., and D. Stephenson, 2007: Climate change - A changing climate for prediction. *Science*, **317**, 207-208.

Cox, W., and S. Chu, 1996: Assessment of interannual ozone variation in urban areas from a climatological perspective. *Atmos Environ*, **30**, 2615-2625.

Dawson, J. P., P. N. Racherla, B. H. Lynn, P. J. Adams, and S. N. Pandis, 2009: Impacts of climate change on regional and urban air quality in the eastern United States: Role of meteorology. *J. Geophys. Res.*, **114**, D05308.

de Noblet-Ducoudre, N., J.-P. Boisier, A. Pitman, and e. al., 2012: Determining Robust Impacts of Land-Use-Induced Land Cover Changes on Surface Climate over North America and Eurasia: Results from the First Set of LUCID Experiments. *J. of Climate*, **25**, 3261-3281.

Delworth, T., and K. Dixon, 2006: Have anthropogenic aerosols delayed a greenhouse gas-induced weakening of the North Atlantic thermohaline circulation? *Geophys Res Lett*. doi:ARTN L02606, DOI 10.1029/2005GL024980.

Delworth, T., V. Ramaswamy, and G. Stenchikov, 2005: The impact of aerosols on simulated ocean temperature and heat content in the 20th century. *Geophys Res Lett*, **32**.

Delworth, T. L., and F. Zeng, 2008: Simulated impact of altered Southern Hemisphere winds on the Atlantic Meridional Overturning Circulation. *Geophys Res Lett*, **35**.

Dentener, F., et al., 2005: The impact of air pollutant and methane emission controls on tropospheric ozone and radiative forcing: CTM calculations for the period 1990-2030. *Atmos. Chem. Phys.*, **5**, 1731-1755.

Dentener, F., et al., 2006: The Global Atmospheric Environment for the Next Generation. *Environmental Science & Technology*, **40**, 3586-3594.

Dery, S. J., M. A. Hernandez-Henriquez, J. E. Burford, and E. F. Wood, 2009: Observational evidence of an intensifying hydrological cycle in northern Canada. *Geophys Res Lett*, **36**.

Deser, C., and A. S. Phillips, 2009: Atmospheric Circulation Trends, 1950–2000: The Relative Roles of Sea Surface Temperature Forcing and Direct Atmospheric Radiative Forcing. *J. Climate*, **22**, 396-413.

Deser, C., A. S. Phillips, and J. W. Hurrell, 2004: Pacific interdecadal climate variability: Linkages between the tropics and the North Pacific during boreal winter since 1900. *J Climate*, **17**, 3109–3124.

Deser, C., A. Phillips, V. Bourdette, and H. Y. Teng, 2012: Uncertainty in climate change projections: the role of internal variability. *Clim Dynam*, **38**, 527-546.

DeWeaver, E. T., E.C. Hunke, and M. M. Holland, 2008: Comment on "On the reliability of simulated Arctic sea ice in global climate models" by I. Eisenman, N. Untersteiner, and J.S. Wettlaufer. *Geoph. Res. Lett.*, **35**.

Dharshana, K. G. T., S. Kravtsov, and J. D. W. Kahl, 2010: Relationship between synoptic weather disturbances and particulate matter air pollution over the United States. *Journal of Geophysical Research-Atmospheres*, **115**.

Diffenbaugh, N. S., and M. Ashfaq, 2010: Intensification of hot extremes in the United States. *Geophys. Res. Lett.*, **37**, L15701.

DiNezio, P., G. A. Vecchi, and A. Clement, 2012: Detectability of Changes in the Walker Circulation in Response to Global Warming. *J. Climate*, **submitted**.

DiNezio, P., A. Clement, G. Vecchi, B. Soden, and B. Kirtman, 2009a: Climate Response of the Equatorial Pacific to Global Warming. *J Climate*. doi:DOI 10.1175/2009JCLI2982.1, 4873-4892.

DiNezio, P. N., A. C. Clement, G. A. Vecchi, B. J. Soden, B. P. Kirtman, and S.-K. Lee, 2009b: Climate Response of the Equatorial Pacific to Global Warming. *Journal of Climate*, **22**, 4873-4892.

Dlugokencky, E. J., E. G. Nisbet, R. Fisher, and D. Lowry, 2011: Global atmospheric methane: budget, changes and dangers. *Philosophical Transactions of the Royal Society A: Mathematical, 				Physical and Engineering Sciences*, **369**, 2058-2072.

Doblas-Reyes, F. J., M. A. Balmaseda, A. Weisheimer, and T. N. Palmer, 2011: Decadal climate prediction with the ECMWF coupled forecast system: Impact of ocean observations. *Journal of Geophysical Research - A*, **116**, D19111.

Doblas-Reyes, F. J., et al., 2009: Addressing model uncertainty in seasonal and annual dynamical ensemble forecasts. *Quarterly Journal of the Royal Meteorological Society*, **135**, 1538-1559.

Doblas-Reyes, F. J., et al., 2012: Initialized near-term regional climate change prediction. *Nature Comms*, **submitted**.

Doherty, R., et al., 2009: Current and future climate- and air pollution-mediated impacts on human health. *Environmental Health*, **8**, -.

Doherty, R. M., et al., 2012: The impact of climate change on surface ozone and intercontinental transport of O3 in a multi-model study. *submitted to J. Geophys. Res.*

Drijfhout, S. S., and W. Hazeleger, 2007: Detecting Atlantic MOC changes in an ensemble of climate change simulations. *J Climate*, **20**, 1571-1582.

Drijfhout, S. S., and G. J. van Oldenborgh, 2012: A comparison of the observed with the modeled pattern of global warming *Geoph. Res. Lett.*, **submitted**.

Du, H., F. J. Doblas-Reyes, J. García-Serrano, V. Guemas, Y. Soufflet, and B. Wouters, 2012: Sensitivity of decadal predictions to the initial atmospheric and oceanic perturbations. *Clim. Dyn.* doi:doi:10.1007/s00382-011-1285-9.

Dunstone, N. J., and D. M. Smith, 2010: Impact of atmosphere and sub-surface ocean data on decadal climate prediction. *Geophys Res Lett*, **37**, L02709.

Dunstone, N. J., D. M. Smith, and R. Eade, 2011: Multi-year predictability of the tropical Atlantic atmosphere driven by the high latitude North Atlantic Ocean. *Geophys Res Lett*, **38**, L14701.

Durack, P. J., and S. E. Wijffels, 2010: Fifty-Year Trends in Global Ocean Salinities and Their Relationship to Broad-Scale Warming. *J Climate*, **23**, 4342-4362.

Dutra, E., C. Schar, P. Viterbo, and P. M. A. Miranda, 2011: Land-atmosphere coupling associated with snow cover. *Geophys Res Lett*, **38**.

Easterling, D. R., and M. F. Wehner, 2009: Is the climate warming or cooling? *Geophys Res Lett*, **36**.

El Nadi, A. H., 1974: The Significance of Leaf Area in Evapotranspiration. *Ann. Bot*, **38 (3)**, 607-611.

Euskirchen, E. S., et al., 2006: Importance of recent shifts in soil thermal dynamics on growing season length, productivity, and carbon sequestration in terrestrial high-latitude ecosystems. *Global Change Biol*, **12**, 731-750.

Evan, A. T., D. J. Vimont, A. K. Heidinger, J. P. Kossin, and R. Bennartz, 2009: The Role of Aerosols in the Evolution of Tropical North Atlantic Ocean Temperature Anomalies. *Science*, **324**, 778-781.

Eyring, V., et al., 2012: Long-term changes in tropospheric and stratospheric ozone and associated climate impacts in CMIP5 simulations. *J. Geophys., Res.*

Eyring, V., et al., 2010: Multi-model assessment of stratospheric ozone return dates and ozone recovery in CCMVal-2 models. *Atmospheric Chemistry and Physics*, **10**, 9451-9472.

Fan, K., and H. J. Wang, 2009: A New Approach to Forecasting Typhoon Frequency over the Western North Pacific. *Weather and Forecasting*, **24**, 974-986.

Fang, Y., et al., 2011: The impacts of changing transport and precipitation on pollutant distributions in a future climate. *J. Geophys. Res.*, **116**, D18303.

Fasullo, J. T., 2010: Robust Land-Ocean Contrasts in Energy and Water Cycle Feedbacks. *J Climate*, **23**, 4677-4693.

Feulner, G., and S. Rahmstorf, 2010: On the effect of a new grand minimum of solar activity on the future climate on Earth. *Geophys Res Lett*, **37**.

Field, C. B., R. B. Jackson, and H. A. Mooney, 1995: Stomatal Responses to Increased Co2 - Implications from the Plant to the Global-Scale. *Plant Cell Environ*, **18**, 1214-1225.

Filleul, L., et al., 2006: The relation between temperature, ozone, and mortality in nine french cities during the heat wave of 2003. *Environmental Health Perspectives*, **114**, 1344-1347.

Fiore, A. M., J. J. West, L. W. Horowitz, V. Naik, and M. D. Schwarzkopf, 2008: Characterizing the tropospheric ozone response to methane emission controls and the benefits to climate and air quality. *J. Geophys. Res.*, **113**, D08307.

Fiore, A. M., D. J. Jacob, B. D. Field, D. G. Streets, S. D. Fernandes, and C. Jang, 2002: Linking ozone pollution and climate change: The case for controlling methane. *Geophys. Res. Lett.*, **29**, 1919.

Fiore, A. M., et al.: Global Air Quality and Climate. *Chem. Soc. Rev.*, **DOI:10.1039/C2CS35095E.**

——, 2012: Global Air Quality and Climate. *Chem. Soc. Rev.*, **DOI:10.1039/C2CS35095E.**

Fiore, A. M., et al., 2009: Multimodel estimates of intercontinental source-receptor relationships for ozone pollution. *J. Geophys. Res.*, **114**, D04301.

Fischer, E. M., and C. Schar, 2009: Future changes in daily summer temperature variability: driving processes and role for temperature extremes. *Clim Dynam*, **33**, 917-935.

——, 2010: Consistent geographical patterns of changes in high-impact European heatwaves. *Nat Geosci*, **3**, 398-403.

Fischer, E. M., J. Rajczak, and C. Schär, 2012: Changes in European summer temperature variability revisited. *Geoph. Res. Lett.*, **submitted**.

Fischer, E. M., S. I. Seneviratne, P. L. Vidale, D. Luthi, and C. Schar, 2007: Soil moisture - Atmosphere interactions during the 2003 European summer heat wave. *J Climate*, **20**, 5081-5099.

Flanner, M. G., C. S. Zender, J. T. Randerson, and P. J. Rasch, 2007a: Present-day climate forcing and response from black carbon in snow. *J. Geophys. Res.*, **112**, D11202.

Flanner, M. G., C. S. Zender, J. T. Randerson, and P. J. Rasch, 2007b: Present-day climate forcing and response from black carbon in snow. *Journal of Geophysical Research-Atmospheres*, **112**.

Flannigan, M. D., M. A. Krawchuk, W. J. de Groot, B. M. Wotton, and L. M. Gowman, 2009: Implications of changing climate for global wildland fire. *International Journal of Wildland Fire*, **18**, 483-507.

Fleming, E., C. Jackman, R. Stolarski, and A. Douglass, 2011: A model study of the impact of source gas changes on the stratosphere for 1850-2100. *Atmospheric Chemistry and Physics*, **11**, 8515-8541.

Fogt, R. L., J. Perlwitz, A. J. Monaghan, D. H. Bromwich, J. M. Jones, and G. J. Marshall, 2009: Historical SAM Variability. Part II: Twentieth-Century Variability and Trends from Reconstructions, Observations, and the IPCC AR4 Models. *J Climate*, **22**, 5346-5365.

Folland, C., J. Knight, H. Linderholm, D. Fereday, S. Ineson, and J. Hurrell, 2009: The Summer North Atlantic Oscillation: Past, Present, and Future. *J Climate*. doi:DOI 10.1175/2008JCLI2459.1, 1082-1103.

Forkel, R., and R. Knoche, 2006: Regional climate change and its impact on photooxidant concentrations in southern Germany: Simulations with a coupled regional climate-chemistry model. *J. Geophys. Res.*, **111**, D12302.

Fowler, H. J., M. Ekstrom, S. Blenkinsop, and A. P. Smith, 2007: Estimating change in extreme European precipitation using a multimodel ensemble. *Journal of Geophysical Research-Atmospheres*, **112**.

Frieler, K., M. Meinshausen, T. S. von Deimling, T. Andrews, and P. Forster, 2011: Changes in global-mean precipitation in response to warming, greenhouse gas forcing and black carbon. *Geophys Res Lett*, **38**.

Funk, C., M. Barlow, and A. Hoell, 2012: The Ocean Atmosphere Hydrodyne and recent rapid warming in the western Pacific   *Clim. Dyn.*, **submitted**.

Fyfe, J. C., W. J. Merryfield, V. Kharin, G. J. Boer, W. S. Lee, and K. von Salzen, 2011: Skillful predictions of decadal trends in global mean surface temperature. *Geophys Res Lett*, **38**.

Gadgil, S., P. N. Vinayachandran, P. A. Francis, and S. Gadgil, 2004: Extremes of the Indian summer monsoon rainfall, ENSO and equatorial Indian Ocean oscillation. *Geophys Res Lett*, **31**.

Galloway, J. N., et al., 2008: Transformation of the Nitrogen Cycle: Recent Trends, Questions, and Potential Solutions. *Science*, **320**, 889-892.

Gangstø, R., A. P. Weigel, M. A. Liniger, and C. Appenzeller, 2012: Comments on the evaluation of decadal predictions. *Climate Research*, **submitted**.

Ganzeveld, L., L. Bouwman, E. Stehfest, D. P. van Vuuren, B. Eickhout, and J. Lelieveld, 2010: Impact of future land use and land cover changes on atmospheric chemistry-climate interactions. *J. Geophys. Res.*, **115**, D23301.

Gao, C. C., A. Robock, and C. Ammann, 2008: Volcanic forcing of climate over the past 1500 years: An improved ice core-based index for climate models. *Journal of Geophysical Research-Atmospheres*, **113**.

García-Serrano, J., and F. J. Doblas-Reyes, 2012: On the assessment of near-surface global temperature and North Atlantic multi-decadal variability in the ENSEMBLES decadal hindcast. *Clim Dynam*, **under review**.

García-Serrano, J., F. J. Doblas-Reyes, and C. A. S. Coelho, 2012: Understanding Atlantic multi-decadal variability prediction skill. *Geoph. Res. Lett.*, **submitted**.

Gastineau, G., L. Li, and H. Le Treut, 2009: The Hadley and Walker Circulation Changes in Global Warming Conditions Described by Idealized Atmospheric Simulations. *J Climate*, **22**, 3993-4013.

Gauss, M., et al., 2003: Radiative forcing in the 21st century due to ozone changes in the troposphere and the lower stratosphere. *Journal of Geophysical Research-Atmospheres*, **108**, -.

Gautam, R., N. C. Hsu, K. M. Lau, and M. Kafatos, 2009: Aerosol and rainfall variability over the Indian monsoon region: distributions, trends and coupling. *Ann Geophys-Germany*, **27**, 3691-3703.

Gillett, N., R. Allan, and T. Ansell, 2005: Detection of external influence on sea level pressure with a multi-model ensemble. *Geophys Res Lett*, **32**.

Gillett, N. P., and D. W. J. Thompson, 2003: Simulation of recent Southern Hemisphere climate change. *Science*, **302**, 273-275.

Gillett, N. P., and P. A. Stott, 2009: Attribution of anthropogenic influence on seasonal sea level pressure. *Geophys Res Lett*, **36**.

Ginoux, P., J. M. Prospero, T. E. Gill, N. C. Hsu, and M. Zhao, 2012: Global scale attribution of anthropogenic and natural dust sources and their emission rates based on MODIS Deep Blue aerosol products. *Reviews of Geophysics*.

Goddard, L., et al., 2012: A verification framework for interannual-to-decadal predictions experiments. *Clim. Dyn.*, **submitted**.

Goldenberg, S. B., C. W. Landsea, A. M. Mestas-Nunez, and W. M. Gray, 2001: The recent increase in Atlantic hurricane activity: Causes and implications. *Science*, **293**, 474-479.

Gorodetskaya, I. V., L. B. Tremblay, B. Liepert, M. A. Cane, and R. I. Cullather, 2008: The influence of cloud and surface properties on the Arctic Ocean shortwave radiation budget in coupled models. *J Climate*, **21**, 866-882.

Gosling, S. N., R. G. Taylor, N. W. Arnell, and M. C. Todd, 2011: A comparative analysis of projected impacts of climate change on river runoff from global and catchment-scale hydrological models. *Hydrol Earth Syst Sc*, **15**, 279-294.

Granier, C., et al., 2006: Ozone pollution from future ship traffic in the Arctic northern passages. *Geophys. Res. Lett.*, **33**, L13807.

Gray, L., et al., 2010: SOLAR INFLUENCES ON CLIMATE. *Reviews of Geophysics*, **48**.

Gregory, J., 2010: Long-term effect of volcanic forcing on ocean heat content. *Geophys Res Lett*. doi:ARTN L22701, DOI 10.1029/2010GL045507, -.

Gregory, J. M., and J. F. B. Mitchell, 1995: Simulation of Daily Variability of Surface-Temperature and Precipitation over Europe in the Current and 2xco(2) Climates Using the Ukmo Climate Model. *Quarterly Journal of the Royal Meteorological Society*, **121**, 1451-1476.

Gregory, J. M., and P. M. Forster, 2008: Transient climate response estimated from radiative forcing and observed temperature change. *Journal of Geophysical Research-Atmospheres*, **113**.

Griffies, S. M., and K. Bryan, 1997: A predictability study of simulated North Atlantic multidecadal variability. *Clim Dynam*, **13**, 459-487.

Grotzner, A., M. Latif, A. Timmermann, and R. Voss, 1999: Interannual to decadal predictability in a coupled ocean-atmosphere general circulation model. *J Climate*, **12**, 2607-2624.

Grousset, F. E., P. Ginoux, A. Bory, and P. E. Biscaye, 2003: Case study of a Chinese dust plume reaching the French Alps. *Geophys Res Lett*, **30**.

Guémas, V., F.J. Doblas-Reyes, F. Lienert, Y. Soufflet, and H. Du, 2012: Identifying the causes of the poor decadal climate prediction skill over the North Pacific. *J. Geophys. Res.*, **submitted**.

Guémas, V. L. A. a. F. J. D.-R., 2012: How to deal with the data dependencies in climate time series when applying statistical tests of hypothesis? *J. Appl. Meteorol. Clim.*, **submitted**.

Guenther, A., T. Karl, P. Harley, C. Wiedinmyer, P. I. Palmer, and C. Geron, 2006: Estimates of global terrestrial isoprene emissions using MEGAN (Model of Emissions of Gases and Aerosols from Nature). *Atmos. Chem. Phys.*, **6**, 3181-3210.

Guo, D. L., and H. Wang, 2012: A projection of permafrost degradation on the Tibetan Plateau during the 21st century. *J. Geophys. Res.*, **17**.

Gutowski, W. J., K. A. Kozak, R. W. Arritt, J. H. Christensen, J. C. Patton, and E. S. Takle, 2007: A possible constraint on regional precipitation intensity changes under global warming. *J Hydrometeorol*, **8**, 1382-1396.

Gutowski, W. J., et al., 2008: Causes of observed changes in extremes and projections of future changes. *Weather and Climate Extremes in a Changing Climate. Regions of Focus: North America, Hawaii, Caribbean, and U.S. Pacific Islands*, T.R. Karl, G.A. Meehl, D.M. Christopher, S.J. Hassol, A.M. Waple, and W. L. Murray, Eds., U.S. Climate Change Science Program and the Subcommittee on Global Change Research.

Haarsma, R. J., and F. M. Selten, 2012: Anthropogenic changes in the Walker Circulation and their impact on the extra-tropical planetary wave structure in the Northern Hemisphere. *Clim. Dyn.* doi:DOI 10.1007/s00382-012-1308-1.

Haarsma, R. J., F. Selten, B. V. Hurk, W. Hazeleger, and X. L. Wang, 2009: Drier Mediterranean soils due to greenhouse warming bring easterly winds over summertime central Europe. *Geophys Res Lett*, **36**.

Haigh, J., A. Winning, R. Toumi, and J. Harder, 2010: An influence of solar spectral variations on radiative forcing of climate. *Nature*, **467**, 696-699.

Haigh, J. D., 1996: The impact of solar variability on climate. *Science*, **272**, 981-984.

Haigh, J. D., M. Blackburn, and R. Day, 2005: The response of tropospheric circulation to perturbations in lower-stratospheric temperature. *J Climate*, **18**, 3672-3685.

Hallquist, M., et al., 2009: The formation, properties and impact of secondary organic aerosol: current and emerging issues. *Atmos. Chem. Phys.*, **9**, 5155-5236.

Han, W., et al., 2012: Pacific decadal sea level change patterns associated with a warming Indo-Pacific Warm Pool. *Nature Geosci*, **submitted**.

Hanel, M., and T. A. Buishand, 2011: Analysis of precipitation extremes in an ensemble of transient regional climate model simulations for the Rhine basin. *Clim Dynam*, **36**, 1135-1153.

Hansen, J., A. Lacis, R. Ruedy, and M. Sato, 1992: Potential Climate Impact of Mount-Pinatubo Eruption. *Geophys Res Lett*, **19**, 215-218.

Hansen, J., R. Ruedy, M. Sato, and K. Lo, 2010: Global Surface Temperature Change. *Reviews of Geophysics*, **48**.

Hansen, J., M. Sato, R. Ruedy, A. Lacis, and V. Oinas, 2000: Global warming in the twenty-first century: An alternative scenario. *Proceedings of the National Academy of Sciences*, **97**, 9875-9880.

Harder, J., J. Fontenla, P. Pilewskie, E. Richard, and T. Woods, 2009: Trends in solar spectral irradiance variability in the visible and infrared. *Geophys Res Lett*, **36**.

Haren, R., G. van Oldenborgh, G. Lenderink, M. Collins, and W. Hazeleger, 2011: SST and circulation trend biases cause an underestimation of European precipitation trends.

——, 2012: SST and circulation trend biases cause an underestimation of European precipitation trends. *Clim. Dyn.* doi:10.1007/s00382-012-1401-5.

Hawkins, E., and R. Sutton, 2009: THE POTENTIAL TO NARROW UNCERTAINTY IN REGIONAL CLIMATE PREDICTIONS. *Bulletin of the American Meteorological Society*. doi:DOI 10.1175/2009BAMS2607.1, 1095-+.

Hawkins, E., and R. Sutton, 2010: The potential to narrow uncertainty in projections of regional precipitation change. *Clim Dynam*. doi:10.1007/s00382-010-0810-6, 1-12.

——, 2011: The potential to narrow uncertainty in projections of regional precipitation change. *Clim Dynam*, **37**, 407-418.

Hazeleger, W., et al., 2012a: Multiyear climate predictions using two initialisation strategies. *Geoph. Res. Lett.*, **submitted**.

Hazeleger, W., et al., 2012b: Predicting multi-year North Atlantic Ocean variability. *J. Geophys. Res.*, **submitted**.

Heald, C. L., et al., 2008: Predicted change in global secondary organic aerosol concentrations in response to future climate, emissions, and land use change. *J. Geophys. Res.*, **113**, D05211.

Hedegaard, G. B., J. Brandt, J. H. Christensen, L. M. Frohn, C. Geels, K. M. Hansen, and M. Stendel, 2008: Impacts of climate change on air pollution levels in the Northern Hemisphere with special focus on Europe and the Arctic. *Atmos. Chem. Phys.*, **8**, 3337-3367.

Heinrich, G., and A. Gobiet, 2011: The future of dry and wet spells in Europe: A comprehensive study based on the ENSEMBLES regional climate models. *Int. J. Climatol.* doi:658 10.1002/joc.2421.

Held, I., and B. Soden, 2006: Robust responses of the hydrological cycle to global warming. *J Climate*. 5686-5699.

Hermanson, L., and R. T. Sutton, 2010: Case studies in interannual to decadal climate predictability. *Clim Dynam*, **35**, 1169-1189.

Hezel, P. j., X. Zhang, C.M. Bitz, and B. P. Kelly, 2012: Projected decline in snow depth on Arctic sea ice casued by progressively later autumn open ocean freeze-up this century. *Geoph. Res. Lett.*, **submitted**.

1   Ho, Hawkins, Shaffrey, and Underwood, 2012: 'Statistical decadal predictions for sea surface temperatures: a
2   benchmark for dynamical GCM predictions'. *Clim. Dyn.*, **submitted**.
3   Hodnebrog, ò., et al., 2012: A model study of the Eastern Mediterranean ozone levels during the hot summer of 2007.
4   *Atmos. Chem. Phys. Discuss.*, **12**, 7617-7675.
5   Hoerling, M., et al., 2011: On North American Decadal Climate for 2011-20. *J Climate*, **24**, 4519-4528.
6   Hogrefe, C., et al., 2004: Simulating changes in regional air pollution over the eastern United States due to changes in
7   global and regional climate and emissions. *J. Geophys. Res.*, **109**, D22301.
8   Hohenegger, C., P. Brockhaus, C. S. Bretherton, and C. Schar, 2009: The Soil Moisture-Precipitation Feedback in
9   Simulations with Explicit and Parameterized Convection. *J Climate*, **22**, 5003-5020.
10 Holland, M. M., J. Finnis, and M. C. Serreze, 2006: Simulated Arctic Ocean freshwater budgets in the twentieth and
11   twenty-first centuries. *J Climate*, **19**, 6221-6242.
12 Holland, M. M., M. C. Serreze, and J. Stroeve, 2008: The sea ice mass budget of the Arctic and its future change as
13   simulated by coupled climate models. *Clim. Dyn.* doi:10.1007/s00382-008-0493-4.
14 Holland, M. M., J. Finnis, A. P. Barrett, and M. C. Serreze, 2007: Projected changes in arctic ocean freshwater budgets.
15   *J Geophys Res-Biogeo*, **112**.
16 Holloway, T., A. Fiore, and M. G. Hastings, 2003: Intercontinental Transport of Air Pollution:‚Äâ Will Emerging
17   Science Lead to a New Hemispheric Treaty? *Environmental Science & Technology*, **37**, 4535-4542.
18 Holloway, T., et al., 2008: Change in ozone air pollution over Chicago associated with global climate change. *J.
19   Geophys. Res.*, **113**, D22306.
20 Holmes, C. D., M. J. Prather, and A. O. Sovde, 2012: Future methane, hydroxyl, and their uncertainties: key parameters
21   for modeling emissions and climate change. *Atmospheric Chemistry and Physics*, **12**.
22 Hoyle, C. R., et al., 2011: A review of the anthropogenic influence on biogenic secondary organic aerosol. *Atmos.
23   Chem. Phys.*, **11**, 321-343.
24 Hsu, J., and M. Prather, 2010: Global long-lived chemical modes excited in a 3-D chemistry transport model:
25   Stratospheric N2O, NOy, O-3 and CH4 chemistry. *Geophys Res Lett*, **37**, -.
26 HTAP, 2010a: *HEMISPHERIC TRANSPORT OF AIR POLLUTION 2010, PART B: Mercury, Air Pollution Studies No.
27   18.* Vol. 18, United Nations, 278 pp.
28 ——, 2010b: *HEMISPHERIC TRANSPORT OF AIR POLLUTION 2010, PART C: Persistent Organic Pollutants.* Vol.
29   19, United Nations, 278 pp.
30 ——, 2010c: *HEMISPHERIC TRANSPORT OF AIR POLLUTION 2010, PART A: OZONE AND PARTICULATE
31   MATTER.* Vol. 17, United Nations, 278 pp.
32 Huang, H.-C., et al., 2008: Impacts of long-range transport of global pollutants and precursor gases on U.S. air quality
33   under future climatic conditions. *J. Geophys. Res.*, **113**, D19307.
34 Huebener, H., U. Cubasch, U. Langematz, T. Spangehl, F. Niehorster, I. Fast, and M. Kunze, 2007: Ensemble climate
35   simulations using a fully coupled ocean-troposphere-stratosphere general circulation model. *Philos T R Soc A.*
36   doi:DOI 10.1098/rsta.2007.2078, 2089-2101.
37 Hungate, B. A., et al., 2002: Evapotranspiration and soil water content in a scrub-oak woodland under carbon dioxide
38   enrichment. *Global Change Biol*, **8**, 289-298.
39 Huntington, T. G., 2006: Evidence for intensification of the global water cycle: Review and synthesis. *J Hydrol*, **319**,
40   83-95.
41 Hurtt, G. C., et al., 2011: Harmonization of land-use scenarios for the period 1500-2100: 600 years of global gridded
42   annual land-use transitions, wood harvest, and resulting secondary lands. *Climatic Change*, **109**, 117-161.
43 Huszar, P., et al., 2011: Effects of climate change on ozone and particulate matter over Central and Eastern Europe.
44   *Climate Research*, **50**, 51-68.
45 Ihara, C., and Y. Kushnir, 2009: Change of mean midlatitude westerlies in 21st century climate simulations. *Geophys
46   Res Lett.* doi:ARTN L13701, DOI 10.1029/2009GL037674, -.
47 Im, E. S., W. J. Gutowski, and F. Giorgi, 2008: Consistent changes in twenty-first century daily precipitation from
48   regional climate simulations for Korea using two convection parameterizations. *Geophys Res Lett*, **35**.
49 Ineson, S., A. Scaife, J. Knight, J. Manners, N. Dunstone, L. Gray, and J. Haigh, 2011: Solar forcing of winter climate
50   variability in the Northern Hemisphere. *Nat Geosci*, **4**, 753-757.
51 IPCC, 2007: *Climate Change 2007: The Physical Science Basis. Contribution of Working Group I to the Fourth
52   Assessment Report of the Intergovernmental Panel on Climate Change (IPCC).* Cambridge University Press, 996
53   pp.
54 ——, 2012: *Managing the Risks of Extreme Events and Disasters to Advance Climate Change Adaptation.* A Special
55   Report of Working Groups I and II of the Intergovernmental Panel on Climate Change. C. B. Field, et al., Eds.,
56   582.
57 Isaksen, I. S. A., et al., 2009: Atmospheric composition change: Climate-Chemistry interactions. *Atmos Environ*, **43**,
58   5138-5192.
59 Ito, A., S. Sillman, and J. E. Penner, 2009: Global chemical transport model study of ozone response to changes in
60   chemical kinetics and biogenic volatile organic compounds emissions due to increasing temperatures:
61   Sensitivities to isoprene nitrate chemistry and grid resolution. *J. Geophys. Res.*, **114**, D09301.
62 JACOB, D., et al., 1993: FACTORS REGULATING OZONE OVER THE UNITED-STATES AND ITS EXPORT TO
63   THE GLOBAL ATMOSPHERE. *Journal of Geophysical Research-Atmospheres*, **98**, 14817-14826.

1   Jacob, D. J., and D. A. Winner, 2009: Effect of climate change on air quality. *Atmos Environ*, **43**, 51-63.
2   Jacob, D. J., J. A. Logan, and P. P. Murti, 1999: Effect of rising Asian emissions on surface ozone in the United States.
3   *Geophys. Res. Lett.*, **26**, 2175-2178.
4   Jacobson, M., 2008a: Effects of wind-powered hydrogen fuel cell vehicles on stratospheric ozone and global climate.
5   *Geophys Res Lett*. doi:ARTN L19803, 10.1029/2008GL035102, -.
6   ——, 2010: Short-term effects of controlling fossil-fuel soot, biofuel soot and gases, and methane on climate, Arctic
7   ice, and air pollution health. *Journal of Geophysical Research-Atmospheres*. doi:ARTN D14209,
8   10.1029/2009JD013795, -.
9   Jacobson, M., and D. Streets, 2009: Influence of future anthropogenic emissions on climate, natural emissions, and air
10   quality. *Journal of Geophysical Research-Atmospheres*. doi:ARTN D08118, 10.1029/2008JD011476, -.
11   Jacobson, M. Z., 2008b: On the causal link between carbon dioxide and air pollution mortality. *Geophys. Res. Lett.*, **35**,
12   L03809.
13   Jaffe, D., D. Chand, W. Hafner, A. Westerling, and D. Spracklen, 2008: Influence of Fires on O3 Concentrations in the
14   Western U.S. *Environmental Science & Technology*, **42**, 5885-5891.
15   Jaffe, D. A., and N. L. Wigder, 2012: Ozone production from wildfires: A critical review. *Atmos Environ*, **51**, 1-10.
16   Jiang, X., Z.-L. Yang, H. Liao, and C. Wiedinmyer, 2010: Sensitivity of biogenic secondary organic aerosols to future
17   climate change at regional scales: An online coupled simulation. *Atmos Environ*, **44**, 4891-4907.
18   Jiang, X., C. Wiedinmyer, F. Chen, Z.-L. Yang, and J. C.-F. Lo, 2008: Predicted impacts of climate and land use
19   change on surface ozone in the Houston, Texas, area. *J. Geophys. Res.*, **113**, D20312.
20   Jickells, T. D., et al., 2005: Global Iron Connections Between Desert Dust, Ocean Biogeochemistry, and Climate.
21   *Science*, **308**, 67-71.
22   John, J. G., A. M. Fiore, V. Naik, L. W. Horowitz, and J. P. Dunne, 2012: Climate versus emission drivers of methane
23   lifetime from 1860–2100. *Atmos. Chem. Phys. Discuss.*, **12**.
24   Johnson, C. E., W. J. Collins, D. S. Stevenson, and R. G. Derwent, 1999: Relative roles of climate and emissions
25   changes on future tropospheric oxidant concentrations. *J. Geophys. Res.*, **104**, 18631-18645.
26   Johnson, C. E., D. S. Stevenson, W. J. Collins, and R. G. Derwent, 2001: Role of climate feedback on methane and
27   ozone studied with a Coupled Ocean‐Atmosphere‐Chemistry Model. *Geophys. Res. Lett.*, **28**,
28   1723-1726.
29   Johnson, N. C., and S. P. Xie, 2010: Changes in the sea surface temperature threshold for tropical convection. *Nat
30   Geosci*, **3**, 842-845.
31   Jolliffe, I. T., 2007: Uncertainty and inference for verification measures. *Weather and Forecasting*, **22**, 637-650.
32   Jolliffe, I. T., and D. B. Stephenson, 2011: *Forecast Verification: A Practitioner's Guide in Atmospheric Science, 2nd
33   Edition.* Wiley and Sons.
34   Jones, G., M. Lockwood, and P. Stott, 2012: What influence will future solar activity changes over the 21st century
35   have on projected global near-surface temperature changes? *Journal of Geophysical Research-Atmospheres*,
36   **117**.
37   Joshi, M., E. Hawkins, R. Sutton, J. Lowe, and D. Frame, 2011: Projections of when temperature change will exceed 2
38   degrees C above pre-industrial levels. *Nat Clim Change*, **1**, 407-412.
39   Jung, M., et al., 2010: Recent decline in the global land evapotranspiration trend due to limited moisture supply. *Nature*,
40   **467**, 951-954.
41   Kang, S., and L. Polvani, 2011: The Interannual Relationship between the Latitude of the Eddy-Driven Jet and the Edge
42   of the Hadley Cell. *J Climate*, **24**, 563-568.
43   Kang, S. M., L. M. Polvani, J. C. Fyfe, and M. Sigmond, 2011: Impact of Polar Ozone Depletion on Subtropical
44   Precipitation. *Science*, **332**, 951-954.
45   Kao, S. C., and A. R. Ganguly, 2011: Intensity, duration, and frequency of precipitation extremes under 21st-century
46   warming scenarios. *Journal of Geophysical Research-Atmospheres*, **116**.
47   Katragkou, E., P. Zanis, I. Kioutsioukis, I. Tegoulias, D. Melas, B. C. Kruger, and E. Coppola, 2011: Future climate
48   change impacts on summer surface ozone from regional climate-air quality simulations over Europe. *Journal of
49   Geophysical Research-Atmospheres*, **116**.
50   Kawase, H., T. Nagashima, K. Sudo, and T. Nozawa, 2011: Future changes in tropospheric ozone under Representative
51   Concentration Pathways (RCPs). *Geophys. Res. Lett.*, **38**, L05801.
52   Keenlyside, N. S., M. Latif, J. Jungclaus, L. Kornblueh, and E. Roeckner, 2008: Advancing decadal-scale climate
53   prediction in the North Atlantic sector. *Nature*, **453**, 84-88.
54   Keller, C. A., D. Brunner, S. Henne, M. K. Vollmer, S. O'Doherty, and S. Reimann, 2011: Evidence for under-reported
55   western European emissions of the potent greenhouse gas HFC-23. *Geophys. Res. Lett.*, **38**, L15808.
56   Kharin, V. V., F. W. Zwiers, X. B. Zhang, and G. C. Hegerl, 2007: Changes in temperature and precipitation extremes
57   in the IPCC ensemble of global coupled model simulations. *J Climate*, **20**, 1419-1444.
58   Kharin, V. V., G.J. Boer, J. W.J. Merryfield, F. Scinocca, and W.-S. Lee, 2012: Statistical adjustment of decadal
59   predictions in a changing climate. *Geoph. Res. Lett.*, **submitted**.
60   Kim, H. M., P. J. Webster, and J. A. Curry, 2012: Evaluation of short-term climate change prediction in multi-model
61   CMIP5 decadal hindcasts. *Geophys Res Lett*, **39**.
62   Kleeman, M. J., 2008: A preliminary assessment of the sensitivity of air quality in California to global change. *Climatic
63   Change*, **87 (Suppl 1)**, S273-S292.

Kleeman, R., Y. M. Tang, and A. M. Moore, 2003: The calculation of climatically relevant singular vectors in the presence of weather noise as applied to the ENSO problem. *J Atmos Sci*, **60**, 2856-2868.

Kloster, S., F. Dentener, J. Feichter, F. Raes, U. Lohmann, E. Roeckner, and I. Fischer-Bruns, 2010a: A GCM study of future climate response to aerosol pollution reductions. *Clim Dynam*, **34**, 1177-1194.

Kloster, S., F. Dentener, J. Feichter, F. Raes, U. Lohmann, E. Roeckner, and I. Fischer-Bruns, 2010b: A GCM study of future climate response to aerosol pollution reductions. *Climate Dynamics*, **34**, 1177-1194.

Kloster, S., et al., 2008: Influence of future air pollution mitigation strategies on total aerosol radiative forcing. *Atmospheric Chemistry and Physics*, **8**, 6405-6437.

Knight, J., R. Allan, C. Folland, M. Vellinga, and M. Mann, 2005: A signature of persistent natural thermohaline circulation cycles in observed climate. *Geophys Res Lett*. doi:ARTN L20708, 10.1029/2005GL024233, -.

KNUTSON, T., and S. MANABE, 1995: TIME-MEAN RESPONSE OVER THE TROPICAL PACIFIC TO INCREASED CO2 IN A COUPLED OCEAN-ATMOSPHERE MODEL. *J Climate*. 2181-2199.

Knutson, T. R., F. Zeng, and A. T. Wittenberg 2012a: Multi-Model Assessment of Regional Surface Temperature Trends: CMIP3 vs CMIP5 Historical (20C3M) Runs *J. Climate*, **submitted**.

——, 2012b: Multi-Model Assessment of Regional Surface Temperature Trends: CMIP3 vs CMIP5 Historical (20C3M) Runs. *J. Climate*, **submitted**.

Knutson, T. R., et al., 2006: Assessment of Twentieth-Century regional surface temperature trends using the GFDL CM2 coupled models. *J. Climate*, **19**.

Knutson, T. R., et al., 2010: Tropical cyclones and climate change. *Nature Geosci*, **3**, 157-163.

Korty, R. L., and T. Schneider, 2008: Extent of Hadley circulations in dry atmospheres. *Geophys Res Lett*, **35**.

Koster, R. D., et al., 2010: Contribution of land surface initialization to subseasonal forecast skill: First results from a multi-model experiment. *Geophys Res Lett*, **37**, L02402.

Krueger, O., and J.-S. von Storch, 2011: A simple empirical model for decadal climate prediction. *J. Climate*, **24**, 1276–1283.

Kumar, S., V. Merwade, D. Niyogi, and J. L. Kinter III, 2012: Evaluation of Temperature and Precipitation Trends and long-term Persistence in CMIP5 20th Century Climate Simulations. *J. Climate*, **submitted**.

Laepple, T., S. Jewson, and K. Coughlin, 2008: Interannual temperature predictions using the CMIP3 multi-model ensemble mean. *Geophys Res Lett*, **35**, L10701.

Lamarque, J.-F., et al., 2011a: Global and regional evolution of short-lived radiatively-active gases and aerosols in the Representative Concentration Pathways. *Climatic Change*. doi:10.1007/s10584-011-0155-0, 1-22.

Lamarque, J.-F. o., et al., 2011b: Global and regional evolution of short-lived radiatively-active gases and aerosols in the Representative Concentration Pathways. *Climatic Change*. doi:10.1007/s10584-011-0155-0, 1-22.

Lamarque, J. F., et al., 2011c: Global and regional evolution of short-lived radiatively-active gases and aerosols in the Representative Concentration Pathways. *Climatic Change*.

Lambert, F. H., and J. C. H. Chiang, 2007: Control of land-ocean temperature contrast by ocean heat uptake. *Geophys Res Lett*, **34**.

Lambert, F. H., and M. J. Webb, 2008: Dependency of global mean precipitation on surface temperature. *Geophys Res Lett*, **35**.

Lambert, F. H., A. R. Stine, N. Y. Krakauer, and J. C. H. Chiang, 2008: How much will precipitation increase with global warming? *EOS Transactions*, **89**.

Lambert, S. J., and B. K. Hansen, 2011: Simulated Changes in the Freezing Rain Climatology of North America under Global Warming Using a Coupled Climate Model. *Atmos Ocean*, **49**, 289-295.

Lammertsma, E. I., H. J. de Boer, S. C. Dekker, D. L. Dilcher, A. F. Lotter, and F. Wagner-Cremer, 2011: Global CO2 rise leads to reduced maximum stomatal conductance in Florida vegetation. *Proc. Natl. Acad. Sci. U. S. A.*, **108**, 4035-4040.

Lang, C., and D. W. Waugh, 2011: Impact of climate change on the frequency of Northern Hemisphere summer cyclones. *Journal of Geophysical Research-Atmospheres*, **116**.

Langner, J., M. Engardt, and C. Andersson, 2012a: European summer surface ozone 1990-2100. *Atmos. Chem. Phys. Discuss.*, **12**, 7705-7726.

Langner, J., et al., 2012b: A multi-model study of impacts of climate change on surface ozone in Europe. *Atmos. Chem. Phys. Discuss.*, **12**.

——, 2012c: A multi-model study of impacts of climate change on surface ozone in Europe. *Atmos. Chem. Phys. Discuss.*, **12**, 4901-4939.

Lanzante, J. R., 2005: A cautionary note on the use of error bars. *J Climate*, **18**, 3699-3703.

Latif, M., M. Collins, H. Pohlmann, and N. Keenlyside, 2006: A review of predictability studies of Atlantic sector climate on decadal time scales. *J Climate*, **19**, 5971-5987.

Latif, M., C. W. Boning, J. Willebrand, A. Biastoch, A. Alvarez-Garcia, N. Keenlyside, and H. Pohlmann, 2007: Decadal to Multidecadal Variability of the Atlantic MOC: Mechanisms and Predictability. - In: "Ocean Circulation: Mechanisms and Impacts - Past and Future Changes of Meridional Overturning". *AGU Mongraph 173*, A. Schmittner, J. C. H. Chiang, and S. R. Hemming, Eds., American Geophysical Union, 149-166.

Lau, K. M., and K. M. Kim, 2006: Observational relationships between aerosol and Asian monsoon rainfall, and circulation. *Geophys Res Lett*, **33**.

Lau, K. M., M. K. Kim, and K. M. Kim, 2006: Asian summer monsoon anomalies induced by aerosol direct forcing: the role of the Tibetan Plateau. *Clim Dynam*, **26**, 855-864.

Lawrence, D. M., and A. G. Slater, 2010: The contribution of snow condition trends to future ground climate. *Clim Dynam*, **34**, 969-981.

Lawrence, D. M., A. G. Slater, V. E. Romanovsky, and D. J. Nicolsky, 2008: Sensitivity of a model projection of near-surface permafrost degradation to soil column depth and representation of soil organic matter. *J Geophys Res-Earth*, **113**.

Lean, J. L., and D. H. Rind, 2009: How will Earth's surface temperature change in future decades? *Geophys Res Lett*, **36**, L15708.

Lee, T. C. K., F. W. Zwiers, X. B. Zhang, and M. Tsao, 2006: Evidence of decadal climate prediction skill resulting from changes in anthropogenic forcing. *J Climate*, **19**, 5305-5318.

Leibensperger, E. M., L. J. Mickley, and D. J. Jacob, 2008: Sensitivity of US air quality to mid-latitude cyclone frequency and implications of 1980–2006 climate change. *Atmos. Chem. Phys.*, **8**, 7075-7086.

Leibensperger, E. M., L. J. Mickley, D. J. Jacob, and S. R. H. Barrett, 2011a: Intercontinental influence of NOx and CO emissions on particulate matter air quality. *Atmos Environ*, **45**, 3318-3324.

Leibensperger, E. M., et al., 2011b: Climatic effects of 1950‚Äì2050 changes in US anthropogenic aerosols ‚Äì Part 2: Climate response. *Atmos. Chem. Phys. Discuss.*, **11**, 24127-24164.

Lenderink, G., and E. Van Meijgaard, 2008: Increase in hourly precipitation extremes beyond expectations from temperature changes. *Nat Geosci*, **1**, 511-514.

Lenderink, G., E. van Meijgaard, and F. Selten, 2009: Intense coastal rainfall in the Netherlands in response to high sea surface temperatures: analysis of the event of August 2006 from the perspective of a changing climate. *Clim Dynam*, **32**, 19-33.

Lenderink, G., H. Y. Mok, T. C. Lee, and G. J. van Oldenborgh, 2011: Scaling and trends of hourly precipitation extremes in two different climate zones - Hong Kong and the Netherlands. *Hydrol Earth Syst Sc*, **15**, 3033-3041.

Leslie, L. M., D. J. Karoly, M. Leplastrier, and B. W. Buckley, 2007: Variability of tropical cyclones over the southwest Pacific Ocean using a high-resolution climate model. *Meteorol Atmos Phys*, **97**, 171-180.

Levermann, A., J. Schewe, V. Petoukhov, and H. Held, 2009: Basic mechanism for abrupt monsoon transitions. *Proc. Natl. Acad. Sci. U. S. A.*, **106**, 20572-20577.

Levin, I., et al., 2010: The global SF6 source inferred from long-term high precision atmospheric measurements and its comparison with emission inventories. *Atmos. Chem. Phys.*, **10**, 2655-2662.

Levy, H., II, L. W. Horowitz, M. D. Schwarzkopf, Y. Ming, J. C. Golaz, V. Naik, and V. Ramaswamy, 2012: The Roles of Aerosol Direct and Indirect Effects in Past and Future Climate Change. *J. Geophys. Res.*, **submitted**.

Li, H. L., H. J. Wang, and Y. Z. Yin, 2012: Interdecadal variation of the West African summer monsoon during 1979–2010 and associated variability. *Clim. Dyn.* doi:10.1007/s00382-012-1426-9.

Li, Q., et al., 2002: Transatlantic transport of pollution and its effects on surface ozone in Europe and North America. *J. Geophys. Res.*, **107**, 4166.

Li, S. L., J. Perlwitz, X. W. Quan, and M. P. Hoerling, 2008: Modelling the influence of North Atlantic multidecadal warmth on the Indian summer rainfall. *Geophys Res Lett*, **35**.

Liang, X.-Z., J. Pan, J. Zhu, K. E. Kunkel, J. X. L. Wang, and A. Dai, 2006: Regional climate model downscaling of the U.S. summer climate and future change. *J. Geophys. Res.*, **111**, D10108.

Liao, H., W.-T. Chen, and J. H. Seinfeld, 2006: Role of climate change in global predictions of future tropospheric ozone and aerosols. *J. Geophys. Res.*, **111**, D12304.

Liao, H., Y. Zhang, W.-T. Chen, F. Raes, and J. H. Seinfeld, 2009: Effect of chemistry-aerosol-climate coupling on predictions of future climate and future levels of tropospheric ozone and aerosols. *J. Geophys. Res.*, **114**, D10306.

Liao, K.-J., et al., 2007: Sensitivities of Ozone and Fine Particulate Matter Formation to Emissions under the Impact of Potential Future Climate Change. *Environmental Science & Technology*, **41**, 8355-8361.

Lienert, F., and F. J. Doblas-Reyes, 2012: Decadal prediction of North Pacific sea surface temperature and its influence on land climate. *Geoph. Res. Lett.*, **submitted**.

Lin, C. Y. C., D. J. Jacob, and A. M. Fiore, 2001: Trends in exceedances of the ozone air quality standard in the continental United States, 1980-1998. *Atmos Environ*, **35**, 3217-3228.

Lin, J.-T., D. J. Wuebbles, and X.-Z. Liang, 2008: Effects of intercontinental transport on surface ozone over the United States: Present and future assessment with a global model. *Geophys. Res. Lett.*, **35**, L02805.

Lin, M., et al., 2012: Transport of Asian ozone pollution into surface air over the western United States in spring. *J. Geophys. Res.*, **117**, D00V07.

Liu, J., D. L. Mauzerall, L. W. Horowitz, P. Ginoux, and A. M. Fiore, 2009: Evaluating inter-continental transport of fine aerosols: (1) Methodology, global aerosol distribution and optical depth. *Atmos Environ*, **43**, 4327-4338.

Liu, J., J. A. Curry, H. Wang, M. Song, and R. M. Horton, 2012: Impact of declining Arctic sea ice on winter snowfall. *Proc. Natl. Acad. Sci. U. S. A.*, **109**, 4074-4079.

Lobell, D. B., and M. B. Burke, 2008: Why are agricultural impacts of climate change so uncertain? The importance of temperature relative to precipitation. *Environ Res Lett*, **3**.

Lockwood, M., 2010: Solar change and climate: an update in the light of the current exceptional solar minimum. *Proceedings of the Royal Society a-Mathematical Physical and Engineering Sciences*, **466**, 303-329.

1	Lockwood, M., R. Harrison, T. Woollings, and S. Solanki, 2010: Are cold winters in Europe associated with low solar
2		activity? *Environ Res Lett*, **5**.
3	Lockwood, M., R. G. Harrison, M. J. Owens, L. Barnard, T. Woollings, and F. Steinhilber, 2011: The solar influence on
4		the probability of relatively cold UK winters in the future. *Environ Res Lett*, **6**.
5	Logan, J. A., 1989: Ozone in Rural Areas of the United States. *J. Geophys. Res.*, **94**, 8511-8532.
6	Lohmann, K., H. Drange, and M. Bentsen, 2009: A possible mechanism for the strong weakening of the North Atlantic
7		subpolar gyre in the mid-1990s. *Geophys Res Lett*, **36**.
8	Lorenz, D., and E. DeWeaver, 2007: Tropopause height and zonal wind response to global warming in the IPCC
9		scenario integrations. *Journal of Geophysical Research-Atmospheres*. doi:ARTN D10119,
10		10.1029/2006JD008087, -.
11	Lu, J., G. Vecchi, and T. Reichler, 2007: Expansion of the Hadley cell under global warming. *Geophys Res Lett*.
12		doi:ARTN L06805, 10.1029/2006GL028443, -.
13	Lu, R. Y., and Y. H. Fu, 2010: Intensification of East Asian Summer Rainfall Interannual Variability in the Twenty-
14		First Century Simulated by 12 CMIP3 Coupled Models. *J Climate*, **23**, 3316-3331.
15	Mahlstein, I., R. Knutti, S. Solomon, and R. W. Portmann, 2011: Early onset of significant local warming in low
16		latitude countries. *Environ Res Lett*, **6**.
17	Mahmud, A., M. Tyree, D. Cayan, N. Motallebi, and M. J. Kleeman, 2008: Statistical downscaling of climate change
18		impacts on ozone concentrations in California. *J. Geophys. Res.*, **113**, D21103.
19	Mahmud, A., M. Hixson, J. Hu, Z. Zhao, S. H. Chen, and M. J. Kleeman, 2010: Climate impact on airborne particulate
20		matter concentrations in California using seven year analysis periods. *Atmos. Chem. Phys.*, **10**, 11097-11114.
21	Mahowald, N. M., 2007: Anthropocene changes in desert area: Sensitivity to climate model predictions. *Geophys. Res.*
22		*Lett.*, **34**, L18817.
23	Mahowald, N. M., and C. Luo, 2003: A less dusty future? *Geophys. Res. Lett.*, **30**, 1903.
24	Mahowald, N. M., D. R. Muhs, S. Levis, P. J. Rasch, M. Yoshioka, C. S. Zender, and C. Luo, 2006: Change in
25		atmospheric mineral aerosols in response to climate: Last glacial period, preindustrial, modern, and doubled
26		carbon dioxide climates. *J. Geophys. Res.*, **111**, D10202.
27	Makkonen, R., A. Asmi, V. M. Kerminen, M. Boy, A. Arneth, P. Hari, and M. Kulmala, 2012: Air pollution control and
28		decreasing new particle formation lead to strong climate warming. *Atmos. Chem. Phys.*, **12**, 1515-1524.
29	Maloney, E. D., et al., 2012: North American Climate in CMIP5 Experiments: Part III: Assessment of 21st Century
30		Projections. *J. Climate*, **submitted**.
31	Manabe, S., R. J. Stouffer, M. J. Spelman, and K. Bryan, 1991: Transient Responses of a Coupled Ocean Atmosphere
32		Model to Gradual Changes of Atmospheric Co2 .1. Annual Mean Response. *J Climate*, **4**, 785-818.
33	Mann, M., et al., 2009: Global Signatures and Dynamical Origins of the Little Ice Age and Medieval Climate Anomaly.
34		*Science*, **326**, 1256-1260.
35	Marengo, J. A., R. Jones, L. M. Alves, and M. C. Valverde, 2009: Future change of temperature and precipitation
36		extremes in South America as derived from the PRECIS regional climate modeling system. *Int J Climatol*, **29**,
37		2241-2255.
38	Mason, S. J., 2004: On using "climatology" as a reference strategy in the Brier and ranked probability skill scores.
39		*Monthly Weather Review*, **132**, 1891-1895.
40	Mason, S. J., and A. P. Weigel, 2009: A Generic Forecast Verification Framework for Administrative Purposes.
41		*Monthly Weather Review*, **137**, 331-349.
42	Masson, D., and R. Knutti, 2011: Climate model genealogy. *Geophys Res Lett*, **38**.
43	Massonnet, F., D. Matei, H. Pohlmann, J. Jungclaus, W. Müller, and H. Haak, 2012: Constraining projections of
44		summer Arctic sea ice. *The Cryosphere*, **submitted**.
45	Matei, D., J. Baehr, J. H. Jungclaus, H. Haak, W. A. Muller, and J. Marotzke, 2012: Multiyear Prediction of Monthly
46		Mean Atlantic Meridional Overturning Circulation at 26.5 degrees N. *Science*, **335**, 76-79.
47	McCabe, G. J., M. A. Palecki, and J. L. Betancourt, 2004: Pacific and Atlantic Ocean influences on multidecadal
48		drought frequency in the United States. *PNAS*, **101**, 4136 – 4141.
49	McGuire, A. D., F. S. Chapin, J. E. Walsh, and C. Wirth, 2006: Integrated regional changes in arctic climate feedbacks:
50		Implications for the global climate system. *Annu Rev Env Resour*, **31**, 61-91.
51	McLandress, C., T. G. Shepherd, J. F. Scinocca, D. A. Plummer, M. Sigmond, A. I. Jonsson, and M. C. Reader, 2011:
52		Separating the Dynamical Effects of Climate Change and Ozone Depletion. Part II Southern Hemisphere
53		Troposphere. *J Climate*, **24**, 1850-1868.
54	Meehl, G., et al., 2006: Climate change projections for the twenty-first century and climate change commitment in the
55		CCSM3. *J Climate*. 2597-2616.
56	Meehl, G. A., and A. X. Hu, 2006: Megadroughts in the Indian monsoon region and southwest North America and a
57		mechanism for associated multidecadal Pacific sea surface temperature anomalies. *J Climate*, **19**, 1605-1623.
58	Meehl, G. A., and J. M. Arblaster, 2011: Decadal Variability of Asian-Australian Monsoon-ENSO-TBO Relationships.
59		*J Climate*, **24**, 4925-4940.
60	Meehl, G. A., and J. M. Arblaster, 2012: Relating the strength of the tropospheric biennial oscillation (TBO) to the
61		phase of the Interdecadal Pacific Oscillation (IPO). *Geoph. Res. Lett.*, **submitted**.
62	Meehl, G. A., and H. Teng, 2012: Decadal hindcasts in the Pacific of the mid-1970s shift and the early 2000s hiatus,
63		and prospects for 2016-2035. *Geoph. Res. Lett.*, **submitted**.

Meehl, G. A., J. M. Arblaster, and W. D. Collins, 2008: Effects of Black Carbon Aerosols on the Indian Monsoon. *J Climate*, **21**, 2869-2882.

Meehl, G. A., A. X. Hu, and C. Tebaldi, 2010: Decadal Prediction in the Pacific Region. *J Climate*, **23**, 2959-2973.

Meehl, G. A., A. Hu, and J. M. Arblaster, 2012a: Externally forced versus internally generated decadal climate variability in the Pacific. *J. Climate*, **submitted**.

Meehl, G. A., J. M. Arblaster, and G. Branstator, 2012b: Mechanisms contributing to the warming hole and the consequent U.S. east-west differential of heat extremes. *J. Climate*, **submitted**.

Meehl, G. A., C. Tebaldi, G. Walton, D. Easterling, and L. McDaniel, 2009a: Relative increase of record high maximum temperatures compared to record low minimum temperatures in the U. S. *Geophys Res Lett*, **36**.

Meehl, G. A., J. M. Arblaster, J. T. Fasullo, A. Hu, and K. E. Trenberth, 2011: Model-based evidence of deep-ocean heat uptake during surface-temperature hiatus periods. *Nat Clim Change*, **1**, 360-364.

Meehl, G. A., et al., 2007a: The WCRP CMIP3 multimodel dataset - A new era in climate change research. *Bulletin of the American Meteorological Society*, **88**, 1383-+.

Meehl, G. A., et al., 2012c: Climate System Response to External Forcings and Climate Change Projections in CCSM4. *J Climate*, **25**, 3661-3683.

Meehl, G. A., et al., 2007b: Global Climate Projections. *Climate Change 2007: The Physical Science Basis. Contribution of Working Group I to the Fourth Assessment Report of the Intergovernmental Panel on Climate Change*, S. Solomon, and D. Qin, Eds., Cambridge University Press.

Meehl, G. A., et al., 2007c: Global Climate Projections. *Climate Change 2007: The Physical Science Basis. Contribution of Working Group I to the Fourth Assessment Report of the Intergovernmental Panel on Climate Change*, Cambridge University Press.

Meehl, G. A., et al., 2009b: DECADAL PREDICTION Can It Be Skillful? *Bulletin of the American Meteorological Society*, **90**, 1467-+.

Meehl, G. A., et al., 2009c: Decadal Prediction. *Bulletin of the American Meteorological Society*, **90**, 1467-1485.

Meehl, G. A., et al., 2012d: Decadal climate prediction: An update from the trenches. *Bulletin of the American Meteorological Society*, **submitted**.

Meinshausen, M., S. Smith, K. Calvin, and J. Daniel, 2011: The RCP greenhouse gas concentrations and their extensions from 1765 to 2300. *Climatic Change*. doi:DOI 10.1007/s10584-011-0156-z.

Meinshausen M, Wigley TML, and R. SCB, 2011: Emulating atmosphere-ocean and carbon cycle models with a simpler model, MAGICC6—Part 2: applications. *Atmos Chem Phys*, **11**, 1457–1471.

Meleux, F., F. Solmon, and F. Giorgi, 2007: Increase in summer European ozone amounts due to climate change. *Atmos Environ*, **41**, 7577-7587.

Menon, S., and et al., 2008: Aerosol climate effects and air quality impacts from 1980 to 2030. *Environ Res Lett*, **3**, 024004.

Merrifield, M. A., 2011: A Shift in Western Tropical Pacific Sea Level Trends during the 1990s. *J Climate*, **24**, 4126-4138.

Mickley, L. J., D. J. Jacob, B. D. Field, and D. Rind, 2004: Effects of future climate change on regional air pollution episodes in the United States. *Geophys. Res. Lett.*, **31**, L24103.

Mickley, L. J., E. M. Leibensperger, D. J. Jacob, and D. Rind, 2011: Regional warming from aerosol removal over the United States: Results from a transient 2010-2050 climate simulation. *Atmos Environ*, **In Press, Accepted Manuscript**.

Miller, R., G. Schmidt, and D. Shindell, 2006a: Forced annular variations in the 20th century intergovernmental panel on climate change fourth assessment report models. *Journal of Geophysical Research-Atmospheres*. doi:ARTN D18101, 10.1029/2005JD006323, -.

Miller, R. L., G. A. Schmidt, and D. T. Shindell, 2006b: Forced annular variations in the 20th century intergovernmental panel on climate change fourth assessment report models. *J Geophys Res-Atmos*, **111**.

Ming, Y., and V. Ramaswamy, 2011: A Model Investigation of Aerosol-induced Changes in Tropical Circulation. *J Climate*. doi:10.1175/2011jcli4108.1.

Ming, Y., V. Ramaswamy, and G. Persad, 2010: Two opposing effects of absorbing aerosols on global-mean precipitation. *Geophys. Res. Lett.*, **37**, L13701.

Ming, Y., V. Ramaswamy, and G. Chen, 2011: A Model Investigation of Aerosol-induced Changes in Boreal Winter Extratropical Circulation. *J Climate*. doi:10.1175/2011jcli4111.1.

Mochizuki, T., et al., 2012: Decadal Prediction Using a Recent Series of MIROC Global Climate Models. *J Meteorol Soc Jpn*, **90A**, 373-383.

Mochizuki, T., et al., 2010: Pacific decadal oscillation hindcasts relevant to near-term climate prediction. *Proc. Natl. Acad. Sci. U. S. A.*, **107**, 1833-1837.

Montzka, S., M. Krol, E. Dlugokencky, B. Hall, P. Jockel, and J. Lelieveld, 2011: Small Interannual Variability of Global Atmospheric Hydroxyl. *Science*, **331**, 67-69.

Morgenstern, O., et al., 2010: Anthropogenic forcing of the Northern Annular Mode in CCMVal-2 models. *Journal of Geophysical Research-Atmospheres*. doi:ARTN D00M03, 10.1029/2009JD013347, -.

Mori, M., et al., 2012: Prediction and Projection of Tropical Cyclone Activity over the Western North Pacific using CMIP5 Near-Term Experiments by MIROC. *J. Meteorology Soc. Japan*, **submitted**.

Morice, C. P., J. J. Kennedy, N. A. Rayner, and P. D. Jones, 2012: Quantifying uncertainties in global and regional temperature change using an ensemble of observational estimates: The HadCRUT4 data set. *J. Geophys. Res.*, **117**.

Moss, R. H., et al., 2010: The next generation of scenarios for climate change research and assessment. *Nature*, **463**, 747-756.

Msadek, R., K. Dixon, T. Delworth, and W. Hurlin, 2010: Assessing the predictability of the Atlantic meridional overturning circulation and associated fingerprints. *Geophys Res Lett*. doi:ARTN L19608, 10.1029/2010GL044517, -.

Müller, A. W., et al., 2012: Forecast skill of multi-year seasonal means in the decadal prediction system of the Max Planck Institute for Meteorology. *Geoph. Res. Lett.*, **submitted**.

Muller, C. J., and P. A. O'gorman, 2011: An energetic perspective on the regional response of precipitation to climate change. *Nat Clim Change*, **1**, 266-271.

Muller, C. J., P. A. O'Gorman, and L. E. Back, 2011: Intensification of Precipitation Extremes with Warming in a Cloud-Resolving Model. *J Climate*, **24**, 2784-2800.

Murazaki, K., and P. Hess, 2006: How does climate change contribute to surface ozone change over the United States? *J. Geophys. Res.*, **111**, D05301.

Murphy, J., et al., 2010: **Towards prediction of decadal climate variability and change**. *Procedia Environmental Science*, **1**, *287-304*.

Murphy, J. M., B. B. B. Booth, M. Collins, G. R. Harris, D. M. H. Sexton, and M. J. Webb, 2007: A methodology for probabilistic predictions of regional climate change from perturbed physics ensembles. *Philos T R Soc A*, **365**, 1993-2028.

Newman, M., 2007: Interannual to decadal predictability of tropical and North Pacific sea surface temperatures. *J Climate*, **20**, 2333-2356.

——, 2012: An empirical benchmark for decadal forecasts of global surface temperature anomalies. *J. Climate*, **submitted**.

Nicolsky, D. J., V. E. Romanovsky, V. A. Alexeev, and D. M. Lawrence, 2007: Improved modeling of permafrost dynamics in a GCM land-surface scheme. *Geophys Res Lett*, **34**.

Nolte, C. G., A. B. Gilliland, C. Hogrefe, and L. J. Mickley, 2008: Linking global to regional models to assess future climate impacts on surface ozone levels in the United States. *J. Geophys. Res.*, **113**, D14307.

NRC, 2009: *Global Sources of Local Pollution:An Assessment of Long-Range Transport of Key Air Pollutants to and from the United States.* The National Academies Press.

——, 2010a: Assessment of intraseasonal to interannual climate prediction and predictability. N. R. Council, Ed., The National Academies Press.

——, 2010b: *Greenhouse Gas Emissions: Methods to Support International Climate Agreements.* National Research Council.

O'connor, F. M., et al., 2010: Possible Role of Wetlands, Permafrost, and Methane Hydrates in the Methane Cycle under Future Climate Change: A Review. *Reviews of Geophysics*, **48**.

O'gorman, P. A., and T. Schneider, 2008: The hydrological cycle over a wide range of climates simulated with an idealized GCM. *J Climate*, **21**, 3815-3832.

——, 2009: The physical basis for increases in precipitation extremes in simulations of 21st-century climate change. *Proc. Natl. Acad. Sci. U. S. A.*, **106**, 14773-14777.

O'gorman, P. A., R. P. Allan, M. P. Byrne, and M. Previdi, 2012: Energetic Constraints on Precipitation Under Climate Change. *Surv Geophys*, **33**, 585-608.

Office), I. I. C. P., 2011: Decadal and bias correction for decadal climate predictions. *CLIVAR Publication Series No.150, 6pp*, International CLIVAR Project Office.

Oman, L., et al., 2010a: Multimodel assessment of the factors driving stratospheric ozone evolution over the 21st century. *Journal of Geophysical Research-Atmospheres*, **115**, -.

Oman, L. D., et al., 2010b: Multimodel assessment of the factors driving stratospheric ozone evolution over the 21st century. *Journal of Geophysical Research-Atmospheres*, **115**, -.

Ordóñez, C., H. Mathis, M. Furger, S. Henne, C. Hüglin, J. Staehelin, and A. S. H. Prévôt, 2005: Changes of daily surface ozone maxima in Switzerland in all seasons from 1992 to 2002 and discussion of summer 2003. *Atmos. Chem. Phys.*, **5**, 1187-1203.

Organization, U. N. E. P. W. M., 2011: Integrated Assessment of Black Carbon and Tropospheric Ozone.

Orlowsky, B., and S. I. Seneviratne, 2011: Global changes in extremes events: Regional and seasonal dimension. Climatic Change. *Climate Change*. doi:DOI 10.1007/s10584-011-0122-9.

Ott, L., et al., 2010: Influence of the 2006 Indonesian biomass burning aerosols on tropical dynamics studied with the GEOS-5 AGCM. *J. Geophys. Res.*, **115**, D14121.

Pacifico, F., S. P. Harrison, C. D. Jones, and S. Sitch, 2009: Isoprene emissions and climate. *Atmos Environ*, **43**, 6121-6135.

Paeth, H., and F. Pollinger, 2010: Enhanced evidence in climate models for changes in extratropical atmospheric circulation. *Tellus Series a-Dynamic Meteorology and Oceanography*, **62**, 647-660.

Pall, P., M. R. Allen, and D. A. Stone, 2007: Testing the Clausius-Clapeyron constraint on changes in extreme precipitation under CO2 warming. *Clim Dynam*, **28**, 351-363.

Palmer, M. D., D. J. McNeall, and N. J. Dunstone, 2011: Importance of the deep ocean for estimating decadal changes in Earth's radiation balance. *Geophys Res Lett*, **38**.

Palmer, T. N., R. Buizza, R. Hagedon, A. Lawrence, M. Leutbecher, and L. Smith, 2006: Ensemble prediction: A pedagogical perspective. *ECMWF Newsletter*, **106**, 10-17.

Palmer, T. N., et al., 2004: Development of a European multimodel ensemble system for seasonal-to-interannual prediction (DEMETER). *Bulletin of the American Meteorological Society*, **85**, 853-+.

Paolino, D. A., J. L. Kinter, B. P. Kirtman, D. H. Min, and D. M. Straus, 2012: The Impact of Land Surface and Atmospheric Initialization on Seasonal Forecasts with CCSM. *J Climate*, **25**, 1007-1021.

Paulot, F., J. D. Crounse, H. G. Kjaergaard, J. H. Kroll, J. H. Seinfeld, and P. O. Wennberg, 2009: Isoprene photooxidation: new insights into the production of acids and organic nitrates. *Atmos. Chem. Phys.*, **9**, 1479-1501.

Pennell, C., and T. Reichler, 2011: On the Effective Number of Climate Models. *J Climate*, **24**, 2358-2367.

PENNER, J., H. EDDLEMAN, and T. NOVAKOV, 1993: TOWARDS THE DEVELOPMENT OF A GLOBAL INVENTORY FOR BLACK CARBON EMISSIONS. *Atmospheric Environment Part a-General Topics*, **27**, 1277-1295.

Persechino, A., J. Mignot, D. Swingedouw, S. Labetoulle, and E. Guilyardi, 2012: Decadal Predictability of the Atlantic Meridional Overturning Circulation and Climate in the IPSL-CM5A-LR model. . *Clim. Dyn.*

Pierce, D. W., T. P. Barnett, R. Tokmakian, A. Semtner, M. Maltrud, J. A. Lysne, and A. Craig, 2004: The ACPI Project, Element 1: Initializing a coupled climate model from observed conditions. *Climate Change*, **62**, 13-28.

Pinto, J., U. Ulbrich, G. Leckebusch, T. Spangehl, M. Reyers, and S. Zacharias, 2007: Changes in storm track and cyclone activity in three SRES ensemble experiments with the ECHAM5/MPI-OM1 GCM. *Clim Dynam*. doi:DOI 10.1007/s00382-007-0230-4, 195-210.

Pitman, A. J., et al., 2009: Uncertainties in climate responses to past land cover change: First results from the LUCID intercomparison study. *Geophys Res Lett*, **36**.

Pohlmann, H., J. H. Jungclaus, A. Köhl, D. Stammer, and J. Marotzke, 2009: Initializing decadal climate predictions with the GECCO oceanic synthesis: Effects on the North Atlantic. *J Climate*, **22**, 3926-3938.

Pohlmann, H., M. Botzet, M. Latif, A. Roesch, M. Wild, and P. Tschuck, 2004: Estimating the decadal predictability of a coupled AOGCM. *J Climate*, **17**, 4463-4472.

Power, S., and R. Colman, 2006: Multi-year predictability in a coupled general circulation model. *Clim Dynam*, **26**, 247-272.

Power, S., T. Casey, C. Folland, A. Colman, and V. Mehta, 1999: Inter-decadal modulation of the impact of ENSO on Australia. *Clim Dynam*, **15**, 319-324.

Power, S. B., 1995: Climate Drift in a Global Ocean General-Circulation Model. *J Phys Oceanogr*, **25**, 1025-1036.

Power, S. B., and G. Kociuba, 2011a: The impact of global warming on the Southern Oscillation Index. *Clim Dynam*, **37**, 1745-1754.

——, 2011b: What Caused the Observed Twentieth-Century Weakening of the Walker Circulation? *J Climate*, **24**, 6501-6514.

Power, S. B., and F. P. Delage, 2012: What won't change in response to global wamring? *Geoph. Res. Lett.*, **submitted**.

Power, S. B., M. Haylock, R. Colman, and X. Wang, 2006: The predictability of interdecadal changes in ENSO and ENSO teleconnections. *J. Climate*, **19**, 4755-4771.

Power, S. B., F. Delage, R. Colman, and A. Moise, 2012: Consensus on 21st century rainfall projections in climate models more widespread than previously thought. *J. Climate*. doi:doi:10.1175/JCLI-D-11-00354.1.

Prather, M., et al., 2001: Atmospheric Chemistry and Greenhouse Gases. *Climate Change 2001: The Scientific Basis*, J. T. H. e. al., Ed., Cambridge University Press, 239-287.

Prather, M., et al., 2003: Fresh air in the 21st century? *Geophys. Res. Lett.*, **30**, 1100.

Prather, M. J., C. D. Holmes, and J. Hsu, 2012: Reactive greenhouse gas scenarios: Systematic exploration of uncertainties and the role of atmospheric chemistry. *Geophys Res Lett*, **39**.

Prather, M. J., et al., 2009: Tracking uncertainties in the causal chain from human activities to climate. *Geophys Res Lett*, **36**, -.

Previdi, M., 2010: Radiative feedbacks on global precipitation. *Environ Res Lett*, **5**.

Prospero, J. M., 1999: Long-term measurements of the transport of African mineral dust to the southeastern United States: Implications for regional air quality. *Journal of Geophysical Research-Atmospheres*, **104**, 15917-15927.

Pye, H. O. T., H. Liao, S. Wu, L. J. Mickley, D. J. Jacob, D. K. Henze, and J. H. Seinfeld, 2009: Effect of changes in climate and emissions on future sulfate-nitrate-ammonium aerosol levels in the United States. *J. Geophys. Res.*, **114**, D01205.

Quesada, B., R. Vautard, P. Yiou, M. Hirschi, and S. Seneviratne, 2012: Asymmetric European summer heat predictability from wet and dry southern winters and springs. *Nat Clim Change*, **in press**.

Quinn, P. K., et al., 2008: Short-lived pollutants in the Arctic: their climate impact and possible mitigation strategies. *Atmos. Chem. Phys.*, **8**, 1723-1735.

Racherla, P. N., and P. J. Adams, 2006: Sensitivity of global tropospheric ozone and fine particulate matter concentrations to climate change. *J. Geophys. Res.*, **111**, D24103.

Racherla, P. N., and P. J. Adams, 2008: The response of surface ozone to climate change over the Eastern United States. *Atmos. Chem. Phys.*, **8**, 871-885.

1   Raes, F., and J. H. Seinfeld, 2009: New Directions: Climate change and air pollution abatement: A bumpy road. *Atmos*
2   *Environ*, **43**, 5132-5133.
3   Raisanen, J., 2008: Warmer climate: less or more snow? *Clim Dynam*, **30**, 307-319.
4   Räisänen, J., 2007: How reliable are climate models? *Tellus*, **59A**, 2-29.
5   Räisänen, J., and L. Ruokolainen, 2006: Probabilistic forecasts of near-term climate change based on a resampling
6   ensemble technique. *Tellus A*, **58**, 461–472.
7   Rajczak, J., P. Pall, and C. Schär, 2012: Projections of extreme precipitation events in regional climate simulations for
8   the European and Alpine regions. *J. Geophys. Res.*, **submitted**.
9   Ramana, M. V., V. Ramanathan, Y. Feng, S. C. Yoon, S. W. Kim, G. R. Carmichael, and J. J. Schauer, 2010: Warming
10   influenced by the ratio of black carbon to sulphate and the black-carbon source. *Nature Geosci*, **3**, 542-545.
11 Ramanathan, V., and G. Carmichael, 2008: Global and regional climate changes due to black carbon. *Nature Geosci*, **1**,
12   221-227.
13 Ramanathan, V., and Y. Feng, 2009: Air pollution, greenhouse gases and climate change: Global and regional
14   perspectives. *Atmos Environ*, **43**, 37-50.
15 Ramanathan, V., et al., 2005: Atmospheric brown clouds: Impacts on South Asian climate and hydrological cycle. *Proc.*
16   *Natl. Acad. Sci. U. S. A.*, **102**, 5326-5333.
17 Rampal, P., J. Weiss, C. Dubois, and J. M. Campin, 2011: IPCC climate models do not capture Arctic sea ice drift
18   acceleration: Consequences in terms of projected sea ice thinning and decline. *J Geophys Res-Oceans*, **116**.
19 Randles, C. A., and V. Ramaswamy, 2010: Direct and semi-direct impacts of absorbing biomass burning aerosol on the
20   climate of southern Africa: a Geophysical Fluid Dynamics Laboratory GCM sensitivity study. *Atmos. Chem.*
21   *Phys.*, **10**, 9819-9831.
22 Rasmussen, D. J., A. M. Fiore, V. Naik, L. W. Horowitz, S. J. McGinnis, and M. G. Schultz, 2011: Surface ozone-
23   temperature relationships in the eastern US: A monthly climatology for evaluating chemistry-climate models.
24   *Atmos Environ*, **submitted**
25
26 Richter, I., and S. P. Xie, 2008: Muted precipitation increase in global warming simulations: A surface evaporation
27   perspective. *Journal of Geophysical Research-Atmospheres*, **113**.
28 Rind, D., 2008: The consequences of not knowing low-and high-latitude climate sensitivity. *Bulletin of the American*
29   *Meteorological Society*. doi:DOI 10.1175/2007BAMS2520.1, 855-864.
30 Robock, A., 2000: Volcanic eruptions and climate. *Reviews of Geophysics*, **38**, 191-219.
31 Robson, J., R. Sutton, K. Lohmann, D. Smith, and M. D. Palmer, 2012a: Causes of the Rapid Warming of the North
32   Atlantic Ocean in the Mid-1990s. *J Climate*, **25**, 4116-4134.
33 Robson, J. I., R. T. Sutton, and D. M. Smith, 2012b: Initialized decadal predictions of the rapid warming of the North
34   Atlantic ocean in the mid 1990s. *Geoph. Res. Lett.*, **submitted**.
35 Roeckner, E., P. Stier, J. Feichter, S. Kloster, M. Esch, and I. Fischer-Bruns, 2006: Impact of carbonaceous aerosol
36   emissions on regional climate change. *Clim Dynam*, **27**, 553-571.
37 Roelofs, G. J., 2012: Aerosol lifetime and climate change. *Atmos. Chem. Phys. Discuss.*, **12**, 16493-16514.
38 Roscoe, H. K., and J. D. Haigh, 2007: Influences of ozone depletion, the solar cycle and the QBO on the Southern
39   Annular Mode. *Quarterly Journal of the Royal Meteorological Society*, **133**, 1855-1864.
40 Rotstayn, L. D., S. J. Jeffrey, M. A. Collier, S. M. Dravitzki, A. C. Hirst, J. I. Syktus, and K. K. Wong, 2012: Aerosol-
41   and greenhouse gas-induced changes in summer rainfall and circulation in the Australasian region: a study using
42   single-forcing climate simulations. *Atmos. Chem. Phys.*, **12**, 6377-6404.
43 Rowell, D. P., 2011: Sources of uncertainty in future change in local precipitation. *Clim. Dyn.* doi:10.1007/s00382-011-
44   1210-2.
45 Rowlands, D. J., et al., 2012: Broad range of 2050 warming from an observationally constrained large climate model
46   ensemble. *Nat Geosci*, **5**, 256-260.
47 Royal Society, 2008: Ground-level ozone in the 21st century: future trends, impacts and policy implicationsISBN: 978-
48   0-85403-713-1.
49 Ruckstuhl, C., and J. R. Norris, 2009: How do aerosol histories affect solar "dimming" and "brightening" over Europe?:
50   IPCC-AR4 models versus observations. *Journal of Geophysical Research-Atmospheres*, **114**.
51 Scaife, A. A., et al., 2012: Climate change projections and stratosphere-troposphere interaction. *Clim Dynam*, **38**, 2089-
52   2097.
53 Scaife, A. A., et al., 2009: The CLIVAR C20C project: selected twentieth century climate events. *Clim Dynam*, **33**,
54   603-614.
55 Schar, C., P. L. Vidale, D. Luthi, C. Frei, C. Haberli, M. A. Liniger, and C. Appenzeller, 2004: The role of increasing
56   temperature variability in European summer heatwaves. *Nature*, **427**, 332-336.
57 Schneider, E. K., B. Huang, Z. Zhu, D. G. DeWitt, J. L. Kinter, K. B.P., and J. Shukla, 1999: Ocean data assimilation,
58   initialization and predictions of ENSO with a coupled GCM. *Monthly Weather Review*, **127**, 1187-1207.
59 Schubert, S., M. J. Suarez, P. J. Pegion, R. D. Koster, and J. T. Bacmeister, 2004: On the cause of the 1930s Dust Bowl.
60   *Science*, **303**, 1855-1859.
61 Schultz, M. G., T. Diehl, G. P. Brasseur, and W. Zittel, 2003: Air Pollution and Climate-Forcing Impacts of a Global
62   Hydrogen Economy. *Science*, **302**, 624-627.

Screen, J. A., and I. Simmonds, 2010: The central role of diminishing sea ice in recent Arctic temperature amplification. *Nature*, **464**, 1334-1337.

Seager, R., N. Naik, W. Baethgen, A. Robertson, Y. Kushnir, J. Nakamura, and S. Jurburg, 2010: Tropical Oceanic Causes of Interannual to Multidecadal Precipitation Variability in Southeast South America over the Past Century. *J Climate*, **23**, 5517-5539.

Selten, F., G. Branstator, H. Dijkstra, and M. Kliphuis, 2004: Tropical origins for recent and future Northern Hemisphere climate change. *Geophys Res Lett*. doi:ARTN L21205, 10.1029/2004GL020739, -.

Semenov, V., M. Latif, J. Jungclaus, and W. Park, 2008: Is the observed NAO variability during the instrumental record unusual? *Geophys Res Lett*. doi:ARTN L11701, 10.1029/2008GL033273, -.

Seneviratne S.I., et al., 2012: Changes in climate extremes and their impacts on the natural physical environment. Chapter 3 in IPCC Special Report on Extreme Events and Disasters (SREX). WMO.

Seneviratne, S. I., et al., 2010: Investigating soil moisture-climate interactions in a changing climate: A review. *Earth-Sci Rev*, **99**, 125-161.

Seneviratne, S. I., et al., 2012: Impact of soil moisture-climate feedbacks on CMIP5 projections: First results from the GLACE-CMIP5 experiment. *Geoph. Res. Lett.*, **submitted**.

Serreze, M. C., A. P. Barrett, A. G. Slater, M. Steele, J. L. Zhang, and K. E. Trenberth, 2007: The large-scale energy budget of the Arctic. *Journal of Geophysical Research-Atmospheres*, **112**.

Shimpo, A., and M. Kanamitsu, 2009: Planetary Scale Land-Ocean Contrast of Near-Surface Air Temperature and Precipitation Forced by Present and Future SSTs. *J Meteorol Soc Jpn*, **87**, 877-894.

Shin, S.-I., and P. D. Sardeshmukh, 2011: Critical influence of the pattern of Tropical Ocean warming on remote climate trends. *Clim Dynam*. doi:10.1007/s00382-009-0732-3.

Shindell, D., J.-F. Lamarque, M. Schulz, M. Flanner, and et_al., 2012a: Radiative forcing in the ACCMIP historical and future climate simulations. *ACP,* **12**.

Shindell, D., M. Schulz, Y. Ming, T. Takemura, G. Faluvegi, and V. Ramaswamy, 2010: Spatial scales of climate response to inhomogeneous radiative forcing. *J. Geophys. Res.*, **115**, D19110.

Shindell, D., et al., 2007: Climate response to projected changes in short-lived species under an A1B scenario from 2000-2050 in the GISS climate model. *Journal of Geophysical Research-Atmospheres*, **112**, -.

Shindell, D., et al., 2006: Simulations of preindustrial, present-day, and 2100 conditions in the NASA GISS composition and climate model G-PUCCINI. *Atmos. Chem. Phys.*, **6**, 4427-4459.

Shindell, D., et al., 2012b: Simultaneously Mitigating Near-Term Climate Change and Improving Human Health and Food Security. *Science*, **335**, 183-189.

Shindell, D. T., and G. A. Schmidt, 2004: Southern Hemisphere climate response to ozone changes and greenhouse gas increases. *Geophys Res Lett*, **31**.

Shindell, D. T., A. Voulgarakis, G. Faluvegi, and G. Milly, 2012c: Precipitation response to regional radiative forcing. *Atmos. Chem. Phys. Discuss.*, **12**, 5015-5037.

Sigmond, M., P. Kushner, and J. Scinocca, 2007: Discriminating robust and non-robust atmospheric circulation responses to global warming. *Journal of Geophysical Research-Atmospheres*. doi:ARTN D20121, 10.1029/2006JD008270, -.

Sillman, J., V. V. Kharin, F. W. Zwiers, and X. Zhang, 2012: (submitted), Climate extreme indices in the CMIP5 multi-model ensemble. Part 2: Future climate projections. *Journal of Geophysical Research-Atmospheres*, **117**.

Sillman, S., and P. J. Samson, 1995: Impact of temperature on oxidant photochemistry in urban, polluted rural and remote environments. *J. Geophys. Res.*, **100**, 11497-11508.

Sillmann, J., M. Croci-Maspoli, M. Kallache, and R. W. Katz, 2011: Extreme Cold Winter Temperatures in Europe under the Influence of North Atlantic Atmospheric Blocking. *J Climate*, **24**, 5899-5913.

Sillmann J., V.V. Kharin, F. W. Zwiers, and X. Zhang, 2012: Climate extreme indices in the CMIP5 multi-model ensemble. Part 2: Future climate projections. *J. Geophys. Res.*, **submitted**.

Simmonds, I., and K. Keay, 2009: Extraordinary September Arctic sea ice reductions and their relationships with storm behavior over 1979-2008. *Geophys Res Lett*, **36**.

Simmons, A. J., K. M. Willett, P. D. Jones, P. W. Thorne, and D. P. Dee, 2010: Low-frequency variations in surface atmospheric humidity, temperature, and precipitation: Inferences from reanalyses and monthly gridded observational data sets. *Journal of Geophysical Research-Atmospheres*, **115**.

Sloyan, B. M., and I. V. Kamenkovich, 2007: Simulation of Subantarctic Mode and Antarctic Intermediate Waters in climate models. *J Climate*, **20**, 5061-5080.

Smith, D. M., S. Cusack, A. W. Colman, C. K. Folland, G. R. Harris, and J. M. Murphy, 2007: Improved surface temperature prediction for the coming decade from a global climate model. *Science*, **317**, 796-799.

Smith, D. M., R. Eade, N. J. Dunstone, D. Fereday, J. M. Murphy, H. Pohlmann, and A. A. Scaife, 2010: Skilful multi-year predictions of Atlantic hurricane frequency. *Nat Geosci*, **3**, 846-849.

Smith, D. M., et al., 2012: Real-time multi-model decadal climate predictions. *Clim. Dyn.*, **submitted**.

Smith, T. M., R. W. Reynolds, T. C. Peterson, and J. Lawrimore, 2008: Improvements to NOAA's historical merged land-ocean surface temperature analysis (1880-2006). *J Climate*, **21**, 2283-2296.

Soden, B. J., R. T. Wetherald, G. L. Stenchikov, and A. Robock, 2002: Global cooling after the eruption of Mount Pinatubo: A test of climate feedback by water vapor. *Science*, **296**, 727-730.

Sohn, B. J., and S.-C. Park, 2010: Strengthened tropical circulations in past three decades inferred from water vapor transport. *J. Geophys. Res.*, **115**, D15112.

Son, S., N. Tandon, L. Polvani, and D. Waugh, 2009a: Ozone hole and Southern Hemisphere climate change. *Geophys Res Lett*. doi:ARTN L15705, 10.1029/2009GL038671, -.

Son, S., et al., 2009b: The Impact of Stratospheric Ozone Recovery on Tropopause Height Trends. *J Climate*. doi:DOI 10.1175/2008JCLI2215.1, 429-445.

Son, S. W., et al., 2008: The impact of stratospheric ozone recovery on the Southern Hemisphere westerly jet. *Science*, **320**, 1486-1489.

Spracklen, D. V., L. J. Mickley, J. A. Logan, R. C. Hudman, R. Yevich, M. D. Flannigan, and A. L. Westerling, 2009: Impacts of climate change from 2000 to 2050 on wildfire activity and carbonaceous aerosol concentrations in the western United States. *J. Geophys. Res.*, **114**, D20301.

Stainforth, D. A., et al., 2005: Uncertainty in predictions of the climate response to rising levels of greenhouse gases. *Nature*, **433**, 403-406.

Stammer, D., 2006: Report of the First CLIVAR Workshop on Ocean Reanalysis: WCRP Informal Publication No. 9/2006, ICPO Publication Series No. 93. World Climate Research Program.

Stan, C., and B. P. Kirtman, 2008: The influence of atmospheric noise and uncertainty in ocean initial conditions on the limit of predictability in a coupled GCM. *J Climate*, **21**, 3487-3503.

Stedman, J., 2004: The predicted number of air pollution related deaths in the UK during the August 2003 heatwave. *Atmos Environ*, **38**, 1087-1090.

Stegehuis, A. I., R. Vautard, P. Ciais, R. Teuling, M. Jung, and P. Yiou, 2012: Summer temperatures in Europe and land heat fluxes in observation-based data and regional climate model simulations. *Clim. Dyn.*, **submitted**.

Steiner, A. L., S. Tonse, R. C. Cohen, A. H. Goldstein, and R. A. Harley, 2006: Influence of future climate and emissions on regional air quality in California. *J. Geophys. Res.*, **111**, D18303.

Steiner, A. L., A. J. Davis, S. Sillman, R. C. Owen, A. M. Michalak, and A. M. Fiore, 2010: Observed suppression of ozone formation at extremely high temperatures due to chemical and biophysical feedbacks. *Proceedings of the National Academy of Sciences*. doi:10.1073/pnas.1008336107.

Stenchikov, G., T. Delworth, V. Ramaswamy, R. Stouffer, A. Wittenberg, and F. Zeng, 2009: Volcanic signals in oceans. *Journal of Geophysical Research-Atmospheres*. doi:ARTN D16104, 10.1029/2008JD011673, -.

Stenchikov, G., K. Hamilton, R. Stouffer, A. Robock, V. Ramaswamy, B. Santer, and H. Graf, 2006: Arctic Oscillation response to volcanic eruptions in the IPCC AR4 climate models. *Journal of Geophysical Research-Atmospheres*, **111**.

Stephens, G. L., and T. D. Ellis, 2008: Controls of Global-Mean Precipitation Increases in Global Warming GCM Experiments. *J Climate*, **21**, 6141-6155.

Stephens, G. L., and Y. X. Hu, 2010: Are climate-related changes to the character of global-mean precipitation predictable? *Environ Res Lett*, **5**.

Stephenson, D. B., C. A. S. Coelho, F. J. Doblas-Reyes, and M. Balmaseda, 2005: Forecast assimilation: a unified framework for the combination of multi-model weather and climate predictions. *Tellus Series a-Dynamic Meteorology and Oceanography*, **57**, 253-264.

Stevenson, D., R. Doherty, M. Sanderson, C. Johnson, B. Collins, and D. Derwent, 2005: Impacts of climate change and variability on tropospheric ozone and its precursors. *Faraday Discussions*, **130**, 41-57.

Stevenson, D. S., P. J. Young, V. Naik, J.-F. Lamarque, D. T. Shindell, R. Skeie, and et al., 2012: Tropospheric ozone changes, attribution to emissions and radiative forcing in the Atmospheric Chemistry and Climate Model Inter-comparison Project (ACCMIP). *Atmos. Chem. Phys. Discuss.*, **12**.

Stevenson, D. S., et al., 2006: Multimodel ensemble simulations of present-day and near-future tropospheric ozone. *J. Geophys. Res.*, **111**, D08301.

Stockdale, T. N., 1997: Coupled ocean–atmosphere forecasts in the presence of climate drift. *Monthly Weather Review*, **125**, 809-818.

Stockdale, T. N., D. L. T. Anderson, J. O. S. Alves, and M. A. Balmaseda, 1998: Global seasonal rainfall forecasts using a coupled ocean-atmosphere model. *Nature*, **392**, 370-373.

Stott, P., D. Stone, and M. Allen, 2004: Human contribution to the European heatwave of 2003. *Nature*, **432**, 610-614.

Stott, P., R. Sutton, and D. Smith, 2008: Detection and attribution of Atlantic salinity changes. *Geophys Res Lett*. doi:ARTN L21702, 10.1029/2008GL035874, -.

Stott, P., N. Gillett, G. Hegerl, D. Karoly, D. Stone, X. Zhang, and F. Zwiers, 2010: Detection and attribution of climate change: a regional perspective. *Wiley Interdisciplinary Reviews: Climate Change*, **1**, 192-211.

Stott, P., Good, P, Jones, G, Gillet, N and Hawkins, E, 2012: Upper range of climate warming projections are inconsistent with past warming. *Nature Geosci*, **submitted**.

Stott, P. A., and J. A. Kettleborough, 2002: Origins and estimates of uncertainty in predictions of twenty-first century temperature rise. *Nature*, **416**, 723-726.

Stott, P. A., and G. Jones, 2012: Observed 21st century temperatures further constrain decadal predictions of future warming. *Atmos Science Letters*, **submitted**.

Strahan, S., et al., 2011: Using transport diagnostics to understand chemistry climate model ozone simulations. *Journal of Geophysical Research-Atmospheres*, **116**, -.

Stroeve, J., M. M. Holland, W. Meier, T. Scambos, and M. Serreze, 2007: Arctic sea ice decline: Faster than forecast. *Geophys Res Lett*, **34**.

Stroeve, J. C., V. Kattsov, A. Barrett, M. Serreze, T. Pavlova, M. Holland, and W. N. Meier, 2012: Trends in Arctic sea ice extent from CMIP5, CMIP3 and observations. *Geoph. Res. Lett.*, **in press**.

Struzewska, J., and J. W. Kaminski, 2008: Formation and transport of photooxidants over Europe during the July 2006 heat wave - observations and GEM-AQ model simulations. *Atmospheric Chemistry and Physics*, **8**, 721-736.

Suckling, E. B., and L. A. Smith, 2012: An evaluation of decadal probability forecasts from state-of-the-art climate models. *J. Climate*, **submitted**.

Sugiura, N., et al., 2008: Development of a four-dimensional variational coupled data assimilation system for enhanced analysis and prediction of seasonal to interannual climate variations. *Journal Geophysical Research C*, **113**, C10017.

Sugiura, N., et al., 2009: Potential for decadal predictability in the North Pacific region. *Geophys Res Lett*, **36**, L20701.

Sun, J., and H. Wang, 2006: Relationship between Arctic Oscillation and Pacific Decadal Oscillation on decadal timescales. *Chinese Science Bulletin*, **51**, 75-79.

Sushama, L., R. Laprise, and M. Allard, 2006: Modeled current and future soil thermal regime for northeast Canada. *Journal of Geophysical Research-Atmospheres*, **111**.

Sutton, R., and D. Hodson, 2005: Atlantic Ocean forcing of North American and European summer climate. *Science*. doi:DOI 10.1126/science.1109496, 115-118.

Sutton, R. T., B. W. Dong, and J. M. Gregory, 2007: Land/sea warming ratio in response to climate change: IPCC AR4 model results and comparison with observations. *Geophys Res Lett*, **34**.

Swingedouw, D., J. Mignot, S. Labetoulle, E. Guilyardi, and G. Madec, 2012: Initialisation and predictability of the AMOC over the last 50 years in a climate model. *Clim. Dyn.*

Szopa, S., D. A. Hauglustaine, R. Vautard, and L. Menut, 2006: Future global tropospheric ozone changes and impact on European air quality. *Geophys. Res. Lett.*, **33**, L14805.

Tagaris, E., et al., 2007: Impacts of global climate change and emissions on regional ozone and fine particulate matter concentrations over the United States. *J. Geophys. Res.*, **112**, D14312.

Tai, A. P. K., L. J. Mickley, and D. J. Jacob, 2010: Correlations between fine particulate matter (PM2.5) and meteorological variables in the United States: Implications for the sensitivity of PM2.5 to climate change. *Atmos Environ*, **44**, 3976-3984.

Tai, A. P. K., L. J. Mickley, and D. J. Jacob, 2012a: Impact of 2000–2050 climate change on fine particulate matter (PM2.5) air quality inferred from a multi-model analysis of meteorological modes. *Atmos. Chem. Phys. Discuss.*, **12**.

Tai, A. P. K., L. J. Mickley, D. J. Jacob, E. M. Leibensperger, L. Zhang, J. A. Fisher, and H. O. T. Pye, 2012b: Meteorological modes of variability for fine particulate matter (PM2.5) air quality in the United States: implications for PM2.5 sensitivity to climate change. *Atmospheric Chemistry and Physics*, **12**, 3131-3145.

Tao, Z., A. Williams, H.-C. Huang, M. Caughey, and X.-Z. Liang, 2007: Sensitivity of U.S. surface ozone to future emissions and climate changes. *Geophys. Res. Lett.*, **34**, L08811.

Taylor, C. M., A. Gounou, F. Guichard, P. P. Harris, R. J. Ellis, F. Couvreux, and M. De Kauwe, 2011: Frequency of Sahelian storm initiation enhanced over mesoscale soil-moisture patterns. *Nat Geosci*, **4**, 430-433.

Taylor, K. E., R. J. Stouffer, and G. A. Meehl, 2012: An Overview of Cmip5 and the Experiment Design. *Bulletin of the American Meteorological Society*, **93**, 485-498.

Tebaldi, C., J. M. Arblaster, and R. Knutti, 2011: Mapping model agreement on future climate projections. *Geophys Res Lett*, **38**.

Tegen, I., M. Werner, S. P. Harrison, and K. E. Kohfeld, 2004: Relative importance of climate and land use in determining present and future global soil dust emission. *Geophys. Res. Lett.*, **31**, L05105.

Teng, H. Y., G. Branstator, and G. A. Meehl, 2011: Predictability of the Atlantic Overturning Circulation and Associated Surface Patterns in Two CCSM3 Climate Change Ensemble Experiments. *J Climate*, **24**, 6054-6076.

Terray, L., L. Corre, S. Cravatte, T. Delcroix, G. Reverdin, and A. Ribes, 2012: Near-Surface Salinity as Nature's Rain Gauge to Detect Human Influence on the Tropical Water Cycle. *J Climate*, **25**, 958-977.

TFHTAP, 2007: Task Force on Hemispheric Transport of Air Pollution 2007 Interim Report. *Air Pollution Studies*, T. J. Keating, and A. Zuber, Eds., United Nations Economic Commission for Europe.

Thompson, D. W. J., and S. Solomon, 2002: Interpretation of recent Southern Hemisphere climate change. *Science*, **296**, 895-899.

Timmermann, A., S. McGregor, and F. Jin, 2010: Wind Effects on Past and Future Regional Sea Level Trends in the Southern Indo-Pacific. *J Climate*. doi:DOI 10.1175/2010JCLI3519.1, 4429-4437.

Timmermann, A., et al., 2007: The influence of a weakening of the Atlantic meridional overturning circulation on ENSO. *J Climate*, **20**, 4899-4919.

Toyoda, T., et al., 2011: Impact of the Assimilation of Sea Ice Concentration Data on an Atmosphere-Ocean-Sea Ice Coupled Simulation of the Arctic Ocean Climate. *Sola*, **7**, 37-40.

Trenberth, K., and A. Dai, 2007: Effects of Mount Pinatubo volcanic eruption on the hydrological cycle as an analog of geoengineering. *Geophys Res Lett*, **34**.

Trenberth, K. E., and J. W. Hurrell, 1994: DECADAL ATMOSPHERE-OCEAN VARIATIONS IN THE PACIFIC. *Clim Dynam*, **9**, 303-319.

1 Trenberth, K. E., and D. J. Shea, 2006: Atlantic hurricanes and natural variability in 2005. *Geophys Res Lett*, **33**.
2 Trenberth, K. E., A. Dai, R. M. Rasmussen, and D. B. Parsons, 2003: The changing character of precipitation. *Bulletin*
3   *of the American Meteorological Society*, **84**, 1205-+.
4 Trenberth, K. E., et al., 2007: Observations: Surface and Atmospheric Climate Change. *Climate Change 2007: The*
5   *Physical Science Basis. Contribution of Working Group I to the Fourth Assessment Report of the*
6   *Intergovernmental Panel on Climate Change*, S. Solomon, et al., Eds., Cambridge, United Kingdom and New
7   York, NY, USA.
8 Tressol, M., et al., 2008: Air pollution during the 2003 European heat wave as seen by MOZAIC airliners. *Atmos.*
9   *Chem. Phys.*, **8**, 2133-2150.
10 Troccoli, A., and T. N. Palmer, 2007: Ensemble decadal predictions from analysed initial conditions. *Philosophical*
11   *Transaction A Math Phys Eng Sci.*, **365**, 2179-2191.
12 Turner, A. J., A. M. Fiore, L. W. Horowitz, V. Naik, and M. Bauer, 2012: Summertime cyclones over the Great Lakes
13   Storm Track from 1860-2100: Variability, trends, and association with ozone pollution. *Atmos. Chem. Phys.*
14   *Discuss.*, **12**.
15 Tziperman, E., L. Zanna, and C. Penland, 2008: Nonnormal thermohaline circulation dynamics in a coupled ocean-
16   atmosphere GCM. *J Phys Oceanogr*, **38**, 588-604.
17 Ulbrich, U., J. Pinto, H. Kupfer, G. Leckebusch, T. Spangehl, and M. Reyers, 2008: Changing northern hemisphere
18   storm tracks in an ensemble of IPCC climate change simulations. *J Climate*. doi:DOI 10.1175/2007JCLI1992.1,
19   1669-1679.
20 UNEP, and WMO, 2011: Integrated Assessment of Black Carbon and Tropospheric Ozone.
21 Unger, N., D. T. Shindell, and J. S. Wang, 2009: Climate forcing by the on-road transportation and power generation
22   sectors. *Atmos Environ*, **43**, 3077-3085.
23 Unger, N., D. T. Shindell, D. M. Koch, and D. G. Streets, 2006a: Cross influences of ozone and sulfate precursor
24   emissions changes on air quality and climate. *Proc. Natl. Acad. Sci. U. S. A.*, **103**, 4377-4380.
25 Unger, N., D. T. Shindell, D. M. Koch, M. Amann, J. Cofala, and D. G. Streets, 2006b: Influences of man-made
26   emissions and climate changes on tropospheric ozone, methane, and sulfate at 2030 from a broad range of
27   possible futures. *J. Geophys. Res.*, **111**, D12313.
28 Unger, N., D. T. Shindell, D. M. Koch, M. Amann, J. Cofala, and D. G. Streets, 2006c: Influences of man-made
29   emissions and climate changes on tropospheric ozone, methane, and sulfate at 2030 from a broad range of
30   possible futures. *Journal of Geophysical Research-Atmospheres*, **111**.
31 van den Dool, H., 2007: *Empirical methods in short-term climate prediction.* Oxford University Press.
32 van der Linden, P., and J. F. B. Mitchell, 2009: ENSEMBLES: Climate change and its impacts. Summary of research
33   and results from the ENSEMBLES project.
34 van Oldenborgh, G., et al., 2009a: Western Europe is warming much faster than expected. *Climate of the Past*, **5**, 1-12.
35 van Oldenborgh, G. J., P. Yiou, and R. Vautard, 2010: On the roles of circulation and aerosols in the decline of mist and
36   dense fog in Europe over the last 30 years. *Atmos. Chem. Phys.*, **10**, 4597-4609.
37 van Oldenborgh, G. J., F. J. Doblas-Reyes, B. Wouters, and W. Hazeleger, 2012: Decadal prediction skill in a multi-
38   model ensemble. *Clim Dynam*, **38**, 1263-1280.
39 van Oldenborgh, G. J., et al., 2009b: Western Europe is warming much faster than expected. *Clim. Past*, **5**, 1-12.
40 van Ruijven, B., J.-F. Lamarque, D. P. van Vuuren, T. Kram, and H. Eerens, 2011: Emission scenarios for a global
41   hydrogen economy and the consequences for global air pollution. *Global Environmental Change*, **21**, 983-994.
42 van Vuuren, D., et al., 2011: The representative concentration pathways: an overview. *Climatic Change*.
43   doi:10.1007/s10584-011-0148-z, 1-27.
44 Vautard, R., P. Yiou, and G. van Oldenborgh, 2009: Decline of fog, mist and haze in Europe over the past 30 years. *Nat*
45   *Geosci*, **2**, 115-119.
46 Vautard, R., C. Honoré, M. Beekmann, and L. Rouil, 2005: Simulation of ozone during the August 2003 heat wave and
47   emission control scenarios. *Atmos Environ*, **39**, 2957-2967.
48 Vavrus, S., M. M. Holland, and D. A. Bailey, 2011: Changes in Arctic clouds during intervals of rapid sea ice loss.
49   *Clim Dynam*, **36**, 1475-1489.
50 Vavrus, S., D. Waliser, A. Schweiger, and J. Francis, 2009: Simulations of 20th and 21st century Arctic cloud amount
51   in the global climate models assessed in the IPCC AR4. *Clim Dynam*, **33**, 1099-1115.
52 Vavrus, S. J., M. M. Holland, A. Jahn, D. A. Bailey, and B. A. Blazey, 2012: Twenty-First-Century Arctic Climate
53   Change in CCSM4. *J Climate*, **25**, 2696-2710.
54 Vecchi, G., and B. Soden, 2007: Global warming and the weakening of the tropical circulation. *J Climate*. doi:DOI
55   10.1175/JCLI4258.1, 4316-4340.
56 Vecchi, G., B. Soden, A. Wittenberg, I. Held, A. Leetmaa, and M. Harrison, 2006: Weakening of tropical Pacific
57   atmospheric circulation due to anthropogenic forcing. *Nature*. doi:DOI 10.1038/nature04744, 73-76.
58 Vecchi, G. A., and A. T. Wittenberg, 2010: El Nino and our future climate: where do we stand? *Wires Clim Change*, **1**,
59   260-270.
60 Vecchi, G. A., et al., 2012a: Technical comment on "Multiyear prediction of monthly mean Atlantic meridional
61   overturning circulation at 26.5ºN. *Science*, **in press**.
62 Vecchi, G. A., et al., 2012b: Multi-year Predictions of North Atlantic Hurricane Frequency: Promise and Limitations. *J.*
63   *Climate*, **submitted**.

1   Vidale, P. L., D. Luethi, R. Wegmann, and C. Schaer, 2007: European summer climate variability in a heterogeneous
2   multi-model ensemble. *Climatic Change*, **81**, 209-232.
3   Vieno, M., et al., 2010: Modelling surface ozone during the 2003 heat-wave in the UK. *Atmos. Chem. Phys.*, **10**, 7963-
4   7978.
5   Vikhliaev, Y., B. Kirtman, and P. Schopf, 2007: Decadal North Pacific bred vectors in a coupled GCM. *J Climate*, **20**,
6   5744-5764.
7   Villarini, G., and G. A. Vecchi, 2012a: 21st Century Projections of North Atlantic Tropical Storms from CMIP5
8   Models. *Nat Clim Change*. doi:Nature Climate Change doi:10:1038/NCLIMATE1530.
9   Villarini, G., and G. A. Vecchi, 2012b: Projected Increases in North Atlantic Tropical Cyclone Intensity from CMIP5
10   Models. *J. Climate*, **submitted**.
11   Villarini, G., G. A. Vecchi, T. R. Knutson, M. Zhao, and J. A. Smith, 2011: North Atlantic Tropical Storm Frequency
12   Response to Anthropogenic Forcing: Projections and Sources of Uncertainty. *J Climate*, **24**, 3224-3238.
13   Vollmer, M. K., et al., 2011: Atmospheric histories and global emissions of the anthropogenic hydrofluorocarbons
14   HFC-365mfc, HFC-245fa, HFC-227ea, and HFC-236fa. *J. Geophys. Res.*, **116**, D08304.
15   Volpi, D., F.J. Doblas-Reyes, J. García-Serrano, and V.Guemas, 2012: Dependance of the climate prediction skill on
16   spatio-temporal scales: quantification of the internal versus radiatively-forced contributions. *Geoph. Res. Lett.*,
17   **submitted**.
18   Voulgarakis, A., V. Naik, J. F. Lamarque, D. T. Shindell, and et al., 2012: Multimodel simulations of present-day and
19   future OH and methane lifetime. *Atmospheric Chemistry and Physics Disc*, **12**.
20   Vukovich, F. M., 1995: Regional-scale boundary layer ozone variations in the eastern United States and their
21   association with meteorological variations. *Atmos. Environ.*, **29**, 2259-2273.
22   Wang, H., et al., 2009: A statistical forecast model for Atlantic seasonal hurricane activity based on the NCEP
23   dynamical seasonal forecast. *J Climate*, **22**, 4481-4500.
24   Wang, M., and J. E. Overland, 2012: Summer Arctic sea ice will be gone sooner or later - an update from CMIP5
25   models. *Geoph. Res. Lett.*, **submitted**.
26   Wang, M., J. Overland, and N. Bond, 2010: Climate projections for selected large marine ecosystems. *Journal of
27   Marine Systems*. doi:DOI 10.1016/j.jmarsys.2008.11.028, 258-266.
28   Wang, M. Y., and J. E. Overland, 2009: A sea ice free summer Arctic within 30 years? *Geophys Res Lett*, **36**.
29   Wang, R. F., L. G. Wu, and C. Wang, 2011: Typhoon Track Changes Associated with Global Warming. *J Climate*, **24**,
30   3748-3752.
31   Weaver, C. P., et al., 2009: A Preliminary Synthesis of Modeled Climate Change Impacts on U.S. Regional Ozone
32   Concentrations. *Bulletin of the American Meteorological Society*, **90**, 1843-1863.
33   Weisheimer, A., T. N. Palmer, and F. J. Doblas-Reyes, 2011: Assessment of representations of model uncertainty in
34   monthly and seasonal forecast ensembles. *Geophys Res Lett*, **38**.
35   West, J. J., A. M. Fiore, L. W. Horowitz, and D. L. Mauzerall, 2006: Global health benefits of mitigating ozone
36   pollution with methane emission controls. *Proc. Natl. Acad. Sci. U. S. A.*, **103**, 3988-3993.
37   Wigley, T., et al., 2009: Uncertainties in climate stabilization. *Climatic Change*, **97**, 85-121.
38   Wild, M., J. Grieser, and C. Schaer, 2008: Combined surface solar brightening and increasing greenhouse effect support
39   recent intensification of the global land-based hydrological cycle. *Geophys Res Lett*, **35**.
40   Wild, O., 2007: Modelling the global tropospheric ozone budget: exploring the variability in current models. *Atmos.
41   Chem. Phys.*, **7**, 2643-2660.
42   Wild, O., and Leipert, 2010: The Earth radiation balance as driver of the global hydrological cycle. *Environ Res Lett*, **5**.
43   Wild, O., et al., 2011: Future changes in surface ozone: A parameterized approach. *Atmos. Chem. Phys. Discuss.*
44   Wild, O., et al., 2012: Modelling future changes in surface ozone: a parameterized approach. *Atmos. Chem. Phys.
45   Discuss.*, **12**.
46   Wilks, D. S., 2006: *Statistical Methods in the Atmospheric Sciences.* Vol. 91, Academic Press, Elsevier, xvii, 627 p. pp.
47   Williams, A., and C. Funk, 2011: A westward extension of the warm pool leads to a westward extension of the Walker
48   circulation, drying eastern Africa. *Clim Dynam*. doi:10.1007/s00382-010-0984-y, 1-19-19.
49   Williams, J., and M. A. Ringer, 2010: Precipitation changes within dynamical regimes in a perturbed climate. *Environ
50   Res Lett*, **5**.
51   Williams, P. D., E. Guilyardi, R. Sutton, J. Gregory, and G. Madec, 2007: A new feedback on climate change from the
52   hydrological cycle. *Geophys Res Lett*, **34**.
53   Winton, M., 2006: Does the Arctic sea ice have a tipping point? *Geophys Res Lett*, **33**.
54   WMO, W. M. O., 2002: Standardised Verification System (SVS) for Long-Range Forecasts (LRF). *New Attachment II-
55   9 to the Manual on the GDPS (WMO-No. 485)*, W. SVS-LRF, Ed., WMO.
56   ——, 2009: Report of the World Climate Conference-3: Better climate information for a better future.
57   Woodward, S., D. L. Roberts, and R. A. Betts, 2005: A simulation of the effect of climate change–induced
58   desertification on mineral dust aerosol. *Geophys. Res. Lett.*, **32**, L18810.
59   Woollings, T., 2010: Dynamical influences on European climate: an uncertain future. *Philos T R Soc A*. doi:DOI
60   10.1098/rsta.2010.0040, 3733-3756.
61   Woollings, T., and M. Blackburn, 2012: The North Atlantic Jet Stream under Climate Change and Its Relation to the
62   NAO and EA Patterns. *J Climate*, **25**, 886-902.

1   Wouters, W., W. Hazeleger, S. Drijfhout, G. J. v. Oldenborgh, and V. Guémas, 2012: Decadal predictability of the
2   North Atlantic subpolar gyre. *Geoph. Res. Lett.*, **submitted**.
3   Wu, P. L., R. Wood, J. Ridley, and J. Lowe, 2010: Temporary acceleration of the hydrological cycle in response to a
4   CO2 rampdown. *Geophys Res Lett*, **37**.
5   Wu, S., L. J. Mickley, J. O. Kaplan, and D. J. Jacob, 2012: Impacts of changes in land use and land cover on
6   atmospheric chemistry and air quality over the 21st century. *Atmospheric Chemistry and Physics*, **12**, 1597-1609.
7   Wu, S., L. J. Mickley, D. J. Jacob, D. Rind, and D. G. Streets, 2008a: Effects of 2000–2050 changes in climate
8   and emissions on global tropospheric ozone and the policy-relevant background surface ozone in the United
9   States. *J. Geophys. Res.*, **113**, D18312.
10 Wu, S., L. J. Mickley, D. J. Jacob, J. A. Logan, R. M. Yantosca, and D. Rind, 2007: Why are there large differences
11   between models in global budgets of tropospheric ozone? *J. Geophys. Res.*, **112**, D05302.
12 Wu, S., L. J. Mickley, E. M. Leibensperger, D. J. Jacob, D. Rind, and D. G. Streets, 2008b: Effects of
13   2000–2050 global change on ozone air quality in the United States. *J. Geophys. Res.*, **113**, D06302.
14 Xie, S., C. Deser, G. Vecchi, J. Ma, H. Teng, and A. Wittenberg, 2010: Global Warming Pattern Formation: Sea
15   Surface Temperature and Rainfall. *J Climate*. doi:DOI 10.1175/2009JCLI3329.1, 966-986.
16 Xoplaki, E., P. Maheras, and J. Luterbacher, 2001: Variability of climate in Meridional Balkans during the periods
17   1675-1715 and 1780-1830 and its impact on human life. *Climatic Change*, **48**, 581-615.
18 Yeager, S., A. Karspeck, G. Danabasoglu, J. Tribbia, and H. Teng, 2012: A Decadal Prediction Case Study: Late 20th
19   Century North Atlantic Ocean Heat Content. *J. Climate*. doi:10.1175/JCLI-D-11-00595.1.
20 Yienger, J. J., et al., 2000: The episodic nature of air pollution transport from Asia to North America. *J. Geophys. Res.*,
21   **105**, 26931-26945.
22 Yin, J. J., M. E. Schlesinger, and R. J. Stouffer, 2009: Model projections of rapid sea-level rise on the northeast coast of
23   the United States. *Nat Geosci*, **2**, 262-266.
24 Yin, J. J., S. M. Griffies, and R. J. Stouffer, 2010: Spatial Variability of Sea Level Rise in Twenty-First Century
25   Projections. *J Climate*, **23**, 4585-4607.
26 Yip, S., C. A. T. Ferro, D. B. Stephenson, and E. Hawkins, 2011: A Simple, Coherent Framework for Partitioning
27   Uncertainty in Climate Predictions. *J Climate*, **24**, 4634-4643.
28 Yokohata, T., J. D. Annan, M. Collins, C. S. Jackson, M. Tobis, M. J. Webb, and J. C. Hargreaves, 2012: Reliability of
29   multi-model and structurally different single-model ensembles. *Clim. Dyn.*, **39**, 599-616.
30 Young, P. J., A. T. Archibald, K. Bowman, J. F. Lamarque, V. Naik, and et al., 2012: Pre-industrial to end 21st century
31   projections of tropospheric ozone from the Atmospheric Chemistry and Climate Model Intercomparison Project
32   (ACCMIP). *Atmospheric Chemistry and Physics*, **12**.
33 Yuan, Y., H. Yang, W. Zhou, and C. Y. Li, 2008: Influences of the Indian Ocean dipole on the Asian summer monsoon
34   in the following year. *Int J Climatol*, **28**, 1849-1859.
35 Yue, X., H. J. Wang, H. Liao, and K. Fan, 2010: Simulation of dust aerosol radiative feedback using the GMOD: 2.
36   Dust-climate interactions. *Journal of Geophysical Research-Atmospheres*, **115**.
37 Zeng, G., J. A. Pyle, and P. J. Young, 2008a: Impact of climate change on tropospheric ozone and its global budgets.
38   *Atmos. Chem. Phys.*, **8**, 369-387.
39 ——, 2008b: Impact of climate change on tropospheric ozone and its global budgets. *Atmospheric Chemistry and
40   Physics*, **8**, 369-387.
41 Zeng, G., O. Morgenstern, P. Braesicke, and J. A. Pyle, 2010a: Impact of stratospheric ozone recovery on tropospheric
42   ozone and its budget. *Geophys. Res. Lett.*, **37**, L09805.
43 ——, 2010b: Impact of stratospheric ozone recovery on tropospheric ozone and its budget. *Geophys Res Lett*, **37**.
44 Zhang, R., and T. L. Delworth, 2006: Impact of Atlantic multidecadal oscillations on India/Sahel rainfall and Atlantic
45   hurricanes. *Geophys Res Lett*, **33**.
46 Zhang, S., **M. J. s. H**arrison, M.J., A. Rosati, and A. A. Wittenberg, 2007a: System design and evaluation of coupled
47   ensemble data assimilation for global oceanic climate studies. *Monthly Weather Review*, **135**, 3541-3564.
48 Zhang, X., et al., 2007b: Detection of human influence on twentieth-century precipitation trends. *Nature*, **448**, 461-465.
49 Zhang, X. D., 2010: Sensitivity of arctic summer sea ice coverage to global warming forcing: towards reducing
50   uncertainty in arctic climate change projections. *Tellus Series a-Dynamic Meteorology and Oceanography*, **62**,
51   220-227.
52 Zhang, Y., J. Wallace, and D. Battisti, 1997: ENSO-like interdecadal variability: 1900-93. *J Climate*. 1004-1020.
53 Zhang, Y., X. Y. Wen, and C. J. Jang, 2010: Simulating chemistry-aerosol-cloud-radiation-climate feedbacks over the
54   continental US using the online-coupled Weather Research Forecasting Model with chemistry (WRF/Chem).
55   *Atmos Environ*, **44**, 3568-3582.
56 Zhang, Y., X.-M. Hu, L. R. Leung, and W. I. Gustafson, Jr., 2008: Impacts of regional climate change on biogenic
57   emissions and air quality. *J. Geophys. Res.*, **113**, D18310.
58 Zhao, M., I. Held, S. Lin, and G. Vecchi, 2009: Simulations of Global Hurricane Climatology, Interannual Variability,
59   and Response to Global Warming Using a 50-km Resolution GCM. *J Climate*. doi:DOI
60   10.1175/2009JCLI3049.1, 6653-6678.
61 Zhou, T., R. Yu, H. Li, and B. Wang, 2008: Ocean forcing to changes in global monsoon precipitation over the recent
62   half-century. *J Climate*. doi:DOI 10.1175/2008JCLI2067.1, 3833-3852.

Zhu, Y. L., H. J. Wang, W. Zhou, and J. H. Ma, 2011: Recent changes in the summer precipitation pattern in East China and the background circulation. *Clim Dynam*, **36**, 1463-1473.

1 **Tables**
2
3 **Table 11.1:** Initialization methods used in models that entered CMIP5 near-term experiments.

CMIP5 Near-Term Players	CMIP5 official model_id	AGCM	OGCM	Initialization				Perturbation	
name of modeling center (or group)				Atmosphere/Land	Ocean	sea ice	anomaly assimilation?	Atmos	Ocean
Beijing Climate Center, China Meteorological Administration (BCC) China	BCC-CSM1.1	2.8ºL26	1ºL40	no	SST, T&S (SODA)	no	no	perturbed atmos/ocean	
Canadian Centre for Climate Modelling and Analysis (CCCMA) Canada	CanCM4	2.8ºL35	.9ºL40	ERA40/Interim	Ocean assimilation (Tang et al. 2004) / forced OGCM	yes	no	ensemble assimilation	
Community Climate System Model (CCSM) USA	CCSM4	0.5ºL30	0.5ºL60	no	forced OGCM / ocean assimilation (DART)				
Centro Euro-Mediterraneo per I Cambiamenti Climatici (CMCC-CM) Italy	CMCC-CM	0.8ºL31	1.2ºL31	no	SST, T&S (INGV ocean analysis)	concentration from ocean analysis	no	ensemble assimilation	
EC-EARTH Consortium (EC-EARTH) Europe	EC-EARTH	1.1ºL62	1ºL42	ERA40/interim	Ocean assimilation (NEMOVAR S3)		no (KNMI & IC3) & yes (SMHI)	start dates and singular vectors	ensemble ocean assim (NEMOVAR)
Max Planck Institute for Meteorology (MPI-M) Germany	MPI-ESM	0.9ºL95	0.5ºL40	no	T&S from forced OGCM	no	yes	yes 1-day lagged	
Geophysical Fluid Dynamics Laboratory (GFDL) USA	GFDL-CM2.1	2ºL24	0.9ºL50	NCEP reanalysis	coupled EnKF	no	no	coupled EnKF	
Met Office Hadley Centre (MOHC) UK	HadCM3	2.5ºL19	1.3ºL20	ERA40/ECMWF operational	SST, T&S (Smith and Murphy 2007)	HADISST	yes	no	SST perturbation
Institut Pierre-Simon Laplace (IPSL) France	IPSL-CM5A-LR	1.9ºL39	2ºL31	reanalysis	SST		yes	no	white nose on SST
AORI/NIES/JAMSTEC (MIROC) Japan	MIROC4h MIROC5	0.6ºL56 1.4ºL40	0.2ºL48 0.8ºL50	no	SST, T&S (Ishii-Kimoto(2009)	no	yes	start dates and ensemble assimilation	

4

1
2   **Chapter 11: Near-term Climate Change: Projections and Predictability**
3
4   **Coordinating Lead Authors:** Ben Kirtman (USA), Scott Power (Australia)
5
6   **Lead Authors:** Akintayo John Adedoyin (Botswana), George Boer (Canada), Roxana Bojariu (Romania),
7   Ines Camilloni (Argentina), Francisco Doblas-Reyes (Spain), Arlene Fiore (USA), Masahide Kimoto
8   (Japan), Gerald Meehl (USA), Michael Prather (USA), Abdoulaye Sarr (Senegal), Christoph Schär
9   (Switzerland), Rowan Sutton (UK), Geert Jan van Oldenborgh (Netherlands), Gabriel Vecchi (USA), Hui-
10   Jun Wang (China)
11
12   **Contributing Authors:** Nathan Bindoff, Yoshimitsu Chikamoto, Thierry Fichefet, Javier García-Serrano,
13   Paul Ginoux, Lesley Gray, Virginie Guémas, Ed Hawkins, Marika Holland, Christopher Holmes, Johnna
14   Infanti, Masayoshi Ishii, Thomas Knutson, Gerhard Krinner, David Lawrence, Jian Lu, Vaishali Naik,
15   Lorenzo Polvani, Alan Robock, Luis Rodrigues, Jan Sedlacek, Andrew Slater, Doug Smith, Bart van den
16   Hurk, Steve Vavrus, Apostolos Voulgarakis, Oliver Wild, Tim Woollings
17
18   **Review Editors:** Pascale Delecluse (France), Tim Palmer (UK), Theodore Shepherd (Canada), Francis
19   Zwiers (Canada)
20
21   **Date of Draft:** 5 October 2012
22
23   **Notes:** TSU Compiled Version
24
25
26

1   **Figures**

2

3

4

5   **Figure 11.1a:** The evolution of observation-based global mean temperature $T(t) = T_f(t) + T_i(t)$ (the black line) as the

6   difference from the 1971–2000 average together with a model-based estimate of the externally forced component T_f (the

7   red line) and the internally generated component T_i (the difference between the black and red lines). An ensemble of

8   forecasts of global annual mean temperature, initialized in 2007, is plotted as thin blue lines and their average, the

9   ensemble mean forecast, as the dark blue line. The shading represent plus and minus one standard deviation for the

10   simulations (light grey shading) and the forecasts (light blue shading). The grey areas along the axis broadly indicate

11   the external forcing associated with volcanoes.

12

13

1

2
3
4   **Figure 11.1b:** Schematic evolution of predictability and error growth in terms of probability. The probability
5   distribution corresponding to the forced component $p(T_f,t)$ is in red with the deeper shades indicating higher probability.
6   The probabilistic representation of the forecast $p(T,t)$ is in blue. The initially sharply peaked distribution broadens with
7   time as information about the initial conditions is lost until the initialized climate prediction becomes indistinguishable
8   from an uninitialized climate projection (based on Branstator and Teng, 2010).
9
10

1

2
3
4   **Figure 11.2:** The global average of the local correlation skill score (solid lines) and the corresponding predictability
5   measure (dashed lines) for temperature averaged over periods from a month to a decade. Results plotted for the monthly
6   average correspond to the first month, those for the annual average to the first year and so on up to the decadal average.
7   The orange lines are the results for initialized forecasts which attempt to predict the evolution of both internally
8   generated and forced components of the climate. The green lines are the results for uninitialized forced climate
9   simulations.
10
11

1

2
3
4 **Figure 11.3:** Predictability examples – Top panel shows results for perfect predictability of the Meridional Overturning
5 Circulation (MOC) based on de-correlation time. Light blue curves correspond to multi-model results from Collins et
6 al. (2006) for strong positive MOC cases, the dark blue curve is the multi-model mean and the dotted blue is de-
7 correlation of persistence. Light red curves correspond to multi-model results from Collins et al. (2006) for strong
8 negative MOC cases, the dark red curve is the multi-model mean and the dotted red is de-correlation of persistence. The
9 think black curve the perfect predictability based on results from Msadek et al. (2010). Bottom panel shows CMIP5
10 multi-model extra-tropical upper (400 m) ocean heat content predictability as measured by potential de-correlation time.
11 The blue curve corresponds to the Pacific and the red curves correspond to the Atlantic. Potential de-correlation (r) time
12 is estimated from the mean squared distance (msd) as r=1−msd/2. The msd is from Branstator and Teng (2012) using an
13 analogue method with a CMIP5 sub-set of models (see Branstator et al., 2012) for details).
14
15

1

Potential predictability variance fractions
Internally generated

2
3
Figure 11.4: The potential predictability of five year and decadal means of temperature (lower panels), the contribution
from the forced component (middle panels) and from the internally generated component (upper panels). These are
multi-model results from CMIP5 RCP4.5 scenario simulations from 17 coupled climate models following the
methodology of Boer (2011). The results apply to the early 21st century.

8
9

1

SAT 60ºS-60ºN CMIP5 Init / rm=12months

2
3
4 **Figure 11.5:** Time series of global-mean sea surface temperature from the multi-model initialized hindcasts, where a
5 different colour has been used for each start date, and the reference data (ERSST) is drawn in black. The hindcasts are
6 displayed in two panels to prevent the curves from consecutive start dates to overlap. All time series have been
7 smoothed out with a 24-month centred moving average that removes data for the first and last years of each time series.
8
9

1

2
3
4 **Figure 11.6:** Decadal prediction forecast quality of several climate indices. Top row: Time series of the 2–5 year
5 average ensemble-mean initialized hindcast anomalies and the corresponding non-initialized experiments for three
6 climate indices: global-mean temperature (left), the Atlantic multidecadal variability (AMV, middle) and interdecadal
7 Pacific oscillation (IPO, right). The observational time series, GISS global-mean temperature and ERSST for the AMV
8 and IPO, are represented with dark grey (positive anomalies) and light grey (negative anomalies) vertical bars, where a
9 four-year running mean has been applied for consistency with the time averaging of the predictions. Predicted time
10 series are shown for three different sets of the CMIP5 Init (solid) and NoInit (dotted) simulations: hindcasts with start
11 dates every five years (eleven systems, green), with start dates every year (five systems, yellow) and the five systems
12 with yearly start dates sampled using only one start date every five years (red), all over the period 1960–2005. The
13 AMV index was computed as the SST anomalies averaged over the region Equator –60ºN and 80º–0ºW minus the SST
14 anomalies averaged over 60ºS–60ºN. The IPO index is the principal component of the leading EOF of each model using
15 SSTs in the region 50ºS–50ºN / 100ºE–290ºE where the mean SST over 60ºS–60ºN for each forecast system and
16 forecast period has been previously removed. Middle row: Ensemble-mean correlation with the observational reference
17 along the forecast time for four-year averages of the three sets of CMIP5 hindcasts for Init (solid) and NoInit (dashed).
18 The one-sided 95% confidence level with a t distribution is represented in grey (dark grey) for the hindcasts with five
19 (one) year start date sampling. The number of degrees of freedom has been computed taking into account the
20 autocorrelation of the observational time series. A two-sided t test (where the number of degrees of freedom has been
21 computed taking into account the autocorrelation of the observational time series) has been used to test the differences
22 between the correlation of the initialized and non-initialized experiments, but no differences where found significant
23 with a confidence equal or higher than 90%. Bottom row: Ensemble-mean root mean square error along the forecast
24 time for four-year averages of the three sets of CMIP5 hindcasts for Init (solid) and NoInit (dashed). A two-sided F test
25 (where the number of degrees of freedom has been computed taking into account the autocorrelation of the
26 observational time series) has been used to test the ratio between the RMSE of the Init and NoInit, and those forecast
27 time with differences significant with a confidence equal or higher than 90% are indicated with an open square. The
28 number of degrees of freedom has been computed taking into account the autocorrelation of the observational time
29 series.
30
31

1

2
3
4   **Figure 11.7:** Near surface air temperature forecast quality for the forecast time 2–5 (left column) and 6–9 (right
5   column) years. Top row: Ensemble-mean correlation of the CMIP5 Init multi-model with five-year interval between
6   start dates over the period 1960–2005. A combination of temperatures from GHCN/CAMS air temperature over land,
7   ERSST and GISTEMP 1200 over the polar areas is used as a reference. Black dots correspond to the points where the
8   correlation is statistically significant with 95% confidence using a one-sided t-test taking into account the
9   autocorrelation of the observational time series. Second row: Ensemble-mean correlation difference between the CMIP5
10   Init and NoInit multi-model experiments. A Fisher Z-transform of the correlations has been computed, the colours
11   showing the Z difference in correlation space. Contours are used for areas where the ensemble-mean correlation of at
12   least 75% of the single forecast systems has the same sign as the multi-model ensemble mean correlation. Dots are used
13   for the points where the Z differences are statistically significant with 90% confidence taking into account the
14   autocorrelation of the observational time series. Third row: Root mean square skill score for the multi-model ensemble
15   mean of CMIP5 Init experiment. Black dots correspond to the points where the skill score is statistically significant
16   with 95% confidence using a one-sided F-test taking into account the autocorrelation of the observation minus
17   prediction time series. Bottom row: Ratio between the ensemble-mean root mean square error of Init and NoInit. Dots
18   are used for the points where the ratio is significantly above or below one with 90% confidence using a two-sided F-test
19   taking into account the autocorrelation of the observation minus prediction time series. Contours are used for areas
20   where the ratio of at least 75% of the single forecast systems has a value above or below one according to the multi-
21   model ensemble mean correlation. Poorly observationally sampled areas are masked in grey. The model original data
22   have been bilinearly interpolated to the observational grid. The ensemble mean of each forecast system has been
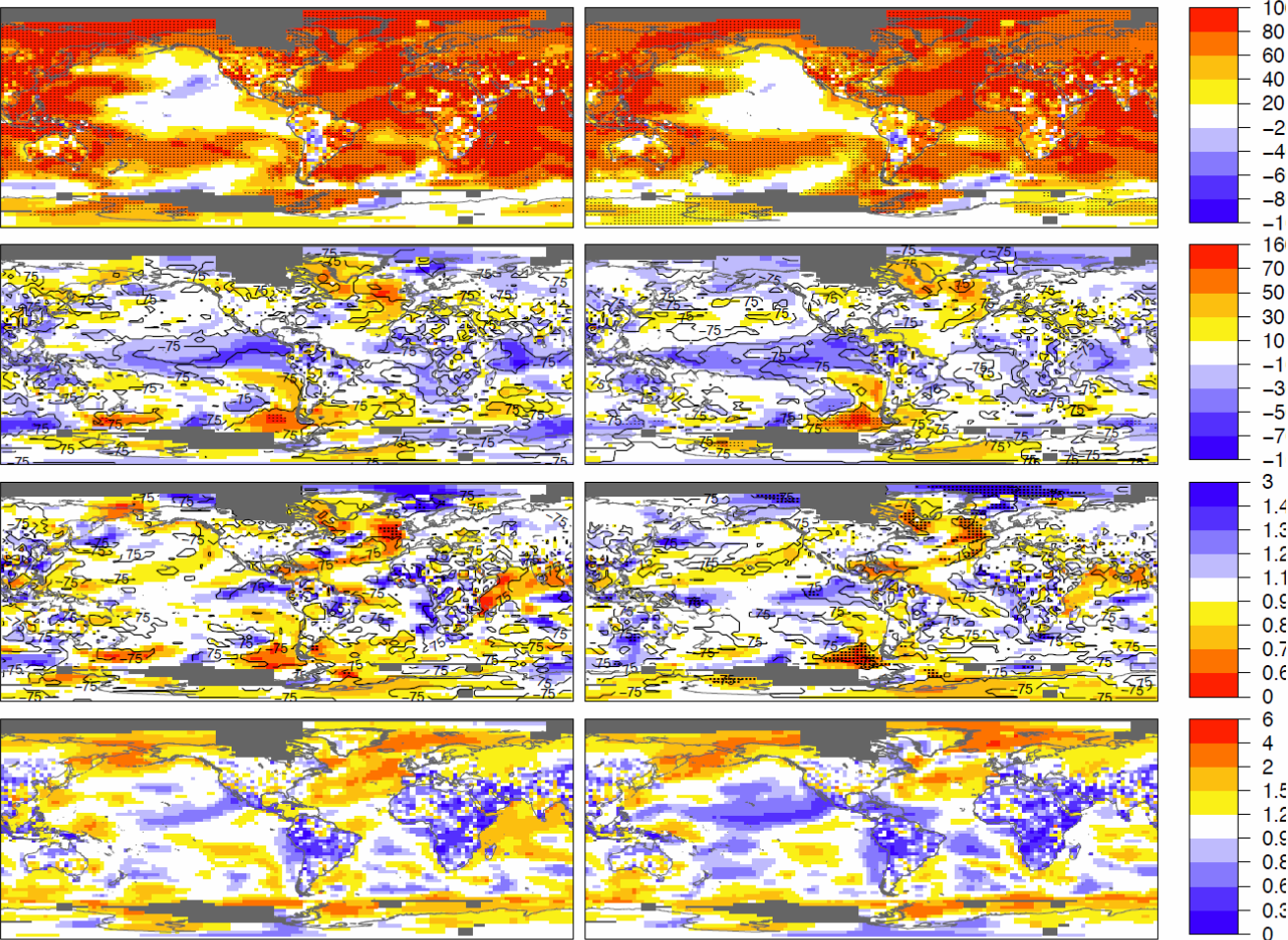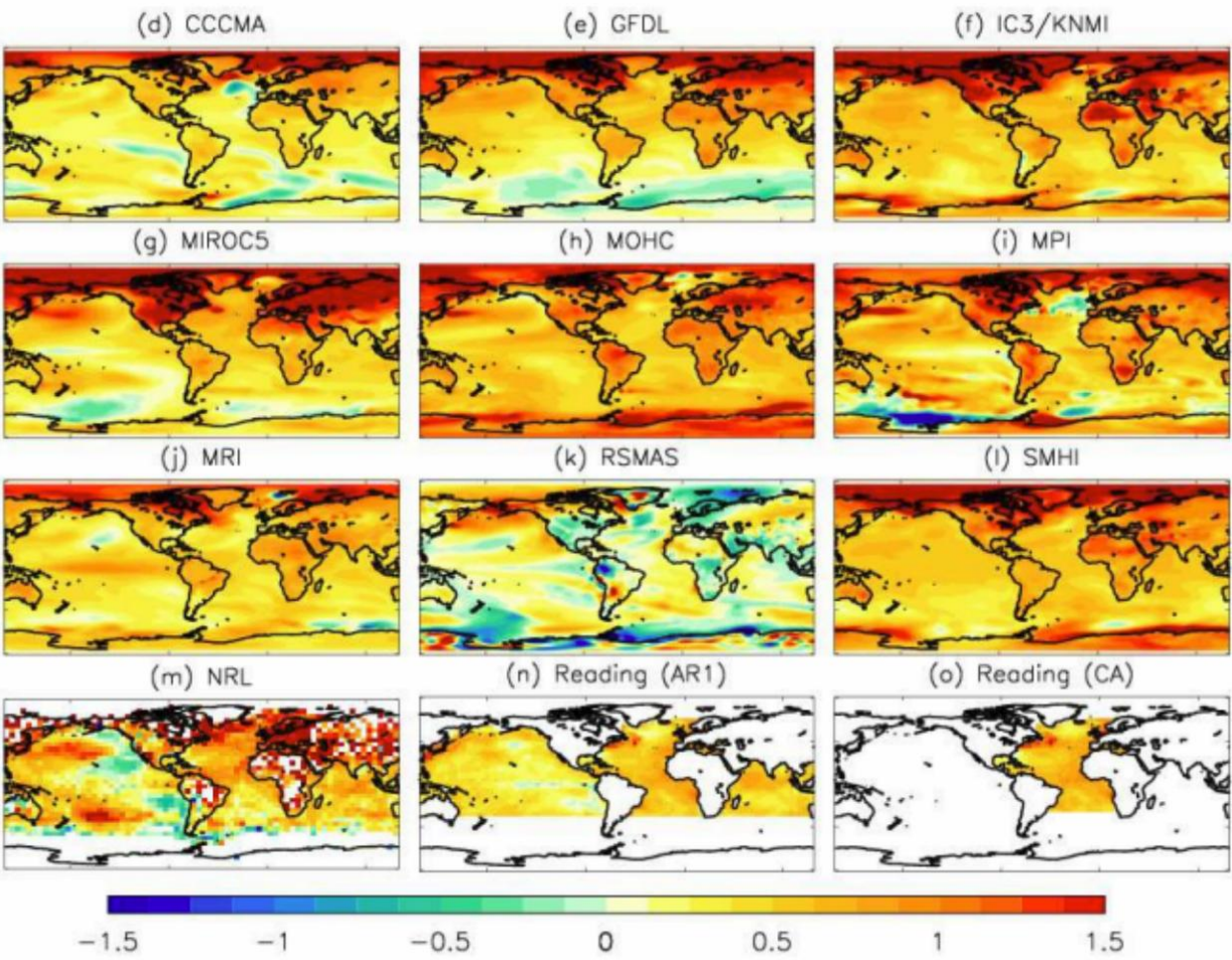23   estimated before computing the multi-model ensemble mean.
24
25

1

2
3
4 **Figure 11.8:** Attributes diagram for the CMIP5 multi-model decadal initialized (panels a and c) and non-initialized
5 (panels b and d) hindcasts for the event 'SST anomalies below the lower tercile' over a) and b) the global oceans
6 (60ºN–60ºS) and c) and d) the North Atlantic (87.5ºN–30ºN, 80ºW–10ºW) for the forecast time 2–5 years. The number
7 of red bullets in the figure corresponds to the number of probability bins (10 in this case) used to estimate forecast
8 probabilities. The size of the bullets represents the number of forecasts in a specific probability category and is a
9 measure of the sharpness of the predictions. The blue horizontal and vertical lines indicate the climatological frequency
10 of the event in the observations and the mean forecast probability, respectively. Grey vertical bars indicate the
11 uncertainty in the observed frequency for each probability category estimated at 95% level of confidence with a
12 bootstrap resampling procedure based on 1000 samples. The longer the bars, the more the vertical position of the bullets
13 may change as new hindcasts become available. The black dashed line separates skilful from unskilled regions in the
14 diagram in the Brier skill score sense. The Brier skill score with respect to the climatological forecast is drawn in the
15 top left corner of each panel.
16
17

1

2
3
4 **Figure 11.9:** Precipitation forecast quality for the forecast time 2–5 (left column) and 6–9 (right column) years. Top
5 row: Ensemble-mean correlation of the CMIP5 Init multi-model with five-year interval between start dates over the
6 period 1960–2005. GPCC precipitation is used as a reference. Black dots correspond to the points where the correlation
7 is statistically significant with 95% confidence using a one-sided t-test taking into account the autocorrelation of the
8 observational time series. Second row: Ensemble-mean correlation difference between the CMIP5 Init and NoInit
9 multi-model experiments. A Fisher Z-transform of the correlations has been computed, the colours showing the Z
10 difference in correlation space. Contours are used for areas where the ensemble-mean correlation of at least 75% of the
11 single forecast systems has the same sign as the multi-model ensemble mean correlation. Dots are used for the points
12 where the Z differences are statistically significant with 90% confidence taking into account the autocorrelation of the
13 observational time series. Third row: Root mean square skill score for the multi-model ensemble mean of CMIP5 Init
14 experiment. Black dots correspond to the points where the skill score is statistically significant with 95% confidence
15 using a one-sided F-test taking into account the autocorrelation of the observation minus prediction time series. Bottom
16 row: Ratio between the ensemble-mean root mean square error of Init and NoInit. Dots are used for the points where the
17 ratio is significantly above or below one with 90% confidence using a two-sided F-test taking into account the
18 autocorrelation of the observation minus prediction time series. Contours are used for areas where the ratio of at least
19 75% of the single forecast systems has a value above or below one according to the multi-model ensemble mean
20 correlation. The model original data have been bilinearly interpolated to the observational grid. The ensemble mean of
21 each forecast system has been estimated before computing the multi-model ensemble mean.
22
23

1

2
3
4   **Figure 11.10a:** Impact of the number of start dates on the air temperature forecast quality of the 2–5 year forecast time
5   with five-year (left) and one-year (right) interval between start dates over the period 1960–2005. Top row: Ensemble-
6   mean correlation of the CMIP5 Init multi-model, where the same multi-model ensemble with five individual forecast
7   systems has been used in both panels. A combination of temperatures from GHCN/CAMS air temperature over land,
8   ERSST and GISTEMP 1200 over the polar areas is used as a reference. Black dots correspond to the points where the
9   correlation is statistically significant with 95% confidence using a one-sided t-test taking into account the
10 autocorrelation of the observational time series. Second row: Ensemble-mean correlation difference between the CMIP5
11 Init and NoInit multi-model experiments. A Fisher Z-transform of the correlations has been computed, the colours
12 showing the Z difference in correlation space. Contours are used for areas where the ensemble-mean correlation of at
13 least 75% of the single forecast systems has the same sign as the multi-model ensemble mean correlation. Dots are used
14 for the points where the Z differences are statistically significant with 90% confidence taking into account the
15 autocorrelation of the observational time series. Third row: Ratio between the ensemble-mean root mean square error of
16 Init and NoInit. Dots are used for the points where the ratio is significantly above or below one with 90% confidence
17 using a two-sided F-test taking into account the autocorrelation of the observation minus prediction time series.
18 Contours are used for areas where the ratio of at least 75% of the single forecast systems has a value above or below
19 one according to the multi-model ensemble mean correlation.
20
21

1

2
3
4 **Figure 11.10b:** Forecast and observed temperature anomalies for 2013–2017 initialized near the end of 2012. a)-j)
5 Ensemble mean forecast from each forecast system. All anomalies are degrees centigrade relative to the average of the
6 period 1971 to 2000.
7
8

1

2
3
4   **Figure 11.10c:** Impact of initialization (initialized minus non-initialized ensemble means) on forecasts of the period
5   2013 to 2017 initialized near the end of 2012. Unstippled regions in (i) indicate a 90% or higher probability that
6   differences between the initialized and non-initialized ensemble means did not occur by chance (based on a 2 tailed t-
7   test of differences between the two ensemble means assuming the ensembles are normally distributed).
8
9

1

2
3
4 **Figure 11.11:** Sources of uncertainty in climate projections as a function of lead time based on an analysis of CMIP5
5 results. a) Projections of global mean decadal mean surface air temperature to 2100 together with a quantification of the
6 uncertainty arising from internal variability (orange), model response uncertainty (blue), and forcing uncertainty
7 (green). b) shows the signal-to-uncertainty ratio for various global and regional averages. The signal is defined as
8 the simulated multi-model mean change in surface air temperature relative to the simulated mean surface air
9 temperature in the period 1986–2005, and the uncertainty is defined as the total uncertainty. c), d), e), f) show the
10 fraction of variance explained by each source of uncertainty for: global mean decadal and annual mean temperature (c),
11 European (30°–75°N, 10°W–40°E) decadal mean boreal winter (December to February) temperature (d) and
12 precipitation (f), and East Asian (5°–45°N, 67.5°–130°E) decadal mean boreal summer (June to August) precipitation
13 (e). See text and Hawkins and Sutton (2009); Hawkins and Sutton (2011) for further details.

1

Figure 11.12: a) Projections of global mean, annual mean surface air temperature 1986–2050 (anomalies relative to 1986–2005) under RCP4.5 from CMIP5 models (grey and blue lines, one ensemble member per model), with four observational estimates (HadCRUT3: Brohan et al., 2006; ERA-Interim: Simmons et al., 2010; GISTEMP: Hansen et al., 2010; NOAA: Smith et al., 2008) for the period 1986–2011 (black lines); b) as a) but showing the 5–95% range (grey shades, with the multi-model median in white) of decadal mean CMIP5 projections using one ensemble member per model from RCP4.5 scenario, and decadal mean observational estimates (black lines). The maximum and minimum values from CMIP5 are shown by the grey lines. An estimate of the projected 5–95% range for decadal mean global mean surface air temperature for the period 2016–2040 derived using the ASK methodology applied to several CMIP5 GCMs (dashed black lines; from Stott, 2012). The red line shows a statistical prediction based on the method of Lean and Rind (2009), updated for RCP 4.5.
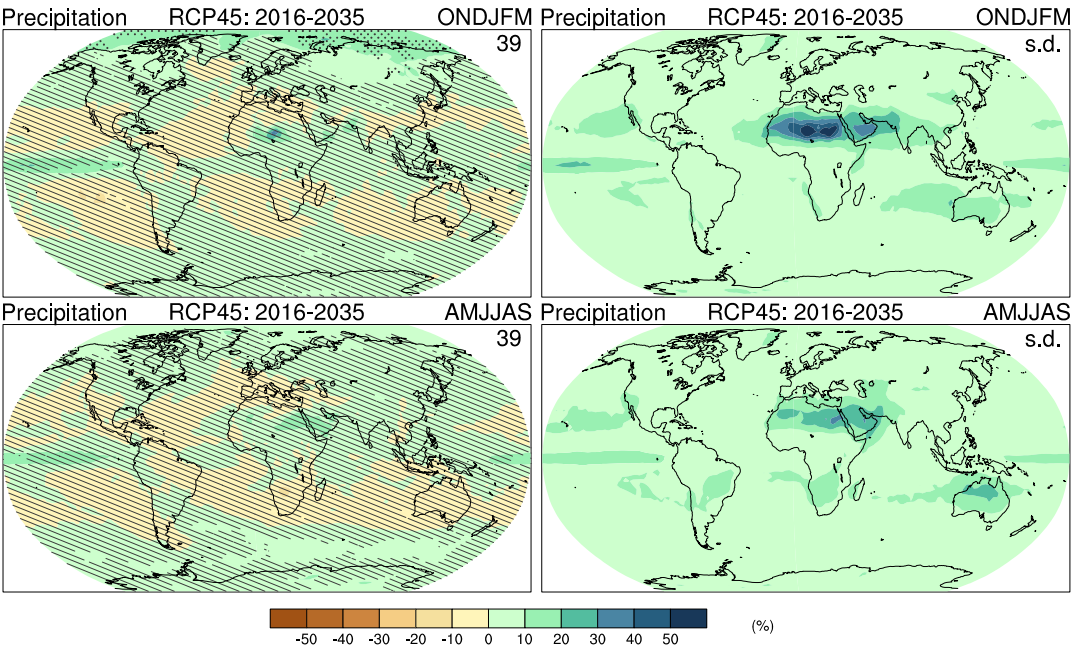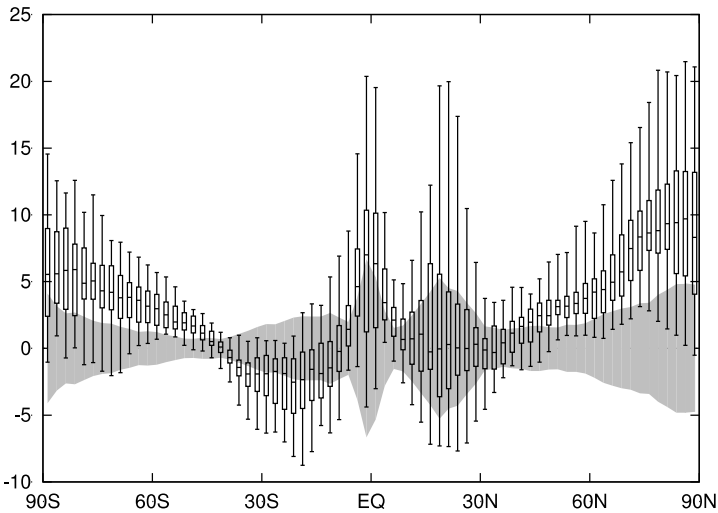
1

Figure 11.13: CMIP5 multi-model ensemble mean of projected changes in surface air temperature for the period 2016–2035 relative to 1986–2005 under RCP4.5 scenario (left panels). The right panels show an estimate of the natural internal variability in the quantity plotted in the left panels (see Annex I Atlas for details of method). Hatching in left-hand panels indicates areas where projected changes are small compared to the natural variability (i.e., smaller than one standard deviation of estimated natural variability of twenty-year means), and stippling indicates regions where the multi-model mean projections deviate significantly from the control (by at least two standard deviations of internal variability in twenty-year means) and where at least 90% of the models agree on the sign of change). See Box 12.1 in Chapter 12 for further details and discussion.

Figure 11.14: Time of emergence of significant local warming derived from CMIP5 models under the RCP 4.5 scenario. Warming is quantified as the half-year mean temperature anomaly relative to 1986–2005, and the noise as the standard deviation of half-year mean temperature derived from a control simulation of the relevant model. Central panels show the median time at which the signal-to-noise ratio exceeds a threshold value of 1 for (left) the October to March half year and (right) the April to September half year, using a spatial resolution of 2.5° x 2.5°. Histograms show the distribution of emergence times for area averages over the regions indicated obtained from the different CMIP5 models. Blue histograms are when using each model's estimate of noise, and green when a median estimate of noise is used. Full details of the methodology may be found in Hawkins and Sutton (2011).

1

2
3
4 **Figure 11.15:** Zonal mean temperature differences, 2016–2035 minus 1986–2005, for the CMIP5 multi-model
5 ensemble (°C), for a) DJF, b) JJA, and C) annual mean. Stippling as in Figure 11.13.
6
7

1

Figure 11.16: CMIP5 multi-model ensemble mean of projected changes in precipitation for the period 2016–2035 relative to 1986–2005 under RCP4.5 in % for October to March (top left-hand panel) and April to September (bottom left-hand panel). The right-hand panels show the corresponding estimates of the natural internal variability in the quantity plotted in the left-hand panels (see Annex I Atlas for details of method). Hatching and stippling in left-hand panels as in Figure11.13.

1

2
3
4 **Figure 11.17:** CMIP5 multi-model projections of changes in annual mean zonal mean precipitation (mm/day) for the
5 period 2016–2035 relative to 1986–2005 under RCP4.5. The box plots indicate projected changes (median, interquartile
6 range, and 5–95% range of model changes). Shading indicates 1 standard deviation of the estimated natural internal
7 variability (see Annex I Atlas for details of method).
8
9

1

2
3
4 **Figure 11.18:** CMIP5 multi-model mean projected changes in annual mean evaporation (%), surface runoff (%), soil
5 moisture (%) and near-surface specific humidity (%) for the period 2016–2035 relative to 1986–2005 under RCP4.5
6 (left panels). All changes are listed as relative changes with respect to control conditions. Right-hand panels and
7 stippling/hatching are defined as in Figure11.13.
8
9

1

Projected Multi-Model Change in Annual-Averaged 850hPa Zonal Wind Velocity

2
3
4 **Figure 11.19:** [PLACEHOLDER FOR FINAL DRAFT: to make final] Projected changes in annual-averaged zonal
5 (west-to-east) wind at 850hPa based on the average of 23 AOGCMs from the CMIP3 (Meehl et al., 2007b) multi-model
6 ensemble, under 21st century Emissions Scenario SRESA1B. Gray shading indicates where the multi-model average
7 AOGCM anomalies are smaller than two standard deviations of the multi-AOGCM estimate of internal variability from
8 the control climate integrations. Values referenced to the 1986–2005 climatology.
9
10

1

2
3
4 **Figure 11.20:** Projected changes in the annual-averaged poleward edge of the Hadley Circulation (horizontal axis) and
5 sub-tropical dry zones (vertical axis) based on 15 AOGCMs from the CMIP5 (Taylor et al., 2012) multi-model
6 ensemble, under 21st century Representative Concentratio Pathway 4.5. Orange symbols show the change in the
7 northern edge of the Hadley Circulation/dry zones, while blue symbols show the change in the southern edge of the
8 Hadley Circulation/dry zones. Open circles indicate the multi-model average, while horizontal and vertical colored lines
9 indicate the ±1-standard deviation range for internal climate variability estimated from each model. Values referenced
10 to the 1986–2005 climatology. Figure based on the methodology of Lu et al. (2007).
11
12

1

Figure 11.21: Projected changes in the strength of the Pacific Walker Circulation, as estimated using the east-west sea level pressure gradient across the equatorial Pacific (Vecchi and Soden, 2007; Vecchi and Soden, 2007), based on 24 AOGCMs from the CMIP3 (Meehl et al., 2007b) multi-model ensemble, under 21st century Emissions Scenario SRESA1B. Thin gray lines indicate the five-year running average for each model, red line indicates the multi-model five-year running average. Blue horizontal lines indicate the 2016–2035 values for each model, with the orange line indicating the multi-model averaged projection for 2016–2035. Values referenced to the 1986–2005 climatology.

Figure 11.22: Global mean projections for the occurrence of (a) warm days, (b) cold days, and (c) wet days from CMIP5 for the RCP2.6, RCP4.5 and RCP8.5 scenarios relative to 1986–2005. Panel (a) shows percentage of warm days (tx90p: Tmax exceeds the 90th percentile), panel (b) shows percentage of cold days (tx10p: Tmax below the 10th percentile), and panel (c) shows relative change of simple precipitation intensity (sdii: average daily precipitation amount for wet days). Results for CMIP3 are also indicated. From Sillmann J. et al. (2012).

Figure 11.23: European-scale projections from the ENSEMBLES regional climate modelling project for 2016–2035 relative to 1986–2005, with top and bottom panels applicable to JJA and DJF, respectively. For temperature, projected changes (°C) are displayed in terms of ensemble mean changes of (a, c) mean seasonal surface temperature, and (b, d) the 90th percentile of daily maximum temperatures. For precipitation, projected changes (%) are displayed in terms of ensemble mean changes of (e, g) mean seasonal precipitation and (f, h) the 95th percentile of daily precipitation. The stippling in (e-h) highlights regions where 80% of the models agree in the sign of the change (for temperature all models agree on the sign of the change). The analysis includes the following 10 RCM-GCM simulation chains for the SRES A1B scenario (naming includes RCM group and GCM simulation): HadRM3Q0-HadCM3Q0, ETHZ-HadCM3Q0, HadRM3Q3-HadCM3Q3, SMHI-HadCM3Q3, HadRM3Q16-HadCM3Q16, SMHI-BCM, DMI-ARPEGE, KNMI-ECHAM5, MPI-ECHAM5, DMI-ECHAM5 (Rajczak et al., 2012; courtesy of Jan Rajczak).

1

2
3
4 **Figure 11.24:** Projected changes in annual-averaged, globally-averaged, depth-averaged ocean temperature based on
5 twelve AOGCMs from the CMIP3 (Meehl et al., 2007b) multi-model ensemble, under 21st century Emissions Scenario
6 SRESA1B. Top panel shows changes of sea surface temperature, middle panel ocean temperature changes averaged
7 over the upper 700 meters of the ocean, bottom panel shows changes averaged over the full ocean depth. Thin black
8 lines show the evolution for each of the twelve AOGCMs, red line shows the average of all twelve projections, the blue
9 line indicates an estimate of the average magnitude of internal variability of all twelve AOGCMs (2sigma).Gray
10 horizontal lines indicate the 2016–2035 average anomaly for each of the twelve AOGCMs, while the orange horizontal
11 line indicates the multi-model average 2016–2035 anomaly. The fifty-year running average from each model's control
12 climate integration was removed from each line. Values referenced to the 1986–2005 climatology of each AOGCM.
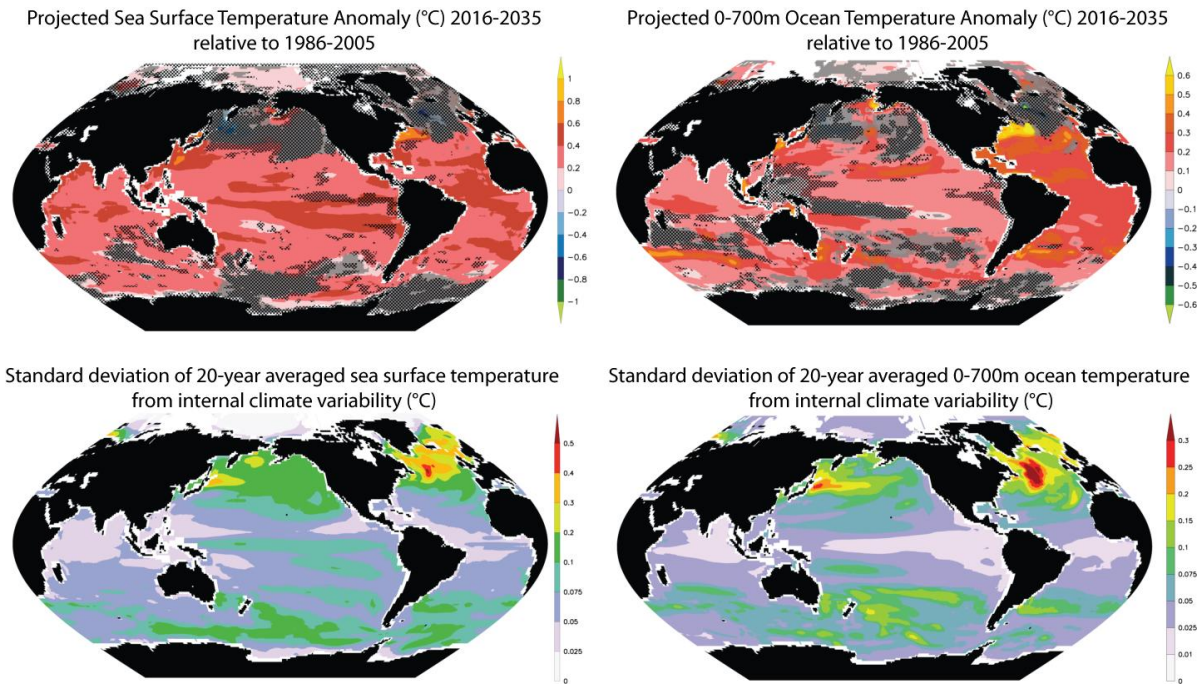13
14

1

2
3
4 **Figure 11.25:** Projected changes, as a function of depth, in annual-averaged, globally-averaged ocean temperature
5 based on the average of twelve AOGCMs from the CMIP3 (Meehl et al., 2007b) multi-model ensemble, under 21st
6 century Emissions Scenario SRESA1B. Gray shading indicates where the multi-model average AOGCM anomalies are
7 smaller than two standard deviations of the multi-AOGCM estimate of internal variability from the control climate
8 integrations. The fifty-year running average from each model's control climate integration was removed from each line.
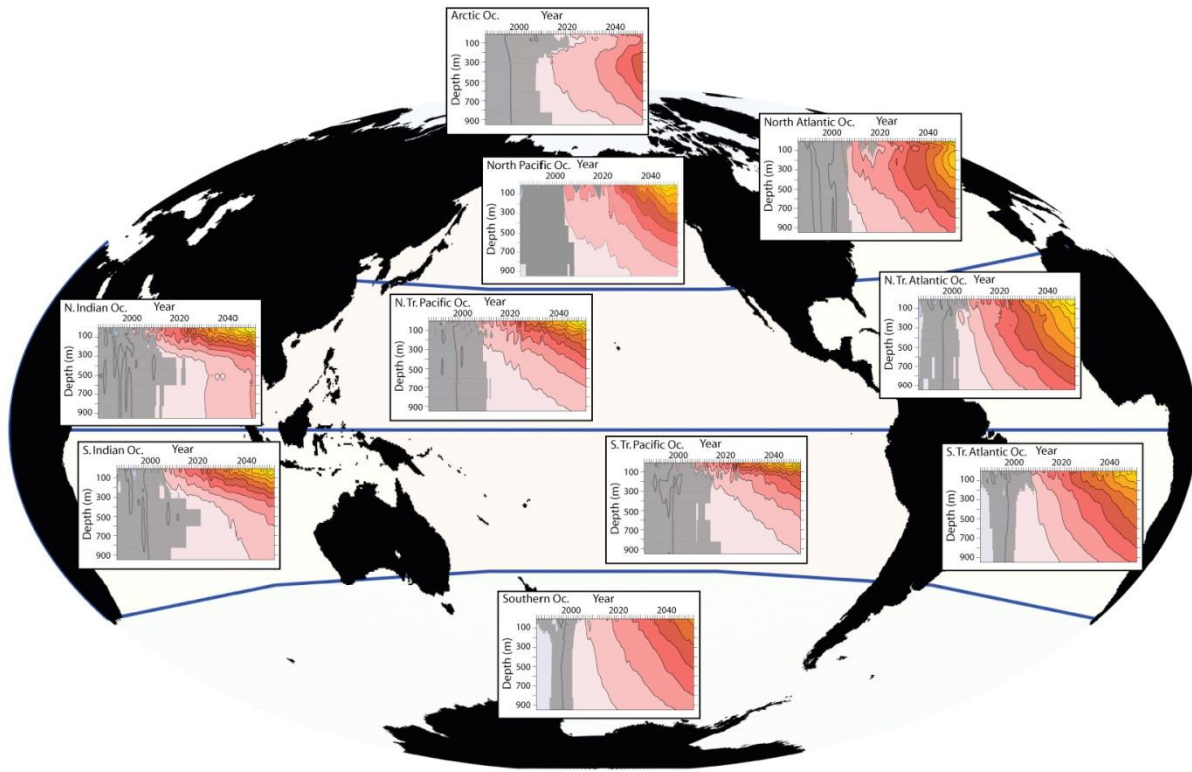9 Values referenced to the 1986–2005 climatology of each AOGCM.

10
11

1

Projected Sea Surface Temperature Anomaly (°C) 2016-2035
relative to 1986-2005

Projected 0-700m Ocean Temperature Anomaly (°C) 2016-2035
relative to 1986-2005

Standard deviation of 20-year averaged sea surface temperature
from internal climate variability (°C)

Standard deviation of 20-year averaged 0-700m ocean temperature
from internal climate variability (°C)

2
3
4   **Figure 11.26:** Upper panels show the projected changes averaged 2016–2035 relative to 1986–2005 in sea surface
5   temperature (left panels) and temperature averaged over the upper 700 meters of the ocean (right panels), as a function
6   of latitude and longitude. Lower panels show the standard deviation of twenty-year averages of sea surface temperature
7   (left panels) and temperature averaged over the upper 700 meters of the ocean (right panels) arising from internal
8   climate variability in these models. Figures based on the average of twelve AOGCMs from the CMIP3 (Meehl et al.,
9   2007b) multi-model ensemble, under 21st century Emissions Scenario SRESA1B. Gray shading indicates where the
10 multi-model average AOGCM anomalies are smaller than two standard deviations of the multi-AOGCM estimate of
11 internal variability from the control climate integrations, black stippling indicates where at least four (1/3) of the models
12 disagree on the sign of the change. The fifty-year running average from each model's control climate integration was
13 removed from each line.
14
15

1

2
3
4   **Figure 11.27:** [PLACEHOLDER FOR FINAL DRAFT: Currently shaded at 1 sigma. Same as Figure 11.25, but for
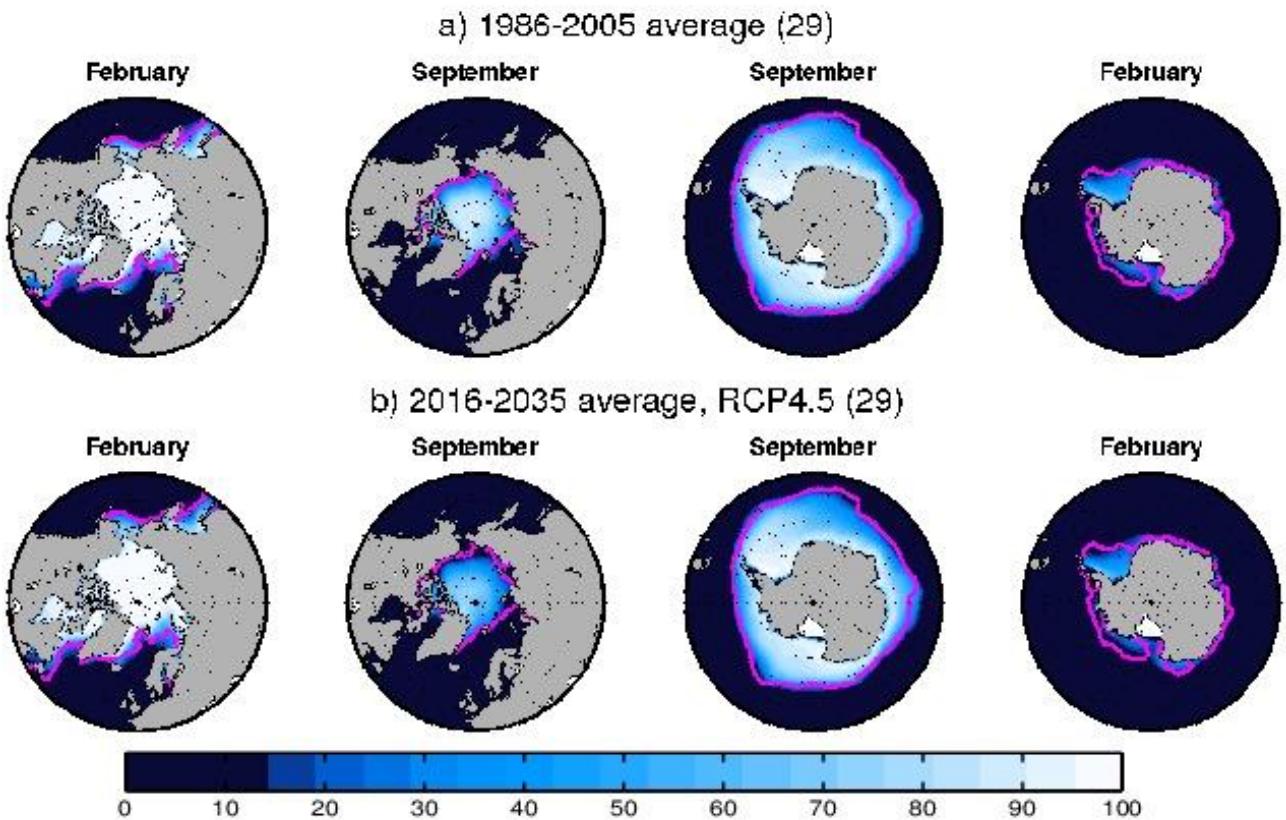5   regional averages.]
6
7

Figure 11.28: February and September CMIP5 multi-model mean sea ice concentrations (%) in the Northern and Southern Hemispheres for the periods (a) 1986–2005, (b) 2016–2035 under RCP4.5. Only one member per model is taken into account in the analysis. The number of models is given in parentheses. The pink lines show the observed 15% sea ice concentration limits averaged over 1986–2005 (Comiso et al., 2008).

1

2
3
4 **Figure 11.29:** Projected CH_4 (a) anthropogenic emissions (Tg–CH_4 yr^{-1}) and (b) atmospheric abundances (ppb) for the
5 four RCP scenarios (2010–2100). The thick solid lines show the published RCP values: red plus, RCP8.5; orange
6 square, RCP6.0; light blue circle, RCP4.5; dark blue asterisk, RCP2.6. Thin lines with markers show values from this
7 assessment based on Holmes et al. (2012). The shaded region shows the ±1 standard deviation from the Monte Carlo
8 calculations that consider uncertainties, including the current magnitude of the anthropogenic emissions.
9
10

1

2
3
4   **Figure 11.30:** Changes in surface O$_3$ (ppb) between year 2000 and 2030 averaged globally and over four northern mid-
5   latitude source regions as used in the Hemispheric Transport of Air Pollution (HTAP) studies (HTAP, 2010c). Results
6   are taken from the literature and include changes driven by climate alone (CLIMATE) as well as those driven by
7   emissions alone, following emission scenarios (SRES A1, A2, B1, B2; RCP 2.6, 4.5, 6.0, 8.5; MFR, CLE). Results
8   from individual studies are labeled by letters underneath the corresponding plot symbols. Solid vertical bars represent a
9   combination of ranges as reported in the literature: (A) multi-model mean and standard deviations in annual mean,
10   spatial averages from the ACCENT/Photocomp study (Dentener et al., 2006); (C) a parameterized model developed
11   from the multi-model HTAP ensemble (Wild et al., 2012). Dotted vertical bars represent spatial ranges as estimated
12   with one model: (S) globally (Stevenson et al., 2005), (V) within each of the HTAP regions (Dentener et al., 2005); (F,
13   D) over Europe (Forkel and Knoche, 2006; Szopa et al., 2006). Filled squares represent: (Q, T, U) regional averages
14   over the globe (Fiore et al., 2008; Unger et al., 2006b; West et al., 2006); and (W) over the United States (Fiore et al.,
15   2002). Regional definitions, methods, and reported metrics (e.g., 24-hour versus daily maximum values over a 1-hour
16   or 8-hour averaging period, annual or seasonal averages) vary across studies, and are the major contributor to the
17   apparent discrepancies between the blue (climate change only) solid and dashed lines (Section 11.3.5.2). Climate
18   change scenarios vary across studies, but are combined into ranges denoted by blue bars because there is little
19   detectable cross-scenario difference in the climate response by 2030 and it would not be detectable with the simulations
20   here (Sections 11.3.5.2.1 and 11.3.6). Adapted from Figure 3 of Fiore et al. (2012).
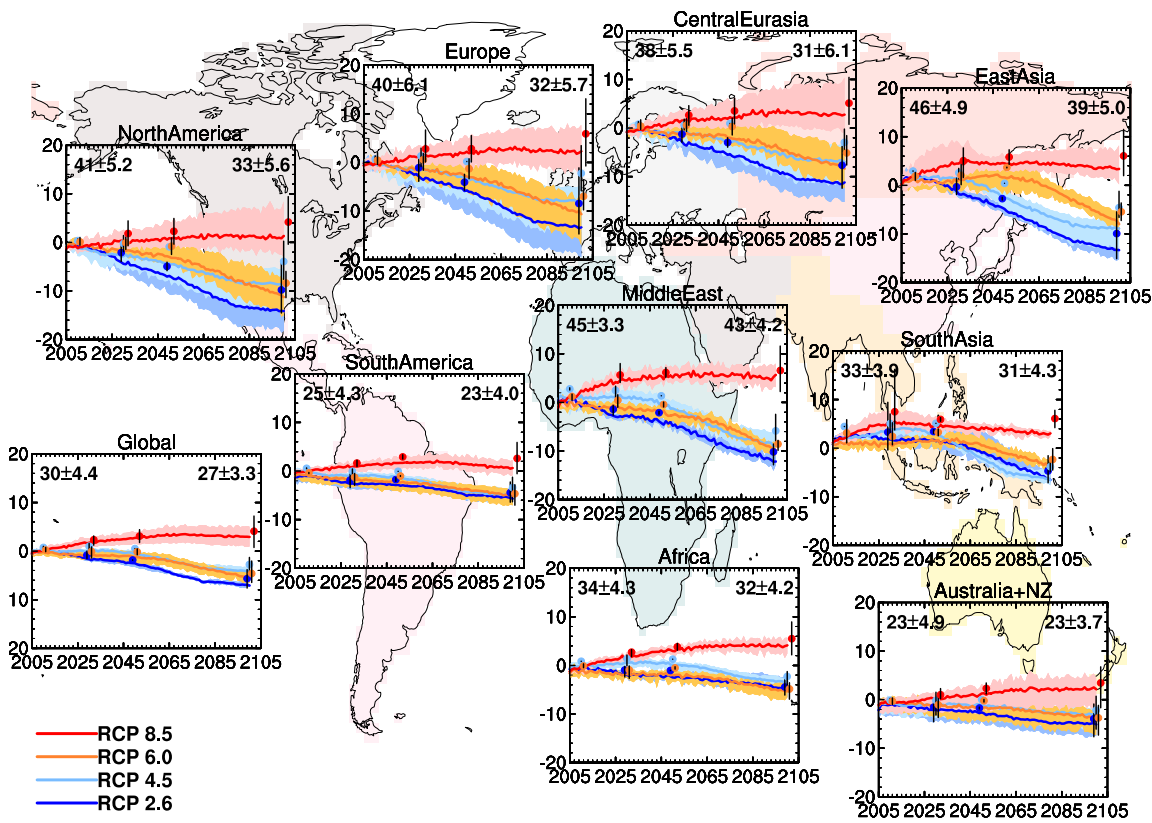21
22

1

2
3
4   **Figure 11.31a:** Projected changes in annual mean surface O_3 (ppb mole fraction) from 2000 to 2100 following the RCP
5   scenarios (8.5 red, 6.0 orange, 4.5 light blue, 2.6 dark blue). Results in each box are averaged over the shaded land
6   regions with continuous colored lines denoting the average of 4 CMIP5 chemistry-climate models (GFDL-CM3, GISS-
7   E2-R, LMDz-ORINCA, NCAR-CAM3.5) and colored dots denoting the average of 3, 9, 2, and 11 (or fewer) ACCMIP
8   models contributing results for the decadal time slices centered on 2010, 2030, 2050 and 2100, respectively. The
9   shading about the lines and the vertical bars on the dots represent the full range across models. Changes are relative to
10 the 1986–2005 reference period for the CMIP5 transient simulations, and relative to the average of the 1980 and 2000
11 decadal time slices for the ACCMIP ensemble. The average value and model standard deviation for the reference period
12 is shown in each panel with CMIP5 models on the upper left and ACCMIP models on the upper right. In cases where
13 multiple ensemble members are available from a single model, they are averaged prior to inclusion in the multi-model
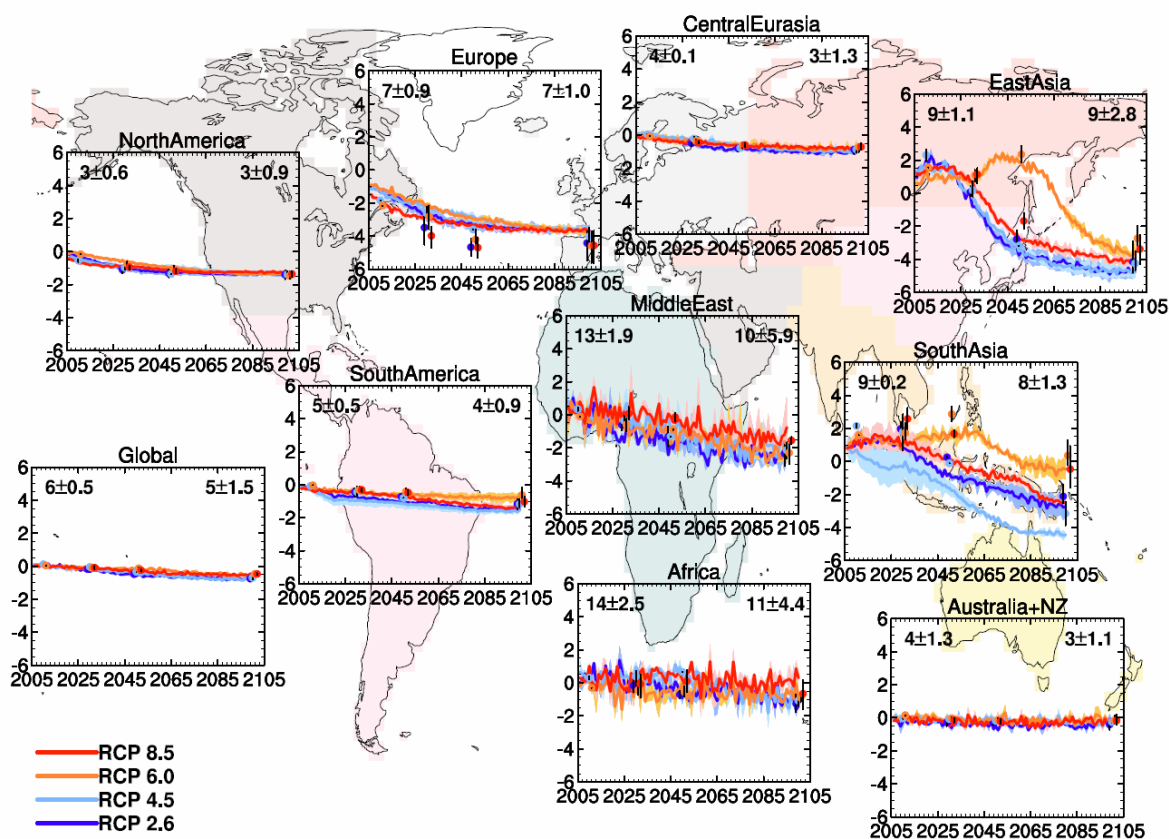14 mean. Adapted from Fiore et al. (2012).
15
16

1

Figure 11.31b: Projected changes in annual-mean surface PM2.5 (ng per g air) from 2000 to 2100 following the RCP scenarios (8.5 red, 6.0 orange, 4.5 light blue, 2.6 dark blue). PM2.5 values are calculated as the sum of individual aerosol components (black carbon + organic carbon + sulfate + secondary organic aerosol + 0.1*dust + 0.25*sea salt). Nitrate was not reported for most models and is not included here. See Figure 11.31a, but note that fewer models contribute: GFDL-E2-R and GFDL-CM3 from CMIP5; CICERO-OsloCTM2, GFDL-AM3, MIROC-CHEM, and NCAR-CAM3.5 from ACCMIP. Adapted from Fiore et al. (2012).

1

2
3
4   **Figure 11.32a:** Near-term increase in global mean surface air temperatures across scenarios. Increases in 10-year mean
5   (2016–2025, 2026–2035, 2036–2045 and 2046–2055) relative to the reference period (1986–2005) of the globally
6   averaged surface air temperatures (K). Results are shown for the CMIP5 model ensembles (see Annex I for listing of
7   models included) for RCP2.6 (dark blue), RCP4.5 (light blue), RCP6.0 (orange), and RCP8.5 (red), respectively) and
8   the CMIP3 model ensemble (22 models for SRES A1b (black). The multi-model median (square), 17–83% (likely)
9   range (wide boxes), 5–95% (very likely) range (whiskers) across all models are shown for each decade and scenario.
10 Also shown are estimates for scenarios that implement technological controls on methane emissions (UNEP CH$_4$) and
11 on emissions of methane and black carbon as well as co-emitted species such as carbon monoxide, organic carbon and
12 nitrogen oxides (UNEP CH$_4$ + BC). These changes are calculated relative to a reference scenario (UNEP Ref) but
13 adjusted to reflect the 1986–2005 reference period shown here. UNEP results are based on two chemistry-climate
14 models and shown only as a range (whiskers) derived from uncertainties in radiative forcing components and climate
15 sensitivity (Shindell et al., 2012b; UNEP and WMO, 2011). The thick horizontal lines indicate increases in global mean
16 surface air temperature relative to a reference period of 1850–1900 (rather than 1986–2005).
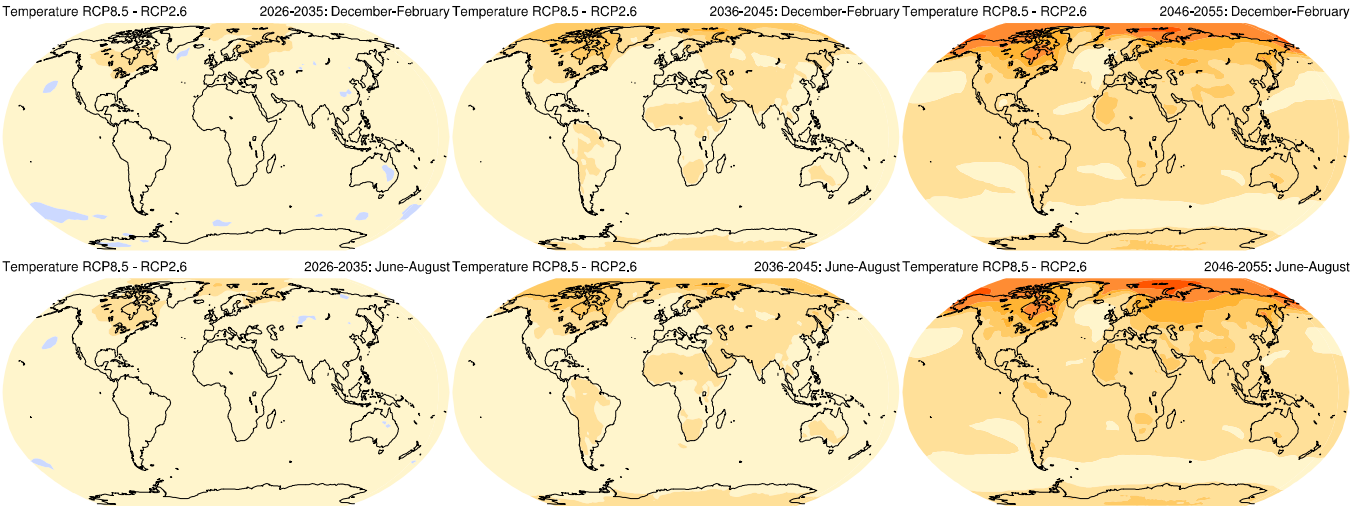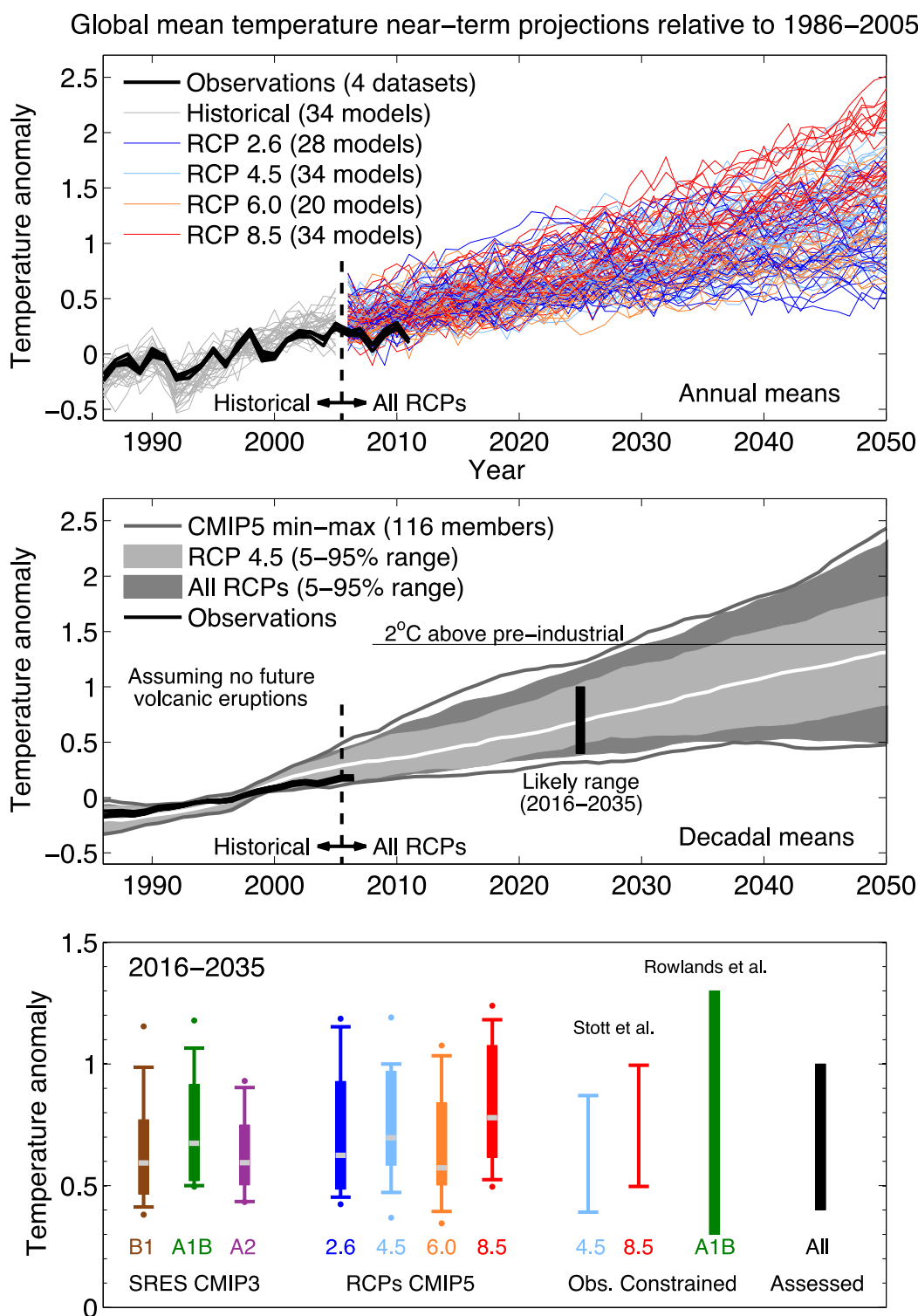17
18

1

2
3
4   **Figure 11.32b:** Global maps of near-term differences in surface air temperature across the RCP scenarios. Differences
5   between the high (RCP8.5) and low (RCP2.6) scenarios for the CMIP5 model ensemble (12 models) are shown for
6   averages over 2026–2035 (left), 2036–2045 (middle) and 2046–2055 (right) in boreal winter (DJF; top row) and
7   summer (JJA; bottom row).
8
9

1

Figure 11.33: Synthesis of near-term projections of global mean surface air temperature. a) Projections of global mean,
annual mean surface air temperature (SAT) 1986–2050 (anomalies relative to 1986–2005) under all RCPs from CMIP5
models (grey and coloured lines, one ensemble member per model), with four observational estimates (HadCRUT3:
Brohan et al., 2006; ERA-Interim: Simmons et al., 2010; GISTEMP: Hansen et al., 2010; NOAA: Smith et al., 2008)
for the period 1986–2011 (black lines); b) as a) but showing the 5–95% range for RCP4.5 (light grey shades, with the
multi-model median in white) and all RCPs (dark grey shades) of decadal mean CMIP5 projections using one ensemble
member per model, and decadal mean observational estimates (black lines). The maximum and minimum values from
CMIP5 are shown by the grey lines. An assessed *likely* range for the mean of the period 2016–2035 is indicated by the
black solid bar. The '2°C above pre-industrial' level is indicated with a thin black line, assuming a warming of global
mean SAT prior to 1986–2005 of 0.6°C. c) A synthesis of ranges for the mean SAT for 2016–2035 using SRES CMIP3,
RCPs CMIP5, observationally constrained projections (Stott et al., 2012; Rowlands et al., 2012; updated to remove

1   simulations with large future volcanic eruptions), and an overall assessment. The box and whiskers represent the *likely*
2   (66%) and *very likely* (90%) ranges. The dots for the CMIP3 and CMIP5 estimates show the maximum and minimum
3   values in the ensemble. The median (or maximum likelihood estimate for Rowlands et al., 2012) are indicated by a grey
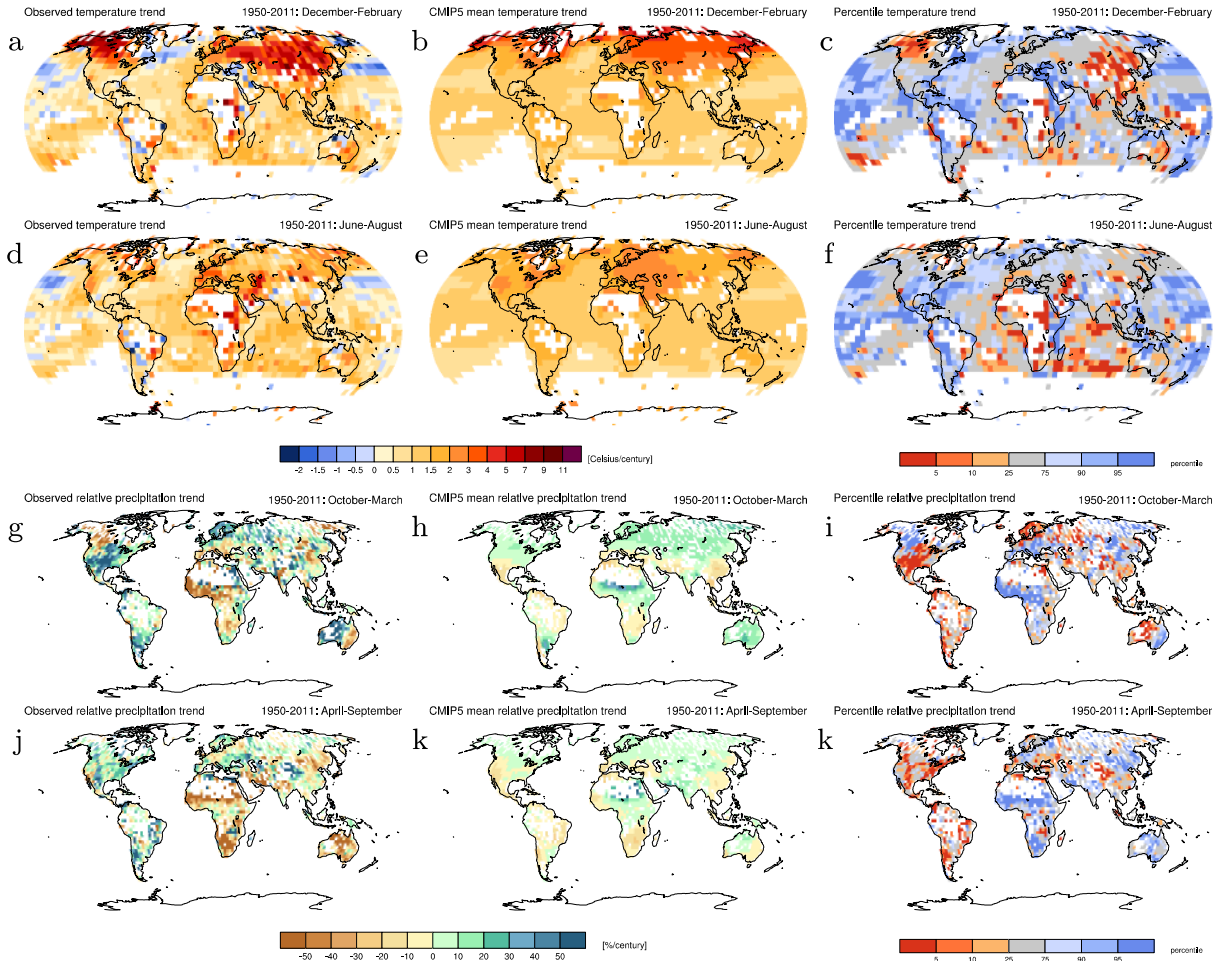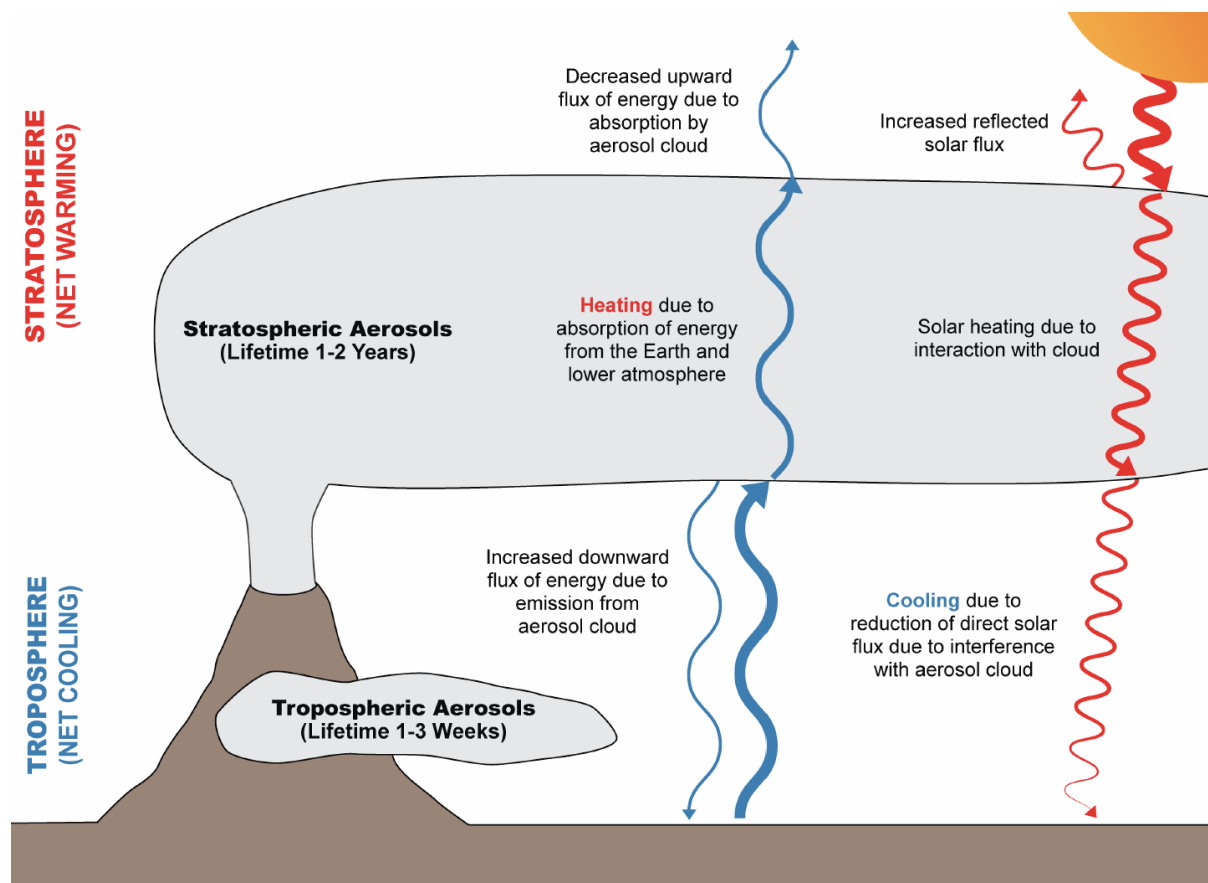4   band.
5
6

1

2
3
Figure 11.34: a) Observed linear December to February temperature trend 1950–2010 (CRUTEM3/HadSST2)
[°C/century], b) the equivelant CMIP5 ensemble mean trend and c) quantile of the observed trend in the ensemble.
d,e,f) Same for June to August. g,h,i) Same for October to March precipitation (CRU TS 3.10.01) [% per century]. j,k,l)
Precipitation in April to September. Based on Räisänen (2007).

8
9

1

2
3
4   **FAQ 11.2, Figure 1:** Schematic of how large tropical or sub-tropical volcanoes impact upper atmospheric
5   (stratospheric) and lower atmospheric (tropospheric) temperatures.
6
7